A potential link between adiposity and the heart: Investigating a posttranscriptional mechanism of cardiac ATM protein regulation in obesity

by
Danélle Botha

Thesis presented in fulfilment of the requirements for the degree of Master of Science in the Faculty of Medicine and Health Sciences at Stellenbosch University

Supervisor: Prof Barbara Huisamen
Co-supervisor: Dr Marguerite Blignaut

March 2021

Declaration

By submitting this thesis electronically, I declare that the entirety of the work contained therein is my own, original work, that I am the sole author thereof (save to the extent explicitly otherwise stated), that reproduction and publication thereof by Stellenbosch University will not infringe any third party rights and that I have not previously in its entirety or in part submitted it for obtaining any qualification.

March 2021

Abstract

Background: Obesity is a risk factor for metabolic abnormalities, including insulin resistance, which precedes type II diabetes and cardiovascular diseases. White adipose tissue (WAT) is an endocrine organ responsible for maintaining systemic energy homeostasis. Obesity results in dramatic changes in WAT behaviour, including ectopic visceral accumulation and dysregulated adipocyte metabolism and secretions, which may adversely affect peripheral organs. Ataxia-telangiectasia mutated kinase (ATM) regulates glucose and redox homeostasis, thereby contributing to normal cellular metabolism. However, ATM protein levels are down-regulated in muscle and cardiac tissues of obese and insulin resistant animals, and therefore represents a potential link between obesity and peripheral metabolic dysfunction. The underlying mechanism of cardiac ATM suppression in obesity, however, remains unknown.

ATM protein levels are suppressed by specific microRNAs (miRNAs) in cancer cells. MiRNAs are short molecules that govern protein translation in health and disease. Therefore, this study investigates whether adipocyte secretions potentially regulate cardiomyoblast ATM protein levels through a miRNA-mediated mechanism in obesity.

Methods: 1) H9c2 cardiomyoblasts were treated with combinations of high free fatty acids (FFAs; palmitic- and oleic acid), glucose and/or insulin (n=3) to establish whether cardiomyoblasts are metabolically sensitive to obese-simulating conditions. ATM levels and activation (phosphorylation), together with other relevant metabolic proteins, were determined through Western blotting. The expression of two miRNAs that target ATM in cancer (miRNA-421 and miRNA-18a) were determined with qRT-PCR.

2) H9c2 cardiomyoblasts were treated with primary adipocyte-derived conditioned media to establish whether cardiomyoblasts are metabolically sensitive to adipocyte secretions. The adipocytes were differentiated from adipose stem cells (ASCs) originating from the subcutaneous and visceral fat depots of lean (control; n=4) and high-fat diet (HFD; n=4) male Wistar rats. The basal metabolic protein profiles of adipocytes were determined through Western blotting and the FFA composition of the conditioned media were determined through GC-FID. Cardiomyoblast ATM levels and activation, together with other relevant metabolic proteins, were determined through Western blotting. The expression of miRNA-421 and miRNA-18a, and four additional metabolic miRNAs that target ATM *in silico* (miRNA-194, miRNA-210, miRNA-322, miRNA-181b), were determined with qRT-PCR.

Results: In H9c2 cells, ATM activity (phospho/total-ratio), but not protein levels, were i) decreased by a combination of high FFAs and insulin compared to FFAs alone and insulin alone, and ii)

increased ($p<0.05$) in response to control- and HFD-derived adipocyte secretions compared to untreated cells. The basal metabolic protein profiles and FFA secretory profiles of adipocytes were not influenced by fat depot or diet, but by the adipocytic differentiation process. Lastly, visceral and subcutaneous adipose secretions down-regulated ($p<0.01$) miRNA-181b levels in H9c2 cells under HFD conditions.

Discussion and conclusion: This study shows, for the first time, that cardiomyoblast i) ATM activity is influenced by high insulin, FFAs and adipose secretions, and ii) miRNA-181b expression is down-regulated in response to HFD-derived adipose secretions. Reduced miRNA-181b levels were previously observed in the myocardium of obese mice and associates with inflammation, insulin resistance and cardiomyopathy. We speculate that cardiomyoblast miRNA-181b down-regulation in response to HFD-derived adipocyte secretions may potentially be an early indicator of metabolic dysfunction.

Opsomming

Agtergrond: Vetsug is ‘n risikofaktor vir metaboliese abnormaliteite, insluitend insulienweerstandigheid, wat lei tot tipe II diabetes en kardiovaskulêre siektes. Wit vetweefsel (WV) is ‘n endokriene orgaan verantwoordelik vir die instandhouding van sistemiese energie homeostase. Vetsug lei tot groot veranderinge in WV funksie, insluitend die ektopiese versameling van vet rondom organe en wangereguleerde adiposietmetabolisme en -sekresie, wat perifere organe nadelig kan beïnvloed. Ataxia-telangiectasia gemuteerde proteïenkinase (ATM) reguleer glukose- en redoks homeostase en dra sodoende by tot normale sellulêre metabolisme. ATM proteïenvlakke word egter onderdruk in spier- en hartweefsel van vetsugtige en insulienweerstandige diere en verteenwoordig dus a moontlike skakel tussen vetsug en perifere metaboliese disfunksie. Die onderliggende meganisme wat lei tot die onderdrukking van ATM in die hart tydens vetsug is egter onbekend.

ATM proteïenvlakke word onderdruk deur spesifieke mikroRNAs (miRNAs) in kankerselle. MiRNAs is kort molekules wat proteïentranslasie onder normale en siektestoestande beheer. Die huidige studie ondersoek dus of adiposietsekresies moontlik ATM proteïenvlakke deur middel van miRNAs in kardiomioblaste tydens vetsug beheer.

Metodes: 1) H9c2 kardiomioblaste is behandel met kombinasies van höe vrye vetsure (VV; palmitaat en oleaat), glukose en/of insulien (n=3) om vas te stel of kardiomioblaste metabolies sensitief is vir kondisies wat vetsug naboots. ATM vlakke en aktivering (fosforilering), asook ander metabolies-verwante proteïene, is bepaal deur middel van Westerse-klad tegniek. Twee miRNAs wat ATM teiken in kanker (miRNA-421 en miRNA-18a) se uitdrukkingsvlakke is met qRT-PCR bepaal.

2) H9c2 kardiomioblaste is behandel met gekondisioneerde media afkomstig van primêre adiposiete om metaboliese sensitiwiteit vir adiposietsekresies te bepaal. Die adiposiete is gedifferensieer vanaf adiposiet stamselle afkomstig van die subkutane en visserale vetkompartemente van kontrole (n=4) en hoë-vet dieet (HVD; n=4) manlike Wistar rotte. Die basale metaboliese proteïenprofiele van die adiposiete is deur middel van Westerse-klad tegniek bepaal en die VV samestelling van die gekondisioneerde media is met GC-FID bepaal. ATM vlakke en aktivering, asook ander relevante metaboliese proteïene, is ook deur middel van Westerse-klad tegniek bepaal. Die uitdrukkingsvlakke van miRNA-421 en miRNA-18a, asook vier addisionele metaboliese miRNAs wat ATM *in silico* teiken (miRNA-194, miRNA-210, miRNA-322, miRNA-181b), is met qRT-PCR bepaal.

Resultate: In H9c2 selle is ATM aktiwiteit (fosfo/totaal-verhouding), maar nie proteïenvlakke nie, i) afgereguleer deur ‘n kombinasie van VV en insulien in vergelyking met VV alleen en insulien alleen en ii) opgereguleer ($p<0.05$) deur gekondisioneerde media van adiposiete afkomstig van kontrole en HVD rotte in vergelyking met onbehandelde selle. Die basale metaboliese proteïenprofiele en VV

sekresieprofiele van adiposiete is nie beïnvloed deur die vetkompartement of dieet nie, maar deur die adiposiet-spesifieke differensiasieproses. Die miRNA-181b vlakke is afgereguleer ($p<0.01$) in H9c2 selle deur visserale en subkutane adiposietsekresies onder HVD kondisies.

Bespreking en gevolgtrekking: Hierdie studie toon vir die eerste keer dat kardiomioblast i) ATM aktiwiteit deur hoë insulien, VV en adiposietsekresies beïnvloed word en ii) miRNA-181b uitdrukkingsvlakke in ‘n HVD omgewing onderdruk word. Onderdrukte miRNA-181b vlakke is voorheen in die miokardium van vetsugtige muise waargeneem en assosieer met inflammasie, insulienweerstandigheid en kardiomiopatie. Ek spekuleer dat HVD-afkomstige adiposietsekresies moontlik miRNA-181b in kardiomioblaste onderdruk voor die aanvang van metaboliese afwykings.

Acknowledgements

I wish to acknowledge and thank the following institutions and individuals for their contributions and support throughout this project:

The division of Medical Physiology, for the opportunity to complete my MSc project. It is a great honour and absolute pleasure to work in such a nurturing and supportive environment that allows for professional and personal growth.

The Harry Crossley Foundation (Stellenbosch University), for providing the necessary funding without which this project would not be possible.

The South African Medical Research Council (SAMRC), for their laboratory facilities, technical assistance and financial support. I would like to especially thank Dr Stephanie Diaz, Dr Paul van Jaarsveld and Dr Rabia Johnson. I sincerely appreciate all that you have done for me.

Dr Hanél Sadie-van Gijsen, for the laboratory work that formed the foundation of this study, as well as availing yourself to help me better understand my data. I truly appreciate it.

Prof Barbara Huisamen, for your invaluable leadership and guidance as my supervisor. Thank you for allowing me to leave my own fingerprint on this project and for keeping me on my toes with important questions. I am honoured to be part of your research-family.

Dr Marguerite Blignaut, for your continued support, patience and assistance as my co-supervisor. Thank you for challenging me throughout the past two years – it has shaped me more than you could know. I am truly grateful for this experience.

Charlize White and Sarah Harries, my dearest friends. Thank you for all your love and time. Your friendships have made for some unforgettable memories and have carried me through some difficult times. It has been a privilege to transition from colleagues to friends!

Neil and Reneé Botha, my wonderful parents. Dad en Mams, baie dankie vir julle oneindige ondersteuning, geduld en liefde. Dankie dat julle dit ‘n prioriteit gemaak het om vir my en Dewie die beste geleenthede te skep. Sonder die fondasie wat julle oor die jare neergelê het, sou ek nie my hoogtes kon bereik het nie. Ek is só lief vir julle.

Lastly, my Sheppard. Thank you for always meeting me where I am and for guiding my feet, step by step. It is through Your grace and faithfulness that I was able to walk to the finish line. I look forward to a lifetime of walking together.

Research outputs associated with this study

Symposium

- **Botha, D.**, Blignaut, M., Sadie-van Gijsen, H., Huisamen, B. "Connecting the dots: Investigating ATM down-regulation as the potential link between adipose tissue and the heart in obesity and insulin resistance". **Oral presentation**, Biomedical Research and Innovation Platform (BRIP), Annual Research Symposium, Cape Town, South Africa (19-20 October 2020).

Conferences

- **Botha, D.**, Blignaut, M., Huisamen, B. "A potential mechanism of cardiac ATM down-regulation in obesity and insulin resistance: Are microRNAs the molecular middlemen?". **Oral presentation**, 47th Conference of the Physiology Society of Southern Africa (PSSA), East London, South Africa (18-21 August 2019).
- **Botha, D.**, Blignaut, M., Sadie-van Gijsen, H., Huisamen, B. "Connecting the dots: Investigating the potential link between adipose tissue and the heart relating to ATM down-regulation in obesity and insulin resistance". **Oral presentation**, Department of Biomedical Sciences Annual Research Day, Tygerberg medical campus, Stellenbosch University, South Africa (21 November 2019).

Awards and achievements

- Overall winner: Wyndham oral presentation competition, 47th Conference of the Physiology Society of Southern Africa (PSSA), East London, South Africa (18-21 August 2019).
- PSSA travel award to attend the PSSA conference, East London, South Africa (18-21 August 2019).
- Faculty of Medicine and Health Sciences, Stellenbosch University travel grant to attend the PSSA conference, East London, South Africa (18-21 August 2019).
- Third prize winner: Oral presentation at the Department of Biomedical Sciences Annual Research Day, Tygerberg medical campus, Stellenbosch University, South Africa (21 November 2019).
- Harry Crossley Foundation project funding (2019 and 2020).
- Harry Crossley Foundation bursary (2019 and 2020).

Table of contents

List of figures

List of tables

List of abbreviations

4E-BP1	Eukaryotic translation initiation factor 4E-binding protein 1
µl	Microlitre
µg	Microgram
ACC	Acetyl-coenzyme A carboxylase
Adipo	Adipocytes
AMP	Adenosine monophosphate
AMPK	AMP-activated protein kinase
ANOVA	Analysis of variance
AS160	Akt substrate of 160 kilodalton
ASCs	Adipose stem cells
ASP	Acylation-stimulating protein
A-T	Ataxia-telangiectasia
ATGL	Adipose triglyceride lipase
ATM	Ataxia-telangiectasia mutated
ATP	Adenosine triphosphate
BAT	Brown adipose tissue
BMI	Body mass index
BSA	Bovine serum albumin
CD36	Cluster of differentiation 36
cDNA	Complimentary DNA
C/EBPα	CCAAT/enhancer binding protein alpha
CM	Conditioned media
Cnt	Control
CPT	Carnitine palmitoyltransferase
Ct	Threshold cycle
Cys	Cysteine

DAG	diacylglycerol
DGCR8	DiGeorge syndrome critical region in gene 8
DMEM	Dulbecco's Modified Eagle Medium
DMSO	Dimethyl sulfoxide
DNA	Deoxyribonucleic acid
DPBS	Dulbecco's phosphate-buffered saline
ds-miRNA	double-stranded miRNA
ECL	Enhanced chemiluminescence
EDL	Extensor digitorum longus
EXP5	Exportin-5
FABP	Fatty acid binding protein
$FABP_{pm}$	Plasmalemmal fatty acid-binding proteins
FAT	Fatty acid translocase
FATP1	Fatty acid transporter protein 1
FBS	Foetal bovine serum
FFAs	Free fatty acids
G6PD	Glucose-6-phosphate dehydrogenase
GC-FID	Gas chromatography-flame ionisation detection
Glu	Glucose
GLUT	Glucose transporter
HFD	High-fat diet
HIF	Hypoxia-inducible factor
HRP	Horseradish peroxidase
IBMX	Isobutylmethylxanthine
IL-6	Interleukin-6
Ins	Insulin
IRS-1	Insulin receptor substrate 1

kDa	Kilodalton
LKB1	Liver kinase B1
Log	Logarithm
M	Molar
mA	Milliampere
MCP-1	Monocyte chemoattractant protein-1
mg	Milligram
miRNAs	MicroRNAs
ml	Millilitre
mM	Millimolar
mRNA	Messenger ribonucleic acid
mTORC	Mammalian target of rapamycin complex
MTT	3-[4,5-dimethylthiazole-2-yl]-2,5-diphenyltetrazolium bromide
NADPH	Nicotinamide adenine dinucleotide phosphate hydrogen
Neg	Negative control
NF-κB	Nuclear factor kappa B
nm	Nanometre
NTC	Non-template control
ORO	Oil red O
p	Phospho
PAI-1	Plasminogen activator inhibitor-1
PBS	Phosphate-buffered saline
PDK1	phosphoinositide-dependent kinase-1
PenStrep	Penicillin-Streptomycin
PI3K	Phosphatidylinositol 3-kinase
PIKK	Phosphatidylinositol 3-kinase-related protein kinase
PIP2	Phosphatidylinositol (4,5)bisphosphate

PIP3	Phosphatidylinositol (3,4,5)triphosphate
PKA	Protein kinase A
PKB	Protein kinase B
Pol II	Polymerase II
PPARα	Proliferator-activated receptor alpha
PPARɣ	Proliferator-activated receptor gamma
PPP	Pentose phosphate pathway
PR	Peri-renal
Pre-miRNA	Precursor microRNA
Pri-miRNA	Primary microRNA
PVDF	Polyvinylidene fluoride
qRT-PCR	Quantitative real-time polymerase chain reaction
R^2	Correlation coefficient
RIN	Ribonucleic acid integrity number
RISC	RNA-induced silencing complex
Rn	Normalised reporter
RNA	Ribonucleic acid
ROS	Reactive oxygen species
RT	Reverse transcription
S6K	S6 kinase
SC	Subcutaneous
SD	Standard deviation
SDS-PAGE	Sodium dodecyl sulfate-polyacrylamide gel electrophoresis
Ser	Serine
shRNA	Short hairpin ribonucleic acid
t	Total
TBS	Tris-buffered saline

TBS-T	Tris-buffered saline with Tween
Thr	Threonine
TNF-α	Tumour necrosis factor alpha
TSC2	Tuberous sclerosis complex 2
ULK1	Unc-51-like kinase 1
UTR	Untranslated region
UV	Ultra-violet
V	Volt
vs.	Versus
WAT	White adipose tissue

Chapter 1

Study introduction

Adipose tissue constitutes an essential organ with a dual function: the rapid storage of energy following feeding and the secretion of various hormones and inflammatory cytokines for vital communication with distant organs (Kershaw and Flier, 2004). Adipose tissue expansion is driven by a positive energy balance, which occurs as a result of chronic overfeeding and a sedentary lifestyle – two characteristics of modern-day living.

Obesity is notoriously associated with metabolic abnormalities, such as insulin resistance, which predispose individuals to the development of type II diabetes and cardiovascular diseases. On an anatomical level, obesity is associated with ectopic adipose tissue accumulation around central organs (Virtue and Vidal-Puig, 2010). On a physiological level, obesity associates with dysregulated adipocyte metabolism and secretions, which may adversely affect other peripheral organs to culminate in systemic disease (Longo *et al.*, 2019). As such, obesity is recognised as a major health threat to the global population (Jaacks *et al.*, 2019).

Ataxia telangiectasia mutated (ATM) is an apical protein kinase responsible for maintaining DNA integrity in response to double-stranded breaks (Lavin and Kozlov, 2007). Furthermore, ATM plays an important metabolic role in the cytoplasm, independent from its participation in the DNA damage repair response. Two major metabolic pathways that rely on ATM activity include insulin signalling (Yang and Kastan, 2000) and redox signalling (Guo *et al.*, 2010). Therefore, individuals with ataxia-telangiectasia (A-T), a rare genetic disorder caused by mutations in the *Atm* gene, are predisposed to the development of cancer, insulin resistance, type II diabetes and ischaemic heart disease (Rothblum-Oviatt *et al.*, 2016). Interestingly, animal studies have shown an association between obesity and decreased peripheral ATM protein levels (Halaby *et al.*, 2008; Huisamen *et al.*, 2016). However, the exact underlying mechanism of this obesity-related ATM reduction is unknown.

MicroRNAs (miRNAs) regulate gene expression through posttranscriptional silencing of messenger RNA (mRNA) transcripts (Bartel, 2004), thereby meticulously controlling the proteins that will be translated under a specific condition. Despite playing important physiological roles, miRNAs have been implicated in various disease states such as cancer (Peng and Croce, 2016), obesity, and type II diabetes (Landrier, Derghal and Mounien, 2019). Therefore, these small regulatory RNAs represent an attractive mechanism to consider for the regulation of ATM protein levels during obesity. In fact, miRNAs have been shown to suppress ATM protein levels in the context of cancer (Hu *et al.*, 2010; Song *et al.*, 2011; Shen and Houghton, 2013; Wu *et al.*, 2013), indicating that ATM is susceptible to

posttranscriptional regulation. Studies investigating their potential involvement in the regulation of ATM in a metabolic context, however, remain lacking.

Due to the involvement of ATM in various metabolic signalling networks, its reduction in obesity might explain some of the metabolic abnormalities that manifest in obese individuals. If the mechanism by which ATM protein levels are dysregulated in obesity is better understood, ATM may serve as a potential novel therapeutic target for alleviating metabolic complications associated with obesity.

Chapter 2

Literature review

2.1. White adipose tissue (WAT)

2.1.1. Introduction to structure and function

Generally known as “fat”, adipose tissue represents a loose connective tissue that is organised into large lobular structures within the body. Two types of adipose tissue exist: brown adipose tissue (BAT), which mainly dissipates energy for thermoregulation in infants, and white adipose tissue (WAT), which enables the storage of energy as triglycerides (Cinti, 2012). WAT is a heterogeneous tissue that consists of mature adipocytes and preadipocytes (adipocyte precursors) situated in a surrounding matrix comprised of collagen fibres, fibroblasts, blood vessels and macrophages (Trayhurn and Beattie, 2001). A characteristic feature that discern mature adipocytes from preadipocytes is the presence of a large, single lipid droplet that occupies the majority of the cytoplasm, thereby displacing the nucleus to the extremity of the cell as more triglycerides are stored within the adipocyte (Cinti, 2012).

WAT is a dominant role player in energy homeostasis as it is the major site for lipid storage and release. This balance of lipid flux is finely regulated by integrative signals of nutrient, neural and hormonal origin (reviewed by Spiegelman and Flier, 1996). In the event where more calories are consumed than is needed for immediate metabolic requirements, various signals mediate the storage of excess free fatty acids (FFAs) as triglycerides within WAT during lipid accumulation. Conversely, in the fasted state, the mobilisation of FFAs from storage is stimulated by opposing signals and results in the release of FFAs from WAT.

In addition to functioning as a biological reservoir for excess energy, WAT is a dynamic organ with important endocrine and metabolic roles. This is due to its ability to secrete a plethora of bioactive compounds into circulation that exert physiological effects at both local (autocrine and paracrine) and systemic (endocrine) levels (Coelho, Oliveira and Fernandes, 2013). The initial indication of this added endocrine potential surfaced in 1987 with the discovery of sex steroid production (Siiteri, 1987) and adipsin secretion (Flier *et al.*, 1987) by adipocytes. Thereafter, the discovery of leptin in 1994 (Zhang *et al.*, 1994) led to the firm recognition of WAT as an endocrine organ in its own right. WAT therefore contains the metabolic machinery to synthesize and secrete circulating factors that enable communication with distant organs (Kershaw and Flier, 2004).

2.1.2. Adipocyte metabolism: roles of AMPK, PKB and mTORC1

Central to adipocyte function is the maintenance of energy homeostasis through its ability to store lipids in times of nutrient excess and to mobilise it again in times of nutrient deficiency. Various protein signalling pathways play important collective or opposing roles in adipocyte metabolism that are dependent on this nutrient availability **(*Figure 2.1*)**. One such protein is adenosine monophosphate (AMP)-activated protein kinase (AMPK), whose activation stimulates energy-producing catabolic processes (fatty acid metabolism; β-oxidation) while inhibiting energy-consuming anabolic processes (lipid synthesis; lipogenesis) in times of nutrient deficiency. AMPK is activated under conditions of elevated AMP (thus decreased adenosine triphosphate; ATP) levels to promote signalling pathways that will restore the ATP balance within the cell. A down-stream target of AMPK is acetyl-coenzyme A carboxylase (ACC), a lipogenic enzyme responsible for the conversion of acetyl-coA to malonyl-coA. In turn, malonyl-coA serves as a substrate for lipogenesis and inhibits FFA uptake into the mitochondria for energy production. Activated AMPK phosphorylates, and thereby inhibits, ACC in order to limit lipogenesis while favouring mitochondrial β-oxidation (Daval, Foufelle and Ferré, 2006).

On the contrary, proteins such as protein kinase B (PKB, also known as Akt) and mammalian target of rapamycin (mTOR) are activated in times of nutrient surplus to promote anabolic processes such as lipogenesis and preadipocyte differentiation into mature adipocytes (adipogenesis). WAT, similar to cardiac and skeletal muscle tissue, is sensitive to insulin, a hormone that is secreted in response to food intake. Once circulating insulin binds to its receptor located in the adipocyte cell membrane, a cascade of protein phosphorylation leads to PKB activation. Activated PKB subsequently targets down-stream proteins to facilitate the storage of excess FFAs and glycerol as triacylglycerol within the lipid droplet. One such down-stream target is mTOR complex 1 (mTORC1), which in turn activates S6-kinase (S6K), to promote lipogenesis and adipogenesis (Caron, Richard and Laplante, 2015). Prolonged activation of the mTORC1/S6K pathway results in the serine phosphorylation, and therefore inhibition, of insulin receptor substrate 1 (IRS-1), an upstream kinase of PKB. Therefore, S6K-facilitated inhibition of IRS-1 leads to the attenuation of PKB activity in a negative feedback loop (Manning, 2004). Additionally, PKB and mTORC1 block various distinctive catabolic processes. For example, PKB negatively regulates β-oxidation by phosphorylating (inhibiting) AMPK on a specific serine residue (Berggreen *et al.*, 2009), whereas mTORC1 negatively regulates lipolysis through the inhibition of adipose triglyceride lipase (ATGL), a lipolytic enzyme (Caron, Richard and Laplante, 2015).

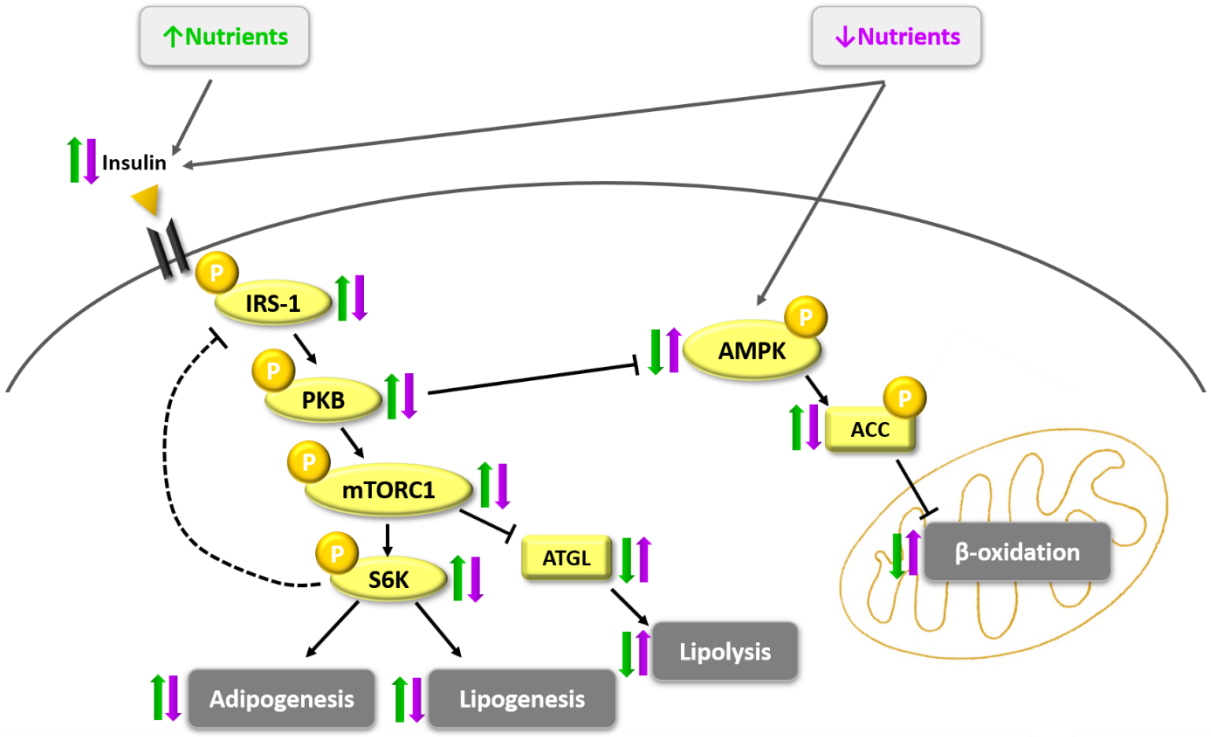

Figure 2.1: Adipocyte metabolism.

In response to nutrient deficiency (purple arrows), pathways in adipocytes are activated to promote catabolic processes. Energy-depletion activates AMPK, which in turn phosphorylates and inhibits ACC to promote mitochondrial β-oxidation. In response to nutrient surplus (green arrows), pathways in adipocytes are activated to promote anabolic processes. Insulin-stimulated PKB phosphorylation leads to the down-stream phosphorylation of the mTORC1/S6K pathway to promote lipogenesis and adipogenesis. S6K, in turn, inhibits IRS-1 in a negative feedback fashion. mTORC1 inhibits ATGL and, subsequently, lipolysis. PKB inhibits AMPK to block mitochondrial β-oxidation. Figure designed in Microsoft PowerPoint Office 365 by the author of the thesis.

As mentioned previously, mTORC1 plays a central role in adipogenesis. Similarly, both AMPK and PKB have been implicated as important role players in this process. Several studies have demonstrated that activated AMPK prevents preadipocyte differentiation by limiting lipid accumulation and inhibiting key adipogenic genes in different cell models (Dagon, Avraham and Berry, 2006; Lee, Jeong and Park, 2018). Conversely, PKB and mTORC1 activation is critical for adipocyte differentiation to commence, as have been shown by PKB (Peng *et al.*, 2003) and mTORC1 (Polak *et al.*, 2008) knock-down studies.

2.1.3. Adipogenesis: from adipose stem cell to adipocyte

In vivo

Increased caloric intake relative to energy output drives WAT expansion in the form of adipocyte hyperplasia, a proliferative occurrence that results in increased adipocyte number. Mature adipocytes are incapable of cell division, therefore hyperplasia relies on the differentiation of adipocyte

precursors to mature adipocytes. Firstly, pluripotent adipose stem cells (ASCs) residing in the WAT vascular stroma are recruited and promoted to commit to the adipocyte phenotype by a surplus energy balance. Once this occurs, ASCs are converted to preadipocytes, which in turn differentiate into mature lipid-carrying adipocytes (reviewed by Tang and Lane, 2012). The chain of events leading to terminally differentiated adipocytes is controlled by transcription factor-mediated gene expression. Particularly, proliferator-activated receptor gamma (PPARɣ) and CCAAT/enhancer binding protein alpha (C/EBPα) are considered to be the fundamental transcription factors induced during adipogenesis and are collectively responsible for initiating the adipogenic gene programme (Siersbæk, Nielsen and Mandrup, 2010).

In vitro

The use of both primary ASCs and clonal preadipocyte cell lines as experimental models have greatly contributed to the general understanding of adipocyte biology. The 3T3-L1 and 3T3-F442A immortalised preadipocyte cell lines (Green and Kehinde, 1974, 1975, 1976) are the most frequently used laboratory models and have guided the characterisation of the adipocyte differentiation program.

Despite the ease of use of a clonal cell line, it is arguable whether cell lines can be manipulated to accurately reflect an *in vivo* environment, and whether they are therefore physiologically relevant. A recent review article highlights the advantages of using primary ASCs as a superior alternative to immortalised cell lines to study adipocyte differentiation and function *ex vivo* (Sadie-Van Gijsen, 2019). Amongst others, the greatest advantage of using a primary ASC model is that these stem cells can be isolated from subjects that have been exposed to experimental interventions *in vivo*, such as a high-fat diet, and the biology of the cells can be studied *ex vivo*. This application allows researchers to gain a more accurate understanding of the physiological impact of the intervention.

The *in vitro* differentiation of primary ASCs and clonal preadipocytes are generally achieved by subjecting post-confluent cells to a hormone-based adipogenic cocktail containing mainly insulin, isobutylmethylxanthine (IBMX) and dexamethasone (Rubin *et al.*, 1978). The degree of adipocyte differentiation can be verified through standard Oil Red O (ORO) staining (Ramírez-Zacarías, Castro-Muñozledo and Kuri-Harcuch, 1992) of the intracellular lipid droplets.

2.1.4. Adipogenic memory

Epigenetic changes refer to modifications to the DNA sequence without altering the sequence itself, resulting in the expression or silencing of specific genes under certain conditions. Andersen and colleagues demonstrated that ASCs are susceptible to epigenetic reprogramming by factors present in their extracellular environment *in vivo* (Andersen *et al.*, 2019), and this phenomenon is supported

by other studies (Nilsson *et al.*, 2014; Rønningen *et al.*, 2015). For example, long term exposure to obesity and type II diabetes can alter the differentiation potential and metabolic activities of these adipocyte precursors. Andersen *et al*. (2019) have demonstrated this when primary ASCs harvested from type II diabetic obese individuals displayed altered differentiation capacity and insulin signalling *in vitro*. This finding suggests that ASCs are not only susceptible to epigenetic modification in response to their environment, but also retain an adipogenic memory of their *in vivo* milieu. This memory of an obese and type II diabetic environment therefore persists when isolated ASCs are differentiated into mature adipocytes in culture.

2.1.5. Obesity and the metabolic syndrome

Even though WAT is necessary to maintain systemic energy and hormonal homeostasis, it has been implicated as a major risk factor for metabolic disease. The commencement of the industrial revolution has facilitated a shift from nutrient deprivation to nutrient excess, which, in combination with other lifestyle factors, has given rise to what is now known as the modern-day obesity epidemic (Caballero, 2007). This epidemic no longer pertains to wealthy Western counties exclusively, but has also started to infiltrate poorer developing countries (Prentice, 2006; Caballero, 2007). By definition, obesity refers to the pathological excess of WAT to a health-threatening extent (James, 2004) and is the central causal risk factor of the metabolic syndrome. The metabolic syndrome is a compound condition that is also characterised by insulin resistance, dyslipidaemia and hypertension, which predisposes individuals to the development of type II diabetes and cardiovascular diseases (Eckel, Grundy and Zimmet, 2005) **(*Figure 2.2*)**. However, not all obese individuals are metabolically challenged, and even lean individuals can exhibit obesity-associated metabolic complications. This obesity paradox (Elagizi *et al.*, 2018) suggests that the WAT mass itself is unlikely to contribute to the health risks associated with obesity.

2.1.6. Subcutaneous and visceral adiposity

The risk of developing obesity-associated diseases relates to the distribution of adiposity rather than total adiposity (Ibrahim, 2009), but the exact mechanism remains a point of discussion. As a result, various hypotheses exist on how excessive adiposity leads to systemic metabolic complications. The most renowned hypothesis is that of limited WAT expandability. WAT can accumulate in two distinct anatomical regions, namely the subcutaneous (superficial to the skin) and visceral (in and around abdominal organs) compartments. The subcutaneous fat depot serves as the normal physiological storehouse for excess energy that accompanies a high-caloric diet. Adipocytes residing in this depot act as metabolic sinks that store surplus FFAs and glycerol as triglycerides (Ibrahim, 2009). In times of chronic nutrient overconsumption, as observed in overweight and obese individuals, subcutaneous

adipocytes respond by increasing in amount (hyperplasia) and size (hypertrophy) to compensate for the additional lipids present in circulation. Once these adipocytes have reached their maximum expansion capacity, a phenomenon known as lipid "spill over" (dyslipidaemia) occurs and excess circulating FFAs are shunted to the liver, kidneys, skeletal muscle, heart and pancreas and stored ectopically as visceral fat. This ectopic deposition of lipids in and around other peripheral tissues that are not equipped for fat storage consequently leads to metabolic defects, such as insulin resistance (Virtue and Vidal-Puig, 2010). Visceral obesity, in particular, is therefore implicated as the central component in the pathogenesis of the metabolic syndrome **(*Figure 2.2*)**.

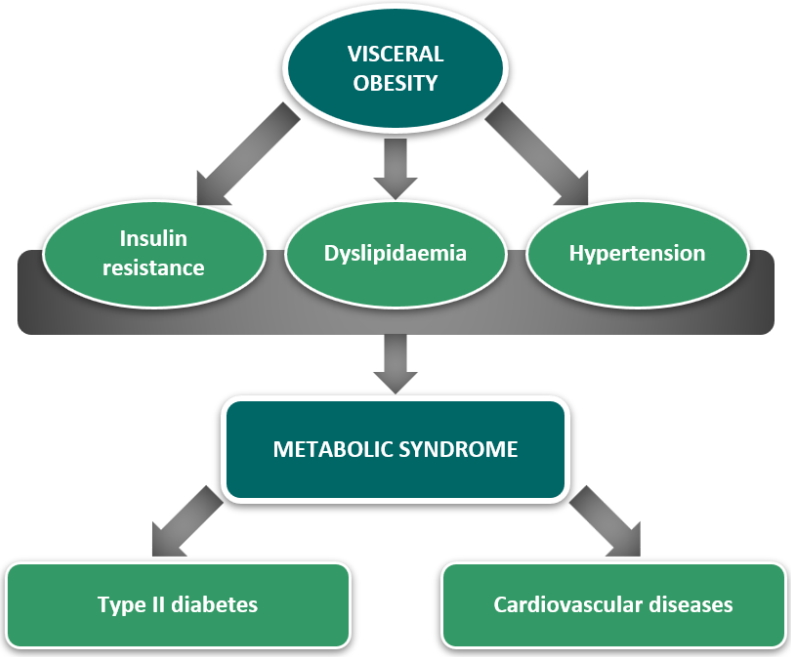

Figure 2.2: Visceral obesity and its relationship to the metabolic syndrome.

Visceral obesity is the main driver of insulin resistance, dyslipidaemia and hypertension. The clustering of these complications is termed the metabolic syndrome, which is a risk factor for the development of type II diabetes and cardiovascular diseases. Figure designed in Microsoft PowerPoint Office 365 by the author of the thesis based on content by Virtue and Vidal-Puig (2010).

2.1.7. Adipose tissue secretions in obesity

Owing to its endocrine function, WAT is not only responsible for the release of FFAs into circulation, but also the secretion of various hormones (referred to as adipokines) and inflammatory cytokines. Obesity, especially in the visceral compartment, and its related metabolic abnormalities are strongly associated with a state of chronic systemic inflammation due to the aberrant release of FFAs, adipokines and pro-inflammatory cytokines from WAT (Kershaw and Flier, 2004). Therefore, in addition to anatomical differences, visceral WAT differs from subcutaneous WAT on an endocrinological level in the obese state.

Free fatty acids (FFAs)

Subcutaneous and visceral WAT display differential lipolytic activities. Insulin opposes lipolysis while promoting lipogenesis within adipocytes. Subcutaneous adipocytes are normally highly sensitive, whereas visceral adipocytes are more resistant, to the anti-lipolytic action of insulin. Therefore, the rate of FFA secretion from visceral adipocytes is suggested to be higher compared to that of subcutaneous adipocytes (Arner, 1995).

In obesity, the circulating FFA concentration is increased and contributes to the development of insulin resistance in peripheral organs (Boden, 2008). In short, circulating FFAs that enter non-adipose cells are either oxidised to produce energy or re-esterified as triglycerides. Chronically elevated levels of circulating FFAs overwhelms the cell's ability to use or store the FFAs, resulting in the accumulation of intracellular triglycerides and metabolites of the re-esterification process. These intermediates contribute to the production of reactive oxygen species (ROS) and consequent oxidative stress, which attenuates insulin signalling and renders the cell insulin resistant.

Studies (Wajchenberg, 2000; Bjørndal *et al.*, 2011) have highlighted a positive correlation between visceral WAT and circulating FFAs in obesity, thereby assuming that visceral adipocytes contribute to systemic FFA levels to a greater degree compared to subcutaneous adipocytes. This may not be the case as the majority of circulating FFAs seem to originate from the abdominal subcutaneous WAT as opposed to visceral WAT in obese individuals (Jensen, 2006), despite a higher lipolytic rate in the visceral depot. This finding focuses attention on the deranged behaviour of subcutaneous adipocytes in the obese condition, which is often overlooked.

Lastly, the plasma composition of dietary FFAs also influences widespread insulin sensitivity. More specifically, saturated FFAs have been found to induce peripheral insulin resistance in rats, whereas the addition of unsaturated FFAs restored insulin sensitivity (Storlien *et al.*, 1991). Studies in humans (Vessby, Tengblad and Lithell, 1994; Hekmatdoost *et al.*, 2011) have corroborated this pattern where increased insulin resistance was strongly associated with increased serum concentrations of saturated FFAs, especially palmitic acid. Lovejoy and colleagues investigated the effects of saturated, unsaturated, and trans FFA-enriched diets on healthy lean and obese individuals (Lovejoy *et al.*, 2002). The authors observed no association between dietary FFA composition and insulin sensitivity in lean subjects, but overweight subjects had a higher propensity for developing insulin resistance while consuming a diet high in saturated FFAs. This suggests that the effect of dietary circulating FFAs on insulin sensitivity might be dependent on the degree of obesity.

Adipokines

WAT also displays differential secretion of adipokines in obesity and related metabolic conditions. Elevated circulating levels of monocyte chemoattractant protein-1 [MCP-1; a macrophage-recruiting hormone] (Takahashi *et al.*, 2003), plasminogen activator inhibitor-1 [PAI-1; an anti-fibrinolytic glycoprotein] (Landin *et al.*, 1990), acylation-stimulating protein [ASP; a lipid storage protein] (Cianflone, Xia and Chen, 2003), resistin [a molecule induced during adipogenesis] (Steppan *et al.*, 2001) and leptin [an insulin-responsive hormone with levels proportional to the amount of WAT] (Considine *et al.*, 1996) correlate with obesity and the development of insulin resistance and type II diabetes. Conversely, reduced circulating levels of adiponectin [a hormone involved in the regulation of nutrient metabolism] is associated with the development of systemic insulin resistance (Weyer *et al.*, 2001).

Pro-inflammatory cytokines

The expression of tumour necrosis factor-α (TNF-α), a pro-inflammatory cytokine secreted by WAT, is markedly elevated in the WAT of obese animals (Hotamisligil, Shargill and Spiegelman, 1993) and humans (Hotamisligil *et al.*, 1995) compared to their lean counterparts, which strongly correlates with peripheral insulin resistance. When comparing TNF-α expression between the two fat depots, studies have shown that TNF-α expression was higher in subcutaneous WAT compared to visceral WAT, but disagreed whether this was in a body mass index (BMI)-dependent (Fain *et al.*, 2004) or -independent (Winkler *et al.*, 2003) manner. Although expressed in subcutaneous WAT, no TNF-α was found to be secreted from this depot in obese individuals (Mohamed-Ali *et al.*, 1997), suggesting that expression does not necessarily correlate with secretion. Lastly, Tsigo and colleagues reported that circulating TNF-α levels were significantly increased in obese individuals with visceral adiposity compared to obese individuals with subcutaneous adiposity (Tsigos *et al.*, 1999), suggesting that WAT distribution affects TNF-α secretion.

Interleukin-6 (IL-6), another pro-inflammatory cytokine secreted by WAT, is also elevated in obesity and has been shown to be secreted at a higher concentration by visceral WAT compared to subcutaneous WAT (Fried, Bunkin and Greenberg, 1998; Fain *et al.*, 2004). The same pattern (visceral > subcutaneous) was observed when adipocytes were isolated from both WAT depots, however these secretions only accounted for approximately 10% of the total IL-6 released from WAT (Fried, Bunkin and Greenberg, 1998).

It is important to note that adipocytes themselves are responsible for only a small percentage of the circulating pro-inflammatory cytokines released from WAT. As WAT expands during obesity, adipocytes employ a local inflammatory response that recruits immune cells, such as macrophages.

These immune cells, in turn, are responsible for the release of the majority of pro-inflammatory cytokines that give rise to the systemic inflammatory profile associated with obesity (Weisberg *et al.*, 2003).

2.1.8. Role of macrophages in obesity

In the obese state, WAT itself becomes insulin resistant and inflamed, which is associated with increased pro-inflammatory macrophage infiltration and activation (Weisberg *et al.*, 2003). Briefly, due to the potent anti-lipolytic action of insulin, insulin resistant hypertrophic adipocytes secrete increased levels of FFAs and MCP-1 into circulation. The latter recruits macrophages to the WAT, where they are directly activated by the elevated FFA levels. Active macrophages express and secrete pro-inflammatory cytokines, which in turn suppress adipogenesis. Since the affected adipocytes are unable to increase in number the cells further increase in size, promoting the continuation of a vicious cycle (for full review, see Virtue and Vidal-Puig, 2010) **(*Figure 2.3*)**.

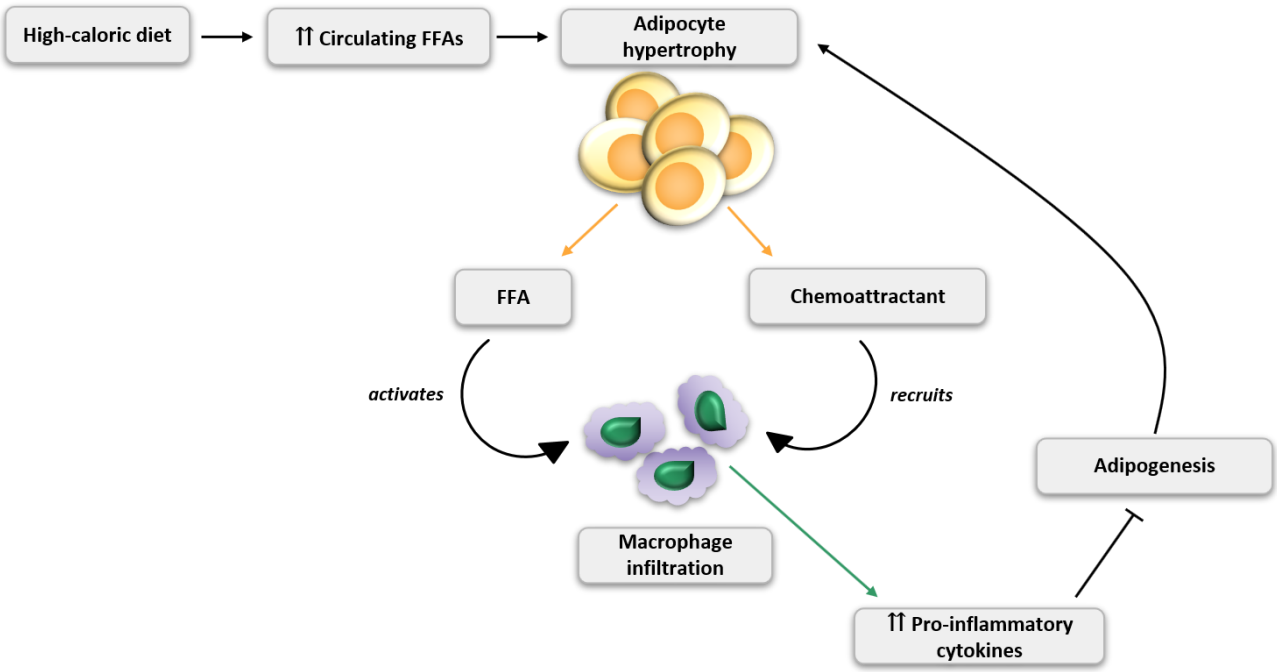

Figure 2.3: Adipocyte hypertrophy and macrophage infiltration during obesity.

During obesity, a high-caloric diet leads to chronically elevated levels of circulating FFAs, which leads to adipose expansion by means of adipocyte hypertrophy. In the insulin resistant individual, the hypertrophic adipocytes are insensitive to the anti-lipolytic action of insulin, resulting in an increase in FFA and MCP-1 secretion. Macrophages are recruited by the circulating MCP-1 to the WAT, where they are activated by the secreted FFAs. Active macrophages secrete pro-inflammatory cytokines that inhibit adipogenesis and drives adipocyte hypertrophy even further. Figure designed in Microsoft PowerPoint Office 365 by the author of the thesis based on content by Virtue and Vidal-Puig (2010).

It has been suggested that hypertrophic adipocytes, rather than hyperplasic adipocytes, are typically more pathological because of their association with increased macrophage infiltration and insulin resistance (Skurk *et al.*, 2007). As *in vivo* adipocytes reside in a collagenous matrix, it is necessary for the matrix to remodel to allow for hypertrophy to occur. Therefore, enlarged adipocytes are likely to experience pressure exerted by the rigid matrix causing them to rupture, leading to an increase in lipid release and subsequent macrophage activation (reviewed by Virtue and Vidal-Puig, 2010).

Taken together, visceral and subcutaneous WAT have unique diet-dependent metabolisms, which are responsible for generating differential secretory profiles that might distinctively affect peripheral organ metabolism. In addition, the role of macrophages and adipocyte hypertrophy play important roles in mediating local WAT and wide-spread systemic inflammation.

2.2. The heart

2.2.1. Cardiomyocyte energy metabolism

The contracting heart is the most energy-intensive organ in the body due to its constant mechanical activity. To meet its high energy requirements, cardiomyocytes are metabolically geared to utilise a variety of fuel substrates, such as carbohydrates and lipids, in order to sustain its continuous need for energy production. Therefore, the myocardial metabolism of these two macronutrients is of particular importance for proper cardiac function.

Glucose

Circulating glucose molecules can only enter cardiomyocytes through facilitative transmembrane glucose transporters (GLUTs). GLUT1 is the constitutively expressed isoform responsible for basal glucose uptake, and GLUT4 is the predominant isoform responsible for the majority of glucose uptake into the adult cardiomyocyte. In the unstimulated cardiomyocyte, the GLUT4 transporters reside within cytoplasmic vesicles. The two major stimuli that induce the translocation of these vesicles to the sarcolemma, are insulin and cellular contraction. The role of insulin and the protein signalling pathway resulting in GLUT4-mediated glucose uptake have been extensively described in literature (Bryant, Govers and James, 2002; Thong, Dugani and Klip, 2005; Chanda, Luiken and Glatz, 2016). In the fed state, increased circulating glucose levels stimulate the secretion of insulin from the pancreas. Insulin binds to the insulin receptor situated in the sarcolemma of cardiomyocytes, resulting in the autophosphorylation of the receptor's tyrosine residues. IRS-1 and phosphatidylinositol 3-kinase (PI3K) are subsequently recruited and phosphorylated, respectively. The latter catalyses the conversion of phosphatidylinositol (4,5)P2 to phosphatidylinositol (3,4,5)P3 [PIP2 → PIP3], which in turn stimulates the phosphorylation of PKB by means of the intermediary kinases,

phosphoinositide-dependent kinase-1 (PDK1) and mTORC2. Akt substrate of 160 kDa (AS160) is a down-stream target of activated PKB and is responsible for initiating the translocation of GLUT4 vesicles to the sarcolemma. Once inserted, GLUT4 facilitates the uptake of extracellular glucose molecules into the cardiomyocyte. AS160 is also activated through contraction, however this activation is suggested to be at least partially mediated by AMPK (Schwenk *et al.*, 2008).

The breakdown of intracellular glucose for ATP production consists of two major processes (reviewed by Chanda, Luiken and Glatz, 2016). The first, glycolysis, occurs in the cytoplasm where glucose molecules are converted to pyruvate through a series of reactions catalysed by various enzymes. Glycolysis can commence under anaerobic conditions, however, it is responsible for merely 10% of the net ATP generated within a healthy heart. The second, glucose oxidation, occurs in the mitochondria where the product of the first process, pyruvate, is further metabolised. Unlike glycolysis, glucose oxidation requires oxygen and contributes to the majority of glucose-derived ATP production **(*Figure 2.4)***.

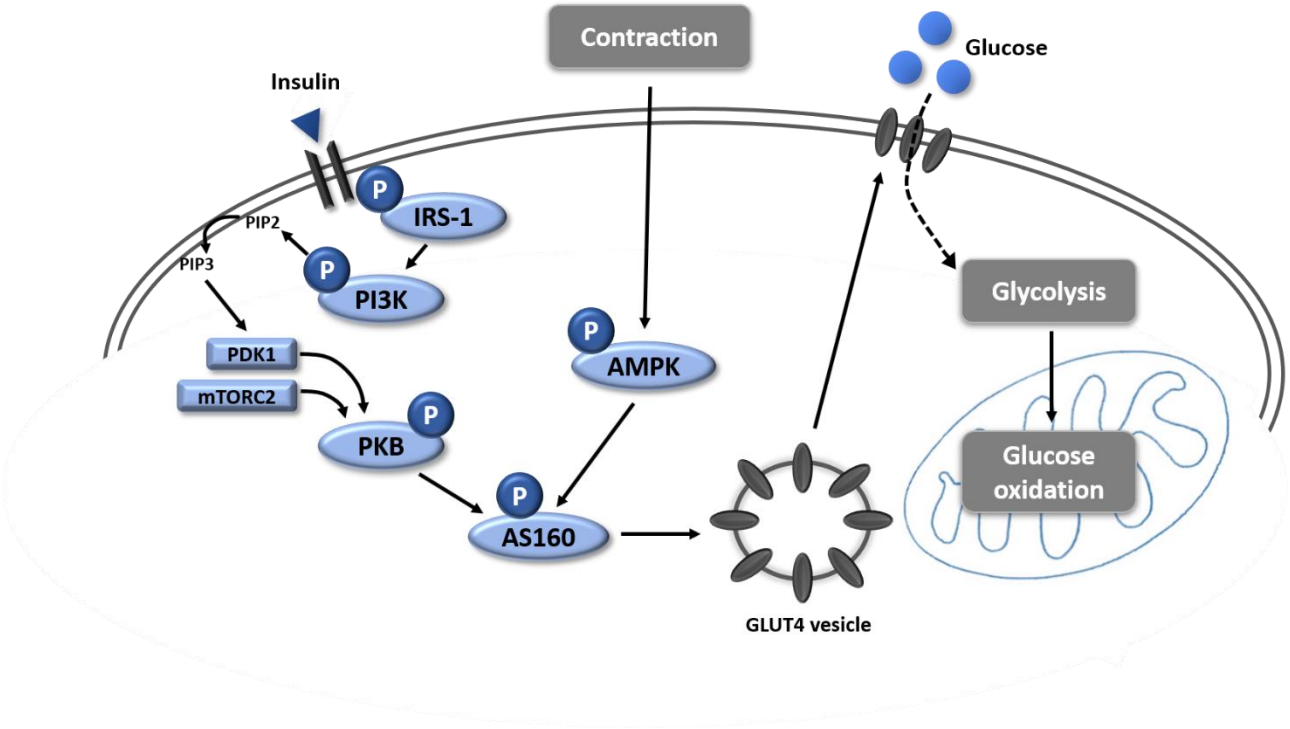

Figure 2.4: Cardiomyocyte glucose metabolism.

In the fed state, insulin binds to its transmembrane receptor and triggers an intracellular phosphorylation cascade. IRS-1 phosphorylation leads to PI3K phosphorylation, which converts PIP2 to PIP3. PIP3, together with PDK1 and mTORC2, stimulate PKB phosphorylation and the subsequent AS160-mediated translocation of GLUT4 vesicles to the sarcolemma for glucose uptake. Intracellular glucose molecules are metabolised through glycolysis (cytoplasm) and oxidation (mitochondria) for energy. Alternatively, AS160 is activated by contraction, possibly by means of AMPK. Figure designed in Microsoft PowerPoint Office 365 by the author of the thesis.

Fatty acids

The utilisation of glucose for ATP generation, however, is not favoured under normal aerobic conditions. Rather, the myocardium switches to and preferentially metabolises FFAs to meet its energy needs (Hue and Taegtmeyer, 2009). In fact, approximately 60-70% of the total ATP required for sufficient myocardial contraction under steady state conditions is obtained through mitochondrial FFA β-oxidation (Van Der Vusse, Van Bilsen and Glatz, 2000).

Initially, circulating FFAs bound to either plasma albumin or lipoproteins are liberated in order to transverse the cardiomyocyte sarcolemma. This crossing is facilitated by plasmalemmal fatty acid-binding proteins ($FABP_{pm}$) and cluster of differentiation 36 (CD36, also known as fatty acid translocase; FAT) (Van Der Vusse, Van Bilsen and Glatz, 2000). Similar to GLUT4, CD36 reside within intracellular vesicles that are shuttled between the cytoplasm and the sarcolemma. This recruitment of CD36 is also stimulated by both the insulin-dependent PKB pathway and the contraction-induced AMPK pathway that converge onto AS160 (Steinbusch *et al.*, 2011).

Once inside the cytoplasm, the FFAs are bound to cardiac-specific fatty acid-binding proteins (FABPs) and converted to long-chain acyl-CoA moieties by the acyl-CoA synthase enzyme. These moieties are shuttled to the mitochondrial matrix by an enzymatic complex consisting of carnitine palmitoyltransferase 1 (CPT1), carnitine:acyl carnitine translocase, and carnitine palmitoyltransferase 2 (CPT2). Here, the long-chain acyl-CoA enters the β-oxidation system where a series of enzymes shorten the moiety during each successive cycle to produce ATP (reviewed by Lopaschuk *et al.*, 2010) **(*Figure 2.5*)**.

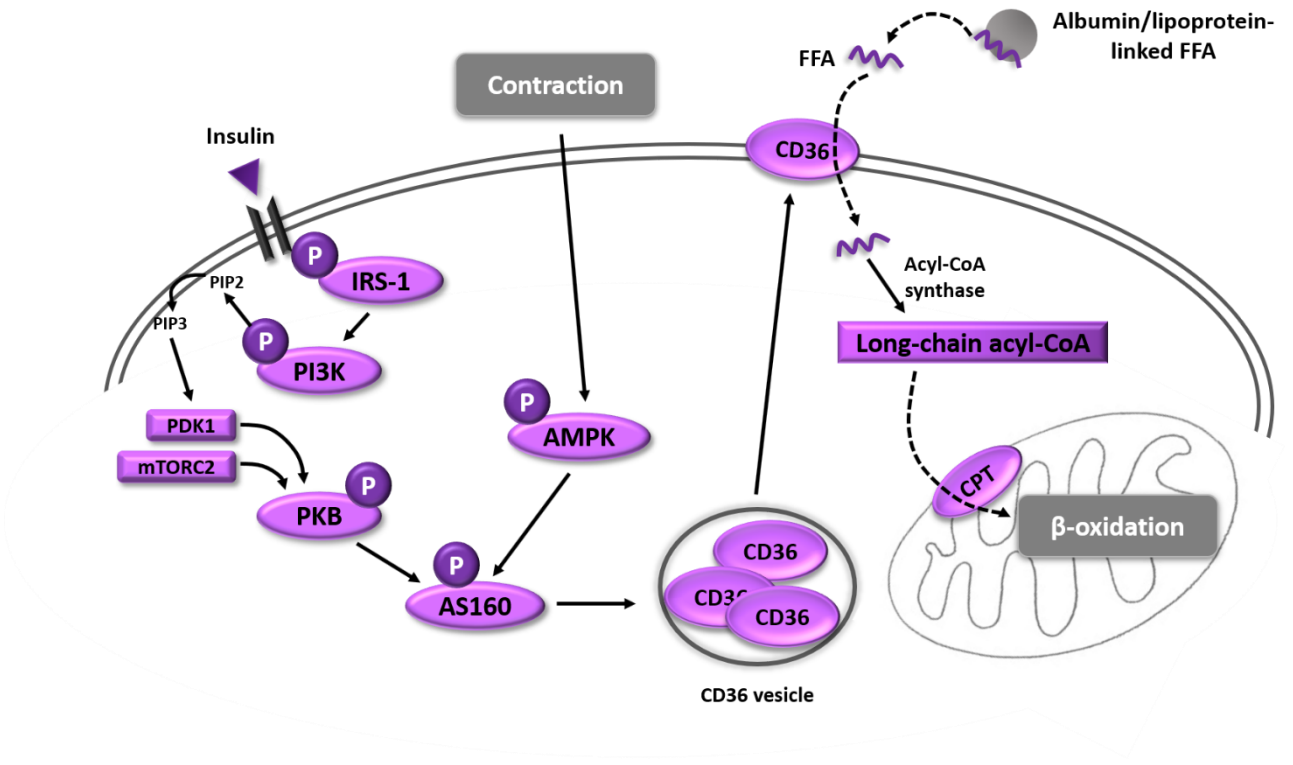

Figure 2.5: Cardiomyocyte fatty acid metabolism.

In the fed state, insulin binds to its transmembrane receptor and triggers an intracellular phosphorylation cascade. IRS-1 phosphorylation leads to PI3K phosphorylation, which converts PIP2 to PIP3. PIP3, together with PDK1 and mTORC2, stimulate PKB phosphorylation and the subsequent AS160-mediated translocation of CD36 vesicles to the sarcolemma for albumin/lipoprotein-linked FFA uptake. Intracellular FFAs are enzymatically converted to long-chain acyl-CoA, which are shuttled into the mitochondria by the CPT complex. The long-chain acyl-CoA moieties are metabolised through β-oxidation for energy. Alternatively, AS160 is activated by contraction, possibly by means of AMPK. Figure designed in Microsoft PowerPoint Office 365 by the author of the thesis.

Taken together, a wide variety of ATP-producing mechanisms are available to the heart under normal conditions, highlighting its metabolic flexibility in order to meet its continuous energetic need.

2.2.2. Metabolic consequences of obesity

Chronically dysregulated nutrient metabolism in the heart and the progression to myocardial dysfunction are closely associated with obesity. Although similar pathways are responsible for GLUT4-facilitated glucose uptake and CD36-facilitated FFA uptake into cardiomyocytes, differences in their subcellular trafficking machinery allows for an imbalance in substrate utilisation in metabolic diseases (Steinbusch *et al.*, 2011). An early metabolic maladaptation observed in the hearts of the obese and insulin resistant is the permanent recruitment of CD36 to the cardiomyocyte sarcolemma, together with the internalisation of GLUT4. This inverse presence of the nutrient transporters means that FFA uptake into cardiomyocytes far outweighs that of glucose. The sarcolemmal amount of CD36 strongly correlates with FFA uptake and intramyocardial triacylglycerol content, while

inversely correlating with insulin-mediated GLUT4 translocation and subsequent glucose uptake. The preferential uptake of FFAs at the expense of glucose, together with the limited oxidative capacity of the mitochondria, result in an intracellular accumulation of lipid metabolites such as ceramide and diacylglycerol (DAG), which contribute to the development of myocardial lipotoxicity and insulin resistance (Schwenk *et al.*, 2008; Steinbusch *et al.*, 2011).

Another metabolic consequence of obesity is oxidative stress due to excessive mitochondrial ROS production. ROS are highly destructive, short-lived molecules that readily reacts with surrounding molecules. The production of basal levels of ROS is an unavoidable consequence of mitochondrial ATP generation. Fortunately, low levels of ROS are metabolically necessary for the regulation of cell signalling, differentiation and proliferation (Hamanaka and Chandel, 2011). Due to the limited capacity of cardiomyocytes to store intracellular FFAs as triglycerides (Unger, Zhou and Orci, 1999), exposure to excess circulating lipids, as is the case in obesity, drives mitochondrial ROS production. When increased ROS production exceeds the level needed for normal physiological processes to the extent where it overwhelms the intracellular antioxidant systems, cardiomyocytes experience oxidative stress due to ROS-induced damage to cellular components. In severe cases, uncontrollable ROS production can ultimately lead to cell death by apoptosis (Ott *et al.*, 2007). Therefore, chronic oxidative stress is an underlying feature of obesity and its related metabolic complications (Roberts and Sindhu, 2009; Marseglia *et al.*, 2015).

2.3. Ataxia-telangiectasia mutated (ATM)

2.3.1. Introduction to ATM

Ataxia-telangiectasia (A-T) is a rare genetic disorder that presents with two hallmark clinical features: uncoordinated movements (ataxia) and dilated oculocutaneous blood vessels (telangiectasia). This debilitating disease is further characterised by several other abnormalities, including cerebellar degeneration, accelerated aging, immune defects, ischaemic heart disease, insulin resistance, type II diabetes and cancer development (Rothblum-Oviatt *et al.*, 2016). The discovery of the origin of the A-T disorder, which results due to mutations occurring throughout the *Ataxia-telangiectasia mutated* (*Atm*) gene (Savitsky *et al.*, 1995), led to the identification of the encoded protein known as Ataxia-telangiectasia mutated (ATM). ATM is a relatively large (350 kDa) serine/threonine protein kinase that forms part of the phosphatidylinositol 3-kinase-related protein kinase (PIKK) family. Some genetic mutations can lead to a reduction in expressed functional protein, whereas others can result in normal amounts of protein with decreased functionality (Lavin *et al.*, 2004).

Once autophosphorylated at serine 1981 (ser1981), nuclear ATM dimers convert to active monomers that orchestrate the signalling network responsible for the repair of double-stranded deoxyribonucleic acid (DNA) breaks, highlighting its crucial role in the prevention of cancer development. Its functional contribution to this defensive mechanism has been well documented (Banin *et al.*, 1998; Canman *et al.*, 1998; Cortez *et al.*, 1999; Pandita *et al.*, 2000; Bakkenist and Kastan, 2003). More recently, the identification of metabolic disturbances among A-T patients, such as type II diabetes and cardiovascular disease (reviewed by Espach *et al.*, 2015), suggests additional functions and has directed research into the metabolic role of ATM in the cytoplasm.

2.3.2. ATM and glucose homeostasis

Insulin-dependent signalling

ATM is an insulin-responsive protein kinase that contributes to glucose metabolism (Yang and Kastan, 2000), however its exact position within the insulin signalling pathway remains controversial **(*Figure 2.6*)**. Depending on the cell type and metabolism, ATM may function either in a PKB-dependent manner, or otherwise independently of PKB at the level of AS160. Viniegra and colleagues showed that ATM is required for the full activation of PKB in Cos and HEK 293T cells, both of which are kidney-derived cell lines (Viniegra *et al.*, 2005). In mouse L6 myotubes, Halaby and colleagues confirmed that ATM is essential for full PKB activation upon insulin stimulation through inhibition of ATM with the ATM-specific inhibitor, KU55933 (Halaby *et al.*, 2008). Similarly, a reduction in insulin-stimulated PKB phosphorylation was noted following treatment of C2C12 (mouse myoblast cell line) cells with KU55933 (Jeong *et al.*, 2010) and in extensor digitorum longus (EDL) muscle tissue from ATM knock-down mice (Ching *et al.*, 2013). Based on these studies, ATM acts as an upstream regulator of PKB in the insulin signalling pathway.

On the other hand, ATM has also been shown to act down-stream of PKB at the level of AS160. Contradicting the findings in the mouse EDL tissue, the soleus tissue of ATM knock-down mice revealed no interruption in PKB phosphorylation upon insulin stimulation, however the phosphorylation of AS160 failed to occur (Ching *et al.*, 2013). This contradiction might be due to differences in muscle metabolism as EDL cells mainly utilise glycolysis and soleus cells mainly utilise oxidative phosphorylation. Conclusions by Jeong *et al.* (2010) verifies this finding when only a reduction in AS160 phosphorylation, and not PKB phosphorylation, was observed in mouse soleus tissue exposed to the KU55933 ATM-inhibitor. The authors further investigated the effect of KU55933 on mouse L6 myotubes and found only AS160 phosphorylation to be reduced, contradicting the findings of Halaby and colleagues (2008).

Regardless of the position of ATM relative to PKB and AS160, the insulin signalling pathway ultimately promotes GLUT4-mediated glucose uptake into the cell, protein synthesis, and cellular growth, while inhibiting protein degradation through autophagy.

Lastly, a recent study showed that ATM activity contributes to glucose homeostasis at the level of GLUT4 by promoting its insulin-mediated translocation to the plasma membrane, while preventing its lysosomal degradation (Cheng *et al.*, 2020). In the cerebral cortex of *Atm* knock-down mice, no differences were observed in general GLUT4 mRNA or protein levels, however GLUT4 levels within isolated lysosomes were significantly increased. Furthermore, wild-type cortical neurons exposed to the ATM-specific inhibitor, KU60019, displayed markedly increased levels of lysosome-associated GLUT4, as well as reduced insulin-mediated GLUT4 translocation to the plasma membrane. These results confirm that ATM-deficiency impedes GLUT4 translocation to the cell membrane by diverting it to the lysosomes for degradation, which ultimately limits cellular glucose uptake ability.

Insulin-independent signalling

ATM has also been shown to play a role in insulin-independent glucose homeostasis **(*Figure 2.6*)**. GLUT1 contains an ATM-specific phosphorylation site (ser490) within its carboxy terminal (Matsuoka *et al.*, 2007), which regulates the cellular localisation and activity of the insulin-independent glucose transporter (Wiemand *et al.*, 2009). This suggests that ATM may play a regulatory role in basal glucose uptake. Interestingly, ATM inhibition reduced GLUT1 localisation to the cell membrane and decreased GLUT1-mediated glucose uptake by nearly 50% in L6 myotubes due to decreased phosphorylation of its ser490 residue. Conversely, ATM activation increased the cell membrane localisation of GLUT1 and the subsequent GLUT1-mediated glucose uptake (Andrisse *et al.*, 2013), confirming the role of ATM in basal glucose homeostasis.

ATM also activates the PKB-mTORC1-S6K pathway in response to insulin-like growth factor 1 (IGF-1) in skeletal muscle, independent of IRS-1 (Ching *et al.*, 2013). C2C12 cells expressing ATM-targeting short hairpin RNA (shRNA), or treated with KU55933 for acute ATM inhibition, and soleus muscle from $Atm^{+/-}$ mice exposed to IGF-1 showed reduced phosphorylation of PKB, mTORC1 and S6K, but not IRS-1. This data indicates that ATM plays a role in insulin-independent glucose homeostasis by participating in IGF-1 signalling, although the exact mechanisms of ATM autophosphorylation in response to IGF-1 binding, and the down-stream phosphorylation of PKB, remain unclear.

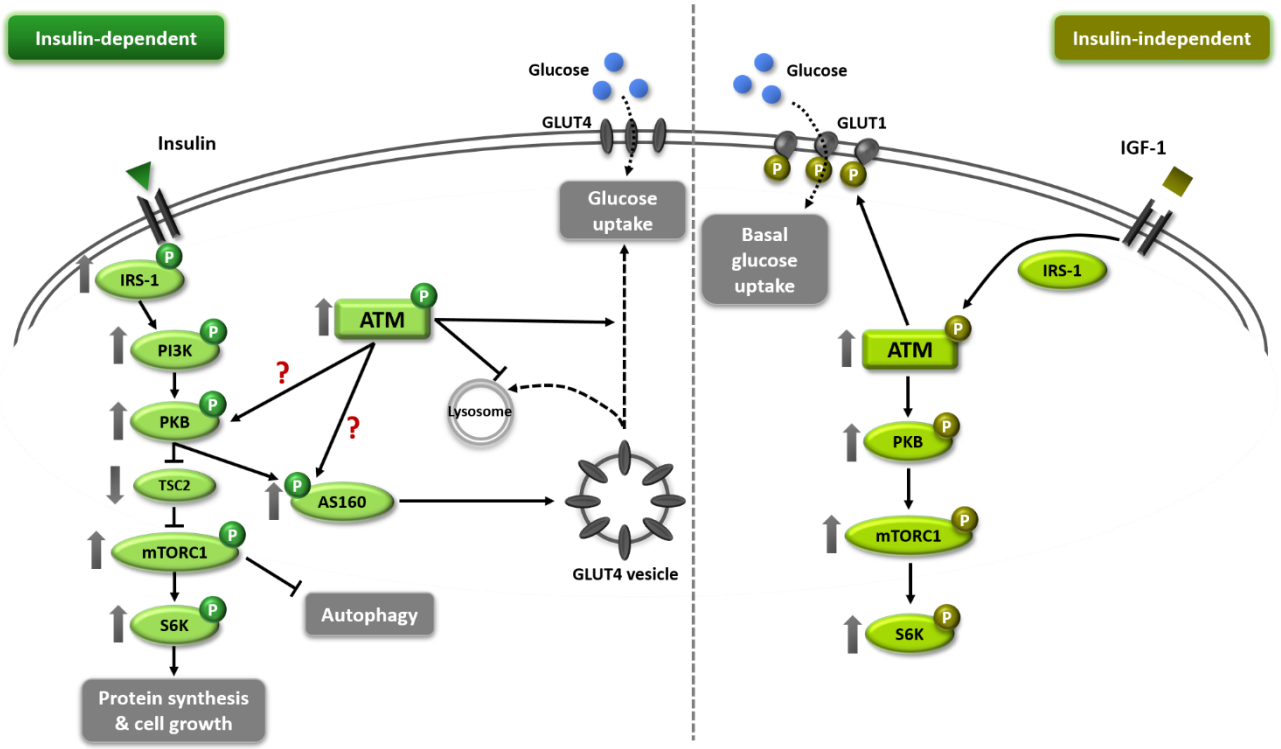

Figure 2.6: ATM participates in insulin-dependent and -independent glucose homeostasis.

ATM participates in insulin-dependent glucose homeostasis: insulin binds to its transmembrane receptor and triggers an intracellular phosphorylation cascade that promotes AS160/GLUT4-mediated glucose uptake and mTORC1/S6K-mediated protein synthesis and cell growth, while inhibiting autophagy. However, it remains unclear whether ATM functions up-stream of PKB, or down-stream of PKB at the level of AS160. In addition, ATM participates in insulin-independent glucose homeostasis: ATM activates the PKB-mTORC1-S6K pathway, independent of IRS-1, in response to IGF-1. Furthermore, ATM phosphorylates GLUT1 at a specific site to promote its localisation to the plasma membrane, thereby regulating basal glucose uptake. Figure designed in Microsoft PowerPoint Office 365 by the author of the thesis.

2.3.3. ATM and redox homeostasis

Another important metabolic function of ATM is its ability to regulate intracellular redox homeostasis in response to oxidative stress, independently of DNA damage **(*Figure 2.7*)**. ATM is directly activated by ROS in the cytoplasm through a mechanism that differs from that of nuclear ATM by double-stranded DNA damage. Instead of monomerization occurring, oxidation by ROS results in the formation of active ATM dimers bound together with intermolecular disulphide bonds between various cysteine (cys) residues, especially cys2991 (Guo *et al.*, 2010).

Once oxidised by ROS, ATM activates the liver kinase B1 (LKB1)/AMPK pathway, resulting in the activation of both tuberous sclerosis complex 2 (TSC2) and unc-51-like kinase 1 (ULK1). TSC2 inhibits mTORC1 to allow the activation of ULK1 and the induction of autophagy (Alexander *et al.*, 2010; Zhang *et al.*, 2015). ROS-activated ATM also directs the selective degradation of peroxisomes through autophagy, a process termed pexophagy. Peroxisomes are metabolic organelles that

participate in the break-down of long-chain fatty acids through β-oxidation, generating ROS as a by-product. Zhang and colleagues demonstrated that ATM is localised to the peroxisome by binding to PEX5, a peroxisome import receptor. ROS-activated ATM phosphorylates PEX5 at ser141, which promotes PEX5 ubiquitination and its subsequent recognition by the autophagy adaptor protein, p62. Finally, the autophagosome is directed to the peroxisome by p62 for pexophagy to occur (Zhang *et al.*, 2015).

In addition, ROS-activated ATM aids in antioxidant defence against oxidative stress by enhancing glucose-6-phosphate dehydrogenase (G6PD) activity within the pentose phosphate pathway (PPP) to produce nicotinamide adenine dinucleotide phosphate hydrogen (NADPH), an important antioxidant co-factor (Cosentino, Grieco and Costanzo, 2011; Zhang *et al.*, 2018).

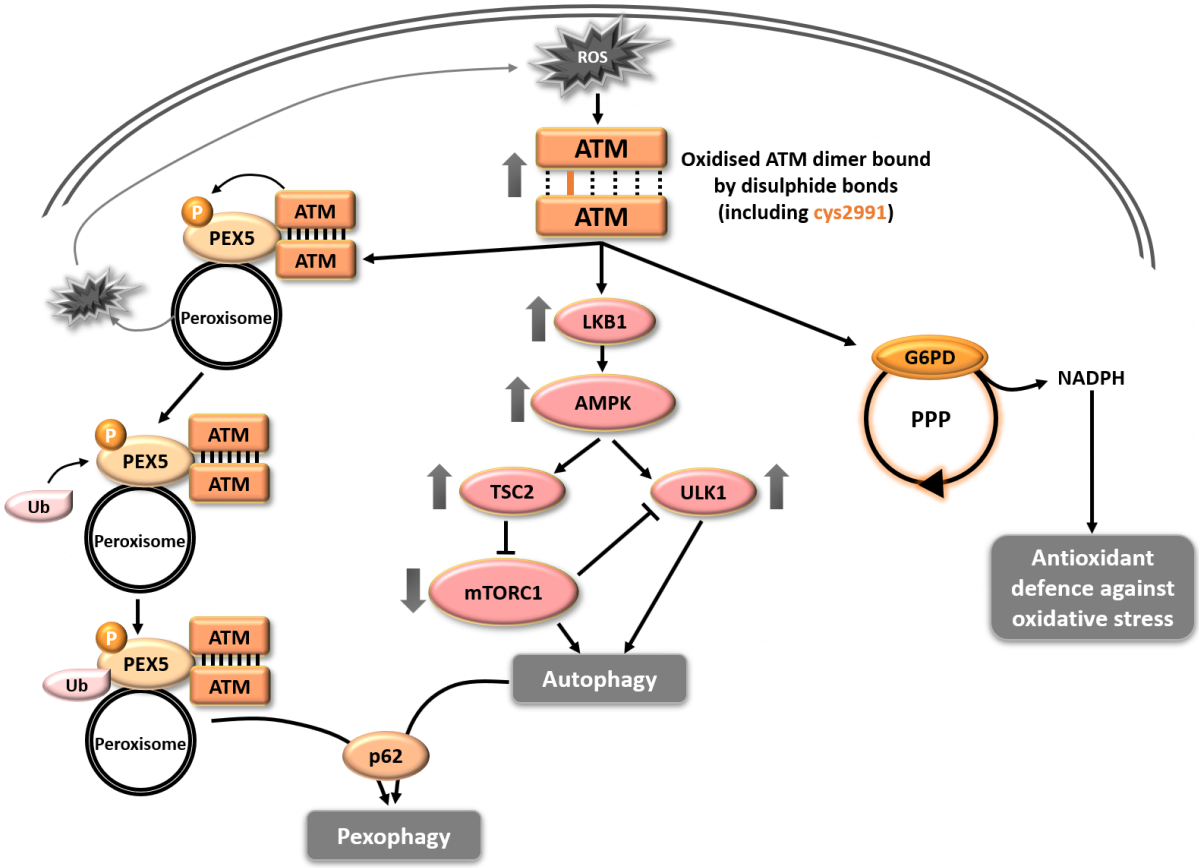

Figure 2.7: ATM participates in redox homeostasis.

ATM is directly activated by ROS. Once oxidised, inactive ATM monomers form active dimers that are bound together by disulphide bonds between various cys residues, especially cys2991. ATM promotes the LKB1/AMPK pathway, which inhibits mTORC1 and activates ULK1 to induce autophagy. ROS-activated ATM also localises to peroxisomes by binding to and phosphorylating PEX5, promoting PEX5 ubiquitination and its subsequent recognition by p62. The latter event directs the autophagosome to the peroxisome for pexophagy. Furthermore, ROS-activated ATM activates G6PD, an enzyme within the PPP, for the production of the antioxidant co-factor, NADPH. Figure designed in Microsoft PowerPoint Office 365 by the author of the thesis.

2.3.4. ATM and the metabolic syndrome

Due to the prominent involvement of ATM in both insulin and ROS signalling networks, it is possible that ATM-deficiency or -dysfunction is central to the development of the metabolic syndrome, a compound disease associated with systemic insulin resistance and oxidative stress. Indeed, various studies have highlighted associations between decreased ATM and key features of the metabolic syndrome.

Reduced ATM protein levels have been linked with obesity and insulin resistance. Halaby *et al.* (2008) were able to show that ATM levels were significantly reduced in the skeletal muscle tissue of high-fat diet-induced insulin resistant rats compared to lean control rats. The authors therefore suggested that decreased ATM contributes to the development of insulin resistance in obesity. Similar results were observed in the cardiac tissue of high-fat fed rats (Huisamen *et al.*, 2016).

ATM-deficiency has further been linked with the development of various other components of the metabolic syndrome. An extensive study by Schneider and colleagues revealed that $Atm^{-/-}ApoE^{-/-}$ mice on a high-fat diet developed abdominal adiposity, hypertension, glucose intolerance, insulin resistance and accelerated atherosclerosis compared to $Atm^{+/+}ApoE^{-/-}$ mice (Schneider *et al.*, 2006). The authors concluded that ATM-deficiency might be a possible contributing mechanism to the development of the metabolic syndrome in obesity. Interestingly, similar studies (Wu *et al.*, 2005; Mercer *et al.*, 2010) showed that even heterozygous $Atm^{+/-}ApoE^{-/-}$ mice on a high-fat diet developed the metabolic features described by Schneider and colleagues (2006), suggesting that ATM haploinsufficiency is sufficient for the development of obesity-related metabolic complications.

A recent comprehensive review article by Wingard and colleagues discussed the parallel nature of the cardiometabolic abnormalities associated with ATM-deficiency and that of diabetic cardiomyopathy (Wingard *et al.*, 2020). While the authors touch on several interesting connection points, only two of these will be mentioned here. Firstly, cardiac ATM expression is increased in response to β-adrenergic receptor (β-AR) stimulation (Foster *et al.*, 2011). Once stimulated by norepinephrine, a catecholamine associated with sympathetic activity, the β-AR modulates heart rate and myocardial contractility. This suggests a role for ATM in the sympathetic response of the heart. The β-AR has been implicated in cardiomyopathy and is down-regulated in heart failure (Wachter and Gilbert, 2012), thereby also implying that decreased ATM may play a role in heart failure development. In fact, ATM-deficiency has been associated with cardiac remodelling (Foster *et al.*, 2012), a key feature of heart failure. And secondly, type II diabetes associates with reduced cardiac angiogenesis (blood vessel formation), which could greatly contribute to the development of related ischaemic heart disease (Costa and Soares, 2013). Similarly, ATM-deficiency as a result of

heterozygous mutations in the *Atm* gene is associated with the development of ischaemic heart disease (Su and Swift, 2000), which could allude to a role for ATM in angiogenesis.

Lastly, ATM-deficiency has been linked with abnormal adipose tissue deposition, altered adipocyte metabolism and impaired adipocyte differentiation (Takagi *et al.*, 2015). *Atm*$^{-/-}$ mice displayed decreased subcutaneous fat accumulation, increased visceral fat accumulation, and reduced serum levels of adiponectin and leptin compared to their wild-type counterparts, suggesting defective adipocyte functioning in the absence of ATM. Furthermore, *in vitro* experiments with *Atm*$^{-/-}$ mouse embryonic fibroblasts (MEFs) confirmed that ATM is necessary for the initiation of the adipocyte differentiation program through the induction of C/EBPα and PPARγ. Based on this novel role for ATM in adipogenesis, ATM-deficiency may be partly responsible for the adipose-related abnormalities observed in obesity, and subsequently the metabolic syndrome.

2.4. MicroRNAs (miRNAs)

2.3.1. Overview of the central dogma

In 1958, Francis Crick famously explained the relation between the three central macromolecules of genetic information, namely DNA, ribonucleic acid (RNA) and proteins, to construct what is known as the central dogma of molecular biology (Crick, 1958). In the simplest form, the dogma states that the genetic message encoded within DNA is transcribed to messenger RNA (mRNA), which is subsequently translated into a functional protein **(*Figure 2.8*)**. Therefore, mRNA plays an important intermediary role within the process of protein synthesis. The simplicity of this process, however, can be misleading as it is, in actual fact, a more complex dynamic with many checkpoints governed by several regulatory mechanisms to ensure proper function. One such mechanism includes RNA interference through small RNAs (Morange, 2009), known as microRNAs (miRNAs).

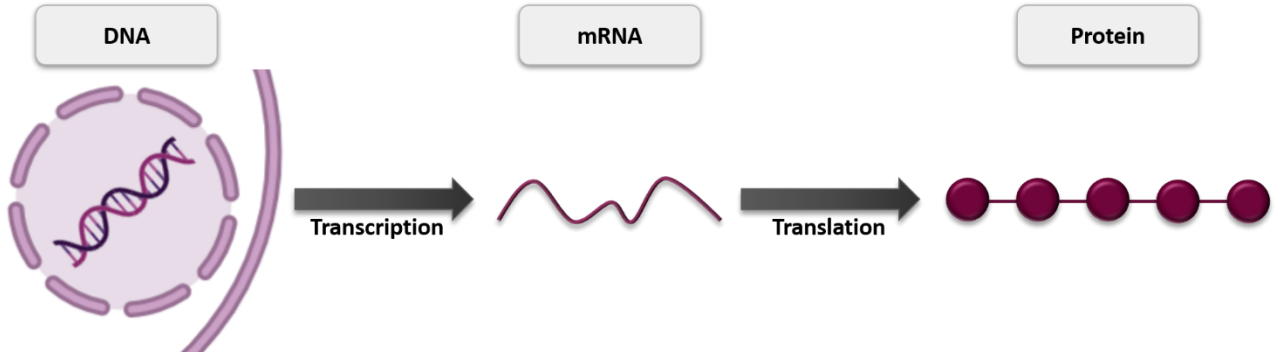

Figure 2.8: The central dogma of molecular biology.

The central dogma of molecular biology states that DNA is transcribed to mRNA, which is translated into protein. Figure designed in Microsoft PowerPoint Office 365 by the author of the thesis based on content from Crick (1958).

2.3.2. miRNA biology

MicroRNAs are short segments (approximately 22 nucleotides in length) of non-coding RNA that play a fundamental role in regulating cellular gene expression, predominantly on a post-transcriptional level, in response to environmental changes. These endogenous RNAs represent an abundant group of gene-governing molecules that have been conserved across evolution, emphasising their important biological role (O'Brien *et al.*, 2018).

miRNA biogenesis

MicroRNA biogenesis is a complex, multi-step process involving an initial nuclear processing phase, followed by a cytoplasmic processing phase (Lee *et al.*, 2002) **(*Figure 2.9*)**. Briefly, depending on a cell's need, specific miRNA genes are transcribed by the RNA polymerase II (pol II) enzyme to produce stem-loop transcripts known as primary miRNA (pri-miRNA). A protein complex consisting of Drosha and DiGeorge syndrome critical region in gene 8 (DGCR8) is responsible for cleaving the pri-miRNA to generate 60-70 nucleotide hairpin intermediates known as precursor miRNA (pre-miRNA). The original pri-miRNA contains the mature miRNA sequence in the arm-portion of the stem-loop structure, which remains conserved in the arm of the pre-miRNA intermediate. To allow for further maturation, the pre-miRNA is recognized by the nuclear transport receptor exportin-5 (EXP5) and subsequently transported to the cytoplasm through a protein pore inserted within the nuclear membrane (Lei and Silver, 2002). Once inside the cytoplasm, the pre-miRNA is further cleaved into a ~22 nucleotide double-stranded miRNA (ds-miRNA) molecule with a forward strand (5'→ 3'; miRNA-5p) and a reverse strand (3' → 5'; miRNA-3p) by the highly specific Dicer enzyme (Park *et al.*, 2011). One strand of the miRNA duplex is generally degraded, whereas the remaining strand (guide miRNA) is integrated into a gene silencing effector complex known as the RNA-induced silencing complex (RISC; Maniataki and Mourelatos, 2005).

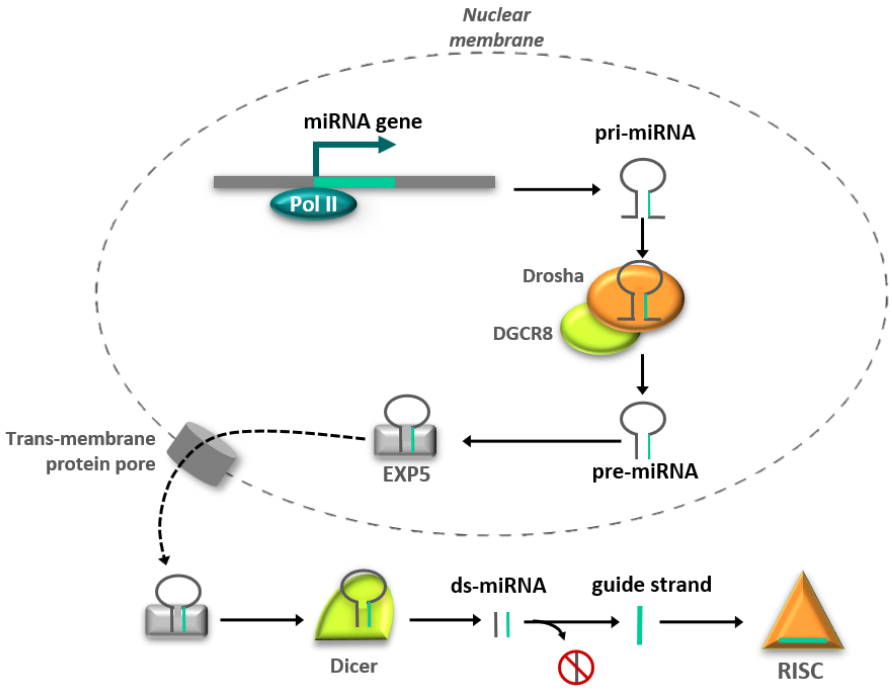

Figure 2.9: The biogenesis of miRNAs.

Nuclear processing of miRNA biogenesis: a specific miRNA gene is transcribed by the RNA pol II enzyme into a pri-miRNA transcript. The DGCR8-complex cleaves the pri-miRNA to produce a pre-miRNA intermediate, which contains the mature miRNA sequence in the arm-portion. Cytoplasmic processing of miRNA biogenesis: the pre-miRNA is exported by EXP5 to the cytoplasm, where it is cleaved into a ds-miRNA molecule by Dicer. One strand is typically discarded, while the remaining (guide) strand is incorporated into RISC for gene silencing. Figure designed in Microsoft PowerPoint Office 365 by the author of the thesis.

miRNA function

MicroRNAs were described for the first time in 1993 in the context of developmental timing in the nematode *Caenorhabditis elegans* with the discovery of *lin-4* miRNA (Lee, Feinbaum and Ambros, 1993; Wightman, Ha and Ruvkun, 1993). However, it was not until 2001 (Lagos-Quintana *et al.*, 2001; Lau *et al.*, 2001; Lee and Ambros, 2001) that the profound role of miRNAs in various physiological processes were realised. Essentially, miRNAs influence protein-coding gene outputs by targeting specific expression messages for silencing. Once incorporated within RISC, the guide miRNA directs the complex to its corresponding target mRNA transcript, which is subsequently silenced through either cleavage or insufficient translation. The choice of repression mechanism depends on the degree of complementarity between the guide miRNA and the binding site sequence in the 3'-untranslated region (UTR) of its target mRNA (Bartel, 2004). Perfectly matched base pairing will result in endonucleolytic cleavage, which occurs at a discrete position near the centre of the overlapping area. In the case of partial complementarity, the translation of the target mRNA will be disrupted. Regardless of the repression mechanism, miRNAs typically guarantee the precision of gene

expression to ensure that the appropriate proteins are synthesised. As such, miRNAs play an integral role as biological regulators in various cellular processes such as proliferation, differentiation, developmental timing and programmed cell death (Ambros, 2004).

Organisms constantly face fluctuations in their environment, such as changes in temperature and limited nutrient availability. Modern humans, on the other hand, face opposite challenges of nutrient excess and lack of physical exercise. When presented with such challenging external conditions, it is critical for cells to regain internal homeostasis in order to survive. In an effort to do so, the cell can implement various stress-associated mechanisms to modulate miRNA activity in response to certain environmental cues (Leung and Sharp, 2010). For example, hypoxia-inducible factor (HIF) has been shown to direct the transcription of miRNA-26a, -107 and -210 in response to limited oxygen (Kulshreshtha *et al.*, 2006). Another example includes the activation of the transcription factor and tumour suppressor, p53. Various studies (Chang *et al.*, 2007; He *et al.*, 2007; Raver-Shapira *et al.*, 2007) have shown that p53-mediated expression of miRNA-34 can occur in response to DNA damage to ultimately prevent cancer development. Therefore, the miRNA transcriptome can be adapted by stress-induced factors to determine the proteins that will be available in the cell under a given stress condition. When the system is unable to counteract a certain stress state, homeostasis is compromised, resulting in disease development such as cancer, diabetes and cardiovascular disease (Leung and Sharp, 2010).

2.3.3. miRNAs in disease

By understanding the physiological role of miRNAs in tailoring the intracellular protein levels in response to a fluctuating environment, we can begin to understand the adversity associated with miRNA dysfunction. As previously mentioned, miRNAs mostly assist with the cell's response to physiologic and pathophysiologic stresses (Leung and Sharp, 2010). This function has been verified through knock-down studies, which concluded that the inhibition of individual miRNAs resulted in aberrant responses to various stress conditions (reviewed by Mendell and Olson, 2012). This forecasts the involvement of abnormally behaving miRNAs in the development of disease.

Cancer

One of the earliest indications of miRNA involvement in a pathological setting derived from studies performed in cancer cells (reviewed by Mendell and Olson, 2012). The initial study that provided evidence for associating miRNAs with cancer development in humans found that miRNA-15 and miRNA-16 are down-regulated in most chronic lymphocytic leukaemia patients (Calin *et al.*, 2002). Following this discovery, the aberrant expression of specific miRNAs has also been implicated in other cancer types (Calin and Croce, 2006), suggesting that cancerous tissue exhibit an altered

miRNA expression profile compared to non-cancerous tissue. This differential expression of miRNAs allows for the creation of distinct miRNA signatures that can be used as biomarkers for diagnostic and prognostic purposes in almost all human malignancies (Calin and Croce, 2006).

Metabolic disease

Likewise, unique miRNA profiles have been identified as potential biomarkers for various metabolic disorders. For example, various miRNAs, some that have been linked with maintaining nutrient homeostasis and some whose functions remain to be established, are differentially expressed in the liver, WAT and skeletal muscle of obese and diabetic animal models compared to their healthy control counterparts (extensively reviewed by Guay *et al.*, 2011). Additionally, miRNAs that originate from non-vascular cells are detected in the blood stream. Profiling of these circulating miRNAs can provide insights into the pathophysiological state of an individual and is currently being considered as potential biomarkers for diagnosing and tracking the disease progression of type II diabetes (Sebastiani *et al.*, 2017; Vaishya, Sarwade and Seshadri, 2018).

2.3.4. miRNA-mediated regulation of ATM

With ATM emerging as a central protein kinase in various cell signalling networks, it is curious that the regulation of its protein levels through miRNA-mediated inhibition has not yet been extensively investigated. Studies in various cancer types established that ATM protein levels are negatively regulated by miRNA-18a (Song *et al.*, 2011; Shen and Houghton, 2013; Wu *et al.*, 2013) and miRNA-421 (Hu *et al.*, 2010; Shen and Houghton, 2013) through posttranscriptional suppression. Shen and Houghton (2013) further demonstrated that these ATM-suppressing miRNAs are upregulated by the PKB-mTORC1-S6K pathway. Therefore, ATM is susceptible to posttranscriptional regulation through an insulin-responsive mechanism in a cancer context, however studies investigating its regulation in a metabolic context are lacking. Even though no direct association has yet been made, there are four miRNAs that have been implicated in metabolic diseases known to be linked with abnormal ATM function **(*Figure 2.10*)**.

Latouche and colleagues performed a series of *in vivo* and *in vitro* experiments to highlight an association between type II diabetes and miRNA-194 levels in skeletal muscle (Latouche *et al.*, 2016). Firstly, miRNA-194 levels were significantly reduced in the skeletal muscle tissue of patients with pre- and established type II diabetes compared to healthy individuals. Secondly, the same phenomenon was observed in the insulin resistant offspring of high-fat fed rats. Lastly, the inhibition of miRNA-194 in L6 myotubes resulted in an increase in insulin-stimulated PKB phosphorylation, glucose uptake and subsequent glucose metabolism. Based on the *in vivo* human and rodent findings, the authors concluded that miRNA-194 is likely regulated during the progression of early insulin

resistance (pre-diabetes) to established type II diabetes. Based on the *in vitro* study, the authors suggested that the involvement of miRNA-194 in various stages of PKB-dependent glucose metabolism might be the reason for its down-regulation in pre-diabetic patients as an adaptive mechanism to the onslaught of insulin resistance. Interestingly, another study identified four significantly increased circulating miRNAs in the sera of patients with metabolic syndrome that progressed to the development of type II diabetes compared to healthy individuals, with miRNA-194 being one of the four. Serum levels of miRNA-194 were also elevated in diabetic mice compared to control mice, highlighting miRNA-194 as a potential predictive biomarker for diabetic disease progression (Jaeger *et al.*, 2018).

Another miRNA that has been linked to the progression of type II diabetes, and suggested as a potential biomarker thereof, is miRNA-210. Ghai and colleagues observed significantly elevated miRNA-210 levels in the sera of pre-diabetic patients who developed type II diabetes compared to pre-diabetic patients who did not (Ghai *et al.*, 2019). This increase was further found to be exacerbated by obesity. In a quest to investigate the role of miRNA-210 in the cellular response to hypoxia, a different research group (Mutharasan *et al.*, 2011) was able to show that PKB increased the induction of miRNA-210 in hypoxic cardiomyoblasts. Although this mechanism has been described in a hypoxic context, with obesity being a chronic hypoxic state, a link between PKB and the regulation of intracellular miRNA-210 levels has been established. The authors further found that overexpression of miRNA-210 in hypoxic cardiomyoblasts appeared to be cardioprotective in response to oxidative stress as it reduced mitochondrial ROS production and cell death.

Min and colleagues highlighted an association between increased miRNA-322 (murine orthologue of human miRNA-424) and the development of obesity-associated insulin resistance in the liver (Min, Yang and Lee, 2018). HepG2 cells treated with a saturated FFA (palmitate) and liver tissue from high-fat diet-induced obese mice displayed elevated miRNA-424/322 levels and impaired insulin signalling. This occurred as a result of decreased expression of the insulin receptor, suggesting that saturated FFA-induced miRNA-424/322 represses the insulin receptor mRNA. A study by Marchand *et al*. confirms that miRNA-322 targets the insulin receptor mRNA (Marchand *et al.*, 2016). *In vitro* experiments with rat vascular smooth muscle cells showed that overexpression of miRNA-322 resulted not only in decreased insulin receptor levels, but also in a significant reduction of insulin-stimulated PKB phosphorylation and subsequent glucose uptake. The authors also reported that miRNA-322 is highly expressed in the cardiac tissue of mice. Interestingly, these animal studies revealed that high-fat fed mice displayed cardiac dysfunction with no changes in miRNA-322 levels compared to control mice, however age-matched *ob/ob* mice exhibited no cardiac dysfunction with markedly elevated levels of miRNA-322 compared to control mice. The authors speculated that

increased miRNA-322 expression could potentially protect the heart against cardiac damage associated with a high-fat diet.

Lastly, reduced expression of miRNA-181b have been implicated in the development of insulin resistance in adipose-derived endothelial cells of high-fat diet-induced obese mice. Once miRNA-181b levels were restored, an improvement in the insulin sensitivity and glucose metabolism were observed (Sun *et al.*, 2016), suggesting that miRNA-181b might play an important role in the regulation of the insulin signalling pathway. Decreased miRNA-181b levels have also been observed in the arterial plaques of *ApoE*$^{-/-}$ rats fed a high-fat diet. Notch1, a transmembrane receptor involved in angiogenesis, was found to be a direct target of miRNA-181b and was therefore up-regulated in these plaques. The authors suggested that this inverse relationship between miRNA-181b and Notch1 might constitute a protective mechanism against the development of obesity-induced atherosclerosis (Sun *et al.*, 2019).

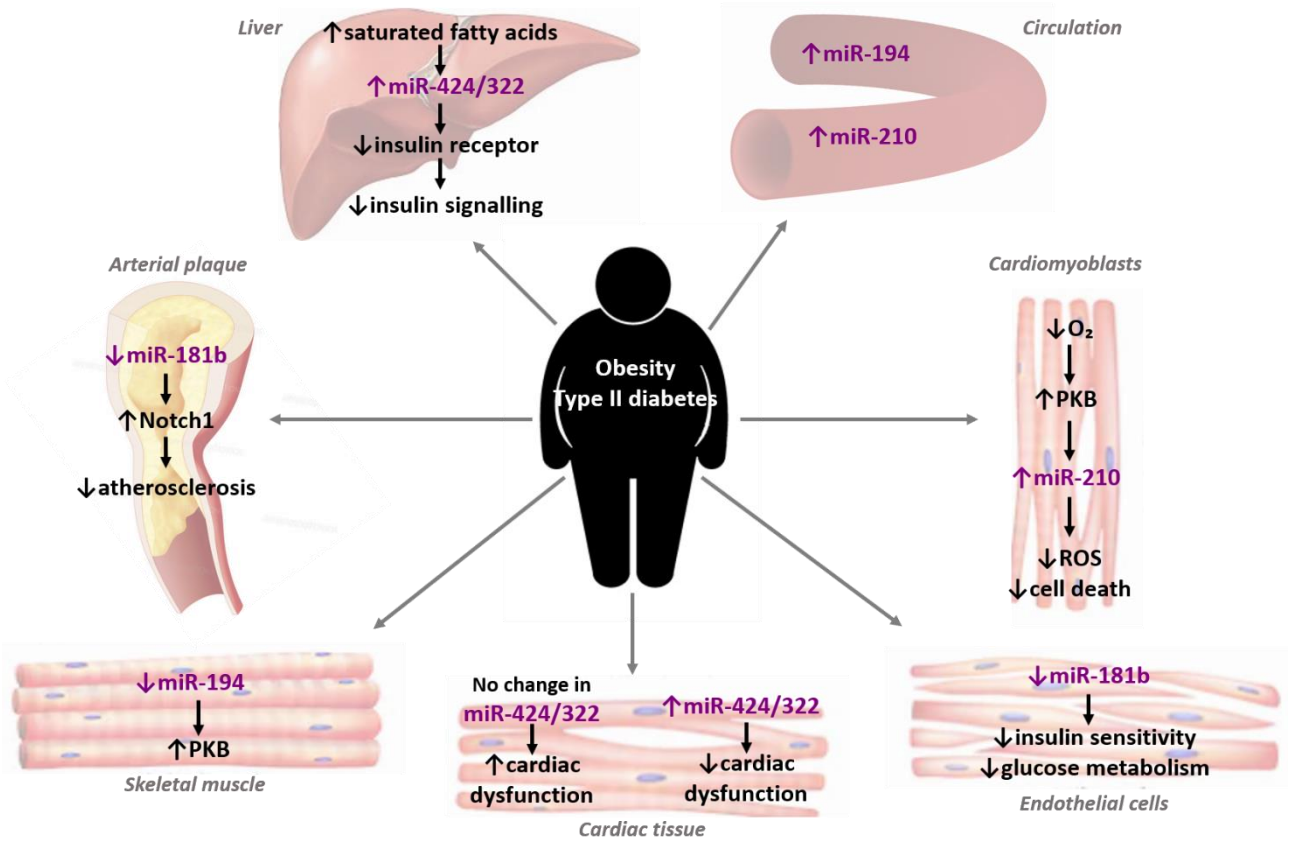

Figure 2.10: Differential expression of four miRNAs have been implicated in obesity and progression to or established type II diabetes in various tissue and cell types.

Four miRNAs (miR-194, -210, -424/322, and -181b) show differential expression in obesity and related type II diabetes in various tissue and cell types, which have in turn been linked with metabolic abnormalities or, at least, adaptive mechanisms against the development of metabolic abnormalities. Figure designed in Microsoft PowerPoint Office 365 by the author of the thesis.

Taken together, the abnormal behaviour of four miRNAs have been implicated in obesity and related metabolic complications, which have in turn been associated with reduced or deficient ATM protein levels. Therefore, the potential pathological regulation of ATM protein levels by these four miRNAs during obesity needs to be explored.

2.5. Concluding remarks, the main study aim, and study objectives

Obesity constitutes a global health risk and is associated with metabolic derangements in various organs that ultimately lead to the development of diseases such as type II diabetes and cardiovascular dysfunction. As a result, the link between obesity and the establishment of peripheral metabolic malfunction has enjoyed extensive research. Obesity is a complex systemic disease due to the endocrine function of WAT, which becomes altered during obesity progression. Furthermore, it is suggested that the pathology associated with obesity correlates with the accumulation of visceral adiposity, indicating a metabolic distinction between the two fat depots.

An interesting observation that has been observed in obesity and insulin resistance is the reduction in protein levels of ATM, a kinase central to the insulin and redox signalling networks, in peripheral tissue (Halaby *et al.*, 2008; Huisamen *et al.*, 2016). However, the respective effects of subcutaneous and visceral obesity on, as well as the underlying mechanism of, reduced peripheral ATM levels are unknown. Even though a miRNA-mediated mechanism for the suppression of ATM protein levels has been described in cancer cells, studies investigating its posttranscriptional regulation under chronic metabolic stress remain lacking. Therefore, the current study aimed to investigate whether adipocyte secretions influence cardiac ATM protein levels in obesity, as previously observed *in vivo* in our laboratory (Huisamen *et al.*, 2016), potentially through a miRNA-mediated mechanism using an *in vitro* cardiomyoblast model. The objectives of the study are as follow:

Objective 1

To establish a suitable *in vitro* cardiomyoblast model that is metabolically sensitive to the effects of obesity. This objective entails the prolonged exposure of H9c2 cardiomyoblasts to high concentrations of nutrients (glucose and FFAs) and/or insulin to investigate the effects on i) cell viability by means of an MTT assay, ii) the total and phosphorylated levels of metabolic proteins (ATM, PKB, mTORC1, S6K and AMPK) through Western blot analysis, and iii) the expression levels of two miRNAs (miR-421 and miR-18a) that regulate ATM protein levels in cancer cells with quantitative real-time polymerase chain reaction (qRT-PCR). This objective is important to establish whether the obese-simulating treatments can influence metabolic protein expression and miRNA levels in H9c2 cells.

Objective 2

To investigate the basal metabolic protein profiles of adipocytes differentiated from primary ASCs originating from the visceral and subcutaneous fat depots harvested from lean and high-fat diet (HFD) rats. More specifically, the total and phosphorylated levels of several metabolic proteins (ATM, mTORC1, S6K, PKB, AMPK, and ACC) will be analysed through Western blot analysis. This objective is important to shed some light on whether adipocytes originating from two different fat depots (subcutaneous and visceral) and dietary backgrounds (control and HFD) display differential basal metabolic profiles.

Objective 3

To determine the respective effects of subcutaneous and visceral adipocyte secretions, under normal and HFD conditions, on the total and phosphorylated levels of various metabolic proteins (ATM, AMPK, mTORC1 and PKB), as well as the expression levels of six miRNAs (miR-421, miR-18a, miR-194, miR-210, miR-322 and miR-181b) in H9c2 cardiomyoblasts through Western blot analysis and qRT-PCR, respectively. This objective involves the treatment of H9c2 cells with conditioned media (CM) derived from the ASCs and their adipocyte counterparts originating from the subcutaneous and visceral fat depots of control and HFD rats (refer to objective 2), followed by the protein and miRNA quantification analyses. Lastly, the FFA composition of the respective CM will be analysed through gas chromatography-flame ionisation detection (GC-FID) by Dr P. van Jaarsveld at the South African Medical Research Council (SAMRC) to investigate the secretory profiles of the adipose-derived cells.

Chapter 3

Materials and Methods

3.1. Cell culture

This study used H9c2(2-1) cardiomyoblasts, an embryonic rat ventricular-derived cell line (Kimes and Brandt, 1976), as an *in vitro* model to investigate the effects of obesity on cardiac metabolism. The H9c2 cells were generously gifted by the Department of Physiology, Stellenbosch University (originally obtained from the ATCC® CRL-1446™). This cell line was selected for its ease of use and phenotypical homogeneity, which is important for the generation of consistent and reproducible results.

Reagents

H9c2 cells were grown in complete Dulbecco's Modified Eagle Medium (DMEM) growth medium, which consisted of high glucose DMEM (4.5 g/l, Lonza™ BioWhittaker™, 12-604F) supplemented with 10% foetal bovine serum (Capricorn, Biocom Biotech, FBS-GI-12A or Hyclone, SV30160.03) and 1% Penicillin-Streptomycin (Sigma-Aldrich, P4333). A 10x dilution of 2.5% Trypsin from Gibco (15090-046) was used to detach cells from the cell culture plate during passaging. Chemicals used for phosphate-buffered saline (PBS) solution (137 mM NaCl, 2.7 mM KCl, 10 mM Na_2HPO_4, 1.8 mM KH_2PO_4; pH 7.4) were purchased from Sigma-Aldrich and Merck.

Method

H9c2 cardiomyoblasts were cultured in accordance with the ATCC® guidelines in a sterile environment. Freezer cultures (previously prepared with 10% dimethyl sulfoxide and complete DMEM media that were stored in the vapour phase of liquid nitrogen) were thawed and plated in 100 mm culture dishes containing complete growth medium. Live cells were adherent to the surface of the culture dish, therefore no attachment factor was necessary. Adherent cells were allowed to grow in a humidified incubator (Shel Lab CO_2 Incubator) containing 5% carbon dioxide at 37°C. Sub-confluent (80-90%) cells were passaged every third day in a 1:3 ratio. For experimental seeding, cells were washed with pre-heated PBS solution, detached form the culture dish surface using 0.25% Trypsin-PBS, and centrifuged (Heraeus Megafuge 16R centrifuge, Thermo Fisher Scientific) at 92 *xg* at 4°C for 4 minutes. The resulting cell pellets were resuspended in complete growth medium, counted using Trypan-blue for dead cell detection on the Countess™ II Automated Cell Counter (Invitrogen, Thermo Fisher Scientific), and live cells were seeded at the desired concentration (live

cells/ml) into new culture dishes for respective experiments **(*Table 3.1*)**, which will be discussed in more detail in the sections to follow.

Table 3.1: Summary of H9c2 cell experimental seeding concentrations, treatment conditions and subsequent analyses.

	Passage	Seeding concentration (live cells per culture dish)	Culture dish size	Treatment	Technical repeats (individual treatment conditions)	Biological repeats (individual experiments)	Subsequent analysis
A	17	*No cell count performed*	100 mm	Insulin	n=2-3	n=1	Western blot
B	Ranging from 17 to 19	5 to 7.5 x 10^5	100 mm	FFAs, glucose, insulin	n=3	n=3	Western blot
C	Ranging from 17 to 19	1.5 to 3 x 10^5	35 mm	FFAs, glucose, insulin	n=3 (pooled)	n=3	qRT-PCR
D	Ranging from 14 to 18	4.5 x 10^5	100 mm	CM	n=3	n=4 per diet group	Western blot
E	Ranging from 14 to 18	1 x 10^5	35 mm	CM	n=3 (pooled)	n=4 per diet group	qRT-PCR
F	19	2 x 10^4 per well	24-well plate	FFAs, glucose, insulin	n=3	n=1	MTT viability assay

Following seeding, H9c2 cells were allowed to adhere to the culture dish surface for at least 24 hours, where after the complete DMEM media were replaced with the respective treatment media.

3.2. Treatment preparation and administration

The effect of obesity on cardiac metabolism was investigated by exposing H9c2 cells to different treatment conditions in two distinct sets of experiments. Firstly, H9c2 cells were treated with different combinations of high FFAs (palmitic acid and oleic acid), glucose and insulin. Secondly, H9c2 cells were treated with adipose-derived CM.

3.2.1. Free fatty acids (FFAs), glucose and insulin

In order to establish whether H9c2 cells represent an appropriate *in vitro* model to study the metabolic effects of obesity on the heart, we investigated whether the cell line is metabolically sensitive to high concentrations of FFAs (palmitic acid and oleic acid), glucose and/or insulin.

Reagents

The palmitic acid (P0500, lot SLBJ3703V) and oleic acid (O1008, lot 0000032783) were purchased from Sigma-Aldrich. The anhydrous D(+)-glucose (108337, lot K49652937813) and ethanol absolute (107017) were purchased from Merck. The Humulin®R insulin (regular biosynthetic human insulin, Eli Lilly (S.A.) (Pty) Ltd, HI0210) was purchased commercially on prescription.

Method

In an initial optimisation experiment **(*Table 3.1 A*)**, H9c2 cells were treated with complete DMEM media supplemented with 100 nM insulin for 15 minutes (acute exposure) and 24 hours (chronic exposure), respectively.

Alternatively, H9c2 cells were treated with various combinations of nutrients and/or insulin for 24 hours **(*Table 3.1 B*** and ***C*)**. Treatment media consisted of complete DMEM media supplemented with either i) 0.2% ethanol (vehicle control), ii) 0.1 mM palmitic acid and 0.1 mM oleic acid, iii) 0.1 mM palmitic acid, 0.1 mM oleic acid and 5.5 mM glucose (DMEM contains 25 mM glucose; final concentration of 30.5 mM glucose), iv) 100 nM insulin, or v) 100 nM insulin, 0.1 mM palmitic acid and 0.1 mM oleic acid. The treatment duration and concentrations for palmitic acid and oleic acid (Wang *et al.*, 2009; Nobuhara *et al.*, 2013), glucose (Cai *et al.*, 2002; Wang *et al.*, 2009; Hu *et al.*, 2016) and insulin (Ha and Pak, 2005) were based on previous studies and have been optimised in our laboratory. The palmitic acid and oleic acid were dissolved in ethanol in a stock solution of 100 mM, respectively. FFAs oxidise readily, therefore the palmitic acid stock solution was prepared on the day of treatment, whereas aliquots of the oleic acid stock solution were exposed to nitrogen gas to displace the oxygen and stored at -20°C for use on experimental days. FFAs are light-sensitive, therefore care was taken to conceal the stock solutions with aluminium foil. Prior to treatment, the palmitic acid stock was heated to 37°C to ensure proper dissolution, whereas the oleic acid stock aliquot was allowed to thaw to room temperature. The combination of palmitic acid and oleic acid will herewith be referred to as the FFA treatment. Prior to treatment, glucose and insulin were directly dissolved in complete growth medium.

Following the treatment duration, cells were prepared for either Western blotting (protein quantification) or qRT-PCR (miRNA quantification) purposes (detail provided in sections **3.4 Western blot analysis** and **3.5 Total RNA isolation and cDNA synthesis**). To avoid performing these subsequent analyses simultaneously, the qRT-PCR cells were treated 24 hours after seeding, whereas the Western blot cells were treated 48 hours after seeding. An experimental timeline is provided in ***Figure 3.1***.

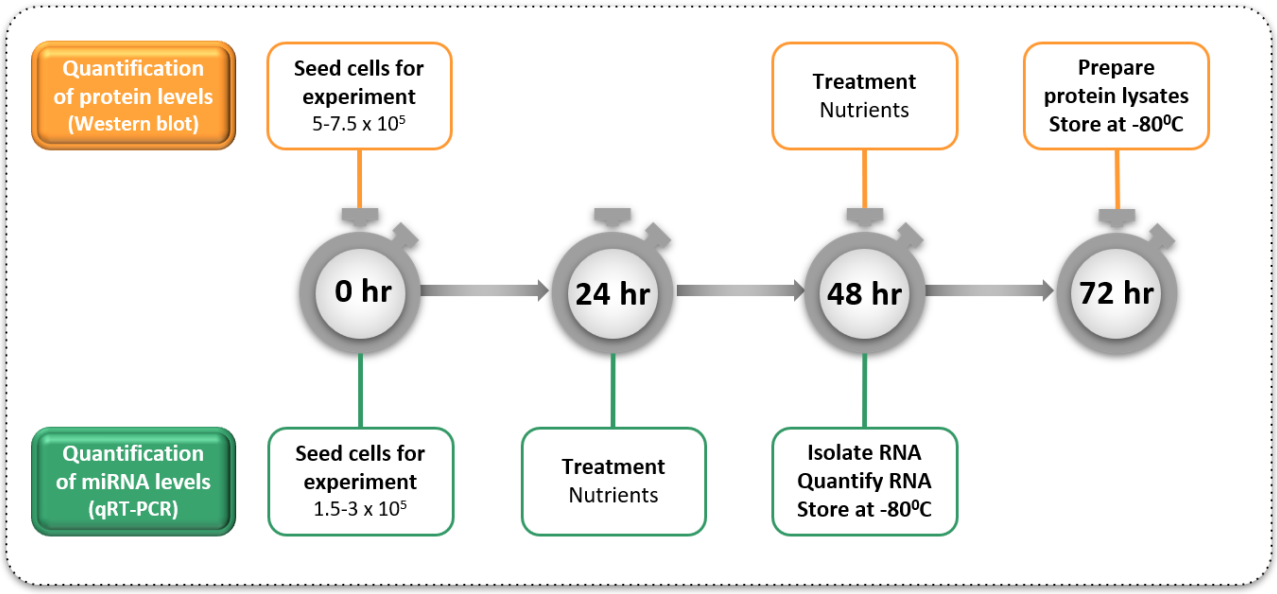

Figure 3.1: Experimental timeline for H9c2 cardiomyoblasts treated with nutrients and/or insulin.

H9c2 cells were treated with complete DMEM media supplemented with either i) 0.1 mM palmitic acid & 0.1 mM oleic acid, ii) 0.1 mM palmitic acid & 0.1 mM oleic acid & 5.5 mM glucose (final concentration of 30.5 mM), iii) 100 nM insulin, or iv) 100 nM insulin & 0.1 mM palmitic acid & 0.1 mM oleic acid for 24 hours and compared to a vehicle control (0.2% ethanol). Following treatment, cells were prepared for Western blotting (protein expression) and qRT-PCR (miRNA expression) analyses, respectively. To avoid conducting these down-stream analyses simultaneously, a staggered approach was followed where the cells intended for qRT-PCR analysis were treated 24 hours after seeding, while cells intended for Western blotting were treated 48 hours after seeding.

3.2.2. Adipose-derived conditioned media (CM)

To further investigate whether H9c2 cells are metabolically sensitive to subcutaneous and visceral adipocyte secretions, respectively, H9c2 cells were exposed to CM derived from adipose cells originating from both fat depots under control and HFD conditions.

The CM used to treat the H9c2 cells **(*Table 3.1 D*** and ***E*)** were derived from ASCs, as well as their differentiated adipocyte counterparts, that were originally harvested from the subcutaneous (SC) and peri-renal (PR; representative of the visceral fat depot) fat depots from control (normal standard chow; n=4) and HFD (n=4) male Wistar rats. For diet compositions, see Appendix A ***Table A1***. Ethical approval was obtained from the Stellenbosch University Research Ethics Committee: Animal Care and Use (ethical clearance number ACU-2018-6786). The feeding and maintenance of the rats, isolation of the ASCs, culturing of the ASCs, and *in vitro* differentiation of the ASCs to adipocytes were conducted by Dr H. Sadie-van Gijsen and is briefly described in Appendix A.

Method

After a subset of the isolated ASCs had been differentiated to mature adipocytes by Dr H. Sadie-van Gijsen (refer to Appendix A), the complete growth media were aspirated from the ASCs (technical n=4) and their differentiated adipocyte counterparts (technical n=4). The cells were washed with pre-heated PBS and fresh complete growth media were placed onto the cells for 24 hours. During this period, the cells were maintained in a humidified incubator containing 5% carbon dioxide at 37°C. Thereafter, the complete growth media, now referred to as CM, were collected. The CM collected from the four technical repeats of ASCs and adipocytes were pooled, respectively, and stored at -80°C for future use i) as treatment for H9c2 cells and ii) for gas chromatography-flame ionisation detection (GC-FID) analysis of the FFA composition. The collection of the CM is summarised in ***Figure 3.2***.

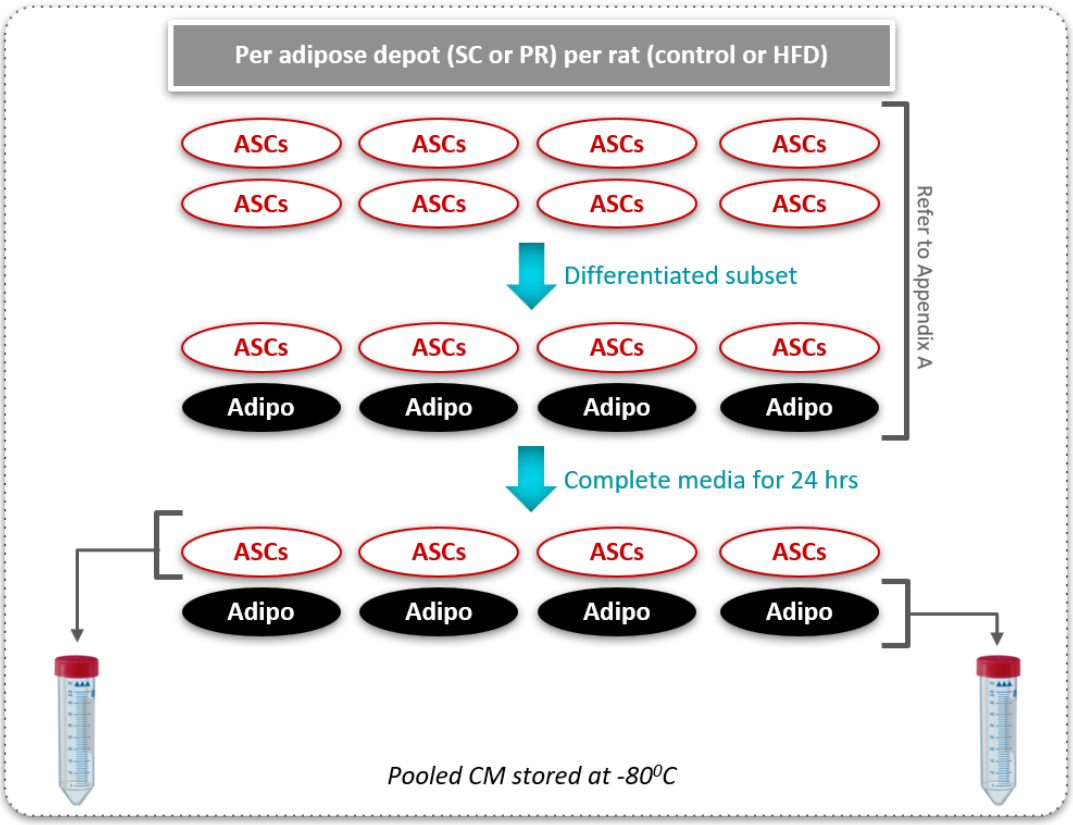

Figure 3.2: Schematic of adipose-derived CM harvested from a particular fat depot (SC and PR) from a particular rat (control and HFD).

50 ml Falcon tubes containing 40 ml each of conditioned medium (CM) harvested from the subcutaneous adipose stem cells (SC ASCs), subcutaneous adipocytes (SC Adipo), peri-renal adipose stem cells (PR ASCs) and peri-renal adipocytes (PR Adipo) were obtained per rat per diet group (control and high-fat) and stored at -80°C.

H9c2 cells were treated with the respective CM for 24 hours. Prior to treatment, the respective CM were thawed and allowed to reach 37°C. To account for the fact that the complete DMEM media from which the CM were derived had already been placed on the ASCs and adipocytes for 24 hours

prior to collection, we included an H9c2 control group that was treated with complete DMEM media 24 hours before the CM were administered to the rest of the H9c2 groups. Similar to the previous set of experiments, the H9c2 cells for qRT-PCR purposes were treated 24 hours after seeding, whereas the H9c2 cells for Western blotting purposes were treated 48 hours after seeding, to avoid performing these subsequent analyses simultaneously. An experimental timeline is provided in ***Figure 3.3***.

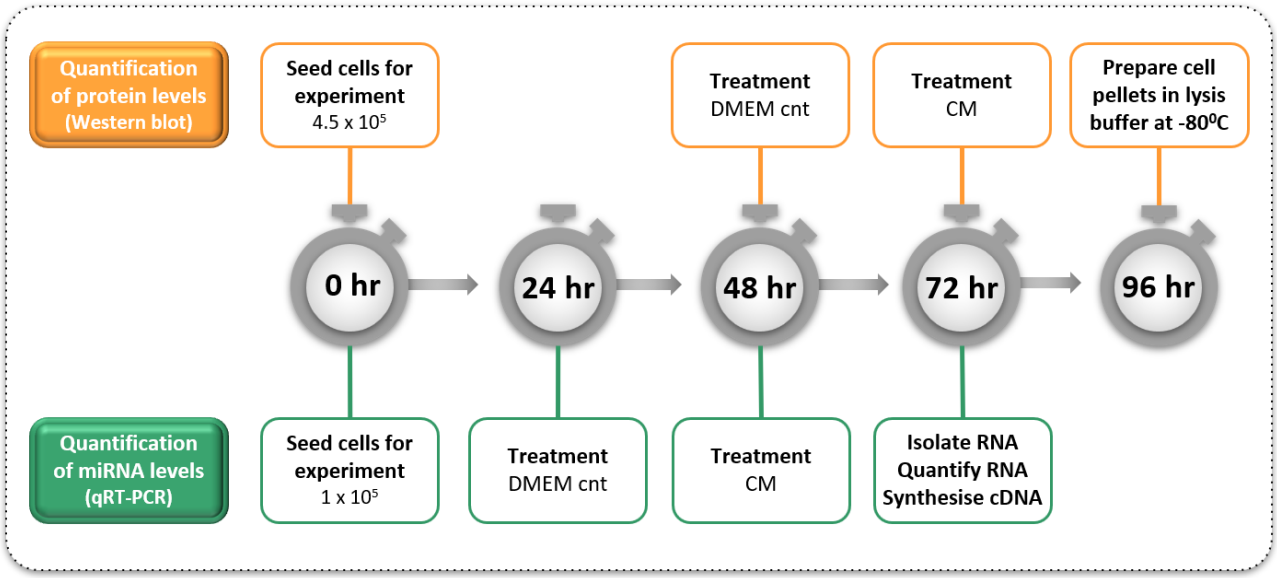

Figure 3.3: Experimental timeline for H9c2 cardiomyoblasts treated with adipose-derived CM.

H9c2 cells were treated with conditioned media (CM) harvested from i) subcutaneous adipose stem cells (SC ASCs), ii) subcutaneous adipocytes (SC Adipo), iii) peri-renal adipose stem cells (PR ASCs), and iv) peri-renal adipocytes (PR Adipo) for 24 hours and compared to a DMEM control. Following treatment, cells were prepared for Western blotting (protein expression) and qRT-PCR (miRNA expression) analyses, respectively. To avoid conducting these down-stream analyses simultaneously, a staggered approach was followed where the cells intended for qRT-PCR analysis were treated 24 hours after seeding, while cells intended for Western blotting were treated 48 hours after seeding.

3.3. MTT viability assay

A 3-[4,5-dimethylthiazole-2-yl]-2,5-diphenyltetrazolium bromide (MTT) colorimetric assay was used to quantitatively determine cell viability of H9c2 cells treated with combinations of FFAs, glucose and insulin (refer to section **3.2.1 Fatty acids, glucose and insulin**). Briefly, the assay relies on a mitochondrial enzyme, succinate dehydrogenase, to catalyse the conversion of soluble tetrazolium salt to insoluble formazan crystals within live cells (Mosmann, 1983). The absorbance of the formazan crystals is directly proportional to mitochondrial function and, therefore, cell viability.

Reagents

The thiazolyl blue tetrazolium bromide (MTT) powder (M5655) and dimethyl sulfoxide (DMSO; D4540) were purchased from Sigma-Aldrich. The Dulbecco's phosphate-buffered saline (DPBS)

with Calcium and Magnesium was purchased from Lonza™ (BioWhittaker™, 17-513F). The chemicals used for the Sorenson's glycine buffer (0.1 M glycine, 0.1 M NaCl; pH 10.5) were purchased from Merck.

Method

H9c2 cells were cultured as described previously (section **3.1 Cell culture**) and seeded into a 24-well plate at a seeding concentration of 2 x 10^4 live cells per plate **(*Table 3.1 F*)**. Cells were allowed to adhere to the surface for at least 24 hours, where after cells were treated with combinations of FFAs, glucose and insulin (refer to section **3.2.1 Free fatty acids (FFAs), glucose and insulin**) in triplicate for 24 hours. A complete DMEM media condition (DMEM control) and complete DMEM supplemented with 0.2% ethanol (vehicle control) were included. After 24 hours, the treatment media were aspirated, cells were washed with 500 µl of pre-heated DPBS, and 500 µl of pre-heated MTT solution (2 mg/ml DPBS) was placed into each well. As the MTT is light-sensitive, the 24-well plate was covered with aluminium foil and allowed to incubate for 2 hours at 37°C. After incubation, the MTT solution was aspirated and 50 µl of room temperature Sorenson's glycine buffer, followed by 400 µl of DMSO, were added to each well. The 24-well plate was once again covered with foil and incubated for 30 minutes. The buffer terminated the enzymatic reaction, whereas the DMSO served as an organic solvent for the water-insoluble formazan crystals. Following the second incubation, the absorbance of the formazan crystals was measured at 570 nm using a FLUOstar® Omega BMG LABTECH microplate reader (refer to Appendix B ***Figure B1*** for absorbance measurements).

3.4. Western blot analysis

The total and phosphorylated levels of the metabolic proteins of interest were quantified using Western blotting (Towbin, Staehelin and Gordon, 1979), an immunodetection technique based on the separation of individual proteins in a sample lysate according to size.

3.4.1. Protein lysate preparation

To analyse the total and phosphorylated levels of individual intracellular proteins, cells have to be lysed in order to release its protein content. This is achieved with a specific lysis buffer containing chemicals that solubilise cellular membranes, as well as enzymes (protease and phosphatase inhibitors) that protect cellular proteins from degradation by proteases and dephosphorylation by phosphatases. We were interested in the proteins contained within the cytoplasm, therefore a lysis buffer specific for cytoplasmic protein extraction was used.

Reagents

The bovine serum albumin (BSA) used for the standard curve was purchased from Sigma-Aldrich. The Bradford solution (0.12 mM Coomassie Brilliant Blue, 4.75% ethanol, 8.5% phosphoric acid) was prepared in-house with chemicals purchased from Sigma-Aldrich or Merck. Reagents for the lysis buffer used for cytoplasmic protein extraction and the 3x Laemmli sample buffer are summarised in ***Table 3.2*** and ***Table 3.3***, respectively.

Table 3.2: Lysis buffer components.

Reagent	Final concentration	Function	Supplier	Product code
Tris-HCl EGTA (pH 7.4)	2 mM 0.1 mM	Buffering salt Ca^{2+}-metalloprotease inhibitor	Merck Sigma-Aldrich	108382 E4378
EDTA	0.01 mM	Mg^{2+}/Mn^{2+}-metalloprotease inhibitor	Sigma-Aldrich	EDS
NaCl	22.5 mM	Buffering salt	Merck	106404
Na_3VO_4	0.1 mM	Tyrosine phosphatase inhibitor	Sigma-Aldrich	S6508
β-glycerophosphate	1 mM	Serine/Threonine phosphatase inhibitor	Sigma-Aldrich	G9422
Tetrasodium pyrophosphate	2.5 mM	Serine/Threonine phosphatase inhibitor	Merck	A364791
PMSF (dissolved in DMSO)	0.3 mM	Serine/Cysteine protease inhibitor	Sigma-Aldrich	P7626
Triton™ X-100	0.1%	Non-ionic membrane detergent	Sigma-Aldrich	T8787
Protease Inhibitor Cocktail	0.5%	Contains serine/cysteine protease and aminopeptidase inhibitors	Sigma-Aldrich	P8340

*DMSO: dimethyl sulfoxide; EDTA: ethylenediaminetetraacetic acid; EGTA: egtazic acid; PMSF: phenylmethylsulfonyl fluoride

Table 3.3: 3x Laemmli sample buffer components.

Reagent	Final concentration	Function	Supplier	Product code
SDS	4%	Denatures proteins & gives each an overall negative charge	Sigma-Aldrich	74255
Glycerol	20%	Weighs samples down in gel wells	Sigma-Aldrich	G5516
Bromophenol blue	0.004%	Colour agent to show front of sample separation	Sigma-Aldrich	B8026
Tris-HCl (pH 6.8)	0.125 M	Buffering salt	Merck	108382
2-mercaptoethanol (add before use)	10%	Denatures proteins & prevents oxidation of cysteine residues	Sigma-Aldrich	M6250

*SDS: sodium dodecyl sulfate

Method

Following the removal of the treatment media from H9c2 cells and the CM from adipose-derived ASCs and differentiated adipocytes, cells were washed with pre-heated PBS. Cells were subsequently scraped from the culture dish surface in 10 ml fresh PBS and centrifuged (Sigma 1-14) at 92 *xg* for 4 minutes at 4°C. The PBS solution was aspirated from the cell pellets, which were resuspended in 400 µl ice-cold lysis buffer. In the case where protein lysates were not directly prepared following this step, the pellets were stored in lysis buffer at -80°C until the protein lysate preparation could commence. Otherwise, the resuspended pellets were transferred to 1.5 ml Eppendorf tubes containing equal amounts of 0.5 mm Zirconium Oxide beads (Next Advance, Biocom Biotech). Cell pellets were homogenised using a BulletBlender™ at 4°C in three consecutive cycles of 1 minute runs (level 4), followed by 5 minute rests after each homogenisation step. The homogenised samples were allowed to rest on ice for 20 minutes, where after the samples were centrifuged at 12 074 *xg* for 20 minutes at 4°C. Cellular membrane debris and nuclei trapped within the resulting pellet were discarded, while the supernatant containing the cytoplasmic proteins were retrieved and transferred to new Eppendorf tubes. The supernatant from this step will hereafter be referred to as the lysate stock samples, which were stored at -80°C until use.

The protein concentrations within each lysate stock sample were determined using the Bradford method (Bradford, 1976) and compared to a standard BSA dilution series (in duplicate). Briefly, a 10x dilution with distilled water was prepared from each lysate stock sample in a final volume of 100 µl, followed by a duplicated second 10x dilution of the first dilution in a final volume of 100 µl. Next, 900 µl of diluted (5x with distilled water) and twice-filtered Bradford solution was added to each of the duplicated BSA standard dilutions and second dilutions of the lysate stock samples. To allow for proper binding of the Coomassie Brilliant Blue dye within the Bradford solution to the proteins within each sample, the samples were left for 15 minutes at room temperature. The absorption measures of each duplicate standard and lysate stock sample were noted using the SPECTRONIC® 20 GENESYS™ or Libra $S4^{+}$ spectrophotometer at a wavelength of 595 nm, which is the absorption maximum of protein-bound dye. Therefore, the absorbance is directly proportional to the amount of protein within each sample. Duplicate absorbance values were averaged, and a linear equation for the known protein concentrations of the BSA standard was used to calculate the unknown protein concentrations within the lysate stock samples.

Lastly, the protein lysates were prepared for gel loading using Laemmli sample buffer (Laemmli, 1970). In a fresh Eppendorf tube, a calculated volume of each lysate stock sample equal to the same amount (µg) of protein were added to Laemmli sample buffer (volume equal to 1/3 of the final volume) and lysis buffer (used to fill to final volume) in a final volume of 150 µl. Complete protein

lysates were boiled for 4 minutes to ensure proper unfolding of sample proteins and stored at -80°C until gel separation could commence.

3.4.2. Protein separation and transfer

Reagents

Chemicals for hand-casted polyacrylamide running gels (0.5% 2,2,2-trichloroethanol, 0.375 M Tris-HCl [pH 8.8], 0.1% SDS, 7.5% acrylamide, 0.05% APS, 0.2% TEMED) and stack gels (0.127 M Tris-HCl [pH 6.8], 0.1% SDS, 4% acrylamide, 0.1% APS, 0.2% TEMED) were purchased from Sigma-Aldrich or Merck, and pre-casted 26-well Criterion™ TGX Stain-Free™ gels (4-20% gradient, Bio-Rad Laboratories, Inc) were purchased from Lasec. Chemicals used for 10x running buffer (250 mM Tris, 1920 mM glycine, 1% SDS) and a modified 1x transfer buffer (25 mM Tris, 192 mM glycine, 10% [v/v] methanol) were purchased from Sigma-Aldrich or Merck.

Method

All protein lysates were thawed on ice and boiled once more for 4 minutes prior to gel loading to ensure proper unfolding of proteins. Protein lysates were loaded into either 10- or 15-well hand-casted polyacrylamide gels or pre-casted 26-well Criterion™ TGX Stain-Free™ gels. Either the HiMark™ Pre-stained Protein Standard ladder (31-460 kDa range), Precision Plus Protein™ Dual Xtra Standards ladder (2-250 kDa range) or PageRuler™ Pre-stained Protein Ladder (10-180 kDa range) was loaded in the first lane as a marker for molecular weight determination. Tanks were filled with 1x running buffer and the loaded gels were subjected to sodium dodecyl sulfate-polyacrylamide gel electrophoresis (SDS-PAGE), which separated the proteins according to molecular weight. The hand-casted gels were subjected to an initial 100 V and 200 mA for 10 minutes, followed by 200 V and 200 mA for 60 minutes. The pre-casted Criterion™ TGX Stain-Free™ gels were subjected to 200 V and 200 mA for 60 minutes. Thereafter, gels were activated and visualised using the ChemiDoc™ MP Imaging System (Bio-Rad Laboratories, Inc.) to establish equal loading and separation of proteins. In short, a stain-free tri-halo compound (2,2,2-trichloroethanol, Sigma-Aldrich, T54801) was incorporated into the gels that catalyses a reaction with the tryptophan residues of the sample proteins in response to ultra-violet (UV) irradiation, which can be detected and imaged by the ChemiDoc™ system. Next, tanks were filled with ice-cold transfer buffer and the proteins were transferred from the gels to polyvinylidene fluoride (PVDF) membranes (Immobilon-P Transfer Membrane, 0.45 µm pore size, Merck) that have been briefly soaked in methanol and ice-cold transfer buffer. The hand-casted gels were subjected to 200 V and 200 mA for 90 minutes, whereas the pre-casted Criterion™ TGX Stain-Free™ gels were subjected to 160 V and 200 mA for 60 minutes.

Following protein transfer, membranes were visualised and imaged using the ChemiDoc™ system to ensure the successful transfer of proteins. The stain-free membrane images (available in Appendices B, C and D) were stored for later use during protein normalisation. Membranes were submerged in methanol for 30 seconds to fix the proteins to the membrane.

3.4.3. Immunodetection of target proteins

Reagents

Chemicals for 10x Tris-buffered saline (TBS) solution (1.37 M NaCl, 200 mM Tris; pH 7.6) were purchased from Merck. Tween® 20 was purchased from Sigma-Aldrich (P1379). The SignalBoost™ solutions for primary antibodies (KP31812) and secondary antibodies (KP31855) were purchased from Merck.

Method

Membranes were blocked with a mixture containing 5% fat-free milk in 1x TBS-Tween (TBS-T; 10% TBS and 1% Tween) for 2 hours at room temperature to prevent non-specific background binding of antibodies. Membranes were subsequently washed with TBS-T for three 5 minute cycles and cut at locations above and below the protein of interest. Membrane pieces were individually incubated in primary rabbit antibodies (optimised concentrations listed in ***Table 3.4***) on a shaker at 4°C overnight. This step allowed for the specific binding of the primary antibody to the protein of interest. Following primary incubation, membrane pieces were washed with TBS-T and incubated in an anti-rabbit immunoglobulin G, horseradish peroxidase (HRP)-conjugated secondary antibody (Cell Signaling Technology, 7074; optimised concentrations listed in ***Table 3.4***) on a shaker at room temperature for 1 hour. This step allowed for the binding of the secondary antibody to the primary antibody. Following secondary incubation, membrane pieces were washed with TBS-T and submerged in Clarity™ enhanced chemiluminescence (ECL) reagent (Bio-Rad Technologies, Inc.) for 5 minutes before a chemiluminescent signal was detected using the ChemiDoc™ system. In short, when the HRP-linked secondary antibody reacts with the ECL, energy is emitted in the form of light. The light is captured by the CCD camera of the ChemiDoc™ and translated into pixels on an image. The signal is proportional to the number of pixels, which in turn relates to the amount of protein, and can therefore be used for protein quantification.

Table 3.4: Optimised antibody dilutions.

Primary (rabbit)						Secondary (anti-rabbit)
Protein	Molecular weight (kilodalton)	Dilution	Incubation time	Supplier	Product code (lot)	Dilution
t-ATM	350	1:1000 TBS-T	16 hours	Abcam	ab199726 (GR3190608-2)	1:4000 TBS-T
p-ATM (ser1981)		1:1000 primary SB	13 hours	CST	5883 (6)	1:4000 secondary SB
t-mTOR	289	1:1000 TBS-T	16 hours	Abcam	ab134903 (GR3266442-4)	1:4000 TBS-T
p-mTOR (ser2448)		1:1000 TBS-T	16 hours	CST	2971 (20)	1:4000 TBS-T
t-ACC1,2	260,280	1:500 TBS-T	16 hours	CST	3662 (4)	1:4000 TBS-T
p-ACC1,2 (ser79)		1:500 TBS-T	16 hours	CST	3661 (9)	1:4000 TBS-T
t-AMPK	62	1:1000 TBS-T	16 hours	CST	2532 (19)	1:4000 TBS-T
p-AMPKα (thr172)		1:1000 TBS-T	16 hours	CST	2535 (21)	1:4000 TBS-T
t-PKB	56	1:1000 TBS-T	16 hours	CST	9272 (28)	1:4000 TBS-T
p-PKB (ser473)		1:500 TBS-T	16 hours	CST	4060 (25)	1:4000 secondary SB

*CST: Cell Signaling Technology; p: phospho; t: total; SB: SignalBoost™

3.4.4. Protein normalisation

Target protein signals were normalised to the total protein transferred to the membranes to determine biological differences in total and phosphorylated levels across the various treatment conditions. This reliable and rapid Stain-Free-based normalisation method considers all the proteins contained within a sample (Gürtler et al., 2013), which negates the use of a house-keeping protein. Automated total protein normalisation using the stain-free membrane blot was performed in Image Lab™ (version 6.0.1, Bio-Rad Technology Inc.), which generated a normalised raw pixel intensity per chemiluminescent protein band. Raw pixel intensity data were inserted into a Microsoft Excel spreadsheet, where the pixel intensities corresponding to each treatment sample were calculated as a fold-change of the mean pixel intensity of the control samples or another designated group (in the case where no control group is present).

3.5. Total RNA extraction and cDNA synthesis

In order to quantify the levels of target miRNAs through qRT-PCR, the total RNA was extracted (*mir*Vana™ miRNA Isolation Kit, with acid-phenol:chloroform, Invitrogen™, Thermo Fisher Scientific) from the treated H9c2 cells (described in section **3.2 Treatment preparation and administration**) and reverse transcribed to complementary DNA (cDNA; TaqMan™ Advanced

miRNA cDNA Synthesis Kit, Applied Biosystems™, Thermo Fisher Scientific). The latter is an important step in stabilising the RNA, as single-stranded RNA sequences are highly susceptible to degradation, whereas double-stranded cDNA is more robust and can be stored for up to two months at -20°C.

Reagents

Nuclease-free water was purchased from Qiagen and pure ethanol was purchased from Sigma-Aldrich (E7023).

Method

Following each treatment duration, the treatment media (refer to section **3.2 Treatment preparation and administration**) were aspirated and the H9c2 cells were washed with pre-heated PBS. Cells within each culture dish were lysed using 100 µl of ice-cold lysis buffer (Lysis/Binding Buffer, component of isolation kit) and scraped from the dish surface. The scraped cells from each respective treatment condition were pooled in 1.5 ml Eppendorf tubes. The total RNA from each pooled sample was extracted as per the manufacturer's instructions. Briefly, the isolation kit is designed to extract high concentrations of ultra-pure RNA molecules, including RNAs as small as 10 nucleotides, by employing a combination of chemical (organic) and solid-phase extraction. The first step, the organic extraction, relies on the use of chaotropic salts, together with acid-phenol-chloroform, to prevent RNA degradation and to purify RNA molecules from any other biological molecules within the cell lysate (Chomczynski and Sacchi, 1987). This entails phase separation through centrifugation to ensure that the hydrophilic RNA remains in the upper aqueous phase, whereas other hydrophobic biomolecules are trapped within the bottom organic phase. The RNA-containing aqueous phase is retrieved and subjected to alcohol precipitation to desalt the RNA. The second step, the solid-phase extraction, relies on the ability of the alcohol to promote the affinity of RNA molecules for silica (Boom *et al.*, 1990), or in this case the glass-fibre filters (component of the kit). A series of washing and filtration steps using the Eppendorf Centrifuge 5410 completed the isolation process, and the resultant RNA molecules were eluted in pre-heated (95°C) nuclease-free water.

The RNA concentration and purity were subsequently determined with the microvolume NanoDrop™ 2000c spectrophotometer (Thermo Fisher Scientific), which employed absorbance measurements. In addition to determining RNA concentration within a sample, which is directly proportional to its absorbance (Schmid, 2001), the spectrophotometer generates absorbance ratios as indicators of RNA purity. Various biomolecules absorb UV light at different wavelengths. The absorbance maxima of nucleic acids and proteins are at 260 and 280 nm, respectively. Therefore, a 260/280 absorbance ratio was used as an indicator of protein contamination, with ratios of

approximately 2.0 considered pure for RNA samples (Desjardins and Conklin, 2010). Furthermore, other organic compounds that typically contaminate RNA samples have absorbance maxima at 230 nm. Therefore, a 260/230 ratio was used as an indicator of organic contamination, with ratios ranging between 1.8 and 2.2 considered pure for RNA samples (Desjardins and Conklin, 2010). Refer to Appendix B **(*Table B1*)** and Appendix D **(*Table D1*)** for RNA concentrations and absorbance ratios of H9c2 cells treated with nutrients and/or insulin and CM, respectively.

Even though RNA purity could be established with absorbance ratios generated by the NanoDrop™ spectrophotometer, RNA integrity had to be assessed to ensure the success of the downstream applications. This was performed with an Agilent 2100 Bioanalyzer, a service provided by the DNA Sequencer Unit of the Central Analytical Facility, Stellenbosch University. In short, a small volume of sample is separated on a gel through electrophoresis and subjected to a fluorescent dye that intercalates with the RNA sequences. The fluorescent signal is detected and translated into peaks on electropherograms, which is used to calculate an RNA Integrity Number (RIN) for each sample. The allocated RIN serves as a measure of RNA quality and ranges on a scale of 1 (low integrity) to 10 (high integrity) (Schroeder *et al.*, 2006). Twelve randomised RNA samples generated from H9c2 cells treated with adipose-derived CM in different experiments were selected and 2.5 µl of each sample was stored separately at -80°C for quality evaluation (see Appendix D ***Figure D5*** for RIN allocations).

RNA does not serve as a suitable template for qRT-PCR for two reasons: RNA is highly susceptible to RNase-facilitated degradation and qRT-PCR relies on the function of a DNA polymerase. Consequently, the RNA sequences were reverse transcribed to cDNA through a series of enzymatic processes during various heating-cooling cycles using the GeneAmp® PCR System 2700 thermal cycler (Applied Biosystems) as outlined in the manufacturer's protocol. Briefly, the total RNA was diluted to an input concentration of 5 ng/µl in a final volume of 2 µl. The first process, polyadenylation, involved the addition of a 3'-adenosine tail to each RNA strand. The second process, adaptor ligation, occurred at the 5'-end of the RNA strands where an adaptor is attached. These extensions serve as the binding sites for the reverse- and forward-primers involved in the subsequent processes. The third process, reverse transcription (RT), involves a universal RT primer that binds to the 3'-polyadenosine tail, which was added during the first process, in order to reverse transcribe the RNA sequence to form a DNA/RNA-hybrid molecule. The fourth and final process, amplification, is necessary to complement the DNA-portion of the hybrid molecule to form cDNA, and to amplify all the cDNA molecules present within the sample through the action of universal forward- and reverse-primers. A non-template control (NTC) was also prepared. The NTC contained nuclease-free water instead of an RNA template, thereby serving as a negative control to ensure the purity of the water

and reagents. The resultant cDNA and NTC samples were stored at -20°C until qRT-PCR could commence. A simplified scheme of the total RNA extraction and cDNA synthesis processes is provided in ***Figure 3.4***.

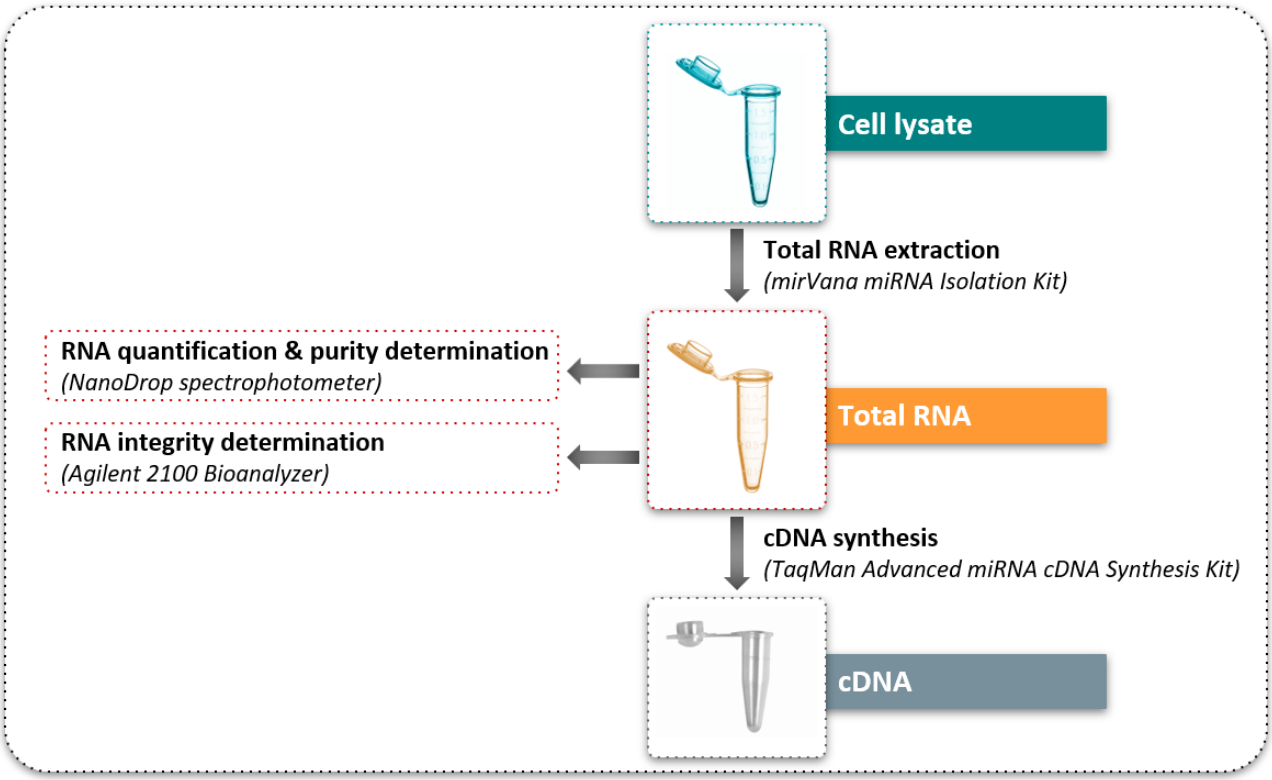

Figure 3.4: Schematic of total RNA extraction and cDNA synthesis of H9c2 cardiomyoblasts following treatment.

3.6. qRT-PCR

PCR is a useful technique that amplifies specific DNA strands of interest for ultimate quantification. In this study, the employment of qRT-PCR using TaqMan™ Advanced miRNA Assays (Applied Biosystems™, Thermo Fisher Scientific) was particularly beneficial as it allows the use of RNA as template, provided it is reverse transcribed to cDNA. Using fluorescence-labelled primers (FAM™-labelled TaqMan™ miRNA assays) that are specific for our target miRNA strands, it was possible to collect amplification data as the PCR process continued (i.e., in real time). To accompany the TaqMan™ Advanced reagents, we used 96-well MicroAmp® Optical Fast Blue Reaction Plates (Life Technologies™, Applied Biosystems™).

Method

Firstly, the cDNA templates were thawed on ice and amplification plots and standard curves (refer to Appendices B and D) for each primer were constructed by combining a small amount of each cDNA sample in a series of 10x dilutions (100%, 10%, 1%, 0.1%, 0.01% and 0.001% using nuclease-free

water) in duplicate (refer to standard curve qRT-PCR plate layouts in Appendix B ***Figure B7*** and Appendix D ***Figure D6***). This was necessary to ensure that i) each miRNA primer could generate a fluorescent signal that exceeded the signal threshold, ii) each miRNA primer met the efficiency criteria (discussed below), iii) the cDNA samples were diluted according to the most ideal dilution factor for the qRT-PCR reaction, and iv) the kit reagents were free of contaminants. For each amplification plot, the ΔRn was plotted on the y-axis against the cycle number on the x-axis to represent the accumulation of product over time. The ΔRn-value, or the normalised reporter value, represents the fluorescent signal of each experimental reaction normalised to the background signal produced by the instrument. The signal threshold refers to the ΔRn-value at which the reaction fluorescence is considered a true signal. The Ct (threshold cycle)-value represents the cycle number at which a fluorescent signal exceeds the signal threshold and is inversely related to the amount of starting RNA. The maximum Ct-value was set at 35 PCR cycles, as samples with a Ct-value greater than 35 required too many cycles to accumulate to threshold. For each standard curve, the logarithm (log) of each known concentration factor in the dilution series were plotted on the y-axis against the corresponding Ct-value on the x-axis to allow for the assessment of reaction performance using several linear line parameters. For example, the slope is a measure of primer efficiency, with an optimal range of -3.58 to -3.10 corresponding to 90% to 110% efficiency, and the correlation coefficient (R^2) is an indication of how well the data points fit the linear standard curve, with an optimal value as close to 1 as possible.

Next, the cDNA templates were diluted (10x) with nuclease-free water. A PCR reaction mix for each target miRNA primer, as well as the endogenous control primer, were prepared as per the manufacturer's protocol (primer information listed in ***Table 3.5***). It was essential to include an endogenous control miRNA as a reference to reliably compare the relative expression of the target miRNAs and to minimise bias caused by experimental variation. The current study used U6 snRNA as a reference miRNA as it is commonly used in literature (Su *et al.*, 2017; Kakimoto *et al.*, 2018; Chen *et al.*, 2019) and is stably expressed in H9c2 cells across various treatment conditions (refer to Appendix B ***Figure B12*** and Appendix D ***Figure D15***). The PCR reaction plates, with each well containing a primer-specific reaction mix and either a cDNA template, NTC or nuclease-free water in duplicate, were prepared and sealed with an optically-clear adhesive cover slip. The nuclease-free water was included as a second negative control (Neg) to ensure the purity of the reaction mix. The qRT-PCR plate layouts are illustrated in Appendix B ***Figure B11*** and Appendix D ***Figure D14***. The plates were inserted into the QuantStudio™ 7 Flex Real-Time PCR Instrument, 96-well FAST (Life Technologies™, Applied Biosystems™) for the amplification process to commence. Briefly, qRT-PCR amplification of the cDNA templates relies on repeated cycles of three temperature-dependent

steps: denaturation, annealing and elongation. With each cycle, the number of copies of a target template is doubled. Each primer (refer to ***Table 3.5***) is labelled with a fluorescent reporter dye (FAM™). Once the primer anneals to its specific cDNA target, a DNA polymerase cleaves the dye during elongation to produce a fluorescent signal that is captured in real time by the QuantStudio™ RT-PCR instrument. The fluorescence is proportional to the number of target copies and is used for relative quantification of miRNA expression.

Table 3.5: TaqMan™ Advanced miRNA primer information.

microRNAs	Sequence	Assay ID	Target species
miR-194-3p	CCAGUGGGGCUGCUGUUAUCU	rno480975_mir	Rat
miR-322-5p	CAGCAGCAAUUCAUGUUUUGGA	rno481051_mir	Rat
miR-210-5p	AGCCACUGCCCACAGCACACUG	rno480994_mir	Rat
miR-181b-5p	AACAUUCAUUGCUGUCGGUGGGU	rno478583_mir	Rat
miR-18a-5p	UAAGGUGCAUCUAGUGCAGAUAG	rno480968_mir	Rat
miR-421-5p	GGCCUCAUUAAAUGUUUGUUG	rno481481_mir	Rat
U6 snRNA (endogenous control)	GTGCTCGCTTCGGCAGCACATATACTAAAA-TTGGAACGATACAGAGAAGATTAGCATGGC-CCCTGCGCAAGGATGACACGCAAATTCGTGA-AGCGTTCCATATTTT	001973	Rat

3.7. GC-FID

To analyse the FFA composition of the adipose-derived CM, samples were subjected to GC-FID. The GC-FID analysis was kindly performed by Dr P. van Jaarsveld at the SAMRC.

Gas chromatography (CG) is commonly used for the separation of various compounds within a sample mixture and is particularly advantageous due to the simplicity, sensitivity and efficiency of the analytical technique. Briefly, samples are introduced into a stream of a chemically inert carrier gas, usually helium, argon or nitrogen. This is referred to as the mobile phase. Liquid samples are then vaporised within a heated vaporisation chamber, and the gas stream containing the evaporated sample mixture is passed through a column that contains the stationary non-volatile phase. The components of the sample mixture pass through the column at velocities that are determined by their affinity for the stationary phase. Compounds that have a higher affinity for the stationary phase are slowed to a greater degree and are consequently separated from compounds with lower affinities. As compounds elute from the column, from lowest to highest affinity, they interact with a flame ionisation detector (FID). FID is highly suitable for the detection of volatile organic compounds that contain hydrocarbons, such as FFAs, however the major disadvantage is that the sample is destroyed and cannot be used for other analyses. The FID consists of a hydrogen/air flame, a positive electrode

at the location where the flame is produced, and a negative collector electrode situated above the flame. The column effluent is mixed with hydrogen and air and ignited. The combustion reaction releases mainly carbon ions from organic compounds, which generate an electrical current between the two electrodes that is proportional to the amount of compound that passes through the flame. The electrical current is measured by an electrometer and transmitted into an integrator for interpretation (information obtained from the Gas Chromatography and Flame Ionisation Detector application sheets, Linde Gases Division, Germany). The data are displayed as peaks on a graph, with the time of compound migration through the column on the x-axis and the area of the peak (indicating the amount of a specific compound) on the y-axis.

3.8. Statistical analyses

Briefly, the data generated from the various laboratory techniques required different processing to generate appropriate input data for statistical testing:

For MTT viability assay analysis, the absorbance values were used to calculate a fold-change as a percentage relative to the DMEM control condition using Microsoft Excel.

For Western blot analysis, the proteins of interest were normalised to the total protein transferred onto the stain-free membrane using Image Lab™ (version 6.0.1, Bio-Rad Technology Inc.). The automatically generated pixel densities were used to calculate a fold-change relative to a reference condition using Microsoft Excel.

For qRT-PCR analysis, the delta-delta Ct ($2^{-\Delta\Delta Ct}$)-method (Livak and Schmittgen, 2001) was employed to calculate the relative expression of a target miRNA normalised to U6 snRNA using Microsoft Excel.

For GC-FID analysis, Dr P. van Jaarsveld kindly provided us with the FFA composition of each CM sample, which were expressed as either µg FFA per ml CM, or as a percentage of the total FFAs per ml CM.

Using GraphPad Prism 5 software, an ordinary one-way Analysis of Variance (ANOVA) was employed where one variable between multiple groups were compared to determine whether a statistical difference existed between the various independent treatment groups or cell types, followed by a Bonferroni multiple-comparison test to correct for multiple testing and to determine whether there were significant differences between specific groups. For analyses where two variables were compared between multiple groups, a two-way ANOVA was employed, followed by a Bonferroni multiple-comparison test. For analyses where one variable between two groups were compared, a Student's t-test was employed. We acknowledge that the sample sizes for each experiment were too

small to determine normality, therefore a normal distribution was assumed. Any difference between various group means were considered statistically significant if the probability value (p-value) was equal to or less than 0.05. All data are expressed as the mean ± standard deviation (SD).

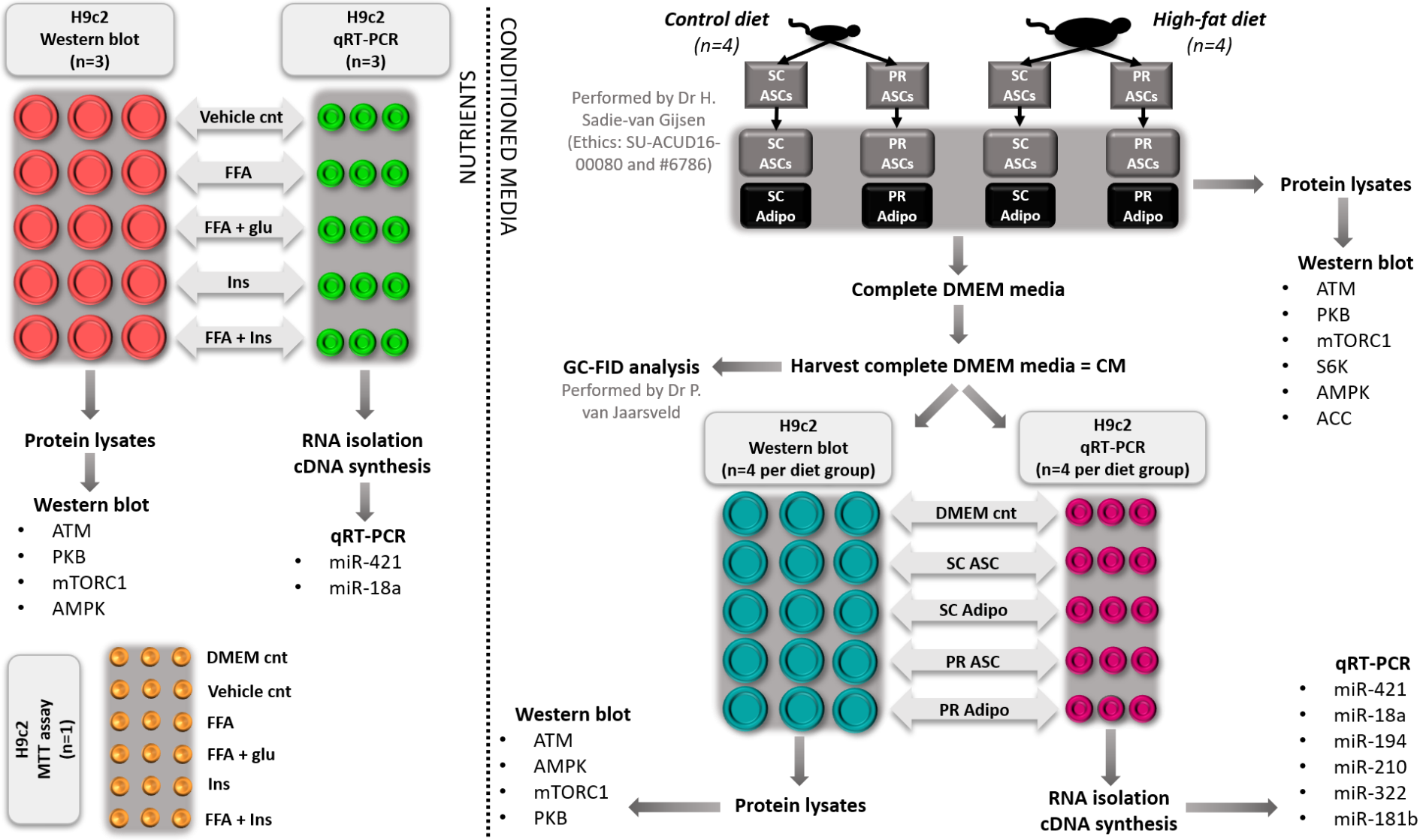

Figure 3.5: Schematic summary of study methods. *Results of H9c2 cells treated with combinations of nutrients and insulin are discussed in Chapter 4; protein quantification results of primary adipose stem cells and adipocytes are discussed in Chapter 5; results of H9c2 cells treated with conditioned media are discussed in Chapter 6.*

Chapter 4

Establishing a suitable *in vitro* cardiomyoblast model that is sensitive to the effects of obesity

In order to investigate the potential metabolic effects of obesity on the heart, we first had to establish a suitable *in vitro* cardiomyoblast model. The H9c2 cardiomyoblast cell line is a well-known *in vitro* cardiac-derived model that has been extensively used as such throughout literature. Although H9c2 cells share some phenotypical properties with skeletal muscle cells once confluency is reached (Kimes and Brandt, 1976), they also share similarities with isolated primary adult cardiomyocytes (Hescheler *et al.*, 1991; Sipido and Marban, 1991). Therefore, we exposed H9c2 cells to various treatments that simulate obesity in order to investigate whether they are metabolically responsive. H9c2 cells were treated with combinations of high FFAs (palmitic acid and oleic acid), glucose and insulin for 24 hours to achieve a chronic obese effect as opposed to an acute nutrient response. Following the treatment period, we analysed H9c2 cell viability by performing an MTT assay, the total and phosphorylated levels of ATM and other metabolic proteins (PKB, mTORC1, S6K and AMPK) through Western blotting, and the expression levels of the two miRNAs (miR-421 and miR-18a) that are known to regulate ATM protein levels in cancer cells with qRT-PCR.

4.1. Prolonged exposure to combinations of excess nutrients and insulin appears to be non-lethal to H9c2 cells

An MTT viability assay was performed after 24 hours of treatment with complete DMEM media supplemented with EtOH (0.2%; vehicle control), 0.2 mM FFAs, 0.2 mM FFAs with 5.5 mM glucose, 100 nM insulin, and 100 nM insulin with 0.2 mM FFAs, respectively **(*Figure 4.1*)**. The MTT assay was performed in a single experiment (biological n=1), with each treatment condition performed in triplicate (technical n=3). No statistical analysis was applied to the single biological replicate, and data are expressed as the mean percentage of viable cells ± SD relative to the untreated (complete DMEM medium-only, from herewith referred to as DMEM control) cells.

There seemed to be no effect on cell viability across the different treatment conditions compared to the DMEM control, therefore any observed cellular changes are likely not due to cell death.

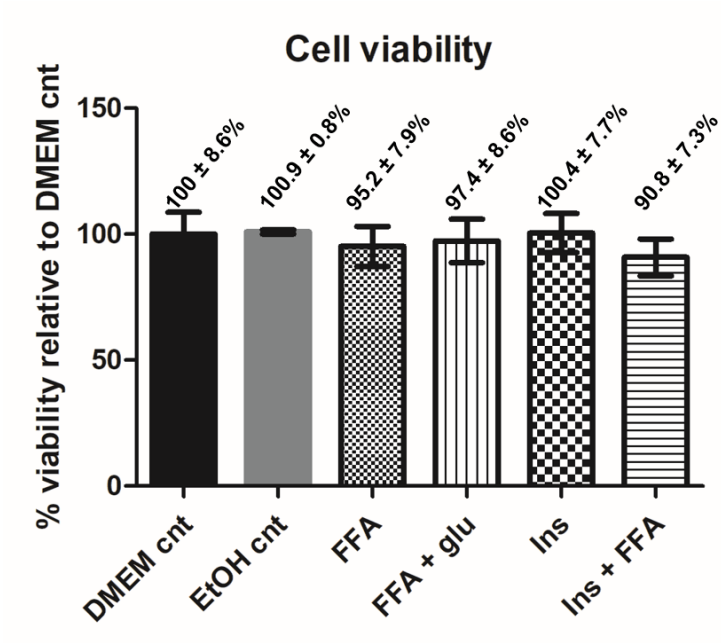

Figure 4.1: Cell viability of H9c2 cardiomyoblasts treated with combinations of nutrients and insulin for 24 hours.

Percentage viability of H9c2 cells treated with combinations of 0.2 mM free fatty acids (FFA; palmitic and oleic), 5.5 mM glucose (glu) and 100 nM insulin (ins), as well as a vehicle control (0.2% EtOH cnt), for 24 hours compared to a DMEM control. No differences in cell viability seemed to be observed (biological n=1; technical n=3; mean ± SD).

4.2. Prolonged insulin stimulation appears to attenuate PKB phosphorylation in H9c2 cells

To determine whether insulin resistance can be induced within H9c2 cardiomyoblasts, cells were subjected to 100 nM insulin for 15 minutes and 24 hours, respectively, to establish the acute and chronic effect on PKB phosphorylation. Following the treatment periods, the total PKB protein and phosphorylated (ser473) levels were determined through Western blot analysis. This experiment consisted of one biological replicate (n=1), where the DMEM control was analysed in duplicate (technical n=2) and the insulin treatments were analysed in triplicate (technical n=3). No statistical analysis was applied to the single biological replicate, and data are presented as the mean fold-change ± SD relative to the DMEM control.

Exposure to 15 minutes of insulin resulted in PKB phosphorylation compared to the DMEM control (5.35 ± 1.12 vs. 1 ± 0.21), whereas 24 hours of insulin stimulation did not result in PKB phosphorylation compared to the DMEM control (2.14 ± 0.28 vs. 1 ± 0.21) **(*Figure 4.2*)**.

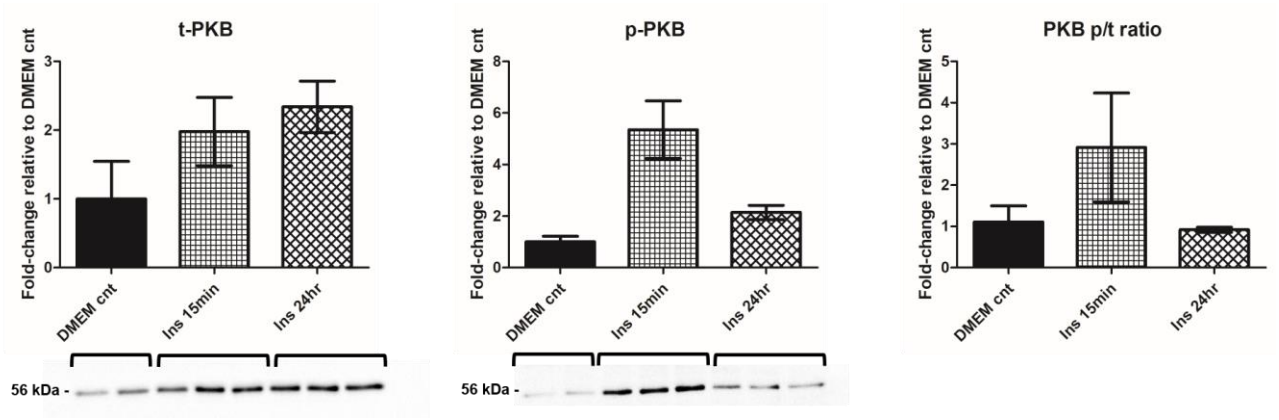

Figure 4.2: H9c2 cardiomyoblast insulin sensitivity following acute and chronic insulin stimulation.

PKB total protein (t) and phosphorylation (p) levels in H9c2 cells following 100 nM insulin (ins) treatment for 15 minutes and 24 hours, respectively, compared to a DMEM control. PKB phosphorylation was observed in cells after 15 minutes of insulin stimulation, but not after 24 hours of insulin stimulation, compared to DMEM controls (technical n=2-3; biological n=1; normalised to total protein; mean ± SD).

The binding of insulin to the transmembrane insulin receptor initiates a cascade of phosphorylation events that ultimately results in glucose uptake. PKB is an insulin-sensitive protein that is phosphorylated on certain amino acid residues for subsequent activation. Apart from threonine 308 (thr308) phosphorylation by PDK1 (Alessi *et al.*, 1997), PKB is phosphorylated on ser473 by the upstream kinase mTORC2 (Sarbassov *et al.*, 2005) in response to insulin stimulation. This phosphorylation site has been used in literature as an indicator of intracellular insulin sensitivity (Coll *et al.*, 2008; Kwon and Querfurth, 2015), and we were therefore able to utilise PKB ser473 phosphorylation in H9c2 cells. Furthermore, it has been established that treatment of cells with a high concentration of insulin for 24 hours is sufficient to render cells insulin resistant (Ha and Pak, 2005), and the results shown in ***Figure 4.2*** correspond with this observation.

4.3. Prolonged exposure to a combination of excess insulin and free fatty acids might reduce ATM activity in H9c2 cells

Following treatment of H9c2 cells with the various nutrient and insulin combinations for 24 hours, the total and phosphorylated levels of ATM, PKB, mTORC1, S6K and AMPK were determined through Western blot analysis. Experiments were performed in triplicate (biological n=3), with the vehicle (EtOH) control condition analysed in duplicate (technical n=2) and each treatment condition analysed in triplicate (technical n=3). The stain-free membranes used for ATM, mTORC1, S6K and AMPK protein quantification originated from 15-well polyacrylamide gels, where the sample lysates of the three individual experiments were unable to fit onto a single gel. No common control was included, thus the results of the three experiments were not pooled and are presented per experiment (experiment 1=A; experiment 2=B; experiment 3=C). No statistical analyses were applied to the

protein quantification data of ATM, mTORC1 and AMPK. 26-well Criterion™ TGX Stain-Free™ gels were used for PKB protein quantification, and common controls were included. Thus, the results of the three experiments were pooled. An ordinary one-way ANOVA was performed, followed by a Bonferroni post-hoc test. Results obtained for S6K could not be replicated and were excluded from the study. All data are presented as mean fold-change ± SD relative to the vehicle (EtOH) control. The p/t-ratio represents the phosphorylated protein as a fraction of the total protein and serves as an indicator of protein activity for all proteins analysed in these experiments.

ATM total protein levels **(*Figure 4.3*)** did not seem to be influenced by the various treatment conditions compared to the vehicle control, however ATM activity (p/t-ratio) showed a decreased trend in H9c2 cells treated with a combination of FFAs and insulin compared to cells treated with insulin alone (experiment B; 0.35 ± 0.31 vs. 1.36 ± 0.07) and FFAs alone (experiment C; 0.33 ± 0.04 vs. 1.19 ± 0.15).

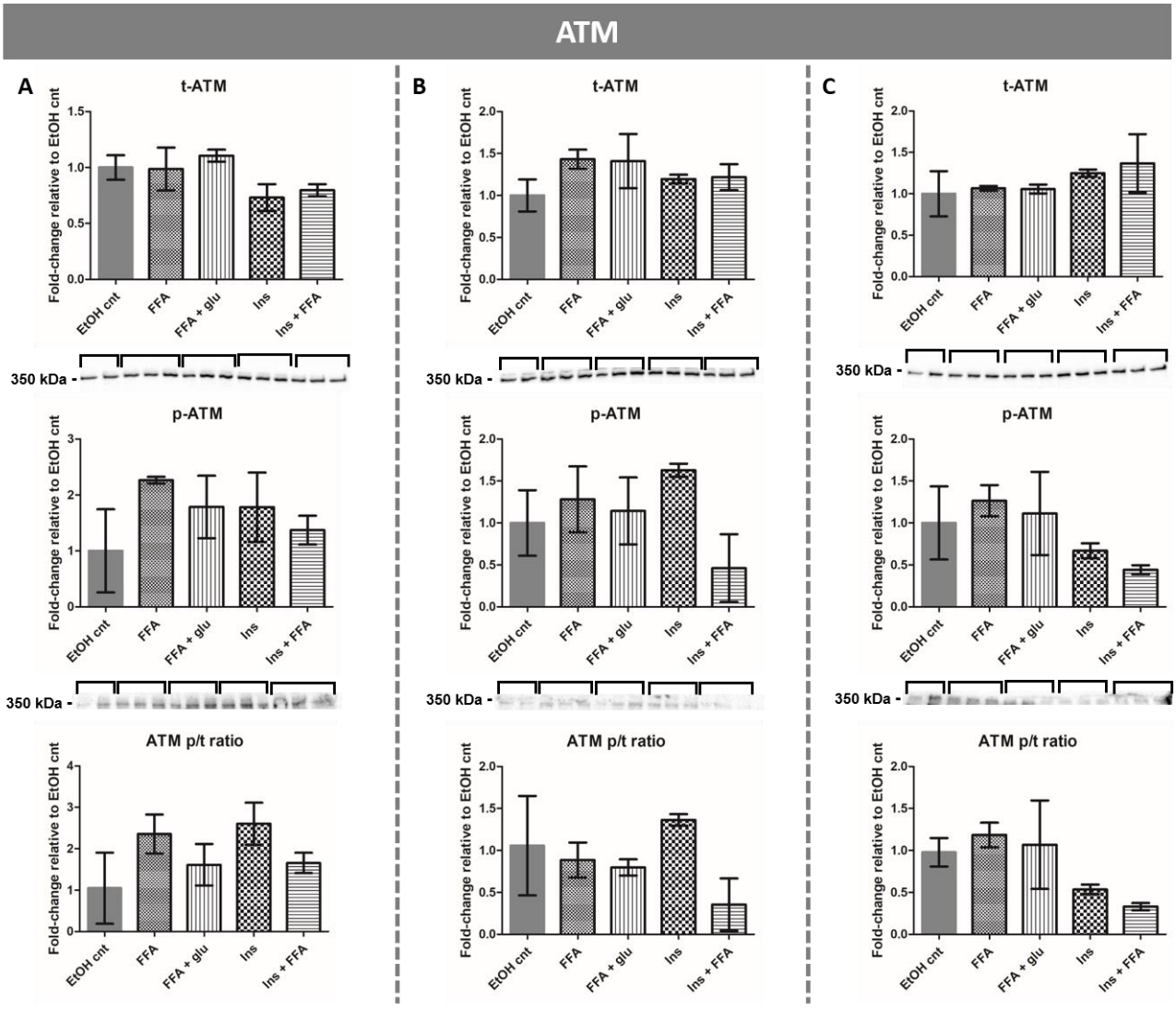

Figure 4.3: Total and phosphorylated levels of ATM in H9c2 cardiomyoblasts treated with combinations of nutrients and insulin for 24 hours.

ATM total (t) and phosphorylated (p) levels in H9c2 cells treated with combinations of 0.2 mM free fatty acids (FFA; palmitic and oleic), 5.5 mM glucose (glu) and 100 nM insulin (ins) for 24 hours compared to a vehicle control (0.2% EtOH). ATM p/t-ratio showed a decreased trend in two of the three biological replicates (B and C) in cells treated with a combination of ins and FFA compared to cells treated with ins alone and FFA alone. Data are presented as three individual experiments (A, B and C; technical n=2-3; normalised to total protein; mean ± SD).

ATM is an insulin-responsive protein kinase (Yang and Kastan, 2000), and its total protein levels are influenced under obese and insulin resistant conditions *in vivo* (Halaby *et al.*, 2008; Huisamen *et al.*, 2016). In the current *in vitro* study, we observed an effect on ATM p/t-ratio in response to a combination of FFAs and insulin compared to FFAs or insulin, individually. These results suggest that ATM activity, but not its protein levels, might be down-regulated in H9c2 cells by high concentrations of insulin and intracellular FFAs. To confirm the uptake of FFAs by the H9c2 cells, we will have to analyse the intracellular FFA concentration with a technique such as Raman spectroscopy (Uematsu *et al.*, 2020), which relies on the detection of molecular vibrations through laser light scattering.

We acknowledge that the ATM phosphorylation site under investigation (ser1981) corresponds with the nuclear activation of ATM in response to DNA damage (Bakkenist and Kastan, 2003), as well as its DNA damage-independent activation by ROS (Guo *et al.*, 2010), but it might not be a true reflection of the metabolic activity of ATM in response to insulin. To the best of our knowledge, no amino acid residue that is specifically phosphorylated in response to insulin stimulation has yet been identified, and ser1981 phosphorylation is generally used as an insulin-mediated activation site throughout literature.

No significant changes were observed in the total and phosphorylated levels of PKB **(*Figure 4.4*)**.

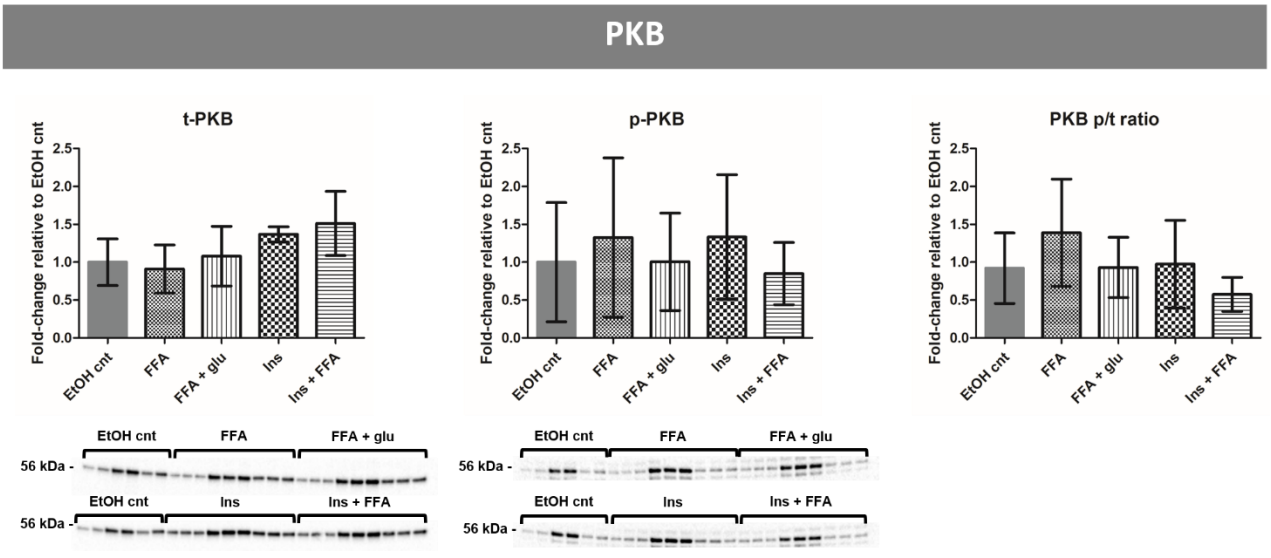

Figure 4.4: Total and phosphorylated levels of PKB in H9c2 cardiomyoblasts treated with combinations of nutrients and insulin for 24 hours.

PKB total (t) and phosphorylated (p) levels in H9c2 cells treated with combinations of 0.2 mM free fatty acids (FFA; palmitic and oleic), 5.5 mM glucose (glu) and 100 nM insulin (ins) for 24 hours compared to a vehicle control (0.2% EtOH). No significant changes were observed. Data of all three experiments are pooled (biological n=3; technical n=2-3; normalised to total protein; one-way ANOVA with Bonferroni post-test; mean ± SD).

Observing no significant changes in PKB activity were unexpected. Obesity is associated with various metabolic abnormalities, including peripheral insulin resistance, which can be facilitated by circulating FFAs secreted from WAT and/or introduced through diet. Oleic acid (mono-unsaturated FFA) and palmitic acid (saturated FFA) are the most abundant dietary and plasma FFAs, which respectively account for approximately 32% and 28% of total circulating FFAs (Staiger *et al.*, 2004). As such, the individual and combined effects of palmitic acid and oleic acid on cellular insulin sensitivity are well-established (Coll *et al.*, 2008; Kwon and Querfurth, 2015; Perdomo *et al.*, 2015). Palmitic acid treatment induces insulin resistance in C2C12 cells and cardiomyocytes by increasing intracellular DAG levels, which phosphorylates and inhibits IRS-1 and, subsequently, reduces PKB phosphorylation in response to insulin. Oleic acid treatment does not elicit this effect, and co-treatment of palmitic acid and oleic acid protects against palmitic acid-induced insulin resistance. Therefore, oleic acid preserves insulin sensitivity in the presence of palmitic acid.

In the current study, we considered the combined effect of equal concentrations of palmitic acid and oleic acid on PKB levels and phosphorylation, as the combination of these two FFAs more accurately reflects the circulating FFA profile in high-fat fed animals (Liu *et al.*, 2015). Assessing the individual effects of these FFAs, however, provides unique insights into the protective effect of oleic acid against the development of insulin resistance when co-treated with palmitic acid, an effect that is likely masked in our results. Therefore, we suggest that the absence of decreased PKB phosphorylation compared to the vehicle control is potentially due to the protective action of oleic acid against the palmitic acid-mediated attenuation of PKB phosphorylation.

No consistent effects were observed on the total and phosphorylated levels of mTORC1 **(*Figure 4.5*)** and AMPK **(*Figure 4.6*)**.

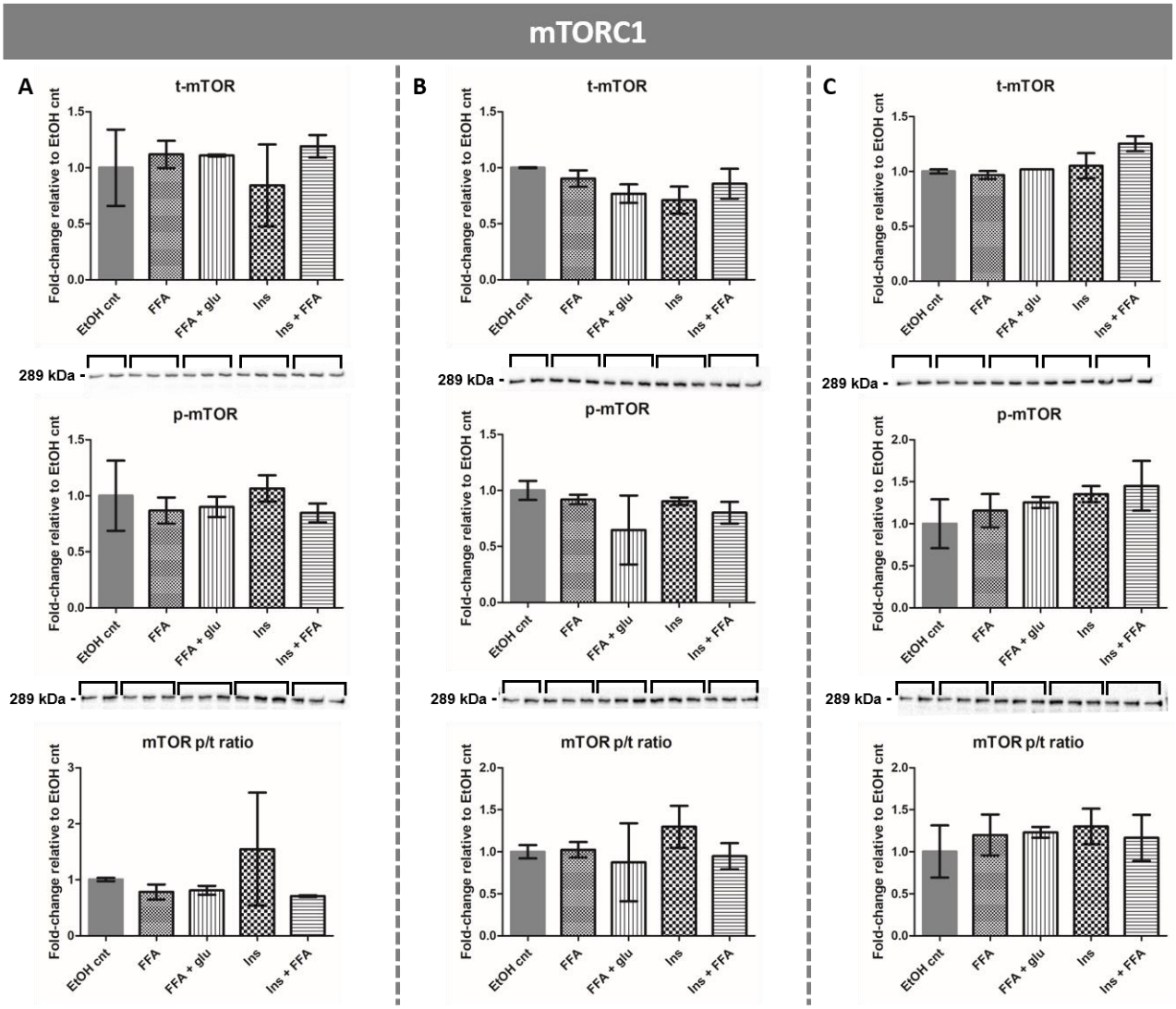

Figure 4.5: Total and phosphorylated levels of mTORC1 in H9c2 cardiomyoblasts treated with combinations of nutrients and insulin for 24 hours.

mTORC1 total (t) and phosphorylated (p) levels in H9c2 cells treated with combinations of 0.2 mM free fatty acids (FFA; palmitic and oleic), 5.5 mM glucose (glu) and 100 nM insulin (ins) for 24 hours compared to a vehicle control (0.2% EtOH). No consistent effects were observed. Data are presented as three individual experiments (A, B and C; technical n=2-3; normalised to total protein; mean ± SD).

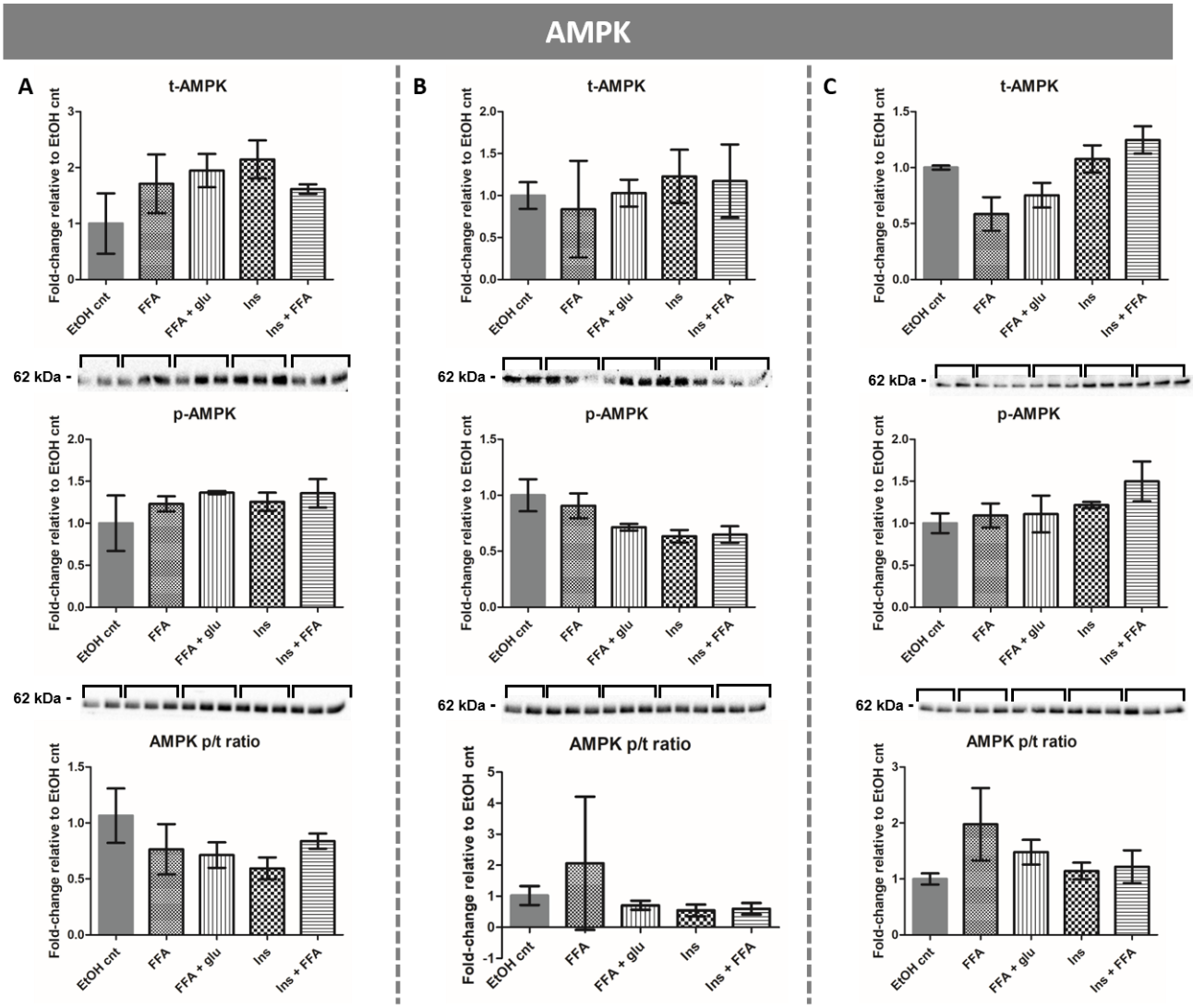

Figure 4.6: Total and phosphorylated levels of AMPK in H9c2 cardiomyoblasts treated with combinations of nutrients and insulin for 24 hours.

AMPK total (t) and phosphorylated (p) levels in H9c2 cells treated with combinations of 0.2 mM free fatty acids (FFA; palmitic and oleic), 5.5 mM glucose (glu) and 100 nM insulin (ins) for 24 hours compared to a vehicle control (0.2% EtOH). No consistent effects were observed. Data are presented as three individual experiments (A, B and C; technical n=2-3; normalised to total protein; mean ± SD).

Although the various treatment conditions seemed to impact the total and phosphorylated levels of mTORC1 and AMPK, no consistent effects were observed across the three biological experiments. The mTORC1 and AMPK pathways play major opposing roles in intracellular energy homeostasis. Saturated and unsaturated FFAs have been shown to differentially affect mTORC1 signalling in an AMPK-dependent manner. C2C12 cells treated with palmitic acid displayed dysregulation of the mTORC1 pathway, as evidenced by increased activation of Raptor (a regulatory subunit of the mTORC1), decreased phosphorylation of eukaryotic translation initiation factor 4E-binding protein 1 (4E-BP1; a down-stream target of mTORC1), increased phosphorylation of S6K (a down-stream target of mTORC1), and decreased phosphorylation of AMPK (a negative regulator of mTORC1),

but no change in mTORC1 activation (ser2448 phosphorylation). Co-treatment of C2C12 cells with palmitic acid and oleic acid completely restored these palmitic acid-induced alterations to levels comparable with the control-treated cells, highlighting the protective role of oleic acid against metabolic dysregulation (Kwon and Querfurth, 2015).

In the current study, we observed no consistent effects on mTORC1 or AMPK activities (p/t-ratios) in H9c2 cells treated with a combination of palmitic acid and oleic acid. Taken together, this might suggest that the protective action of oleic acid restores the palmitic acid-induced dysregulation of the mTORC1 and AMPK pathways. This will have to be confirmed by analysing the individual effects of the FFAs, as well as the effect on other proteins within the mTORC1 pathway.

4.4. Prolonged exposure to combinations of excess nutrients and insulin does not affect miR-421 or miR-18a levels in H9c2 cells

MiR-421 and miR-18a regulate ATM levels in cancer cells (Hu *et al.*, 2010; Song *et al.*, 2011; Shen and Houghton, 2013; Wu *et al.*, 2013), however they have not been associated with ATM regulation in a metabolic context. Therefore, we investigated whether miR-421 and miR-18a levels can be influenced by combinations of excess nutrients and/or insulin to potentially regulate ATM protein levels in H9c2 cells. Following 24 hours of treatment, the total RNA was extracted and the expression levels of miR-421 and miR-18a were determined with qRT-PCR. Each individual experiment (biological n=3) consisted of the respective treatment conditions performed in triplicate (technical n=3), which were pooled. Each pooled sample was analysed in duplicate and the fold-changes were calculated using the $2^{-\Delta\Delta Ct}$ method. U6 snRNA was used as endogenous control for normalisation. An ordinary one-way ANOVA was performed, followed by a Bonferroni post-hoc test, and data are presented as the mean fold-change ± SD relative to the vehicle (EtOH) control.

We observed no significant changes in miR-421 **(*Figure 4.7 A*)** and miR-18a **(*Figure 4.7 B*)** expression levels.

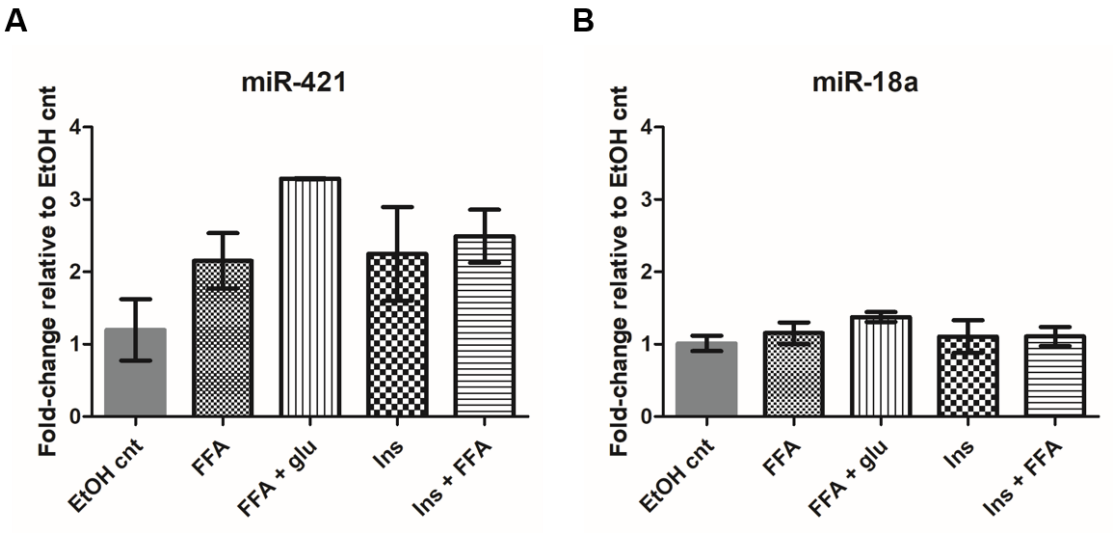

Figure 4.7: Expression levels of target miRNAs in H9c2 cardiomyoblasts treated with combinations of nutrients and insulin for 24 hours.

The relative expression levels of miR-421 (A) and miR-18a (B) in H9c2 cells treated with combinations of 0.2 mM free fatty acids (FFA: palmitic and oleic), 5.5 mM glucose (glu) and 100 nM insulin (ins) for 24 hours compared to a vehicle control (0.2% EtOH). No significant changes were observed (biological n=3; pooled technical n=3; normalised to U6 snRNA; $2^{-\Delta\Delta Ct}$ method; one-way ANOVA with Bonferroni post-test; mean ± SD).

In addition to cancer, abnormal miR-421 and miR-18a expression have been implicated in metabolic disorders. MiR-18a is down-regulated in the renal tissue of diabetic mice compared to non-diabetic mice (Xu *et al.*, 2017), whereas increased levels of miR-18a in human peripheral blood mononuclear cells is associated with an increased risk of developing type II diabetes (Wang *et al.*, 2017). On the other hand, miR-421 has been implicated in myocardial dysfunction relating to mitochondrial fragmentation (Wang *et al.*, 2015). The authors showed that the E2F1 transcription factor induced the expression of miR-421, which in turn suppressed the translation of the mitochondrial maintenance protein, Pink1. Reduced Pink1 levels resulted in mitochondrial fragmentation and subsequent cardiomyocyte apoptosis.

In the current study, no significant differences in miR-421 and miR-18a levels were observed, suggesting that miR-421 and miR-18a expression levels are not influenced by combinations of excess nutrients and/or insulin in H9c2 cells.

Chapter conclusion

Taken together, H9c2 cells seem to be metabolically sensitive to extracellular factors (glucose, FFAs and insulin), and is therefore an appropriate *in vitro* model to use for experiments with adipose-derived CM. Furthermore, cardiomyoblast ATM activity, rather than its protein levels, is likely

influenced by a combination of FFAs and insulin, whereas no significant effects on miR-421 and miR-18a expression levels were observed.

Chapter 5

Investigating the basal metabolic protein profiles of subcutaneous and visceral adipocytes harvested from lean and high-fat diet animals

Two WAT-associated pathologies that manifest during obesity are the ectopic fat deposition around abdominal organs, which is referred to as visceral adiposity, and the dysregulation of adipocyte metabolism and subsequent secretions. Although the central aim of this study is to investigate the effect of adipocyte secretions on cardiac metabolism in obesity, we first investigated whether differences in the basal metabolic protein profiles exist between adipocytes originating from the subcutaneous and visceral fat depots, and whether these profiles are influenced by diet **(*Figure 5.1*)**. ASCs retain an adipogenic memory of their *in vivo* environment, which is regained once differentiated in culture (Andersen *et al.*, 2019). Therefore, we investigated the total and phosphorylated levels of ATM, PKB, mTORC1, S6K, AMPK and ACC of adipocytes differentiated from visceral and subcutaneous ASCs harvested from lean and HFD rats through Western blot analysis. Each stain-free membrane included the ASCs and differentiated adipocytes (abbreviated as Adipo in figures) from the subcutaneous (abbreviated as SC in figures) and visceral (peri-renal; abbreviated as PR in figures) fat depots in triplicate (technical n=3) per rat (biological n=4 per diet). No common control was included, therefore the data are presented separately per rat and we were unable to compare results between the two diet groups. Rats A-D represent four control rats, whereas rats E-H represent four HFD rats within each figure. No statistical analyses were applied to the single biological replicates, and all data are presented as the mean fold-change ± SD relative to the SC ASCs. Results obtained for PKB and S6K could not be replicated and were excluded from the study. The p/t-ratio represents the phosphorylated protein as a fraction of the total protein and serves as an indicator of either protein activity (ATM, mTORC1 and AMPK) or inactivity (ACC).

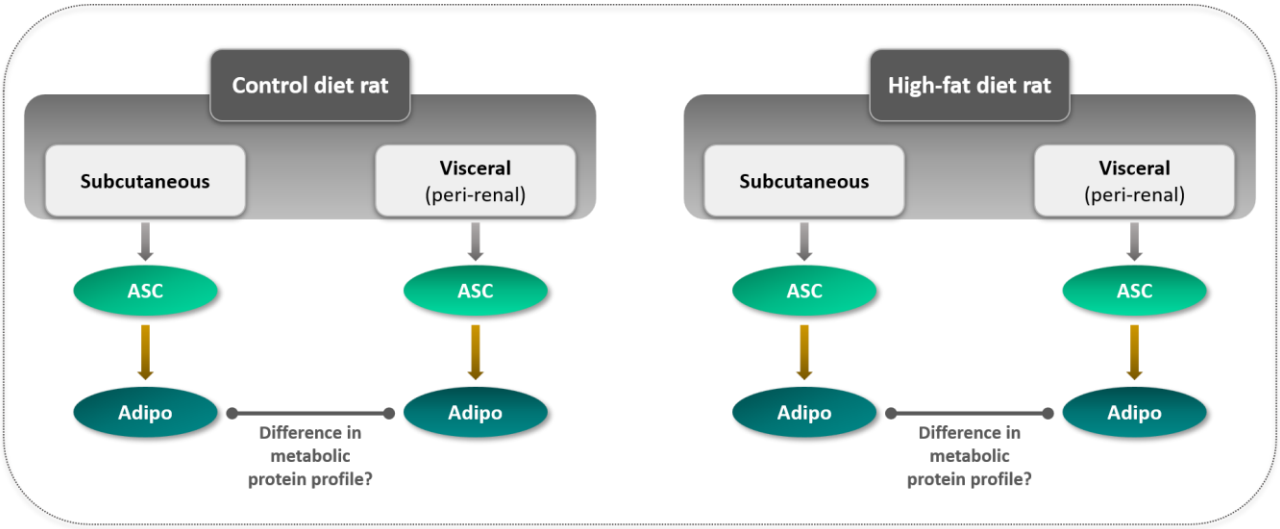

Figure 5.1: Schematic of the comparison between the basal metabolic profiles of adipocytes differentiated from subcutaneous and visceral ASCs harvested from control and HFD rats.

5.1. ATM

ATM protein levels seemed to be lower in the visceral adipocytes compared to the subcutaneous adipocytes in rats A (1.12 ± 0.18 vs. 1.60 ± 0.08) and C (0.57 ± 0.21 vs. 0.99 ± 0.08) under control conditions **(*Figure 5.2*)**, which was not observed under HFD conditions **(*Figure 5.3*)**. ATM phosphorylation (activation) and p/t-ratio did not appear to differ between the subcutaneous and visceral adipocytes in either diet group. Although the effect of adipocyte differentiation on the basal metabolic profiles was not an objective of this study, we observed a trend towards lower ATM activity (p/t-ratio) in the subcutaneous adipocytes compared to their ASC counterparts in control rats A (0.32 ± 0.11 vs. 1.03 ± 0.34), B (0.51 ± 0.14 vs. 1.02 ± 0.17) and D (0.31 ± 0.04 vs. 1.03 ± 0.30) and HFD rats E (0.24 ± 0.08 vs. 1.03 ± 0.23) and F (0.32 ± 0.05 vs. 1.00 ± 0.24). This potential differentiation-dependent effect will not be discussed but is worth mentioning.

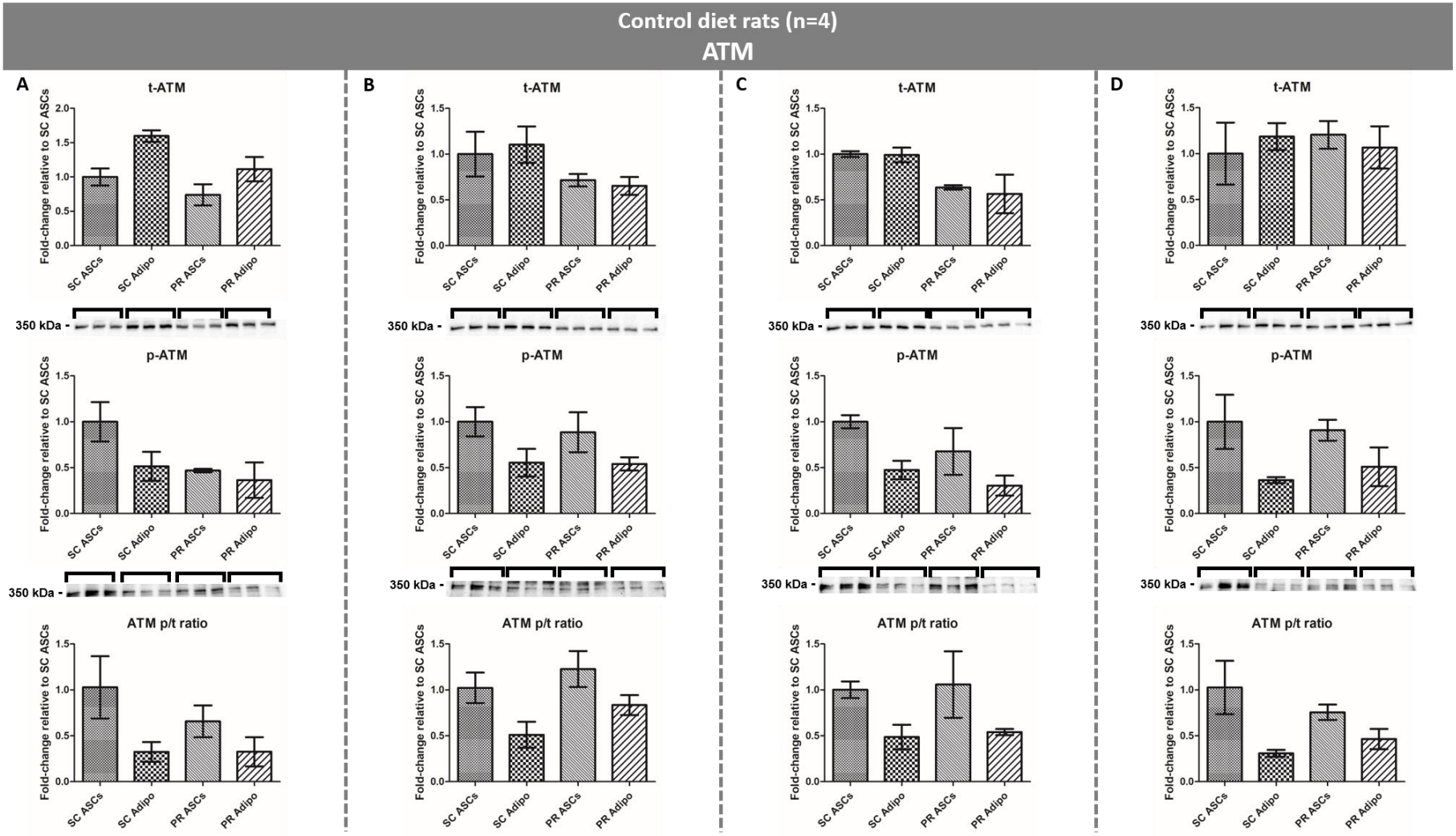

Figure 5.2: Total and phosphorylated levels of ATM in adipose-derived cells that originated from control diet rats.

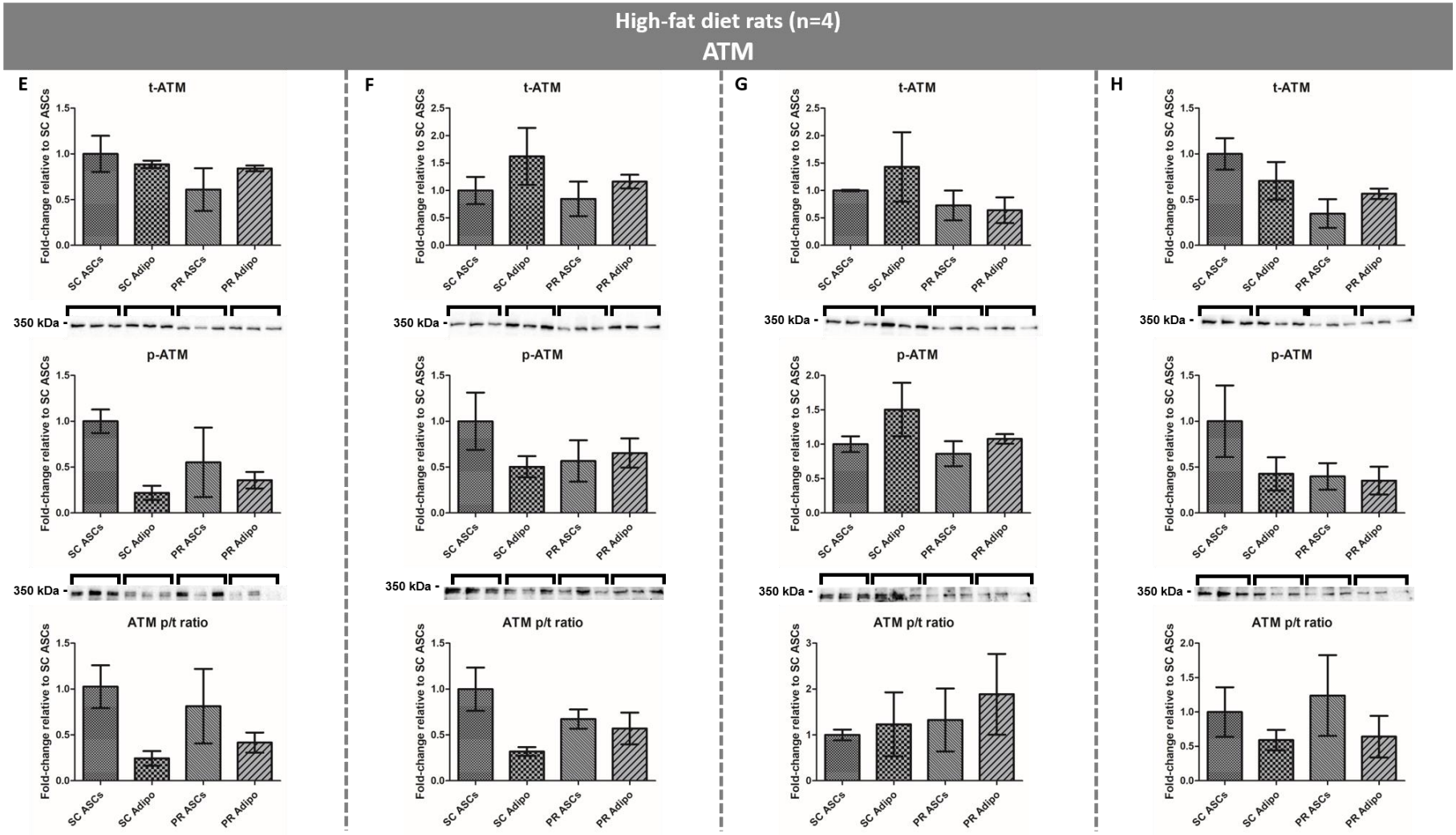

Figure 5.3: Total and phosphorylated levels of ATM in adipose-derived cells that originated from HFD rats.

Total (t) and phosphorylated (p) levels of ATM in adipose stem cells (ACSs) and differentiated adipocytes (Adipo) originating form subcutaneous (SC) and visceral (PR) depots of control diet (A-D) and HFD (E-H) rats. Total ATM levels seemed to be lower in visceral compared to subcutaneous adipocytes under control conditions, but not HFD conditions (biological n=4 per diet group; technical n=3; normalised to total protein; mean ± SD).

The metabolic role of ATM has been widely investigated in various cell and tissue types, however studies investigating its role in adipocyte metabolism remain limited. Le Guezennec *et al*. showed that *ApoE*$^{-/-}$ mice deficient in Wip1, a protein phosphatase responsible for ATM dephosphorylation (inhibition), displayed a reduction in overall lipid accumulation and visceral fat depot size compared to *ApoE*$^{-/-}$ *Wip1*$^{+/+}$ mice (Le Guezennec *et al.*, 2012). While the focus of their study was on the role of ATM regulation in foam cell formation during the development of atherosclerosis, their data suggest that ATM protects against WAT accumulation, particularly in the visceral depot. In a pioneering study by Takagi and colleagues, a novel role for ATM in adipose tissue distribution and adipogenesis (adipocyte differentiation) was described (Takagi *et al.*, 2015). The authors showed that *Atm*$^{-/-}$ mice displayed a shift towards increased visceral WAT accumulation at the expense of subcutaneous accumulation compared to wild-type mice, confirming that ATM protects against visceral obesity. *In vitro* experiments with mouse embryonic fibroblasts (MEFs) derived from *Atm*$^{-/-}$ mice further revealed that ATM plays a central role in initiating the adipocyte differentiation program through the induction of C/EBPα and PPARγ.

In the current study, ATM levels appeared to be lower in visceral adipocytes compared to subcutaneous adipocytes originating from lean rats, however this did not necessarily result in lower ATM phosphorylation (activation). No apparent differences in ATM levels or phosphorylation were observed between the subcutaneous and visceral adipocytes originating from HFD rats. Based on previous studies, ATM activity is inversely related to lipid accumulation. Our data indicate similar levels of ATM activity between subcutaneous and visceral adipocytes, which is consistent with the observation that there was no significant difference in intracellular lipid quantity between subcutaneous and visceral adipocytes (refer to Appendix A ***Figure A2*** for lipid quantification analysis). Taken together, our results suggest that there is no difference in lipid accumulation between subcutaneous and visceral adipocytes under control or HFD conditions in the rat model that this study is based on.

To the best of our knowledge, no prior study has investigated the total or phosphorylated levels of ATM in adipocytes originating from the visceral and subcutaneous fat depots under control or HFD conditions.

5.2. mTORC1

No apparent differences in total or phosphorylated (activated) mTORC1 levels were observed between the subcutaneous and visceral adipocytes under control **(*Figure 5.4*)** or HFD **(*Figure 5.5*)** conditions.

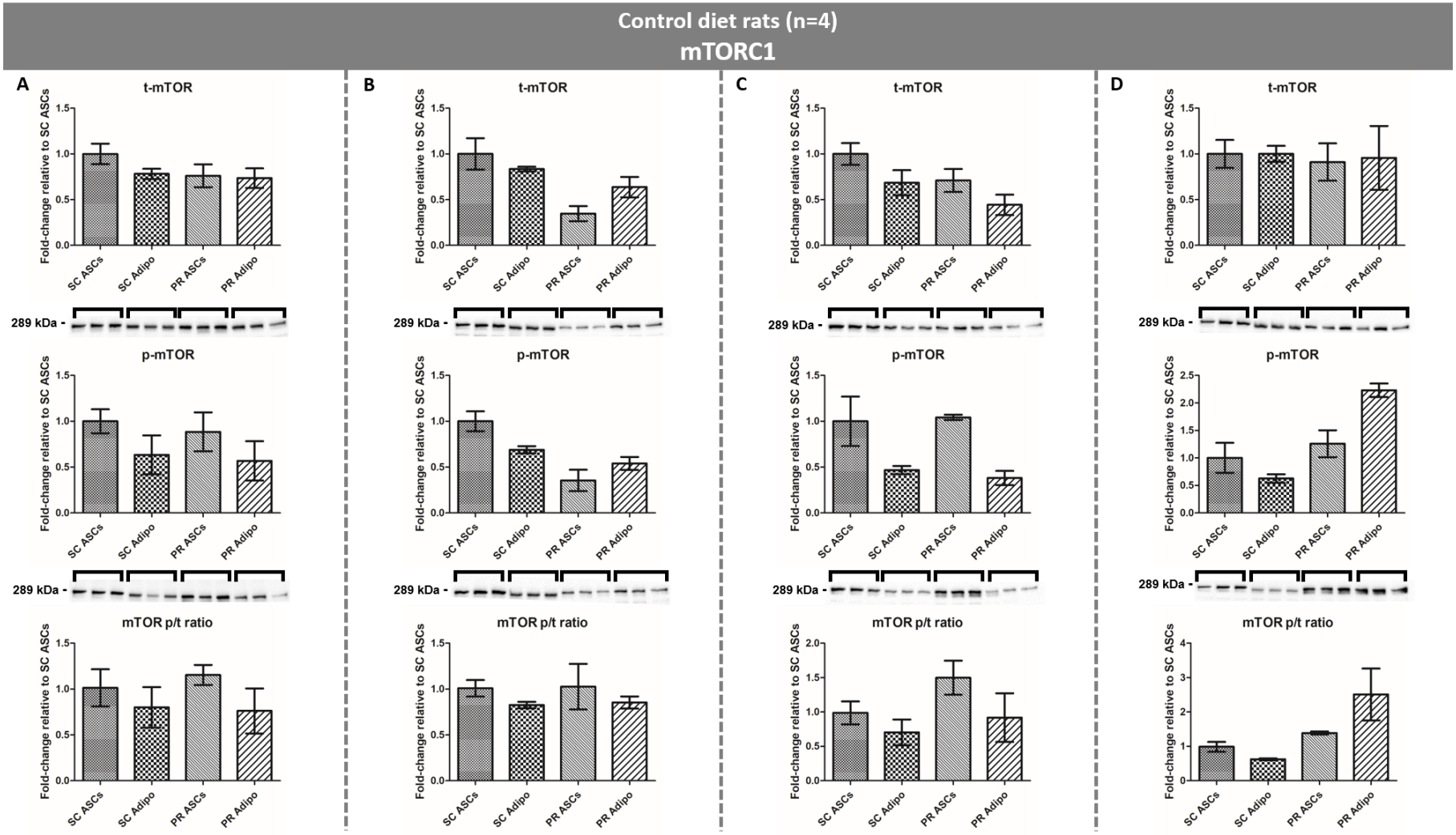

Figure 5.4: Total and phosphorylated levels of mTORC1 in adipose-derived cells that originated from control diet rats.

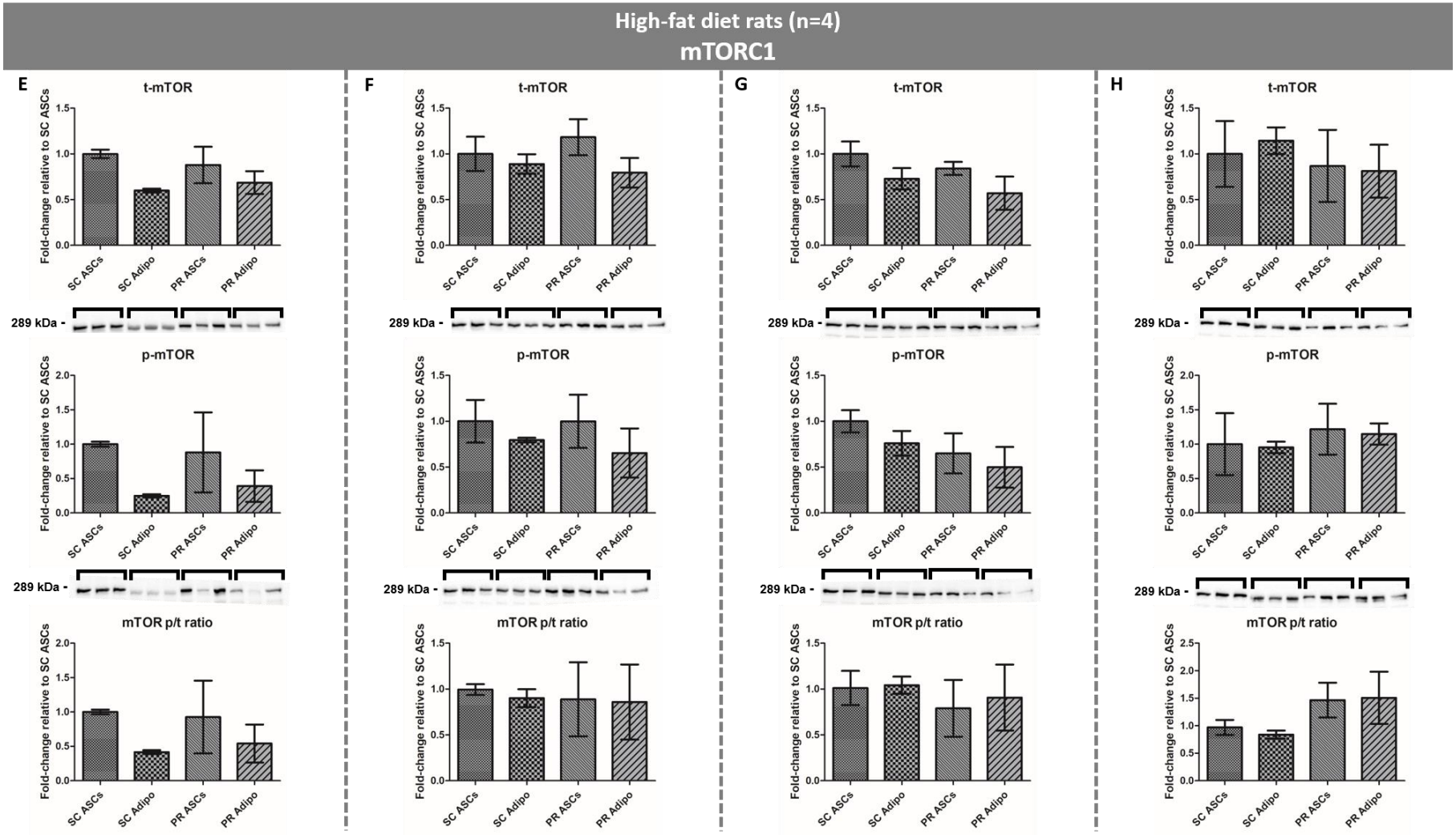

Figure 5.5: Total and phosphorylated levels of mTORC1 in adipose-derived cells that originated from HFD rats.

Total (t) and phosphorylated (p) levels of mTORC1 in adipose stem cells (ACSs) and differentiated adipocytes (Adipo) originating form subcutaneous (SC) and visceral (PR) depots of control diet (A-D) and HFD (E-H) rats. No apparent differences in total or phosphorylated mTORC1 levels were observed between subcutaneous and visceral adipocytes in either diet group (biological n=4 per diet group; technical n=3; normalised to total protein; mean ± SD).

mTORC1 is a master regulator of various aspects of adipocyte metabolism. Specifically, mTORC1 plays a central role in nutrient- and insulin-mediated adipogenesis (Bell, Grunder and Sorisky, 2000; Kim and Chen, 2004) and lipid accumulation (Polak *et al.*, 2008; Chang *et al.*, 2009) by positively regulating the expression of adipogenic and lipogenic genes. Obesity is characterised by increased WAT size, especially in the visceral depot, which arises from increased adipogenesis and fat accumulation. As such, mTORC1 activity is markedly up-regulated in various tissue types, including WAT, of obese animals (Um *et al.*, 2004; Khamzina *et al.*, 2005; Tremblay *et al.*, 2007).

In the current study, no apparent differences in mTORC1 levels or phosphorylation (activation) were observed between the subcutaneous and visceral adipocytes under control or HFD conditions. Similar to ATM, our data indicate no difference in mTORC1 activity between subcutaneous and visceral adipocytes, which is consistent with similar intracellular lipid quantities (refer to Appendix A ***Figure A2*** for lipid quantification analysis). Taken together, our results suggest that there is no difference in lipid accumulation between subcutaneous and visceral adipocytes under control or HFD conditions in the rat model that this study is based on.

5.3. AMPK

AMPK protein levels seemed to be lower in the visceral adipocytes compared to the subcutaneous adipocytes in control rats B (0.69 ± 0.12 vs. 2.28 ± 0.16) and D (1.02 ± 0.02 vs. 2.19 ± 0.24) (***Figure 5.6***) and HFD rats E (1.97 ± 0.41 vs. 4.50 ± 0.45) and H (1.97 ± 0.31 vs. 5.36 ± 0.40) (***Figure 5.7***). No apparent differences in AMPK phosphorylation (activation) or p/t-ratio were observed between subcutaneous and visceral adipocytes under control or HFD conditions.

Although the effect of adipocyte differentiation on the basal metabolic profiles was not an objective of this study, we observed a trend towards higher AMPK total protein levels in the subcutaneous adipocytes compared to their ASC counterparts in control rats B (2.28 ± 0.16 vs. 1.00 ± 0.05), C (1.36 ± 0.09 vs. 1.00 ± 0.10) and D (2.19 ± 0.24 vs. 1.00 ± 0.07) and HFD rats E (4.50 ± 0.45 vs. 1.00 ± 0.19), F (2.00 ± 0.32 vs. 1.00 ± 0.12) and H (5,36 ± 0.40 vs. 1.00 ± 0.13). We also observed this trend between visceral adipocytes and their ASC counterparts in all four control rats (A: 1.00 ± 0.12 vs. 0.57 ± 0.07, B: 0.69 ± 0.12 vs. 0.13 ± 0.03, C: 1.74 ± 0.14 vs. 1.29 ± 0.10, D: 1.02 ± 0.02 vs. 0.30 ± 0.12) and HFD rats E (1.97 ± 0.41 vs. 0.57 ± 0.18), F (3.29 ± 0.50 vs. 1.50 ± 0.12) and H (1.97 ± 0.31 vs. 0.39 ± 0.06).

Interestingly, AMPK activity (p/t-ratio) appeared to be lower in the subcutaneous adipocytes compared to their ASC counterparts in control rats A (0.38 ± 0.17 vs. 1.00 ± 0.15), B (0.19 ± 0.05 vs. 1.00 ± 0.04) and D (0.20 ± 0.05 vs. 1.00 ± 0.12) and HFD rats E (0.08 ± 0.01 vs. 1.00 ± 0.20), F (0.30 ± 0.07 vs. 1.00 ± 0.10) and H (0.08 ± 0.01 vs. 1.00 ± 0.13). We observed a similar trend in the visceral

adipocytes compared to their ASC counterparts in control rats B (0.33 ± 0.01 vs. 1.32 ± 0.15), C (0.44 ± 0.31 vs. 1.29 ± 0.34) and D (1.71 ± 0.19 vs. 6.28 ± 1.83) and all four HFD rats (E: 0.20 ± 0.13 vs. 1.66 ± 0.97, F: 0.09 ± 0.07 vs. 0.85 ± 0.15, G: 0.30 ± 0.26 vs. 1.45 ± 0.37, H: 0.13 ± 0.01 vs. 1.69 ± 0.49). Again, this differentiation-dependent effect will not be discussed but is worth mentioning.

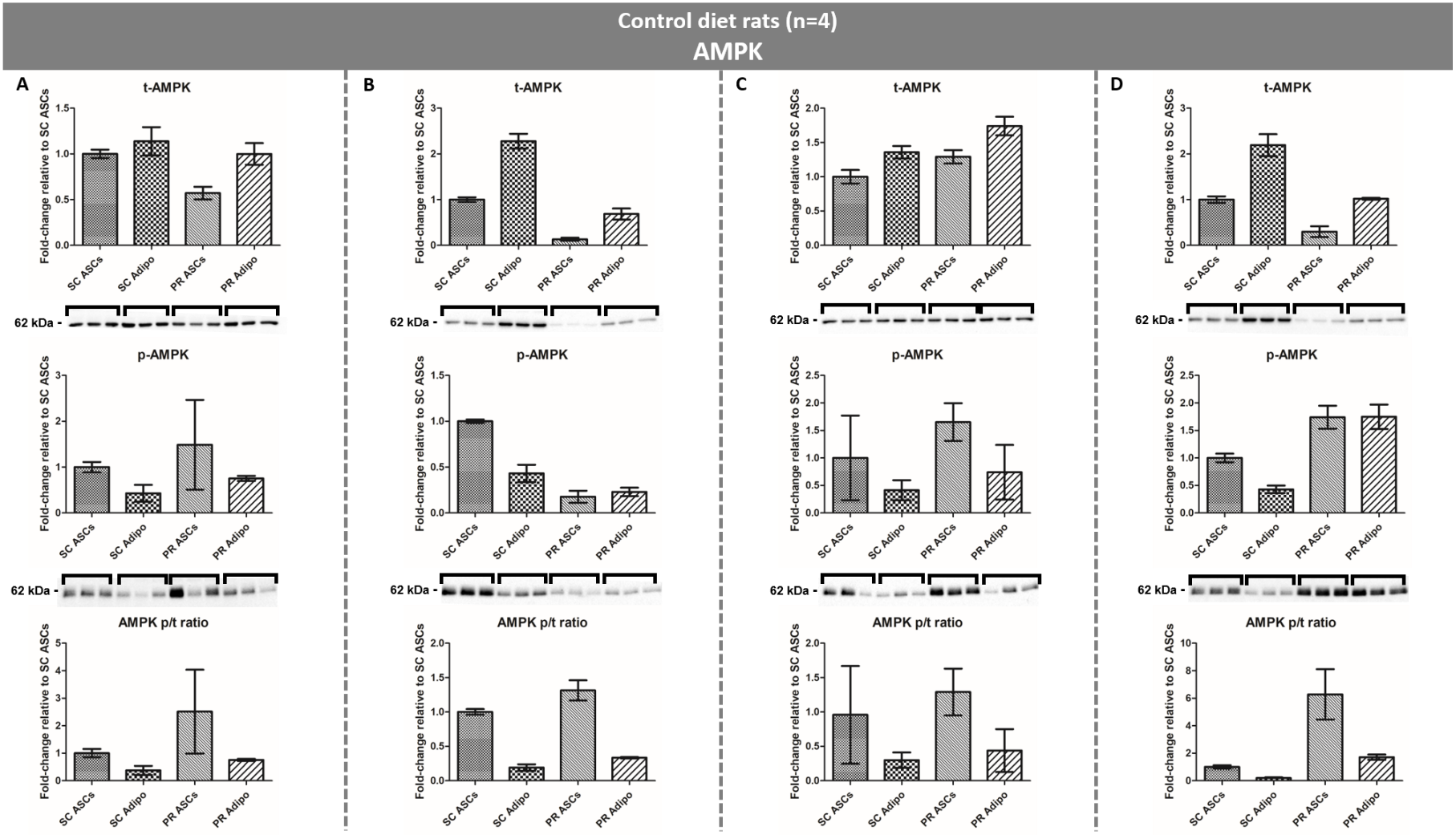

Figure 5.6: Total and phosphorylated levels of AMPK in adipose-derived cells that originated from control diet rats.

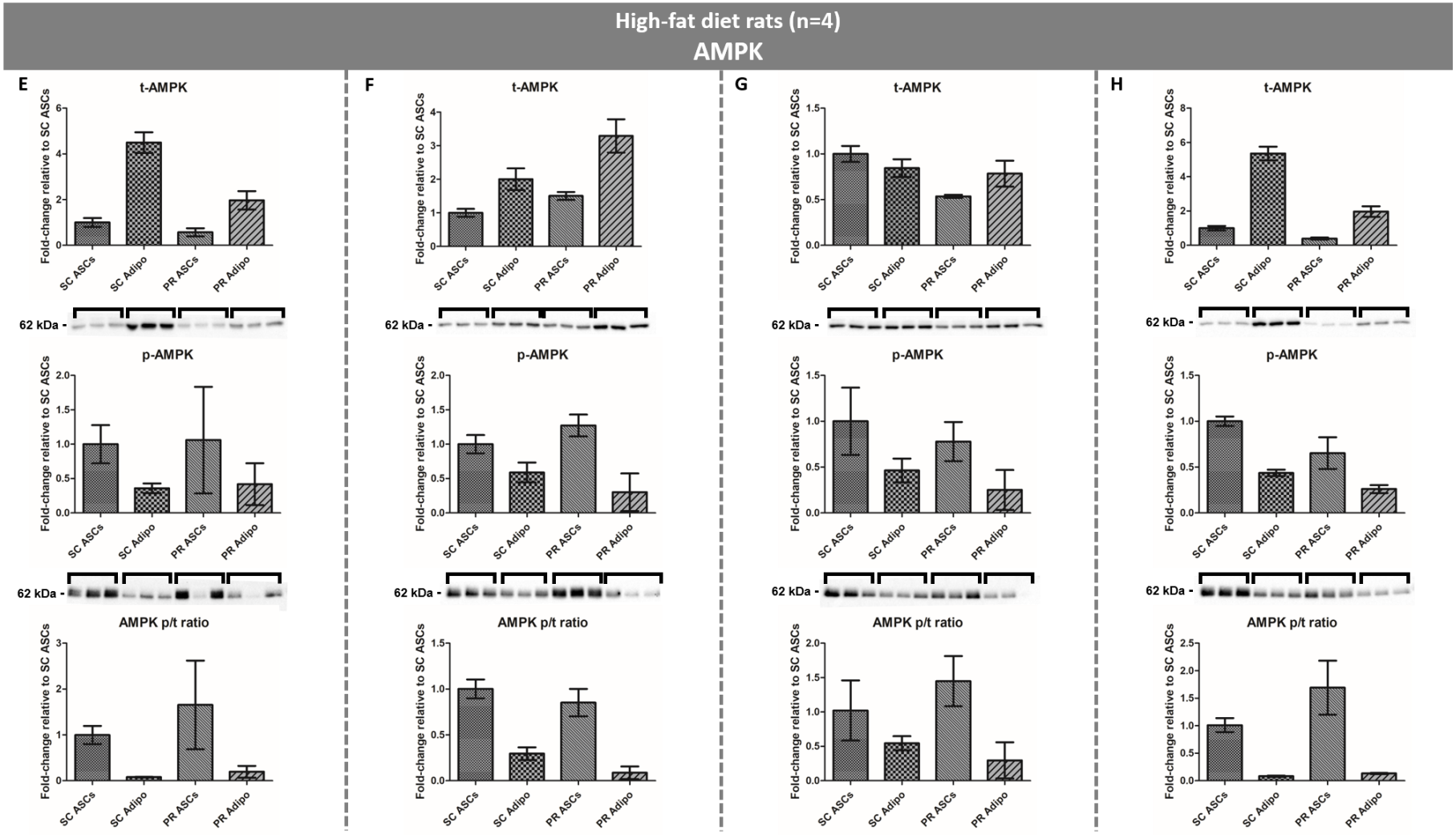

Figure 5.7: Total and phosphorylated levels of AMPK in adipose-derived cells that originated from HFD rats.

Total (t) and phosphorylated (p) levels of AMPK in adipose stem cells (ACSs) and differentiated adipocytes (Adipo) originating form subcutaneous (SC) and visceral (PR) depots of control diet (A-D) and HFD (E-H) rats. Total AMPK levels seemed to be lower in visceral compared to subcutaneous adipocytes in both diet groups (biological n=4 per diet group; technical n=3; normalised to total protein; mean ± SD).

AMPK is another major regulator of adipocyte metabolism. Activated AMPK limits lipid accumulation (Villena *et al.*, 2004) and FFA secretion (Anthony, Gaidhu and Ceddia, 2009), while promoting β-oxidation (Kim *et al.*, 2016). Abnormal AMPK expression or function in WAT has therefore been implicated in obesity and associated metabolic conditions. AMPK activity is down-regulated by overnutrition during obesity (Coughlan *et al.*, 2013), which is associated with the development of insulin resistance (Xu *et al.*, 2012). This is because decreased AMPK activity results in increased mTORC1/S6K signalling, which in turn suppresses the insulin-mediated pathway through negative feedback inhibition of IRS-1 (Saha *et al.*, 2011). Interestingly, AMPK activity was found to be lower in the visceral compared to subcutaneous WAT of obese individuals (Gauthier *et al.*, 2011), highlighting a distinction between the two fat depots in obesity.

In the current study, AMPK levels seemed to be lower in visceral adipocytes compared to subcutaneous adipocytes originating from lean and HFD rats, however this was not necessarily accompanied by lower AMPK phosphorylation (activation). Similar to ATM and mTORC1, our data indicate no apparent difference in AMPK activity between subcutaneous and visceral adipocytes, which is consistent with similar intracellular lipid quantities (refer to Appendix A ***Figure A2*** for lipid quantification analysis). Taken together, our results suggest that there is no difference in lipid accumulation between subcutaneous and visceral adipocytes under control or HFD conditions in the rat model that this study is based on.

5.4. ACC

Acetyl-coenzyme A carboxylase (ACC) was expressed in the adipocytes, but not the ASCs, originating from both fat depots under control **(*Figures 5.8*** and ***5.10*)** and HFD **(*Figures 5.9*** and ***5.11*)** conditions. ACC is an important enzyme that regulates fatty acid metabolism by catalysing the conversion of acetyl-coA to malonyl-coA. In turn, malonyl-coA serves a dual function as either a substrate for lipogenesis or an inhibitor of CPT1-mediated transport of fatty acids into the mitochondria, thereby limiting β-oxidation. This dual function is dependent on the respective actions of the two main ACC isoforms: ACC1 and ACC2 (Munday, 2002).

5.4.1. ACC1

Total and phosphorylated (inhibited) levels of ACC1 seemed to be lower in the visceral adipocytes compared to subcutaneous adipocytes in control rats B (total: 0.05 ± 0.04 vs. 1.00 ± 0.06, phospho: 0.004 ± 0.003 vs. 1.00 ± 0.13), C (total: 0.57 ± 0.10 vs. 1.00 ± 0.11, phospho: 0.36 ± 0.15 vs. 1.00 ± 0.31) and D (total: 0.19 ± 0.04 vs. 1.00 ± 0.07, phospho: 0.07 ± 0.03 vs. 1.00 ± 0.11) (***Figure 5.8***) and HFD rats E (total: 0.22 ± 0.09 vs. 1.00 ± 00.19, phospho: 0.12 ± 0.04 vs. 1.00 ± 0.27), G (total:

0.45 ± 0.05 vs. 1.00 ± 0.10, phospho: 0.50 ± 0.08 vs. 1.00 ± 0.12) and H (total: 0.29 ± 0.08 vs. 1.00 ± 0.18, phospho: 0.06 ± 0.05 vs. 1.00 ± 0.45) (***Figure 5.9***).

ACC1 p/t-ratio, an indicator of ACC1 inactivity, appeared to be lower in visceral adipocytes compared to subcutaneous adipocytes in control rats B (0.16 ± 0.16 vs. 1.00 ± 0.08) and D (0.34 ± 0.12 vs. 1.00 ± 0.16) and HFD rats F (0.61 ± 0.16 vs. 1.00 ± 0.14) and H (0.23 ± 0.20 vs. 1.00 ± 0.26).

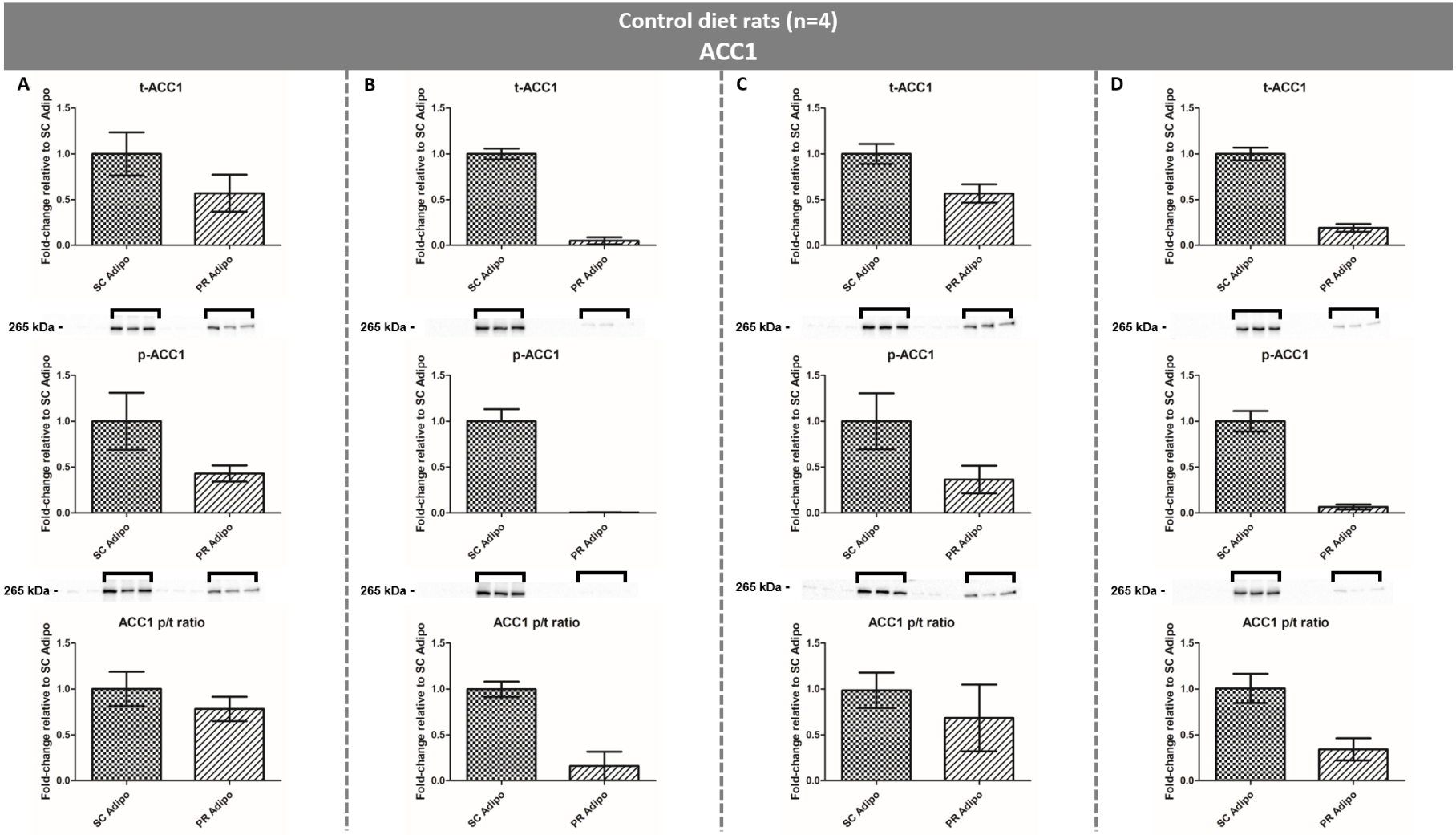

Figure 5.8: Total and phosphorylated levels of ACC1 in adipose-derived cells that originated from control diet rats.

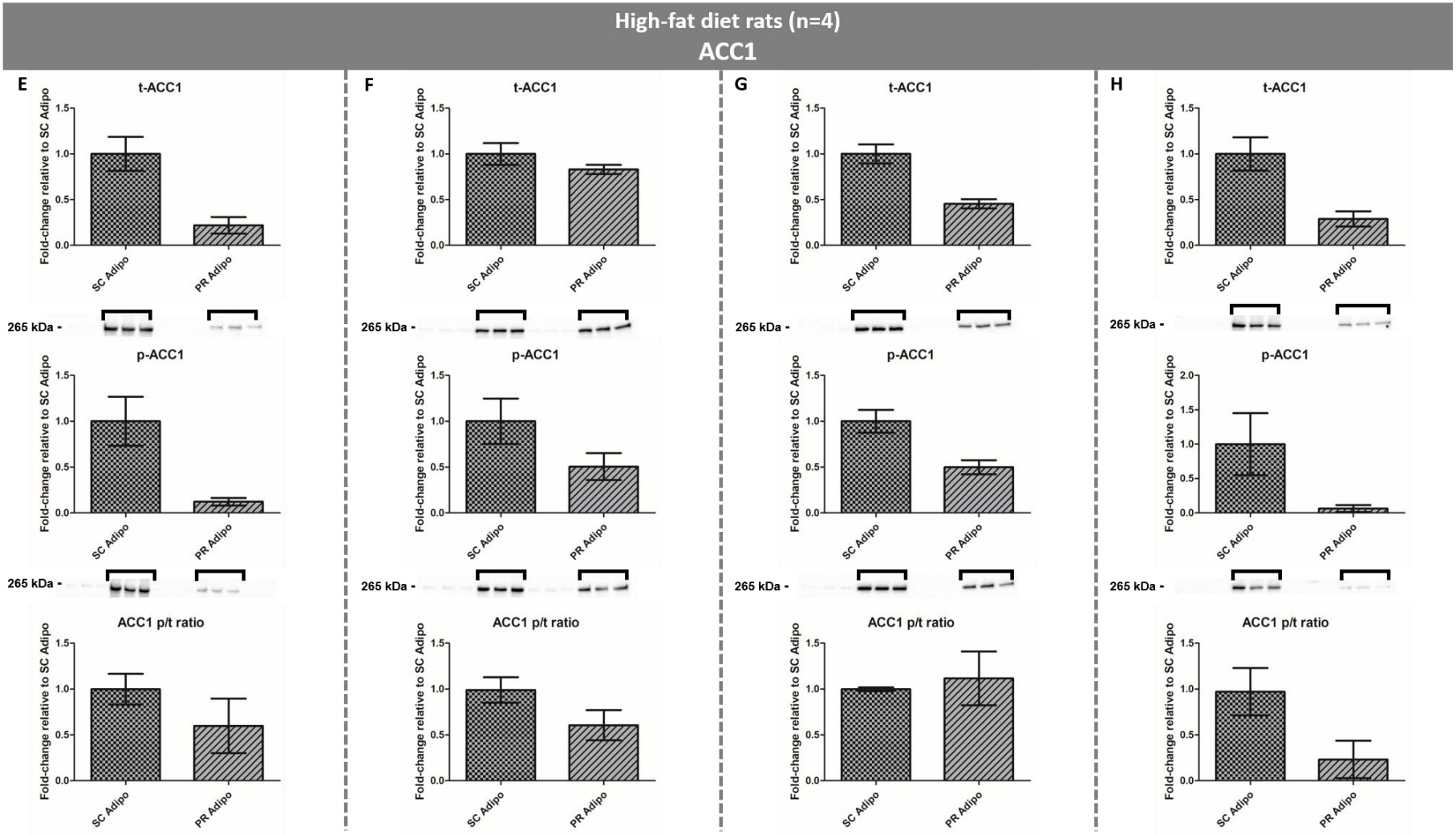

Figure 5.9: Total and phosphorylated levels of ACC1 in adipose-derived cells that originated from HFD rats.

Total (t) and phosphorylated (p) levels of ACC1 expressed in differentiated adipocytes (Adipo) originating from the subcutaneous (SC) and visceral (PR) depots of control diet (A-D) and HFD (E-H) rats. Total and phosphorylated levels seemed to be lower in visceral compared to subcutaneous adipocytes in both diet groups (biological n=4 per diet group; technical n=3; normalised to total protein; mean ± SD).

Although ACC1 is widely expressed in the cytoplasm of various tissue types, its expression is enriched within WAT because the malonyl-coA product specifically feeds into the lipogenesis pathway. Once phosphorylated on ser79 by AMPK, ACC1 is inhibited and lipogenesis is subsequently blocked (Hardie and Pan, 2002). The role of ACC1 in the development of obesity-associated pathology has been investigated, however results remain inconclusive. ACC1 expression (mRNA levels) was reported to be lower in the subcutaneous WAT of obese individuals compared to that of lean individuals, with no difference in expression in visceral WAT (Auguet *et al.*, 2014; Guiu-Jurado *et al.*, 2015). These results suggest that lipogenesis in the subcutaneous depot is reduced during obesity, whereas lipogenesis in the visceral depot remains unchanged. In contrast, Ortega and colleagues reported a decrease in ACC1 expression in the visceral WAT of obese individuals compared to that of lean individuals (Ortega *et al.*, 2010), suggesting that lipogenesis in the visceral depot is in fact affected by obesity.

In the current study, ACC1 was exclusively expressed in the adipocytes, and not the ASCs. ACC1 levels seemed to be lower in the visceral adipocytes compared to the subcutaneous adipocytes under control and HFD conditions. ACC1 phosphorylation (inhibition) also appeared lower in the visceral adipocytes compared to the subcutaneous adipocytes in both diet groups, which could be explained by the lower amount of ACC1 protein available for phosphorylation in the visceral adipocytes. Interestingly, the p/t-ratios seemed to be lower in the visceral adipocytes compared to the subcutaneous adipocytes in both diet groups, suggesting that a bigger proportion of ACC1 is in the non-phosphorylated activated state in the visceral adipocytes. However, since the absolute levels of active ACC1 within the subcutaneous and visceral adipocytes are unknown, the biological significance of the observation is unclear. Lastly, we are unable to correlate AMPK phosphorylation (activation) with ACC1 phosphorylation (inhibition), since ACC1 displays differential total protein levels between the subcutaneous and visceral adipocytes.

5.4.2. ACC2

Total and phosphorylated (inhibited) ACC2 levels seemed to be lower in the visceral adipocytes compared to subcutaneous adipocytes in control rats A (total: 0.36 ± 0.17 vs. 1.00 ± 0.06, phospho: 0.34 ± 0.20 vs. 1.00 ± 0.25), B (total: 0.06 ± 0.05 vs. 1.00 ± 0.14, phospho: 0.004 ± 0.0008 vs. 1.00 ± 0.29) and D (total: 0.14 ± 0.03 vs. 1.00 ± 0.13, phospho: 0.06 ± 0.02 vs. 1.00 ± 0.26) (***Figure 5.10***) and HFD rats E (total: 0.34 ± 0.16 vs. 1.00 ± 0.07, phospho: 0.31 ± 0.10 vs. 1.00 ± 0.36) and H (total: 0.39 ± 0.14 vs. 1.00 ± 0.19, phospho: 0.08 ± 0.03 vs. 1.00 ± 0.19) (***Figure 5.11***). ACC2 was not detected in visceral adipocytes from rat G. ACC2 p/t-ratio, an indicator of ACC2 inactivity, appeared to be lower in visceral adipocytes compared to subcutaneous adipocytes in control rat B (0.15 ± 0.17 vs. 1.00 ± 0.25) and HFD rat H (0.22 ± 0.10 vs. 1.00 ± 0.25).

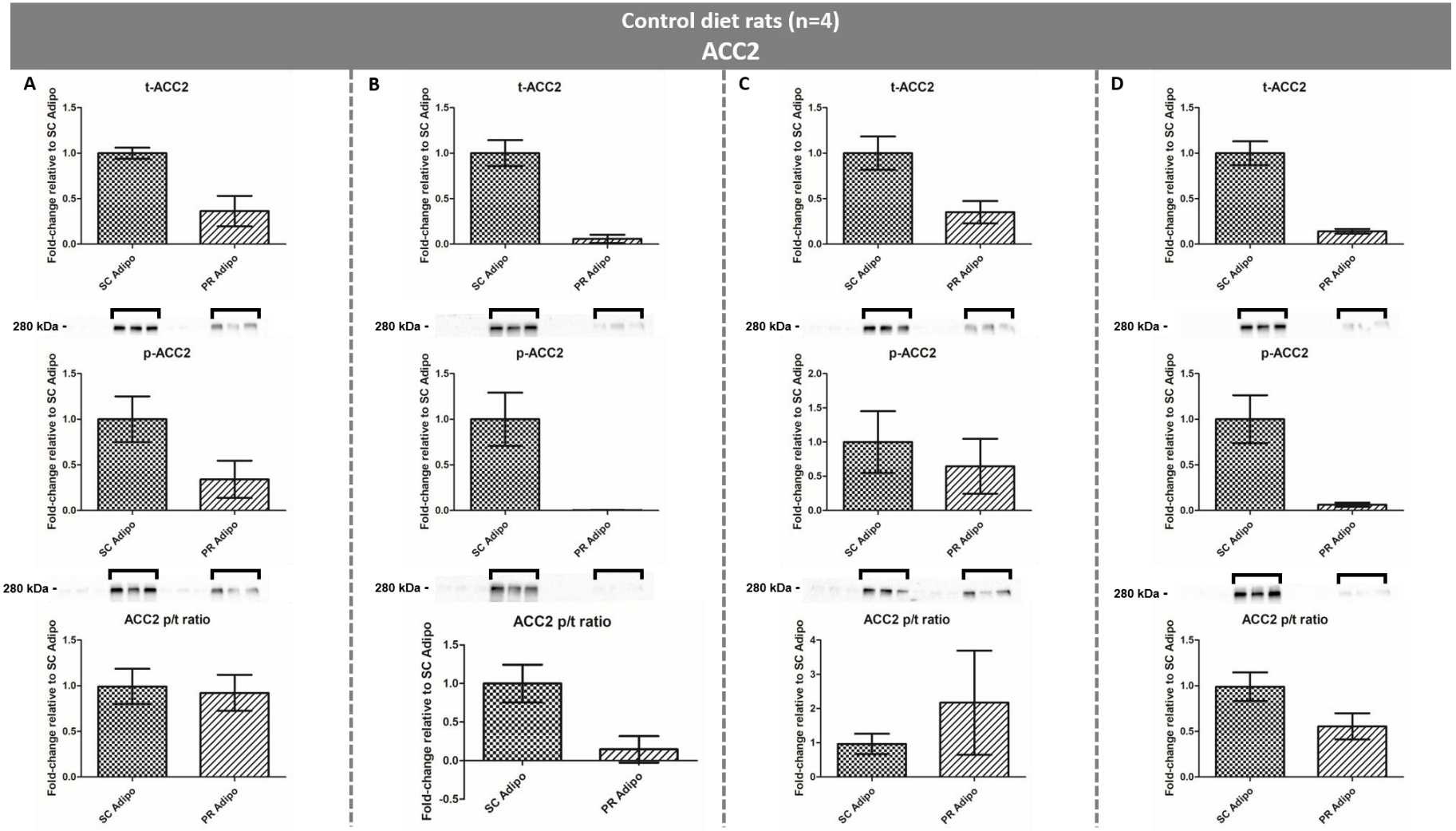

Figure 5.10: Total and phosphorylated levels of ACC2 in adipose-derived cells that originated from control diet rats.

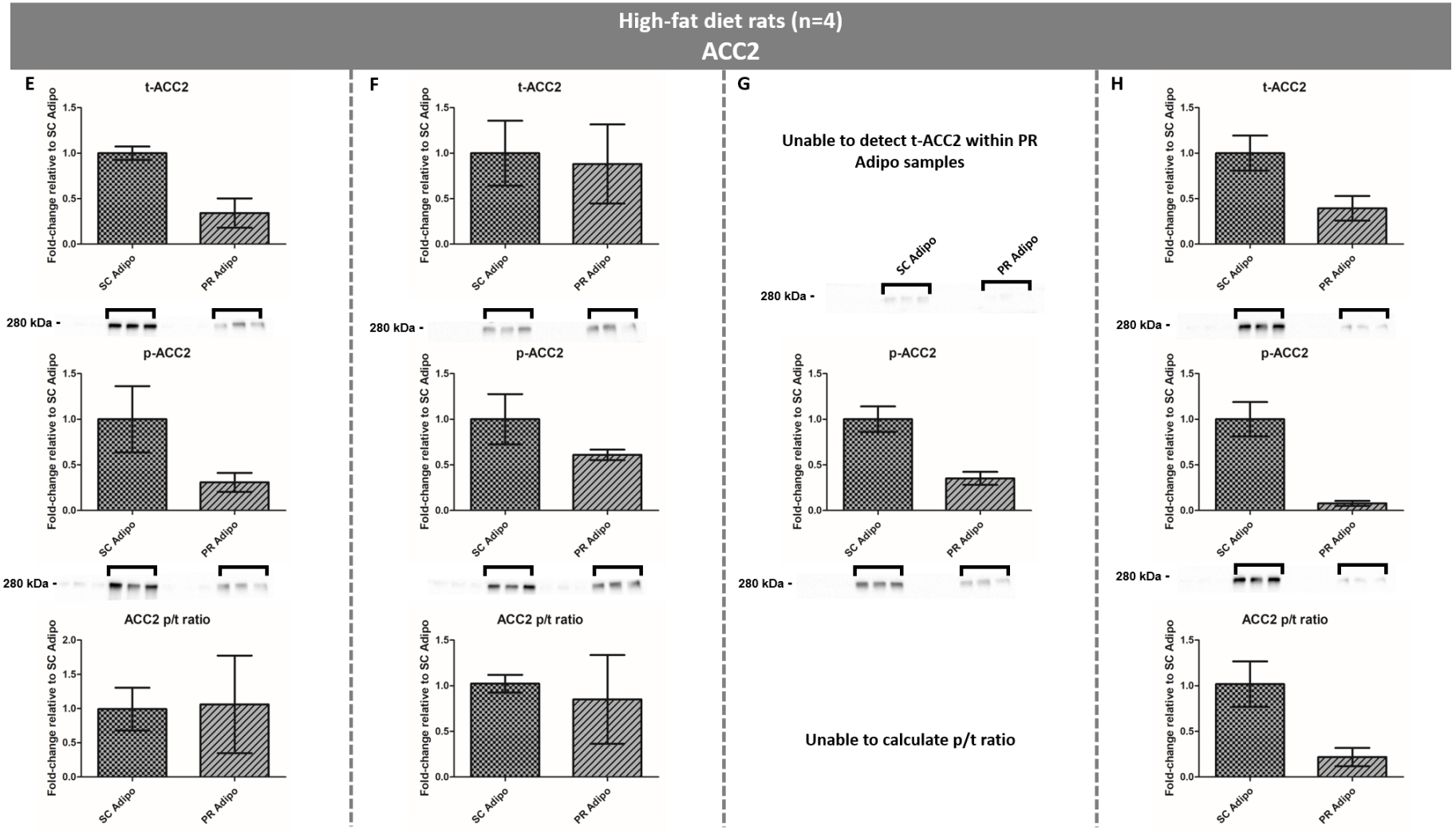

Figure 5.11: Total and phosphorylated levels of ACC2 in adipose-derived cells that originated from HFD rats.

Total (t) and phosphorylated (p) levels of ACC2 expressed in differentiated adipocytes (Adipo) originating from the subcutaneous (SC) and visceral (PR) depots of control diet (A-D) and HFD (E-H) rats. Total and phosphorylated levels seemed to be lower in visceral compared to subcutaneous adipocytes in both diet groups. ACC2 was not detected in the visceral adipocytes of rat G (biological n=4 per diet group; technical n=3; normalised to total protein; mean ± SD).

ACC2 is highly expressed in oxidative tissues of animals such as skeletal muscle and cardiac tissue, with lower expression in WAT (Oh *et al.*, 2005). Whereas ACC1 is mainly localised in the cytoplasm, ACC2 co-localises with the CPT1 transporter in the mitochondrial membrane, where its malonyl-coA product inhibits CPT1-mediated β-oxidation (Wakil and Abu-Elheiga, 2009). ACC2 is also a down-stream target of AMPK, which phosphorylates and inhibits ACC2 on an amino acid residue (ser219) that is the conserved equivalent of ser79 in ACC1 (Hardie and Pan, 2002). The role of ACC2 in obesity has been described in various other tissues. ACC2 expression was shown to be up-regulated in the liver, pancreas and skeletal muscle of obese and diabetic rats compared to lean control rats (Kreuz *et al.*, 2009). Furthermore, ACC2-deficient mice on a HFD were protected against obesity and the development of type II diabetes, partly due to increased β-oxidation in the skeletal muscle and liver (Abu-Elheiga *et al.*, 2003). Because ACC2 is not the predominant isoform in animal WAT (Oh *et al.*, 2005), its role in WAT-related pathology during obesity requires further investigation.

In the current study, ACC2 was exclusively expressed in the adipocytes, and not in ASCs. Similar to ACC1, ACC2 total and phosphorylated (inhibited) levels showed a trend towards lower levels in the visceral adipocytes compared to the subcutaneous adipocytes under control and HFD conditions. The p/t-ratios were not necessarily lower in the visceral adipocytes compared to the subcutaneous adipocytes in both diet groups, suggesting that a similar proportion of ACC2 is in the non-phosphorylated activated state in visceral and subcutaneous adipocytes. Since the absolute levels of active ACC2 within the subcutaneous and visceral adipocytes are unknown, the biological significance of the observation is unclear. Similar to ACC1, we are unable to correlate AMPK phosphorylation (activation) with ACC2 phosphorylation (inhibition), since ACC2 also displays differential total protein levels between the subcutaneous and visceral adipocytes.

Chapter conclusion

Taken together, the fat depot had seemingly no effect on the metabolic activities of ATM, mTORC1 or AMPK within adipocytes under control or HFD conditions. Although the diet groups were not compared, the biometric data of the four control and four HFD rats (collected by Dr H. Sadie-van Gijsen) from which the ASCs were harvested revealed that the HFD did not lead to a significant increase in body weight or visceral fat accumulation compared to the control diet (refer to Appendix A ***Figure A1***). Furthermore, the HFD did not cause insulin resistance compared to the control diet, despite a non-significant trend towards increased insulin resistance in the HFD rats (refer to Appendix A ***Figure A1***). ACC showed adipocyte-specific expression, with seemingly lower protein levels of both isoforms (1 and 2) in visceral adipocytes compared to subcutaneous adipocytes in both diet

groups. ACC1 phosphorylation (inhibition) might be further regulated in visceral adipocytes, however the biological significance thereof remains unclear.

Interestingly, we observed potential changes in ATM activity levels in the subcutaneous fat depot, and AMPK total and activity levels in both fat depots, between the ASCs and their adipocyte counterparts originating from control and HFD rats. These results indicate a possible differentiation-dependent effect on these two metabolic proteins. However, the impact of adipocyte differentiation on basal metabolic protein profiles lies beyond the scope of the current study and was therefore not discussed.

Chapter 6

Investigating a posttranscriptional mechanism of cardiomyoblast ATM protein regulation during obesity

During obesity, adipocyte metabolism becomes dysregulated, which leads to abnormal endocrine function. Abnormal WAT secretions in circulation, in turn, might influence the metabolism of peripheral organs. ATM protein levels are down-regulated in the hearts of obese and insulin resistant animals (Huisamen *et al.*, 2016), suggesting a potential link between obesity and dysregulated cardiac metabolism. However, the mechanism linking ectopic adiposity and reduced cardiac ATM levels remains unclear. To address this unknown, the current study aimed to investigate whether adipocyte secretions can affect cardiomyoblast ATM protein levels in obesity *in vitro*, and if it can be through a miRNA-mediated mechanism. To achieve this aim, H9c2 cells were exposed to CM derived from the visceral and subcutaneous ASCs and adipocytes (analysed in Chapter 5) for 24 hours. The CM represents a more physiological treatment compared with treatments consisting of individual FFAs (investigated in Chapter 4). The FFA composition of the CM was analysed by the SAMRC using GC-FID to establish whether fat depot and diet influence the FFA secretory profiles of adipocytes. We investigated the respective effects of visceral and subcutaneous adipose secretions on cardiomyoblast ATM levels, as well as other metabolic proteins (PKB, mTORC1 and AMPK), through Western blotting. Furthermore, as a potential posttranscriptional mechanism of ATM protein regulation in obesity, we analysed the expression levels of two miRNAs that are known to regulate ATM in cancer cells (miR-421 and miR-18a), and four metabolic miRNAs that target ATM mRNA *in silico* and display aberrant expression in obesity and related co-morbidities (miR-194, miR-210, miR-322 and miR-181b), with qRT-PCR. These six miRNAs have not been associated with the posttranscriptional regulation of ATM protein levels in a metabolic context before.

6.1. Diet and fat depot do not influence the adipocyte secretion of palmitic-, stearic- and oleic acid, the most abundant secreted free fatty acids

The GC-FID analysis of the CM was kindly performed by Dr P. van Jaarsveld in collaboration with the SAMRC to establish the FFA profiles secreted by the adipose cells. The FFA composition of each CM sample (SC ASC, SC Adipo, PR ASC, PR Adipo) were analysed per rat (n=3 per diet group). A two-way ANOVA was performed, followed by a Bonferroni post-hoc test, and data are presented as mean percentage per ml CM ± SD.

The FFA composition of the CM derived from subcutaneous and visceral ASCs and adipocytes originating from control and HFD rats revealed differences in secreted FFA profiles **(*Figure 6.1*)**.

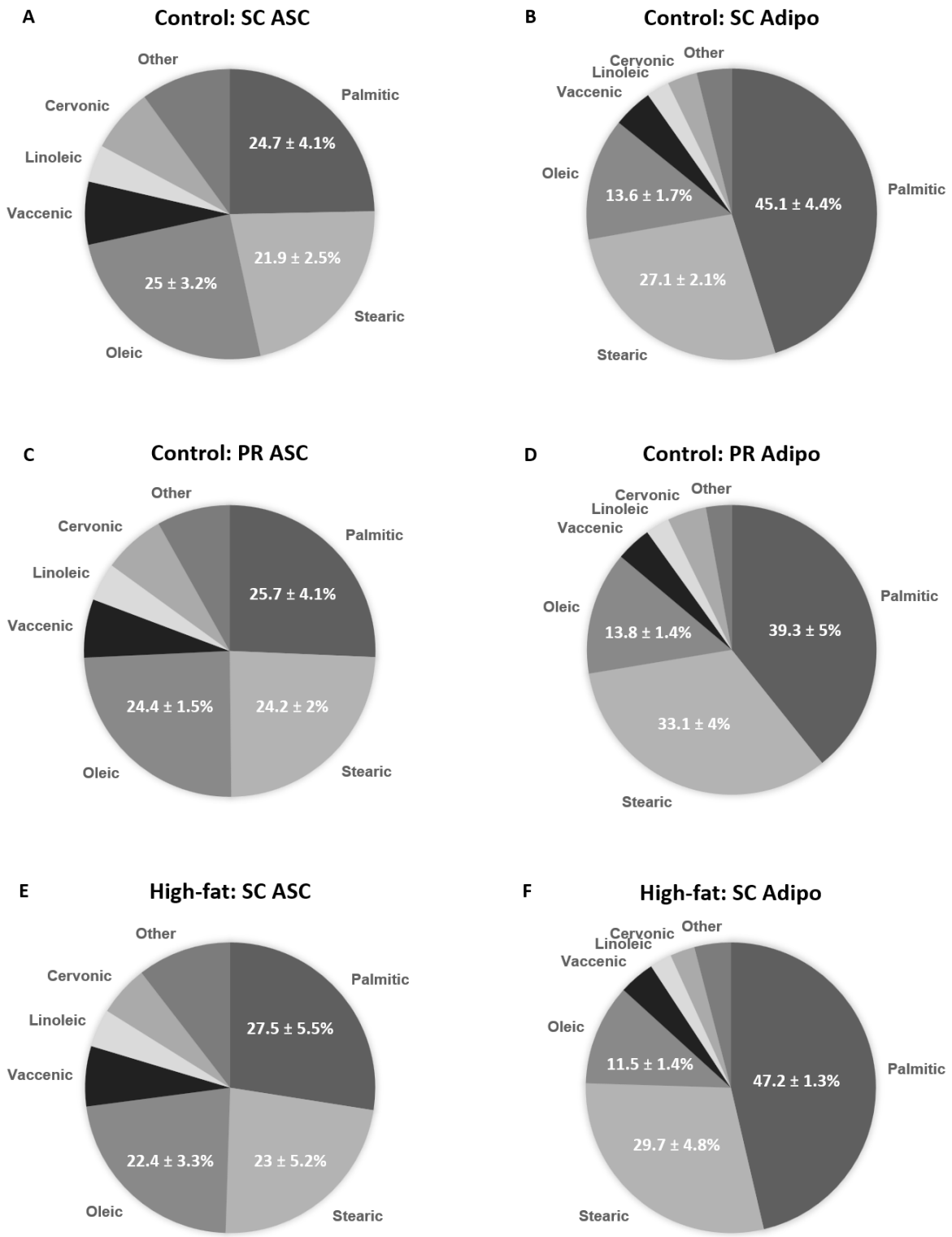

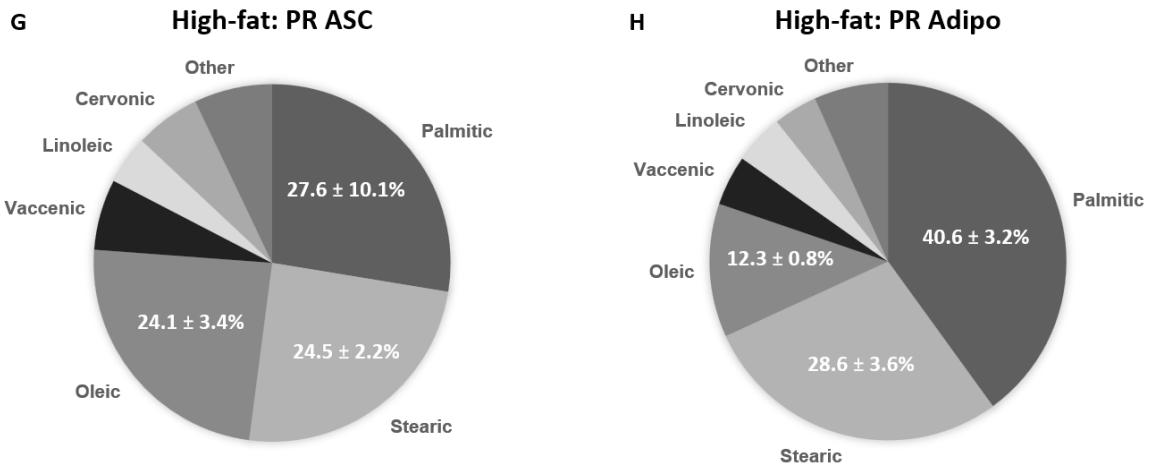

Figure 6.1: FFA secretory profiles of adipose-derived cells.

The FFA composition per 1 ml CM: subcutaneous adipose stem cells originating from control rats (A); subcutaneous adipocytes originating from control rats (B); peri-renal adipose stem cells originating from control rats (C); peri-renal adipocytes originating from control rats (D); subcutaneous adipose stem cells originating from HFD rats (E); subcutaneous adipocytes originating from HFD rats (F); peri-renal adipose stem cells originating from HFD rats (G); peri-renal adipocytes originating from HFD rats (H) (n=3 per diet group; each FFA is presented as a percentage ± SD of the total FFA content).

Based on the CM composition data, we were interested in determining whether the adipose cells originating from different depots and dietary backgrounds displayed differential secretion of the three most abundant FFAs, which were palmitic acid (16-carbon saturated FFA), stearic acid (18-carbon saturated FFA) and oleic acid (18-carbon mono-unsaturated FFA).

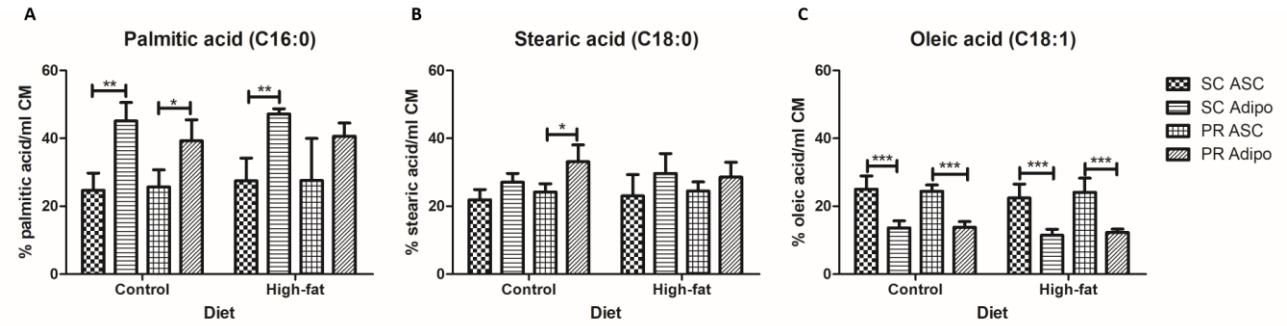

Figure 6.2: Differential secretion of palmitic acid, stearic acid and oleic acid from adipose-derived cells.

*Palmitic acid (A), stearic acid (B) and oleic acid (C) secreted from subcutaneous (SC) and visceral (peri-renal; PR) adipose stem cells (ASCs) and adipocytes (Adipo) originating from control and HFD rats. Differential secretion was observed in palmitic acid and oleic acid between the adipocytes and their ASC counterparts in both depots and diet groups, with no differences between diet groups (n=3 per diet group; two-way ANOVA with Bonferroni post-test; mean percentage of FFA per ml CM ± SD; *p<0.05; **p<0.01; ***p<0.001).*

We observed no significant differences in palmitic-, stearic-, or oleic acid secretion between the subcutaneous and visceral adipocytes, or between adipocytes originating from control and HFD rats **(*Figure 6.2*)**. Interestingly, the subcutaneous and visceral adipocytes secreted higher levels of palmitic acid compared to their ASC counterparts in both diet groups **(*Figure 6.2 A*)**, whereas the subcutaneous and visceral adipocytes secreted lower levels of oleic acid compared to their ASC counterparts in both diet groups **(*Figure 6.2 C*)**.

Circulating FFAs are increased in obesity and are suggested to be a major contributing factor to the development of systemic insulin resistance and inflammation, which precedes metabolic diseases such as type II diabetes and cardiovascular diseases (Boden, 2008). However, it is important to consider the type of circulating FFAs, because saturated and unsaturated FFAs have differential effects on systemic health. Whereas saturated FFAs (such as palmitic acid) promotes peripheral insulin resistance and inflammation, unsaturated FFAs (such as oleic acid) protect against these metabolic risk factors (Palomer *et al.*, 2018). In a study by Liu and colleagues, the serum FFA composition of rats fed a HFD showed that saturated FFAs constituted 47% of total FFAs (compared to 45% in control rats), whereas poly-unsaturated FFAs constituted 31% of total FFAs (compared to 23% in control rats), and mono-unsaturated FFAs the remaining 22% (compared to 32% in control rats) (Liu *et al.*, 2015), demonstrating that diet affects the circulating FFA composition.

Our results indicate that fat depot and diet did not influence the secretion of palmitic-, stearic- or oleic acid from adipocytes. However, adipocyte differentiation influenced palmitic- and oleic acid secretion, where adipocytes secreted more palmitic acid, but less oleic acid, compared to their ASC counterparts. Although not significant, the pattern of stearic acid secretion from the adipose cells mimics that of palmitic acid secretion, suggesting that the adipocytes secrete higher levels of the two most abundant saturated FFAs compared to their ASC counterparts. This differentiation-dependent effect on FFA secretion is consistent with the differentiation-dependent effect observed on basal metabolic protein profiles but lies beyond the scope of this study.

6.2. Cardiomyoblast AMPK and mTORC1, but not ATM, protein levels are down-regulated by adipocyte secretions in response to high-fat feeding

The total and phosphorylated levels of ATM, as well as the metabolic proteins PKB, mTORC1 and AMPK, were determined in H9c2 cells treated with the respective CM or complete DMEM media only (control) for 24 hours. Each treatment condition was performed in triplicate (technical n=3) per experiment, and each experiment was repeated four times (biological n=4 per diet group). Due to insufficient amounts of protein (<10 μg protein per 15 μl cell lysate) from H9c2 cells treated with the CM derived from one control animal and one HFD animal, an n=3 per diet group was used for

Western blot analysis. In order to compare results between individual experiments, a common DMEM control was included (refer to Appendix D). The common DMEM control was used to calculate the fold-change of each treatment condition. The technical repeats per treatment conditions were averaged and a two-way ANOVA was performed, followed by a Bonferroni post-hoc test. Data are presented as mean fold-change ± SD relative to the common DMEM control. The p/t-ratio represents the phosphorylated protein as a fraction of the total protein and serves as an indicator of protein activity for all proteins analysed in these experiments.

Neither visceral nor subcutaneous adipocyte secretions under HFD conditions had a significant effect on cardiomyoblast ATM protein levels **(*Figure 6.3*)**, however the p/t-ratios (activity) were significantly increased by the CM compared to the common DMEM control ($p<0.05$) in both diet conditions.

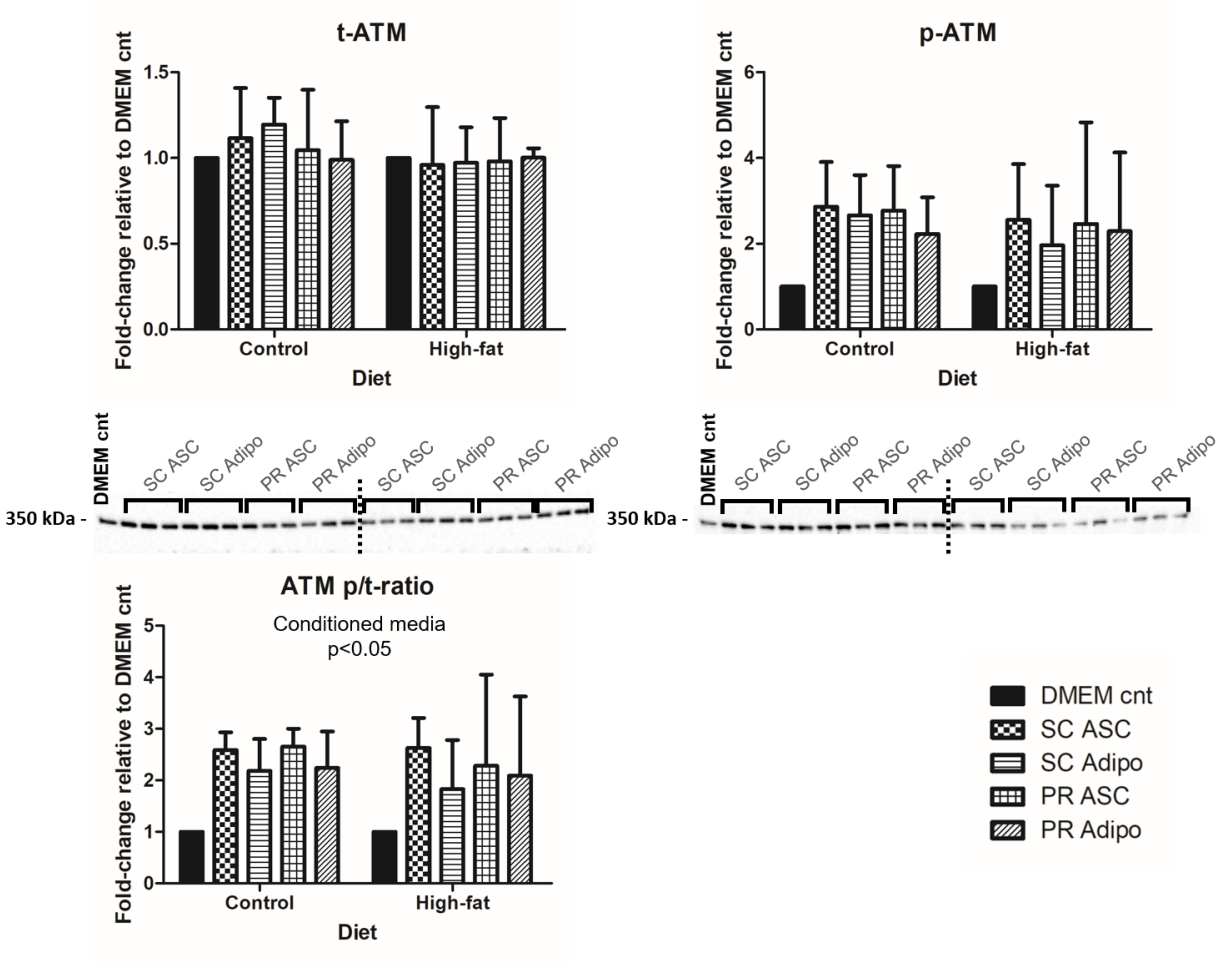

Figure 6.3: Total and phosphorylated levels of ATM in H9c2 cardiomyoblasts treated with adipose-derived CM.

The total (t) and phosphorylated (p) levels of ATM in H9c2 cells treated with CM derived from subcutaneous adipose stem cells (SC ASC), subcutaneous adipocytes (SC Adipo), peri-renal adipose stem cells (PR ASC) and peri-renal adipocytes (PR Adipo) harvested from control and HFD rats for 24 hours compared to a common DMEM control. ATM activation (p/t-ratio) was significantly up-regulated by the respective CM derived from both diet groups, an effect that

*was driven by a non-significant increase in phosphorylated levels (biological n=3 per diet group; technical n=3; normalised to total protein; two-way ANOVA with Bonferroni post-test; mean ± SD; *p<0.05).*

ATM is a metabolic protein that participates in the insulin-mediated PKB/mTORC1 pathway (Yang and Kastan, 2000), which negatively regulates AMPK activity. Furthermore, ATM acts as a redox sensor that is directly activated by ROS (Guo *et al.*, 2010), a by-product of nutrient metabolism. ROS-activated ATM induces autophagy by activating AMPK, which in turn inhibits mTORC1 (Alexander *et al.*, 2010). These two signalling pathways highlight the different relationships between ATM, mTORC1 and AMPK.

Our data indicate that the total levels of cardiomyoblast ATM were not affected by the HFD-derived CM, which does not mimic what has been observed *in vivo* in obese and insulin resistant rats (Huisamen *et al.*, 2016). Rather, our results suggest that the CM up-regulated ATM activity in cardiomyoblasts, which could be due to a requirement for nutrient metabolism brought about by the adipose secretions, and/or as a result of ROS production during said nutrient metabolism. Interestingly, ATM activity was non-significantly lower in response to the adipocyte secretions, which contained higher levels of palmitic acid and lower levels of oleic acid, compared to ASC secretions. Lastly, we have previously observed (Chapter 4) that cardiomyoblast ATM activity is down-regulated in response to a combination of high FFAs (palmitic- and oleic acid) and insulin. The CM contained no additional insulin but may contain adipose-secreted cytokines and adipokines. These results suggest that ATM activity might be influenced by insulin and/or adipose-secreted factors.

No significant differences in phosphorylated AMPK levels were observed **(*Figure 6.4*)**, suggesting that either the ROS-mediated pathway or insulin-mediated PKB/mTORC1 pathway could potentially mediate increased ATM activation. However, AMPK protein levels were significantly down-regulated under HFD conditions compared to control conditions ($p<0.05$). Since a smaller amount of AMPK protein is available for activation in response to an HFD, it could account for a loss of increased phosphorylated levels that we would expect to see in the ROS-activated pathway. The pattern of AMPK activation (p/t-ratio) in response to the respective CM, however, showed an inverse pattern compared to ATM activation under control and HFD conditions, suggesting that the insulin-mediated PKB/mTORC1 pathway, rather than the ROS-mediated pathway, predominates. No significant differences were observed between the subcutaneous- and visceral-derived CM, suggesting adipose depot-independent regulation of total AMPK levels.

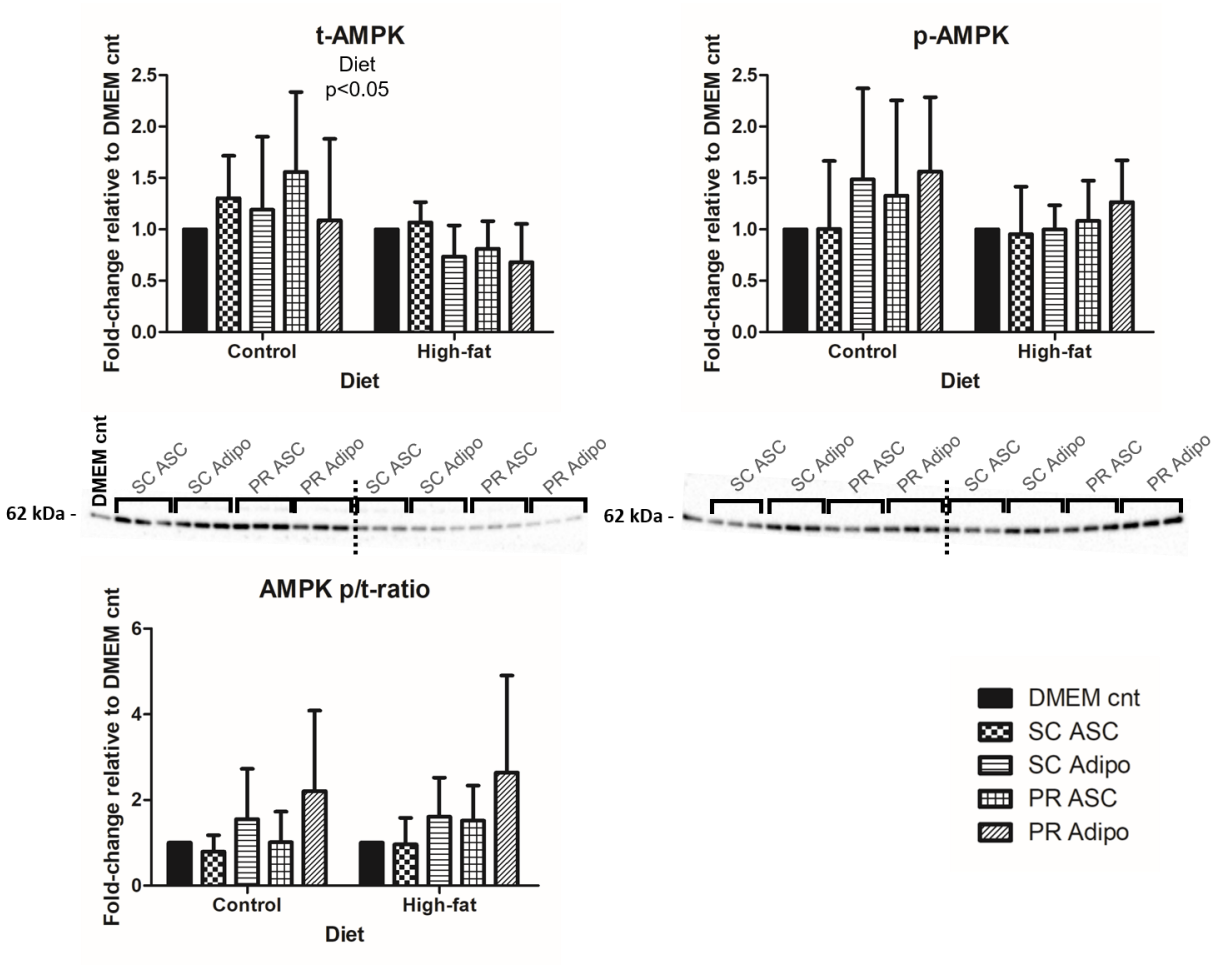

Figure 6.4: Total and phosphorylated levels of AMPK in H9c2 cardiomyoblasts treated with adipose-derived CM.

*The total (t) and phosphorylated (p) levels of AMPK in H9c2 cells treated with CM derived from subcutaneous adipose stem cells (SC ASC), subcutaneous adipocytes (SC Adipo), peri-renal adipose stem cells (PR ASC) and peri-renal adipocytes (PR Adipo) harvested from control and HFD rats for 24 hours compared to a common DMEM control. AMPK levels (t) were significantly down-regulated by the CM derived from HFD rats compared to control rats (biological n=3 per diet group; technical n=3; normalised to total protein; two-way ANOVA with Bonferroni post-test; mean ± SD; *p<0.05).*

AMPK is a nutrient sensor that activates catabolic pathways for energy production, while inhibiting anabolic pathways that consume energy in times of nutrient deprivation. As mentioned previously, AMPK also regulates autophagy through the inhibition of mTORC1 in response to ROS (Alexander *et al.*, 2010). The role of AMPK in the development of obesity-associated metabolic dysfunction have been widely investigated in skeletal muscle and the liver. Overall, decreased AMPK activation (phosphorylation) is thought to be an early event in the development of insulin resistance due to chronic nutrient overload (reviewed by Coughlan *et al.*, 2015). However, the role of AMPK in obesity-related cardiac dysfunction remains inconclusive. Niemann and colleagues investigated the effect of obesity on the AMPK signalling pathway in human cardiac tissue, and reported an increase

in LKB1-mediated AMPK activation (p/t-ratio) in obese compared to lean patients (Niemann *et al.*, 2013). However, they observed no changes in mTORC1 phosphorylation, or any other down-stream AMPK targets, between the obese and control groups and concluded that AMPK might remain inactive albeit phosphorylated during obesity. Conversely, Ko *et al.* reported a non-significant decrease in AMPK protein levels and a significant reduction in the AMPK p/t-ratio in the cardiac tissue of diet-induced obese mice compared to control mice (Ko *et al.*, 2009). Finally, neither total nor phosphorylated AMPK levels showed significant differences in the cardiac tissue between diet-induced obese rats and control rats (Nascimento *et al.*, 2011). Interestingly, the HFD applied in the latter study failed to affect the serum FFA and triglyceride levels in the obese rats, and there were no evidence of altered triglyceride content or lipid peroxidation (a consequence of increased ROS) in the cardiomyocytes. As such, the lipid-associated aspect of obesity and its effect on cardiac metabolism is not accurately reflected in their study, but it highlights a link between the presence of lipotoxicity and altered AMPK signalling in the heart.

Our results indicate that cardiac AMPK protein levels were down-regulated in response to adipose secretions in a HFD setting, with no significant changes in phosphorylated levels. Therefore, we speculate that this down-regulation might be an early adaptive response to metabolic overload driven by the HFD-derived adipose secretions in an attempt to keep its activation levels comparable with normal conditions. By doing so, the cells restrict excess fatty acid uptake and subsequent oxidation in order to limit lipotoxicity and excessive ROS production, an unavoidable by-product of cellular metabolism that activates AMPK in an ATM-dependent positive feedback loop.

No significant differences were observed in phosphorylated mTORC1 levels **(*Figure 6.5*)**, however the activation (p/t-ratio) levels in response to both the control- and HFD-derived CM display an opposite pattern to that of AMPK activation levels, confirming their inverse relationship. Interestingly, mTORC1 protein levels were also down-regulated in response to HFD conditions compared to control conditions ($p<0.05$). Since less mTORC1 protein was available for activation under HFD conditions, but no significant reduction in its phosphorylated levels were observed, it could suggest that the positive regulation of mTORC1 activity by ATM within the insulin-mediated PKB pathway predominates the negative regulation of mTORC1 activity by ATM in response to ROS. In fact, the pattern of mTORC1 activation (p/t-ratio) in response to the respective CM mimics the activation pattern of ATM under control and HFD conditions, which is consistent with the activity of the PKB/mTORC1 pathway rather than the ROS-mediated pathway. Lastly, no significant differences were observed between the subcutaneous- and visceral-derived CM, suggesting adipose depot-independent regulation of mTORC1 levels.

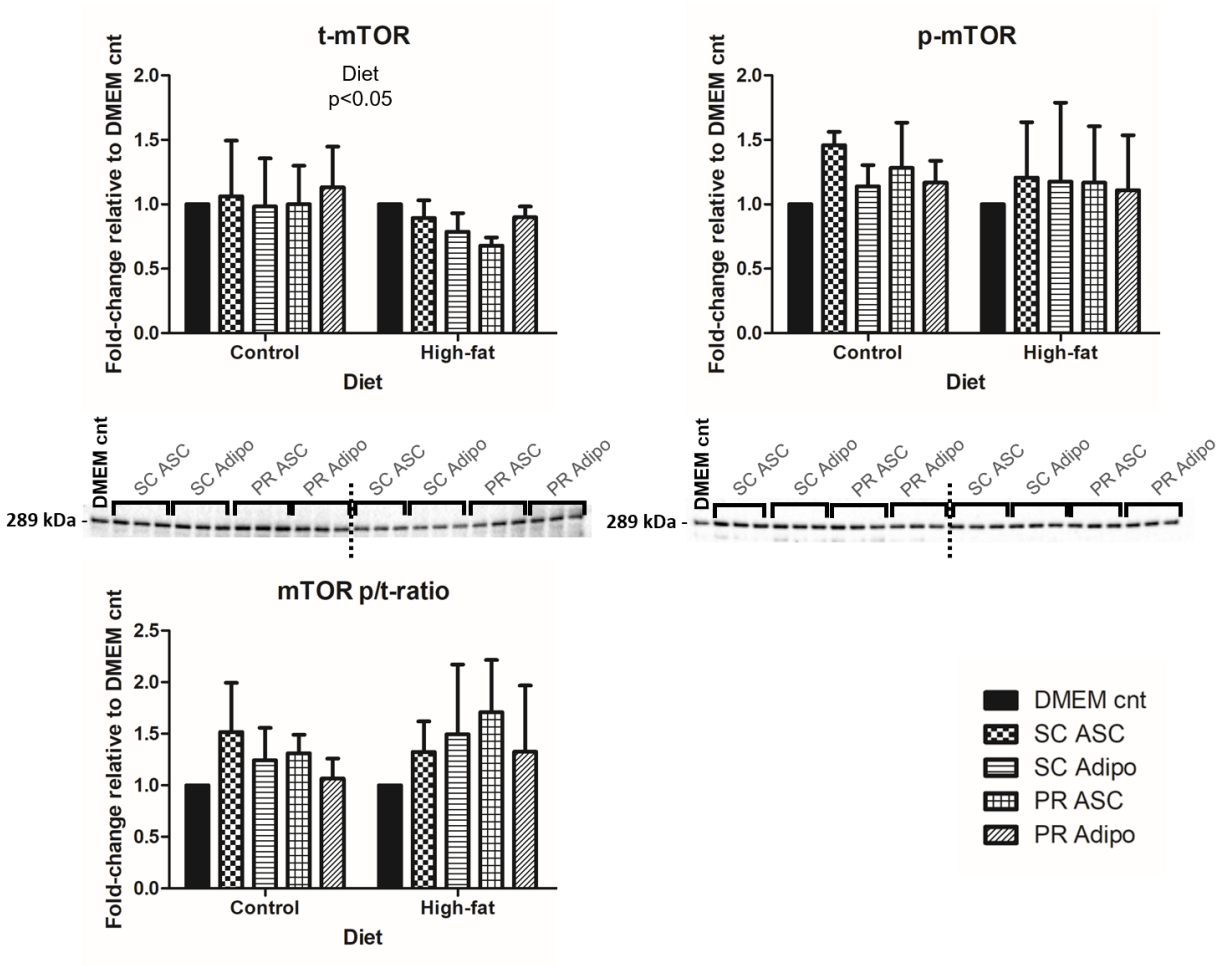

Figure 6.5: Total and phosphorylated levels of mTORC1 in H9c2 cardiomyoblasts treated with adipose-derived CM.

*The total (t) and phosphorylated (p) levels of mTORC1 in H9c2 cells treated with CM derived from subcutaneous adipose stem cells (SC ASC), subcutaneous adipocytes (SC Adipo), peri-renal adipose stem cells (PR ASC) and peri-renal adipocytes (PR Adipo) harvested from control and HFD rats for 24 hours compared to a common DMEM control. mTORC1 levels (t) were significantly down-regulated by the CM derived from HFD rats compared to control rats (biological n=3 per diet group; technical n=3; normalised to total protein; two-way ANOVA with Bonferroni post-test; mean ± SD; *p<0.05).*

mTORC1 is another important metabolic sensor that is activated in response to growth hormones, such as insulin and IGF-1, and nutrients, such as amino acids. The mTORC1 pathway promotes anabolic processes such as protein synthesis, while inhibiting catabolic processes such as autophagy. In addition, mTORC1 plays an important role in lipid metabolism by regulating the fatty acid transporter protein 1 (FATP1)-mediated uptake of long-chain fatty acids through S6K (Arif *et al.*, 2017), as well as promoting cardiac β-oxidation (Zhu *et al.*, 2013). Studies indicate that mTORC1 activity is up-regulated during obesity and related metabolic conditions in various tissues (Khamzina *et al.*, 2005), including the heart (Li *et al.*, 2012; Uchinaka *et al.*, 2017). It is thought to be as a result of either increased PKB activity or reduced AMPK activity in response to metabolic overload

(Sciarretta, Volpe and Sadoshima, 2014), and is consequently associated with suppressed autophagy (Che *et al.*, 2018) and the development of insulin resistance through the negative feedback inhibition of S6K on IRS-1 (Khamzina *et al.*, 2005). Interestingly, in pigs fed a high-fat/high-cholesterol diet, total cardiac mTORC1 levels were significantly up-regulated compared to control animals. However, mTORC1 levels strongly correlated with serum cholesterol and high-density lipoprotein levels, with no correlation between mTORC1 levels and serum triglycerides (Glazer *et al.*, 2009), highlighting differential effects between different types of circulating lipids on cardiac mTORC1 expression.

Similar to AMPK, our results show that cardiac mTORC1 protein levels are down-regulated in response to adipose secretions in a HFD setting, with no significant changes in phosphorylated levels. We therefore speculate that this down-regulation is also an early adaptive response aimed at lowering mTORC1 activity to normal levels in order to counteract the elevated mTORC1 activation (and suppressed autophagy) associated with obesity.

PKB protein levels were slightly increased under control and HFD conditions compared to the common DMEM control, although not significantly **(*Figure 6.6*)**. Despite no significant differences in phosphorylated levels, the pattern of PKB activation (p/t-ratio) in response to the respective CM corresponds to that of ATM and mTORC1, but displays an inverse pattern to that of AMPK, under control conditions. This confirms the likelihood that the PKB/mTORC1 pathway predominates, as opposed to the ROS-mediated pathway. Interestingly, an inverse pattern in PKB activation is observed under HFD conditions, which is an unexpected observation as it rather correlates with AMPK activation. Again, no significant differences were observed between the subcutaneous- and visceral-derived CM.

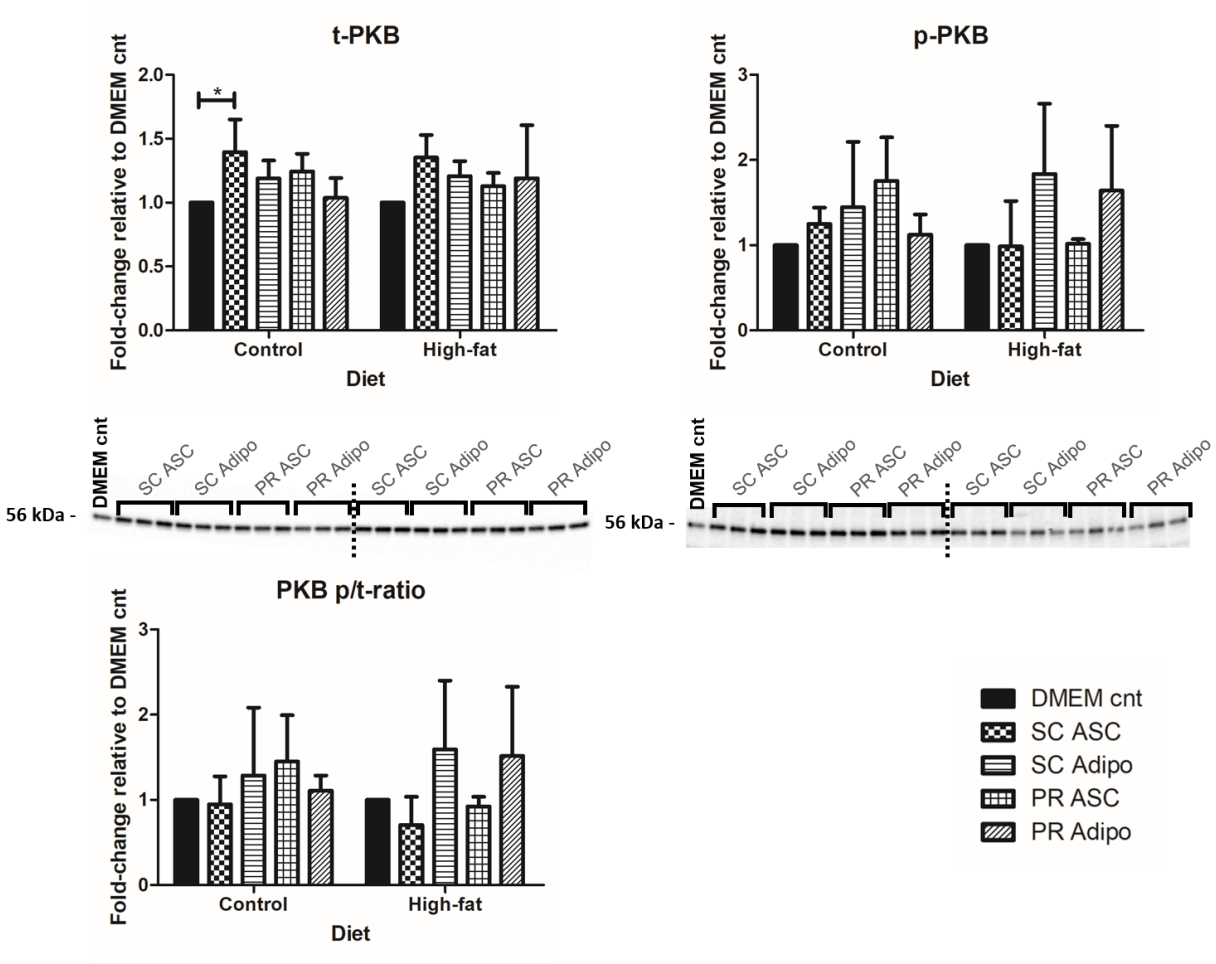

Figure 6.6: Total and phosphorylated levels of PKB in H9c2 cardiomyoblasts treated with adipose-derived CM.

*The total (t) and phosphorylated (p) levels of PKB in H9c2 cells treated with CM derived from subcutaneous adipose stem cells (SC ASC), subcutaneous adipocytes (SC Adipo), peri-renal adipose stem cells (PR ASC) and peri-renal adipocytes (PR Adipo) harvested from control and HFD rats for 24 hours compared to a common DMEM control. PKB levels (t) were significantly up-regulated by the SC ASC CM derived from control rats compared to the DMEM control (biological n=3 per diet group; technical n=3; normalised to total protein; two-way ANOVA with Bonferroni post-test; mean ± SD; *p<0.05).*

PKB is an insulin-responsive positive regulator of nutrient metabolism essential for cell growth and survival. PKB promotes anabolic processes by activating AS160/GLUT4-mediated glucose uptake (for glycogenesis), AS160/CD36-mediated FFA uptake (for lipogenesis) and mTORC1/S6K-mediated protein synthesis, while limiting catabolic processes through the inhibition of AMPK. Furthermore, ATM has been suggested to facilitate the full activation of PKB in response to insulin stimulation in some cell types (Viniegra *et al.*, 2005; Halaby *et al.*, 2008; Jeong *et al.*, 2010; J. Ching *et al.*, 2013).

Different aspects of obesity, such as increased blood glucose, insulin, lipid and pro-inflammatory cytokine levels, have been linked with the development of insulin resistance in peripheral tissue (Ye,

2013), which in turn associates with decreased glucose uptake and utilisation. In particular, fatty acid-induced insulin resistance can arise due to a build-up of intracellular fatty acid metabolites, such as DAG and ceramide, which leads to the serine phosphorylation and inhibition of IRS-1, and a consequent reduction in PKB phosphorylation (Shulman, 2000). Although established insulin resistance is generally associated with various insulin signalling pathway alterations, including decreased PKB phosphorylation, early molecular signs of cellular insulin resistance is thought to be only observed at the level of GLUT4, and not PKB. In fact, insulin signalling to PKB remains unaltered, but a disruption in GLUT4 translocation is responsible for the initial reduction in cellular glucose uptake (Abel, O'Shea and Ramasamy, 2012).

In the current study, no significant differences in PKB phosphorylation were observed. The only source of insulin was from the DMEM in the growth media, which formed the background of all the CM. The only other factors that might affect insulin signalling in H9c2 cells are adipose-secreted pro-inflammatory cytokines, adipokines and FFAs, which had no differential effects on PKB activity between the subcutaneous and visceral fat depots, or between the control and HFD conditions. Although not significant, the adipocyte secretions under HFD conditions resulted in increased PKB activation compared to the control counterparts, which could suggest an early adaptation to greater metabolic pressure without the presence of established insulin resistance. A final interesting observation is that the pattern of PKB activity in the HFD setting deviates from that in the control setting, resembling the pattern of AMPK rather than those of ATM and mTORC1. This could further indicate an early change in cardiomyoblast PKB activity in response to adipose secretions during high-fat feeding.

6.3. miR-18a, miR-194, miR-210, miR-181b and miR-322 are able to target rat ATM mRNA *in silico*

Previous studies have shown that miR-421 and miR-18a function down-stream of the nutrient sensor mTORC1 (Shen and Houghton, 2013) to target ATM mRNA in human and mouse cancer cells (Hu *et al.*, 2010; Song *et al.*, 2011; Wu *et al.*, 2013). Although miRNAs are generally well conserved among different animal species (Bartel, 2004), mRNA binding sites of target proteins are not necessarily conserved. In the current study, *in silico* analysis using the TargetScan and miRMap algorithm software confirmed that miR-18a targets ATM mRNA in rats **(*Figure 6.7 A*)**, but not miR-421. Furthermore, miR-194 **(*Figure 6.7 B*)**, -210, **(*Figure 6.7 C*)** -181b **(*Figure 6.7 D*)** and -322 **(*Figure 6.7 E*)** are able to target rat ATM mRNA.

Figure 6.7: In silico analysis showing the exact binding locations on the ATM 3' UTR for the target miRNAs.

The exact binding positions (nucleotides) on the 3' untranslated region (UTR) of ATM mRNA for miR-18a-5p (A), miR-194-3p (B), miR-210-5p (C), miR-181b-5p (D), and miR-322-5p (E). Figure designed in Microsoft PowerPoint Office 365 by the author of the thesis based on information accessible on TargetScan and miRMap algorithm software.

6.4. Cardiomyoblast miR-181b is down-regulated by normal adipocyte secretions, and more so by adipocyte secretions in response to high-fat feeding

The relative expression levels of miR-421, miR-18a, miR-194, miR-210, miR-181b and miR-322 were determined in H9c2 cells treated with the respective CM or complete DMEM media only (control) for 24 hours. Each treatment condition was performed in triplicate (technical n=3) and pooled per experiment, each experiment was repeated four times (biological n=4 per diet group), and samples were analysed in duplicate. Upon review of the amplification plots and standard curves for each miRNA, miR-194 was excluded from the qRT-PCR analysis based on poor primer efficiency (Appendix D ***Figure D9***). No accurate conclusions from the relative expression data of miR-421, miR-18a or miR-210 could be formulated as their respective primer efficiencies were too high (Appendix D ***Figures D7***, ***D8*** and ***D10***). NanoDrop™ spectrophotometry revealed sufficient RNA concentration and purity per sample (Appendix D ***Table D1***), and RIN allocations revealed high RNA integrity across individual experiments (Appendix D ***Figure D5***). Therefore, we speculate that either the design of the primers or their compatibility with the H9c2 cell line were suboptimal and

responsible for poor primer performance. In order to compare results between individual experiments, the Ct-values of each DMEM control-treated group were averaged for each miRNA and used to calculate the fold-change for each treatment group (refer to Appendix D ***Figure D16***). A two-way ANOVA was performed, followed by a Bonferroni post-hoc test, and data are presented as mean fold-change ± SD relative to the DMEM control.

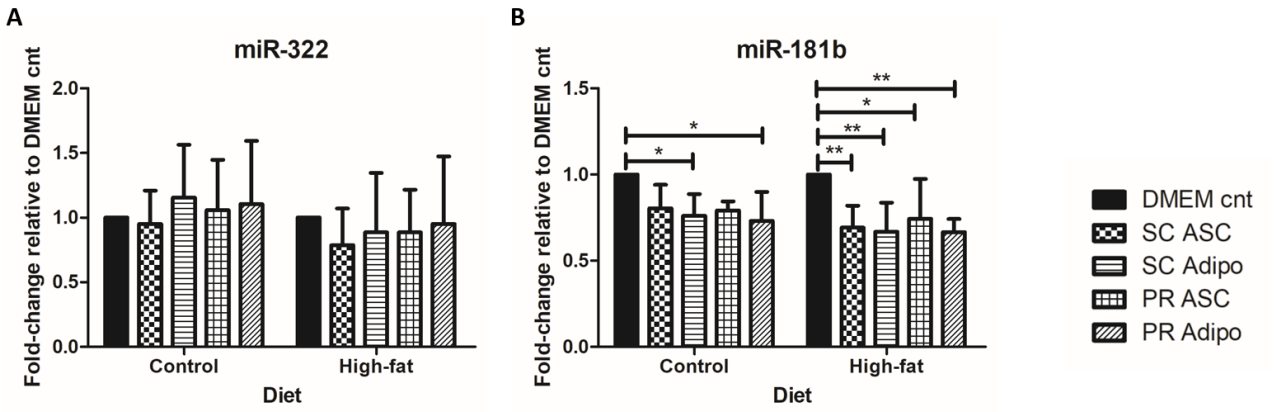

Figure 6.8: Expression levels of target miRNAs in H9c2 cardiomyoblasts treated with adipose-derived CM.

*The relative expression levels of miR-322 (A) and miR-181b (B) in H9c2 cells treated with CM derived from subcutaneous adipose stem cells (SC ASC), subcutaneous adipocytes (SC Adipo), peri-renal adipose stem cells (PR ASC) and peri-renal adipocytes (PR Adipo) harvested from control and HFD rats for 24 hours compared to a DMEM control. The CM from PR Adipo derived from control diet rats, as well as all HFD-derived CM, significantly down-regulated miR-181b in H9c2 cells (biological n=4 per diet group; pooled technical n=3; normalised to U6 snRNA; $2^{-\Delta\Delta Ct}$ method; two-way ANOVA with Bonferroni post-test; mean ± SD; *p<0.05; **p<0.01).*

No significant differences in miR-322 expression were observed **(*Figure 6.8 A*)**. Ectopic miR-322 expression has been linked with the development of insulin resistance. By negatively regulating the insulin receptor mRNA, overexpressed miR-322 leads to decreased insulin receptor expression, decreased down-stream PKB phosphorylation and reduced glucose uptake in rat vascular smooth muscle cells (Marchand *et al.*, 2016). The authors further investigated the role of miR-322 in the development of cardiac dysfunction in obesity. Interestingly, it was observed that HFD mice with cardiac dysfunction displayed no significant changes in cardiac miR-322 levels compared to control mice, whereas age-matched *ob/ob* mice with no cardiac dysfunction displayed increased cardiac miR-322 levels. The authors concluded that elevated miR-322 levels might be cardioprotective in response to metabolic overload in a HFD setting.

Based on the animal study by Marchand and colleagues (2016), it is tempting to speculate that no significant changes in miR-322 levels in response to the adipose secretions under HFD conditions could be indicative of cardiac dysfunction, however cardiac dysfunction would have to be defined in

terms of H9c2 cells and confirmed by additional analyses. No change in miR-322 expression could, however, suggest that insulin resistance is likely not induced within the CM-treated H9c2, which is supported by no significant decreases in phosphorylated PKB levels **(*Figure 6.6*)**.

The most interesting finding was that miR-181b was significantly down-regulated by subcutaneous and visceral adipocyte secretions compared to the DMEM control ($p<0.05$) under normal conditions, and even more so by secretions from subcutaneous ASCs ($p<0.01$), subcutaneous adipocytes ($p<0.01$), visceral ASCs ($p<0.05$) and visceral adipocytes ($p<0.01$) compared to the DMEM control under HFD conditions **(*Figure 6.8 B*)**. It is noticeable that the ASC secretions only had a significant effect on miR-181b expression levels under HFD conditions but not under control conditions.

Interestingly, despite also being linked with the suppression of ATM when ectopically expressed in breast cancer (Bisso *et al.*, 2013), miR-181b down-regulation has been linked with various aspects of obesity. Firstly, miR-181b negatively regulates cellular inflammation by targeting importin-α3, a protein required for the translocation of nuclear factor kappa B (NF-κB) to the nucleus for the transcription of inflammatory mediators (Sun *et al.*, 2012). The authors showed that endothelial miR-181b was down-regulated in response to pro-inflammatory molecules, which resulted in increased NF-κB signalling and, subsequently, cellular inflammation. Therefore, reduced cellular miR-181b might be associated with a pro-inflammatory state. Secondly, miR-181b is thought to play an important role in the regulation of the insulin signalling pathway, as its down-regulation in adipose-derived endothelial cells of obese mice was associated with the development of insulin resistance. Furthermore, miR-181b was also down-regulated in cultured endothelial cells exposed to either palmitate, glucose or TNF-α, indicating that miR-181b expression can be influenced by nutrients and pro-inflammatory cytokines (Sun *et al.*, 2016). Lastly, cardiac miR-181b expression was shown to be down-regulated in HFD-induced obese mice and was associated with the development of cardiomyopathy. This reduction in miR-181b levels in the heart correlated with circulating levels, highlighting miR-181b as a promising potential biomarker of cardiac dysfunction during obesity (Copier *et al.*, 2017). In addition, the authors observed a significant down-regulation in cardiac miR-322 levels in obese mice compared to control mice, which also correlated with circulating levels.

In the current study, we show for the first time that cardiomyoblast miR-181b expression is further down-regulated in response to subcutaneous and visceral ASC and adipocyte secretions in a HFD setting. This down-regulation was not consistent with increased ATM protein levels **(*Figure 6.3*)**, however this does not discount the hypothesis that miR-181b might regulate ATM under metabolic stress. Furthermore, these results suggest that adipose secretions within a HFD setting, and even adipocyte secretions under normal conditions, might trigger a miR-181b-mediated inflammatory response in the heart. Our novel results indicate that miR-181b is sensitive to diet-dependent adipose

secretions *in vitro*, and therefore might be a potential early indicator of metabolic dysregulation in the heart, prior to the development of insulin resistance, in response to high-fat feeding.

Chapter conclusion

Taken together, ATM activity is regulated in H9c2 cells in response to adipose secretions, independent of fat depot or diet. Furthermore, alterations in AMPK and mTORC1 total protein levels in response to HFD conditions might be an early adaptive mechanism employed by cardiomyoblasts to keep the activation levels of these nutrient sensors comparable to control conditions. Lastly, we show, for the first time, that cardiomyoblast miR-181b levels are further down-regulated in response to adipose secretions in a HFD setting, which might be an early indicator of diet-induced metabolic dysfunction.

Chapter 7

Study conclusion

The observation that ATM protein levels are down-regulated in the peripheral tissue of obese and insulin resistant animals introduces a potential link between obesity and peripheral metabolic dysfunction. ATM plays a central role in maintaining intracellular metabolic homeostasis, therefore decreased cardiac ATM in response to an HFD might be a key event in the development of insulin resistance and cardiac dysfunction. The underlying mechanism of peripheral ATM protein down-regulation in obesity, however, remains unclear. Various cancer studies have shown that ATM protein levels are down-regulated by specific miRNAs, and we were thus interested in investigating whether cardiac ATM is also susceptible to miRNA-mediated regulation in obesity.

WAT constitutes a multicellular organ with important endocrine functions that are collectively responsible for systemic energy homeostasis. Obesity results in dramatic changes in WAT behaviour, including ectopic deposition around central organs and dysregulated adipocyte metabolism. In the current study, we determined the basal metabolic protein levels and activities of ATM, mTORC1 and AMPK, but observed no apparent differences between visceral and subcutaneous adipocytes under control or HFD conditions. Although the metabolic impact of adipocyte differentiation lies beyond the scope of this study, we observed a potential differentiation-dependent effect on the basal metabolic protein profiles.

Abnormal circulating FFAs, adipokines and pro-inflammatory cytokines secreted by WAT have been suggested to link obesity with the development of peripheral insulin resistance and inflammation. In the current study, we analysed the FFA composition of the respective CM to determine the secretory profiles of the visceral and subcutaneous adipose cells under control and HFD conditions. Fat depot and diet did not significantly influence the secretion of the three most abundant FFAs, namely palmitic-, stearic-, and oleic acid, by adipocytes. However, adipocytes showed higher secretion of palmitic acid, but lower secretion of oleic acid, compared to the ASCs, emphasising a strong differentiation-dependent effect.

Cardiac ATM total protein levels are influenced in HFD-induced obese rats, and we hypothesised that it might be due to miRNA-mediated regulation. In the current study, we were able to show that high concentrations of FFAs and insulin (Chapter 4) and adipocyte secretions (Chapter 6) influence cardiomyoblast ATM activity *in vitro*, but not its total protein levels. Even though these results do not mimic that of the animal study, perhaps it is important to consider that the factors secreted by adipocytes alone do not necessarily influence peripheral ATM total levels. Rather, it might be a

combination of high circulating FFAs, glucose, insulin, adipokines and pro-inflammatory cytokines that accompany an obesogenic diet that drive the dysregulation of cardiac ATM total protein levels. Furthermore, we were able to show that adipose secretions further down-regulate the expression levels of miR-181b, a metabolic miRNA that targets ATM mRNA *in silico*, in a HFD setting. Previous studies have shown that miR-181b expression is influenced by nutrients (such as palmitate) and pro-inflammatory molecules (such as TNF-α), and its down-regulation has been associated with intracellular inflammation, insulin resistance and cardiomyopathy. Although we observed no significant differences in the secreted FFA profiles between the adipocytes originating from different dietary backgrounds, it might be possible that other secreted factors, such as adipokines or cytokines, influence cardiomyoblast miR-181b levels. Therefore, we show, for the first time, that the down-regulation of cardiomyoblast miR-181b levels is exacerbated in response to HFD-derived adipose secretions, before the dysregulation of metabolic protein activities are observed in the cardiomyoblasts, and before clinical signs of obesity and systemic insulin resistance manifest (see the biometric data of the HFD rats compared to control rats in Appendix A ***Table A2*** and ***Figure A1***). We speculate that reduced miR-181b levels might be an early indicator of metabolic dysfunction in cardiomyoblasts.

Taken together, we demonstrate that adipocyte hypertrophy (ASC differentiation into adipocytes is characterised by increased lipid accumulation) alters the metabolic protein expression and FFA secretion, which in turn influence peripheral (cardiomyoblast) metabolic protein levels (AMPK and mTORC1) and activity (ATM), as well as miRNA expression (miR-181b).

Future directions

Chapter 5: We observed a potential differentiation-dependent effect on the basal metabolic protein profiles between ASCs and their adipocyte counterparts. The roles of these metabolic signalling proteins in the adipocytic differentiation of ASCs have not yet been elucidated and warrant further investigation, specifically pertaining to depot-specific differences and responses to different dietary conditions.

Chapter 6: In accordance with the metabolic protein profiles, we also observed a strong differentiation-dependent effect on the FFA secretory profiles, which warrant further investigation. In order to improve our understanding of the potential posttranscriptional regulation of cardiac ATM in obesity, the ATM mRNA levels will have to be analysed. Although we did not observe significant differences in ATM total protein levels, it does not necessarily conclude that ATM levels are not regulated on the posttranscriptional level. Due to differential regulation, mRNA and protein levels show poor correlation in many cases, such as during stress responses (Liu, Beyer and Aebersold,

2016). We have the isolated total RNA of H9c2 cells treated with the respective CM in -80°C storage, as well as an ATM mRNA primer, for future analysis. Furthermore, obesity is associated with oxidative stress, and ATM is directly activated by ROS, therefore the analysis of intracellular ROS levels in CM-treated cells will provide additional insights into the regulation of ATM in obesity. Lastly, other components present within the CM will have to be analysed, such as adipokines and cytokines, as these molecules can also affect metabolic protein expression and miRNA levels in cardiomyoblasts.

Study limitations

We acknowledge that all the *in vitro* experiments were underpowered, and that a larger n-value will have to be considered in order to confirm our results.

Chapter 5: Two major limitations of this chapter included our inability to (i) pool the protein quantification data of the four biological replicates per diet group and (ii) compare the basal metabolic protein profiles between the two diet groups to investigate the effect of the HFD. This could have been achieved through the inclusion of a common control on each stain-free membrane. It is also important to emphasise that we investigated the metabolic protein profiles in adipose stem cells and differentiated adipocytes, which represent only two cell type within WAT. Therefore, we were unable to formulate conclusions regarding WAT as a multicellular organ.

Chapter 6: We did not include the control media samples for the GC-FID analysis, therefore our data lacks a baseline to exclude background FFAs that are present in the FBS used for the complete DMEM media. In addition to metabolic stimuli, ATM is activated in response to double-stranded DNA breaks. However, we did not consider DNA damage as a mechanism for ATM activation, which could interfere with the interpretation of our results. Another limitation was that the volume of CM available to this study was very limited, therefore we were unable to perform a cell viability assay or assess apoptosis in the CM-treated H9c2 cells. Due to extreme time constraints, we were unable to assess fatty acid metabolism proteins, such as PPARα, or down-stream targets of AMPK (TSC2 and ACC) and mTORC1 (S6K and autophagy markers such as LC3) through Western blotting in CM-treated H9c2 cells, which would have aided our understanding of how the H9c2 cells responded metabolically to the CM.

Chapter 8

References

Abel, E. D., O'Shea, K. M. and Ramasamy, R. (2012) 'Insulin resistance: Metabolic mechanisms and consequences in the heart', *Arteriosclerosis, Thrombosis, and Vascular Biology*, 32(9), pp. 2068–2076.

Abu-Elheiga, L. *et al.* (2003) 'Acetyl-CoA carboxylase 2 mutant mice are protected against obesity and diabetes induced by high-fat/high-carbohydrate diets', *Proceedings of the National Academy of Sciences of the United States of America*, 100(18), pp. 10207–10212.

Alessi, D. R. *et al.* (1997) 'Characterization of a 3-phosphoinositide-dependent protein kinase which phosphorylates and activates protein kinase Bα', *Current Biology*, 7(4), pp. 261–269.

Alexander, A. *et al.* (2010) 'ATM signals to TSC2 in the cytoplasm to regulate mTORC1 in response to ROS', *PNAS*, 107(9), pp. 4153–4158.

Ambros, V. (2004) 'The functions of animal microRNAs', *Nature*, 431(7006), pp. 350–355.

Andersen, E. *et al.* (2019) 'Preadipocytes from obese humans with type 2 diabetes are epigenetically reprogrammed at genes controlling adipose tissue function', *International Journal of Obesity*, 43(2), pp. 306–318.

Andrisse, S. *et al.* (2013) 'ATM and GLUT1-S490 Phosphorylation Regulate GLUT1 Mediated Transport in Skeletal Muscle', *PLoS ONE*, 8(6), p. e66027.

Anthony, N. M., Gaidhu, M. P. and Ceddia, R. B. (2009) 'Regulation of visceral and subcutaneous adipocyte lipolysis by acute AICAR-induced AMPK activation', *Obesity*, 17(7), pp. 1312–1317.

Arif, A. *et al.* (2017) 'EPRS is a critical mTORC1-S6K1 effector that influences adiposity in mice', *Nature*, 542(7641), pp. 357–361.

Arner, P. (1995) 'Differences in lipolysis between human subcutaneous and omental adipose tissues', *Annals of Medicine*, 27(4), pp. 435–438.

Auguet, T. *et al.* (2014) 'Downregulation of lipogenesis and fatty acid oxidation in the subcutaneous adipose tissue of morbidly obese women', *Obesity*, 22(9), pp. 2032–2038.

Bakkenist, C. and Kastan, M. (2003) 'DNA damage activates ATM through intermolecular autophosphorylation and dimer dissociation', *Nature*, 421, pp. 499–506.

Banin, S. *et al.* (1998) 'Enhanced phosphorylation of p53 by ATM in response to DNA damage',

Science, 281(5383), pp. 1674–1677.

Bartel, D. (2004) 'MicroRNAs: Genomics, Biogenesis, Mechanism, and Function', *Cell*, 116(2), pp. 281–297.

Bell, A., Grunder, L. and Sorisky, A. (2000) 'Rapamycin inhibits human adipocyte differentiation in primary culture', *Obesity Research*, 8(3), pp. 249–254.

Berggreen, C. *et al.* (2009) 'Protein kinase B activity is required for the effects of insulin on lipid metabolism in adipocytes', *American Journal of Physiology: Endocrinology and Metabolism*, 296(4), pp. E635–E646.

Bisso, A. *et al.* (2013) 'Oncogenic miR-181a/b affect the DNA damage response in aggressive breast cancer', *Cell Cycle*, 12(11), pp. 1679–1687.

Bjørndal, B. *et al.* (2011) 'Different adipose depots: Their role in the development of metabolic syndrome and mitochondrial response to hypolipidemic agents', *Journal of Obesity*, 2011, pp. 1–15.

Boden, G. (2008) 'Obesity and Free Fatty Acids', *Endocrinology and Metabolism Clinics of North America*, 37(3), pp. 635–646.

Boom, R. *et al.* (1990) 'Rapid and Simple Method for Purification of Nucleic Acids', *Journal of Clinical Microbiology*, 28(3), pp. 495–503.

Bradford, M. (1976) 'A Rapid and Sensitive Method for the Quantitation of Microgram Quantities of Protein Utilizing the Principle of Protein-Dye Binding', *Analytical Biochemistry*, 72, pp. 248–254.

Bryant, N. J., Govers, R. and James, D. E. (2002) 'Regulated transport of the glucose transporter GLUT4', *Nature Reviews: Molecular Cell Biology*, 3(4), pp. 267–277.

Caballero, B. (2007) 'The global epidemic of obesity: An overview', *Epidemiologic Reviews*, 29(1), pp. 1–5.

Cai, L. *et al.* (2002) 'Hyperglycemia-induced apoptosis in mouse myocardium: mitochondrial cytochrome c-mediated caspase-3 activation pathway', *Diabetes*, 51(6), pp. 1938–1948.

Calin, G. A. *et al.* (2002) 'Frequent deletions and down-regulation of microRNA genes miR15 and miR16 at 13q14 in chronic lymphocytic leukemia', *Proceedings of the National Academy of Sciences of the United States of America*, 99(24), pp. 15524–15529.

Calin, G. A. and Croce, C. M. (2006) 'MicroRNA-cancer connection: The beginning of a new tale', *Cancer Research*, 66(15), pp. 7390–7394.

Canman, C. E. *et al.* (1998) 'Activation of the ATM kinase by ionizing radiation and phosphorylation of p53', *Science*, 281(5383), pp. 1677–1679.

Caron, A., Richard, D. and Laplante, M. (2015) 'The Roles of mTOR Complexes in Lipid Metabolism', *Annual Review of Nutrition*, 35, pp. 321–348.

Chanda, D., Luiken, J. J. F. P. and Glatz, J. F. C. (2016) 'Signaling pathways involved in cardiac energy metabolism', *FEBS Letters*, 590, pp. 2364–2374.

Chang, G. R. *et al.* (2009) 'Rapamycin protects against high fat diet-induced obesity in C57BL/6J mice', *Journal of Pharmacological Sciences*, 109(4), pp. 496–503.

Chang, T. *et al.* (2007) 'Transactivation of miR-34a by p53 broadly influences gene expression and promotes apoptosis', *Molecular Cell*, 26(5), pp. 745–752.

Che, Y. *et al.* (2018) 'Role of autophagy in a model of obesity: A long-term high fat diet induces cardiac dysfunction', *Molecular Medicine Reports*, 18(3), pp. 3251–3261.

Chen, C. H. *et al.* (2019) 'MicroRNA-21 Mediates the Protective Effect of Cardiomyocyte-Derived Conditioned Medium on Ameliorating Myocardial Infarction in Rats', *Cells*, 8(8), pp. 935–952.

Cheng, A. *et al.* (2020) 'ATM loss disrupts the autophagy-lysosomal pathway', *Autophagy*, pp. 1–13.

Ching, J. *et al.* (2013) 'Impaired insulin-stimulated glucose transport in ATM-deficient mouse skeletal muscle', *Applied Physiology, Nutrition, and Metabolism*, 38(6), pp. 589–596.

Ching, J. K. *et al.* (2013) 'Ataxia telangiectasia mutated impacts insulin-like growth factor 1 signalling in skeletal muscle', *Experimental Physiology*, 98(2), pp. 526–535.

Chomczynski, P. and Sacchi, N. (1987) 'Single step method of RNA isolation by acid guanidinium thiocyanate-phenol-cloroform extraction', *Anal Biochem*, 162(1), pp. 156–159.

Cianflone, K., Xia, Z. and Chen, L. Y. (2003) 'Critical review of acylation-stimulating protein physiology in humans and rodents', *Biochimica et Biophysica Acta*, 1609(2), pp. 127–143.

Cinti, S. (2012) 'The adipose organ at a glance', *Disease Models & Mechanisms*, 5(5), pp. 588–594.

Coelho, M., Oliveira, T. and Fernandes, R. (2013) 'Biochemistry of adipose tissue: an endocrine organ', *Archives of Medical Science*, 9(2), pp. 191–200.

Coll, T. *et al.* (2008) 'Oleate reverses palmitate-induced insulin resistance and inflammation in skeletal muscle cells', *Journal of Biological Chemistry*, 283(17), pp. 11107–11116.

Considine, R. V. *et al.* (1996) 'Serum immunoreactive-leptin concentrations in normal-weight and

obese humans', *New England Journal of Medicine*, 334(5), pp. 292–295.

Copier, C. U. *et al.* (2017) 'Circulating miR-19b and miR-181b are potential biomarkers for diabetic cardiomyopathy', *Scientific Reports*, 7(13514).

Cortez, D. *et al.* (1999) 'Requirement of ATM-dependent phosphorylation of Brca1 in the DNA damage response to double-strand breaks', *Science*, 286(5442), pp. 1162–1166.

Cosentino, C., Grieco, D. and Costanzo, V. (2011) 'ATM activates the pentose phosphate pathway promoting anti-oxidant defence and DNA repair', *EMBO Journal*, 30(3), pp. 546–555.

Costa, P. Z. and Soares, R. (2013) 'Neovascularization in diabetes and its complications. Unraveling the angiogenic paradox', *Life Sciences*, 92(22), pp. 1037–1045.

Coughlan, K. A. *et al.* (2013) 'Nutrient Excess in AMPK Downregulation and Insulin Resistance', *Journal of endocrinology, diabetes & obesity*, 1(1), p. 1008.

Crick, F. (1958) 'On protein synthesis', *Symposia of the Society for Experimental Biology*, 12, pp. 138–163.

Dagon, Y., Avraham, Y. and Berry, E. (2006) 'AMPK activation regulates apoptosis, adipogenesis, and lipolysis by eIF2α in adipocytes', *Biochemical and Biophysical Research Communications*, 340(1), pp. 43–47.

Daval, M., Foufelle, F. and Ferré, P. (2006) 'Functions of AMP-activated protein kinase in adipose tissue', *Journal of Physiology*, 574(1), pp. 55–62.

Desjardins, P. R. and Conklin, D. S. (2010) 'NanoDrop microvolume quantitation of nucleic acids', *Journal of Visualized Experiments*, 45(2565), pp. 1–4.

Eckel, R., Grundy, S. and Zimmet, P. (2005) 'The metabolic syndrome', *Lancet*, 365(9468), pp. 1415–1428.

Elagizi, A. *et al.* (2018) 'An Overview and Update on Obesity and the Obesity Paradox in Cardiovascular Diseases', *Progress in Cardiovascular Diseases*, 61(2), pp. 142–150.

Espach, Y. *et al.* (2015) 'ATM Protein Kinase Signaling, Type 2 Diabetes and Cardiovascular Disease', *Cardiovascular Drugs and Therapy*, 29, pp. 51–58.

Fain, J. N. *et al.* (2004) 'Comparison of the release of adipokines by adipose tissue, adipose tissue matrix, and adipocytes from visceral and subcutaneous abdominal adipose tissues of obese humans', *Endocrinology*, 145(5), pp. 2273–2282.

Flier, J. S. *et al.* (1987) 'Severely impaired adipsin expression in genetic and acquired obesity', *Science*, 237(4813), pp. 405–408.

Foster, C. *et al.* (2012) 'Lack of ATM induces structural and functional changes in the heart: Role in β-adrenergic receptor-stimulated apoptosis', *Experimental Physiology*, 97(4), pp. 506–515.

Foster, C. R. *et al.* (2011) 'Ataxia telangiectasia mutated kinase plays a protective role in β-adrenergic receptor-stimulated cardiac myocyte apoptosis and myocardial remodeling', *Molecular and Cellular Biochemistry*, 353(1–2), pp. 13–22.

Fried, S., Bunkin, D. and Greenberg, A. (1998) 'Omental and Subcutaneous Adipose Tissues of Obese Subjects Release Interleukin-6: Depot Difference and Regulation by Glucocorticoid', *Journal of Clinical Endocrinology & Metabolism*, 83(3), pp. 847–850.

Gauthier, M. S. *et al.* (2011) 'Decreased AMP-activated protein kinase activity is associated with increased inflammation in visceral adipose tissue and with whole-body insulin resistance in morbidly obese humans', *Biochemical and Biophysical Research Communications*, 404(1), pp. 382–387.

Ghai, V. *et al.* (2019) 'Circulating RNAs as predictive markers for the progression of type 2 diabetes', *Journal of Cellular and Molecular Medicine*, 23(4), pp. 2753–2768.

Glazer, H. P. *et al.* (2009) 'Hypercholesterolemia is associated with hyperactive cardiac mTORC1 and mTORC2 signaling', *Cell Cycle*, 8(11), pp. 1738–1746.

Green, H. and Kehinde, O. (1974) 'Sublines of mouse 3T3 cells that accumulate lipid', *Cell*, 1, pp. 113–116.

Green, H. and Kehinde, O. (1975) 'An established preadipose cell line and its differentiation in culture II. Factors affecting the adipose conversion', *Cell*, 5(1), pp. 19–27.

Green, H. and Kehinde, O. (1976) 'Spontaneous heritable changes leading to increased adipose conversion in 3T3 cells', *Cell*, 7(1), pp. 105–113.

Guay, C. *et al.* (2011) 'Diabetes mellitus, a microRNA-related disease?', *Translational Research*, 157(4), pp. 253–264.

Le Guezennec, X. *et al.* (2012) 'Wip1-dependent regulation of autophagy, obesity, and atherosclerosis', *Cell Metabolism*, 16(1), pp. 68–80.

Guiu-Jurado, E. *et al.* (2015) 'Downregulation of de novo fatty acid synthesis in subcutaneous adipose tissue of moderately obese women', *International Journal of Molecular Sciences*, 16(12), pp. 29911–29922.

Guo, Z. *et al.* (2010) 'ATM Activation by Oxidative Stress', *Science*, 330(6003), pp. 517–521.

Gürtler, A. *et al.* (2013) 'Stain-Free technology as a normalization tool in Western blot analysis',

Analytical Biochemistry, 433(2), pp. 105–111.

Ha, H. and Pak, Y. (2005) 'Modulation of the caveolin-3 and Akt status in caveolae by insulin resistance in H9c2 cardiomyoblasts', *Experimental and Molecular Medicine*, 37(3), pp. 169–178.

Halaby, M. *et al.* (2008) 'ATM protein kinase mediates full activation of Akt and regulates glucose transporter 4 translocation by insulin in muscle cells', *Cellular Signalling*, 20, pp. 1555–1563.

Hamanaka, R. B. and Chandel, N. S. (2011) 'Mitochondrial reactive oxygen species regulate cellular signaling and dictate biological outcomes', *Trends in Biochemical Sciences*, 35(9), pp. 505–513.

Hardie, D. G. and Pan, D. A. (2002) 'Regulation of fatty acid synthesis and oxidation by the AMP-activated protein kinase', *Biochemical Society Transactions*, 30(6), pp. 1064–1070.

He, L. *et al.* (2007) 'A microRNA component of the p53 tumour suppressor network', *Nature*, 447(7148), pp. 1130–1134.

Hekmatdoost, A. *et al.* (2011) 'Dietary fatty acid composition and metabolic syndrome in Tehranian adults', *Nutrition*, 27(10), pp. 1002–1007.

Hescheler, J. *et al.* (1991) 'Morphological, biochemical, and electrophysiological characterization of a clonal cell (H9c2) line from rat heart', *Circulation Research*, 69(6), pp. 1476–1486.

Hotamisligil, G. *et al.* (1995) 'Increased adipose tissue expression of tumor necrosis factor-alpha in human obesity and insulin resistance', *The Journal of Clinical Investigation*, 95(5), pp. 2409–2415.

Hotamisligil, G., Shargill, N. and Spiegelman, B. (1993) 'Adipose expression of tumor necrosis factor-alpha: direct role in obesity-linked insulin resistance', *Science*, 259(5091), pp. 87–91.

Hu, H. *et al.* (2010) 'ATM is down-regulated by N-Myc-regulated microRNA-421', *Proceedings of the National Academy of Sciences of the United States of America*, 107(4), pp. 1506–1511.

Hu, M. *et al.* (2016) 'Metformin Protects H9C2 Cardiomyocytes from High-Glucose and Hypoxia/Reoxygenation Injury via Inhibition of Reactive Oxygen Species Generation and Inflammatory Responses: Role of AMPK and JNK', *Journal of Diabetes Research*, 2016, pp. 1–9.

Hue, L. and Taegtmeyer, H. (2009) 'The Randle cycle revisited: a new head for an old hat', *American Journal of Physiology: Endocrinology and Metabolism*, 297(3), pp. E578–E591.

Huisamen, B. *et al.* (2016) 'Is low ATM protein responsible for myocardial insulin resistance

associated with obesity?', *Cardiovascular Research*, 111(Suppl 1), pp. S88–S89.

Ibrahim, M. M. (2009) 'Subcutaneous and visceral adipose tissue: structural and functional differences', *Obesity reviews: Etiology and Pathophysiology*, 11, pp. 11–18.

Jaacks, L. M. *et al.* (2019) 'The obesity transition: stages of the global epidemic', *The Lancet Diabetes and Endocrinology*, 7(3), pp. 231–240.

Jaeger, A. *et al.* (2018) 'Circulating microRNAs -192 and -194 are associated with the presence and incidence of diabetes mellitus', *Scientific Reports*, 8, pp. 1–14.

James, P. T. (2004) 'Obesity: The worldwide epidemic', *Clinics in Dermatology*, 22(4), pp. 276–280.

Jensen, M. D. (2006) 'Adipose tissue as an endocrine organ: Implications of its distribution on free fatty acid metabolism', *European Heart Journal Supplements*, 8(Suppl_B), pp. B13–B19.

Jeong, I. *et al.* (2010) 'Role of ataxia telangiectasia mutated in insulin signaling of muscle-derived cell lines and mouse soleus', *Acta Physiologica*, 198(4), pp. 465–475.

Kakimoto, Y. *et al.* (2018) 'Overexpression of miR-221 in sudden death with cardiac hypertrophy patients', *Heliyon*, 4(6), p. e00639.

Kershaw, E. and Flier, J. (2004) 'Adipose Tissue as an Endocrine Organ', *The Journal of Endocrinology & Metabolism*, 89(6), pp. 2548–2556.

Khamzina, L. *et al.* (2005) 'Increased activation of the mammalian target of rapamycin pathway in liver and skeletal muscle of obese rats: Possible involvement in obesity-linked insulin resistance', *Endocrinology*, 146(3), pp. 1473–1481.

Kim, J. E. and Chen, J. (2004) 'Regulation of peroxisome proliferator-activated receptor-γ activity by mammalian target of rapamycin and amino acids in adipogenesis', *Diabetes*, 53(11), pp. 2748–2756.

Kim, S. *et al.* (2016) 'AMPK Phosphorylates Desnutrin/ATGL and Hormone-Sensitive Lipase To Regulate Lipolysis and Fatty Acid Oxidation within Adipose Tissue', *Molecular and cellular biology*, 36(14), pp. 1961–1976.

Kimes, B. and Brandt, B. (1976) 'Properties of a clonal muscle cell line from rat heart', *Experimental Cell Research*, 98(2), pp. 367–381.

Ko, H. *et al.* (2009) 'Nutrient stress activates inflammation and reduces glucose metabolism by suppressing AMP-activated protein kinase in the heart', *Diabetes*, 58(11), pp. 2536–2546.

Kreuz, S. *et al.* (2009) 'Acetyl-CoA carboxylases 1 and 2 show distinct expression patterns in rats and humans and alterations in obesity and diabetes', *Diabetes/Metabolism Research and*

Reviews, 25(6), pp. 577–586.

Kulshreshtha, R. *et al.* (2006) 'A MicroRNA Signature of Hypoxia', *Molecular and Cellular Biology*, 27(5), pp. 1859–1867.

Kwon, B. and Querfurth, H. W. (2015) 'Palmitate activates mTOR/p70S6K through AMPK inhibition and hypophosphorylation of raptor in skeletal muscle cells: Reversal by oleate is similar to metformin', *Biochimie*, 118, pp. 141–150.

Laemmli, U. (1970) 'Cleavage of structural proteins during the assembly of the head of bacteriophage T4.', *Nature*, 227(5259), pp. 680–685.

Lagos-Quintana, M. *et al.* (2001) 'Identification of novel genes coding for small expressed RNAs', *Science*, 294(5543), pp. 853–858.

Landin, K. *et al.* (1990) 'Abdominal obesity is associated with an impaired fibrinolytic activity and elevated plasminogen activator inhibitor-1', *Metabolism*, 39(10), pp. 1044–1048.

Landrier, J.-F., Derghal, A. and Mounien, L. (2019) 'MicroRNAs in Obesity and Related Metabolic Disorders', *Cells*, 8(8), p. 859.

Latouche, C. *et al.* (2016) 'MicroRNA-194 modulates glucose metabolism and its skeletal muscle expression is reduced in diabetes', *PLoS ONE*, 11(5), pp. 1–20.

Lau, N. *et al.* (2001) 'An abundant class of tiny RNAs with probable regulatory roles in Caenorhabditis elegans', *Science*, 294(5543), pp. 858–862.

Lavin, M. F. *et al.* (2004) 'Functional consequences of sequence alterations in the ATM gene', *DNA Repair*, 3(8–9), pp. 1197–1205.

Lavin, M. F. and Kozlov, S. (2007) 'ATM activation and DNA damage response', *Cell Cycle*, 6(8), pp. 931–942.

Lee, J. H., Jeong, J. K. and Park, S. Y. (2018) 'AMPK Activation Mediated by Hinokitiol Inhibits Adipogenic Differentiation of Mesenchymal Stem Cells through Autophagy Flux', *International Journal of Endocrinology*, 2018.

Lee, R. and Ambros, V. (2001) 'An extensive class of small RNAs in Caenorhabditis elegans', *Science*, 294(5543), pp. 862–864.

Lee, R., Feinbaum, R. and Ambros, V. (1993) 'The C. elegans heterochronic gene lin-4 encodes small RNAs with antisense complementarity to lin-14', *Cell*, 75(5), pp. 843–854.

Lee, Y. *et al.* (2002) 'MicroRNA maturation: Stepwise processing and subcellular localization', *EMBO Journal*, 21(17), pp. 4663–4670.

Lei, E. P. and Silver, P. A. (2002) 'Protein and RNA export from the nucleus', *Developmental Cell*, 2(3), pp. 261–272.

Leung, A. and Sharp, P. (2010) 'MicroRNA Functions in Stress Responses', *Molecular Cell*, 40(2), pp. 205–215.

Li, Z. L. *et al.* (2012) 'Transition from obesity to metabolic syndrome is associated with altered myocardial autophagy and apoptosis', *Arteriosclerosis, Thrombosis, and Vascular Biology*, 32(5), pp. 1132–1141.

Liu, T. *et al.* (2015) 'High-fat diet alters serum fatty acid profiles in obesity prone rats: implications for in-vitro studies', *Lipids*, 50(10), pp. 997–1008.

Liu, Y., Beyer, A. and Aebersold, R. (2016) 'On the Dependency of Cellular Protein Levels on mRNA Abundance', *Cell*, 165(3), pp. 535–550.

Livak, K. and Schmittgen, T. (2001) 'Analysis of Relative Gene Expression Data Using Real- Time Quantitative PCR and the 2^-DDCT Method', *Methods*, 26, pp. 402–408.

Longo, M. *et al.* (2019) 'Adipose tissue dysfunction as determinant of obesity-associated metabolic complications', *International Journal of Molecular Sciences*, 20(9), p. 2358.

Lopaschuk, G. D. *et al.* (2010) 'Myocardial fatty acid metabolism in health and disease', *Physiological Reviews*, 90(1), pp. 207–258.

Lovejoy, J. *et al.* (2002) 'Effects of diets enriched in saturated (palmitic), unsaturated (oleic), or trans (elaidic) fatty acids on insulin sensitivity and substrate oxidation in healthy adults', *Diabetes Care*, 25(8), pp. 1283–1288.

Maniataki, E. and Mourelatos, Z. (2005) 'A human, ATP-independent, RISC assembly machine fueled by pre-miRNA', *Genes & Development*, 19(24), pp. 2979–2990.

Manning, B. D. (2004) 'Balancing Akt with S6K: Implications for both metabolic diseases and tumorigenesis', *The Journal of Cell Biology*, 167(3), pp. 399–403.

Marchand, A. *et al.* (2016) 'miR-322 regulates insulin signaling pathway and protects against metabolic syndrome-induced cardiac dysfunction in mice', *Biochimica et Biophysica Acta*, 1862, pp. 611–621.

Marseglia, L. *et al.* (2015) 'Oxidative stress in obesity: A critical component in human diseases', *International Journal of Molecular Sciences*, 16(1), pp. 378–400.

Matsuoka, S. *et al.* (2007) 'ATM and ATR substrate analysis reveals extensive protein networks responsive to DNA damage', *Science*, 316(5828), pp. 1160–1166.

Mendell, J. and Olson, E. (2012) 'MicroRNAs in Stress Signaling and Human Disease', *Cell*, 148(6), pp. 1172–1187.

Mercer, J. R. *et al.* (2010) 'DNA damage links mitochondrial dysfunction to atherosclerosis and the metabolic syndrome', *Circulation Research*, 107(8), pp. 1021–1031.

Min, K. H., Yang, W. M. and Lee, W. (2018) 'Saturated fatty acids-induced miR-424–5p aggravates insulin resistance via targeting insulin receptor in hepatocytes', *Biochemical and Biophysical Research Communications*, 503(3), pp. 1587–1593.

Mohamed-Ali, V. *et al.* (1997) 'Subcutaneous adipose tissue releases interleukin-6, but not tumor necrosis factor-α, in vivo', *Journal of Clinical Endocrinology and Metabolism*, 82(12), pp. 4196–4200.

Morange, M. (2009) 'The Central Dogma of Molecular Biology: A Retrospective after Fifty Years', *Resonance*, 14(3), pp. 236–247.

Mosmann, T. (1983) 'Rapid colorimetric assay for cellular growth and survival: Application to proliferation and cytotoxicity assays', *Journal of Immunological Methods*, 65(1–2), pp. 55–63.

Munday, M. R. (2002) 'Regulation of mammalian acetyl-CoA carboxylase', *Biochemical Society Transactions*, 30(6), pp. 1059–1064.

Mutharasan, R. K. *et al.* (2011) 'microRNA-210 is upregulated in hypoxic cardiomyocytes through Akt- and p53-dependent pathways and exerts cytoprotective effects', *American Journal of Physiology: Heart and Circulatory Physiology*, 301(4), pp. H1519–H1530.

Nascimento, A. F. *et al.* (2011) 'Long-term high-fat diet-induced obesity decreases the cardiac leptin receptor without apparent lipotoxicity', *Life Sciences*, 88(23–24), pp. 1031–1038.

Niemann, B. *et al.* (2013) 'Age and obesity-associated changes in the expression and activation of components of the AMPK signaling pathway in human right atrial tissue', *Experimental Gerontology*, 48(1), pp. 55–63.

Nilsson, E. *et al.* (2014) 'Altered DNA methylation and differential expression of genes influencing metabolism and inflammation in adipose tissue from subjects with type 2 diabetes', *Diabetes*, 63(9), pp. 2962–2976.

Nobuhara, M. *et al.* (2013) 'Mitochondrial dysfunction caused by saturated fatty acid loading induces myocardial insulin-resistance in differentiated H9c2 myocytes: A novel ex vivo myocardial insulin-resistance model', *Experimental Cell Research*, 319(7), pp. 955–966.

O'Brien, J. *et al.* (2018) 'Overview of microRNA biogenesis, mechanisms of actions, and

circulation', *Frontiers in Endocrinology*, 9(402), pp. 1–12.

Oh, W. K. *et al.* (2005) 'Glucose and fat metabolism in adipose tissue of acetyl-CoA carboxylase 2 knockout mice', *Proceedings of the National Academy of Sciences of the United States of America*, 102(5), pp. 1384–1389.

Ortega, F. J. *et al.* (2010) 'The gene expression of the main lipogenic enzymes is downregulated in visceral adipose tissue of obese subjects', *Obesity*, 18(1), pp. 13–20.

Ott, M. *et al.* (2007) 'Mitochondria, oxidative stress and cell death', *Apoptosis*, 12(5), pp. 913–922.

Palomer, X. *et al.* (2018) 'Palmitic and Oleic Acid: The Yin and Yang of Fatty Acids in Type 2 Diabetes Mellitus', *Trends in Endocrinology and Metabolism*, 29(3), pp. 178–190.

Pandita, T. K. *et al.* (2000) 'Ionizing radiation activates the ATM kinase throughout the cell cycle', *Oncogene*, 19(11), pp. 1386–1391.

Park, J. E. *et al.* (2011) 'Dicer recognizes the 5′ end of RNA for efficient and accurate processing', *Nature*, 475(7355), pp. 201–205.

Peng, X. ding *et al.* (2003) 'Dwarfism, impaired skin development, skeletal muscle atrophy, delayed bone development, and impeded adipogenesis in mice lacking Akt1 and Akt2', *Genes and Development*, 17(11), pp. 1352–1365.

Peng, Y. and Croce, C. M. (2016) 'The role of microRNAs in human cancer', *Signal Transduction and Targeted Therapy*, 1(15004).

Perdomo, L. *et al.* (2015) 'Protective role of oleic acid against cardiovascular insulin resistance and in the early and late cellular atherosclerotic process', *Cardiovascular Diabetology*, 14(75), pp. 1–12.

Polak, P. *et al.* (2008) 'Adipose-Specific Knockout of raptor Results in Lean Mice with Enhanced Mitochondrial Respiration', *Cell Metabolism*, 8(5), pp. 399–410.

Prentice, A. (2006) 'The emerging epidemic of obesity in developing countries', *International Journal of Epidemiology*, 35, pp. 93–99.

Ramírez-Zacarías, J., Castro-Muñozledo, F. and Kuri-Harcuch, W. (1992) 'Quantitation of adipose conversion and triglycerides by staining intracytoplasmic lipids with oil red O', *Histochemistry*, 97(6), pp. 493–497.

Raver-Shapira, N. *et al.* (2007) 'Transcriptional Activation of miR-34a Contributes to p53-Mediated Apoptosis', *Molecular Cell*, 26(5), pp. 731–743.

Roberts, C. K. and Sindhu, K. K. (2009) 'Oxidative stress and metabolic syndrome', *Life Sciences*.,

84(21–22), pp. 705–712.

Rønningen, T. *et al.* (2015) 'Epigenetic priming of inflammatory response genes by high glucose in adipose progenitor cells', *Biochemical and Biophysical Research Communications*, 467(4), pp. 979–986.

Rothblum-Oviatt, C. *et al.* (2016) 'Ataxia telangiectasia: a review', *Orphanet Journal of Rare Diseases*, 11(159).

Rubin, C. S. *et al.* (1978) 'Development of hormone receptors and hormonal responsiveness in vitro', *The Journal of Biological Chemistry*, 253(20), pp. 7570–7578.

Sadie-Van Gijsen, H. (2019) 'Adipocyte biology: It is time to upgrade to a new model', *Journal of Cellular Physiology*, 234(3), pp. 2399–2425.

Sadie-Van Gijsen, H., Kotzé-Hörstmann, L. and Huisamen, B. (2020) 'An In Vivo/Ex Vivo Study Design to Investigate Effects of Chronic Conditions and Therapeutic Compounds on Adipose Stem Cells in Animal Models', *Clinical and Preclinical Models for Maximizing Healthspan: Methods and Protocols*, 2138, pp. 101–118.

Saha, A. K. *et al.* (2011) 'Insulin resistance due to nutrient excess: Is it a consequence of AMPK downregulation?', *Cell Cycle*, 10(20), pp. 3447–3451.

Sarbassov, D. D. *et al.* (2005) 'Phosphorylation and regulation of Akt/PKB by the rictor-mTOR complex', *Science*, 307(5712), pp. 1098–1101.

Savitsky, K. *et al.* (1995) 'A single ataxia telangiectasia gene with a product similar to PI-3 kinase', *Science*, 268(5218), pp. 1749–1753.

Schmid, F. (2001) 'Biological Macromolecules : UV-visable Spectrophotometry', *Encyclopedia of Life Sciences*, pp. 1–4.

Schneider, J. *et al.* (2006) 'ATM-dependent suppression of stress signaling reduces vascular disease in metabolic syndrome', *Cell Metabolism*, 4(5), pp. 377–389.

Schroeder, A. *et al.* (2006) 'The RIN: An RNA integrity number for assigning integrity values to RNA measurements', *BMC Molecular Biology*, 7(3).

Schwenk, R. W. *et al.* (2008) 'Regulation of sarcolemmal glucose and fatty acid transporters in cardiac disease', *Cardiovascular Research*, 79(2), pp. 249–258.

Sciarretta, S., Volpe, M. and Sadoshima, J. (2014) 'mTOR Signaling in Cardiac Physiology and Disease', *Circulation Research*, 114(3), pp. 549–564.

Sebastiani, G. *et al.* (2017) 'Circulating microRNAs and diabetes mellitus: a novel tool for disease

prediction, diagnosis, and staging?', *Journal of Endocrinological Investigation*, 40(6), pp. 591–610.

Shen, C. and Houghton, P. (2013) 'The mTOR pathway negatively controls ATM by up-regulating miRNAs', *Proceedings of the National Academy of Sciences of the United States of America*, 110(29), pp. 11869–11874.

Shulman, G. (2000) 'Cellular mechanisms of insulin resistance', *The Journal of Clinical Investigation*, 106(2), pp. 171–176.

Siersbæk, R., Nielsen, R. and Mandrup, S. (2010) 'PPARγ in adipocyte differentiation and metabolism - Novel insights from genome-wide studies', *FEBS Letters*, 584(15), pp. 3242–3249.

Siiteri, P. (1987) 'Adipose tissue as a source of hormones', *The American Journal of Clinical Nutrition*, 45(1), pp. 277–282.

Sipido, K. R. and Marban, E. (1991) 'L-Type Calcium Channels , Potassium Channels , and Novel Nonspecific Cation Channels in a Clonal Muscle Cell Line Derived From Embryonic Rat Ventricle', *Circulation Research*, 69(6), pp. 1487–1499.

Skurk, T. *et al.* (2007) 'Relationship between adipocyte size and adipokine expression and secretion', *Journal of Clinical Endocrinology and Metabolism*, 92(3), pp. 1023–1033.

Song, L. *et al.* (2011) 'MiR-18a impairs DNA damage response through downregulation of Ataxia telangiectasia mutated (ATM) kinase', *PLoS ONE*, 6(9), p. e25454.

Spiegelman, B. M. and Flier, J. S. (1996) 'Adipogenesis and obesity: rounding out the big picture', *Cell*, 87(3), pp. 377–389.

Staiger, H. *et al.* (2004) 'Palmitate-induced interleukin-6 expression in human coronary artery endothelial cells', *Diabetes*, 53(12), pp. 3209–3216.

Steinbusch, L. K. M. *et al.* (2011) 'Subcellular trafficking of the substrate transporters GLUT4 and CD36 in cardiomyocytes', *Cellular and Molecular Life Sciences*, 68(15), pp. 2525–2538.

Steppan, C. *et al.* (2001) 'The hormone resistin links obesity to diabetes', *Nature*, 409(6818), pp. 301–312.

Storlien, L. *et al.* (1991) 'Influence of dietary fat composition on development of insulin resistance in rats. Relationship to muscle triglyceride and omega-3 fatty acids in muscle phospholipid', *Diabetes*, 40(2), pp. 280–289.

Su, Q. *et al.* (2017) 'MiRNA Expression Profile of the Myocardial Tissue of Pigs with Coronary

Microembolization', *Cellular Physiology and Biochemistry*, 43(3), pp. 1012–1024.

Su, Y. and Swift, M. (2000) 'Mortality Rates among Carriers of Ataxia-Telangiectasia Mutant Alleles', *Annals of Internal Medicine*, 133(10), pp. 770–778.

Sun, P. *et al.* (2019) 'MiR-181b regulates atherosclerotic inflammation and vascular endothelial function through Notch1 signaling pathway', *European Review for Medical and Pharmacological Sciences*, 23(7), pp. 3051–3057.

Sun, X. *et al.* (2012) 'MicroRNA-181b regulates NF-kB – mediated vascular inflammation, *The Journal of Clinical Investigation*, 122(6), pp. 1973–1990.

Sun, X. *et al.* (2016) 'MicroRNA-181b Improves Glucose Homeostasis and Insulin Sensitivity by Regulating Endothelial Function in White Adipose Tissue', *Circulation Research*, 118(5), pp. 810–821.

Takagi, M. *et al.* (2015) 'ATM Regulates Adipocyte Differentiation and Contributes to Glucose Homeostasis', *Cell Reports*, 10(6), pp. 957–967.

Takahashi, K. *et al.* (2003) 'Adiposity Elevates Plasma MCP-1 Levels Leading to the Increased CD11b-positive Monocytes in Mice', *The Journal of Biological Chemistry*, 278(47), pp. 46654–46660.

Tang, Q. Q. and Lane, M. D. (2012) 'Adipogenesis: From Stem Cell to Adipocyte', *Annual Review of Biochemistry*, 81, pp. 715–736.

Thong, F. S. L., Dugani, C. B. and Klip, A. (2005) 'Turning signals on and off: GLUT4 traffic in the insulin-signaling highway', *Physiology*, 20(4), pp. 271–284.

Towbin, H., Staehelin, T. and Gordon, J. (1979) 'Electrophoretic transfer of proteins from polyacrylamide gels to nitrocellulose sheets: Procedure and some applications', *Proceedings of the National Academy of Sciences of the United States of America*, 76(9), pp. 4350–4354.

Trayhurn, P. and Beattie, J. H. (2001) 'Physiological role of adipose tissue: white adipose tissue as an endocrine and secretory organ', *Proceedings of the Nutrition Society*, 60(3), pp. 329–339.

Tremblay, F. *et al.* (2007) 'Identification of IRS-1 Ser-1101 as a target of S6K1 in nutrient- and obesity-induced insulin resistance', *Proceedings of the National Academy of Sciences of the United States of America*, 104(35), pp. 14056–14061.

Tsigos, C. *et al.* (1999) 'Circulating tumor necrosis factor alpha concentrations are higher in abdominal versus peripheral obesity', *Metabolism: Clinical and Experimental*, 48(10), pp. 1332–1335.

Uchinaka, A. *et al.* (2017) 'Effects of mTOR inhibition on cardiac and adipose tissue pathology and glucose metabolism in rats with metabolic syndrome', *Pharmacology Research and Perspectives*, 5(4), p. e00331.

Uematsu, M. *et al.* (2020) 'Multiplex fatty acid imaging inside cells by Raman microscopy', *The FASEB Journal*, 34, pp. 10357–10372.

Um, S. H. *et al.* (2004) 'Absence of S6K1 protects against age- and diet-induced obesity while enhancing insulin sensitivity', *Nature*, 431(7005), pp. 200–205.

Unger, R., Zhou, Y. and Orci, L. (1999) 'Regulation of fatty acid homeostasis in cells: Novel role of leptin', *Proceedings of the National Academy of Sciences of the United States of America*, 96(5), pp. 2327–2332.

Vaishya, S., Sarwade, R. D. and Seshadri, V. (2018) 'MicroRNA, proteins, and metabolites as novel biomarkers for prediabetes, diabetes, and related complications', *Frontiers in Endocrinology*, 9, pp. 1–12.

Vessby, B., Tengblad, S. and Lithell, H. (1994) 'Insulin sensitivity is related to the fatty acid composition of serum lipids and skeletal muscle phospholipids in 70-year-old men', *Diabetologia*, 37(10), pp. 1044–1050.

Villena, J. A. *et al.* (2004) 'Induced Adiposity and Adipocyte Hypertrophy in Mice Lacking the AMP-Activated Protein Kinase-alpha2 Subunit', *Diabetes*, 53, pp. 2242–2249.

Viniegra, J. *et al.* (2005) 'Full activation of PKB/Akt in response to insulin or ionizing radiation is mediated through ATM', *Journal of Biological Chemistry*, 280(6), pp. 4029–4036.

Virtue, S. and Vidal-Puig, A. (2010) 'Adipose tissue expandability, lipotoxicity and the Metabolic Syndrome - An allostatic perspective', *Biochimica et Biophysica Acta*, 1801(3), pp. 338–349.

Van Der Vusse, G. J., Van Bilsen, M. and Glatz, J. F. C. (2000) 'Cardiac fatty acid uptake and transport in health and disease', *Cardiovascular Research*, 45(2), pp. 279–293.

Wachter, S. B. and Gilbert, E. M. (2012) 'Beta-adrenergic receptors, from their discovery and characterization through their manipulation to beneficial clinical application', *Cardiology*, 122(2), pp. 104–112.

Wajchenberg, B. (2000) 'Subcutaneous and Visceral Adipose Tissue: Their Relationship to the Metabolic Syndrome', *Endocrine Reviews*, 21(6), pp. 697–738.

Wakil, S. J. and Abu-Elheiga, L. A. (2009) 'Fatty acid metabolism: Target for metabolic syndrome', *Journal of Lipid Research*, 50(Suppl), pp. S138–S143.

Wang, K. *et al.* (2015) 'E2F1-dependent miR-421 regulates mitochondrial fragmentation and myocardial infarction by targeting Pink1', *Nature Communications*, 6(7619), pp. 1–13.

Wang, S. S. *et al.* (2017) 'Expression of miR-18a and miR-34c in circulating monocytes associated with vulnerability to type 2 diabetes mellitus and insulin resistance', *Journal of Cellular and Molecular Medicine*, 21(12), pp. 3372–3380.

Wang, X. *et al.* (2009) 'Adverse effects of high glucose and free fatty acid on cardiomyocytes are mediated by connective tissue growth factor', *American Journal of Physiology: Cell Physiology*, 297(6), pp. 1490–1500.

Weisberg, S. *et al.* (2003) 'Obesity is associated with macrophage accumulation in adipose tissue', *The Journal of Clinical Investigation*, 112(12), pp. 1796–1808.

Weyer, C. *et al.* (2001) 'Hypoadiponectinemia in Obesity and Type 2 Diabetes: Close Association with Insulin Resistance and Hyperinsulinemia', *The Journal of Clinical Endocrinology and Metabolism*, 86(5), pp. 1930–1935.

Wiemand, H. *et al.* (2009) 'An essential role for the Glut1 PDZ-binding motif in growth factor regulation of Glut1 degradation and trafficking', *Biochemical Journal*, 418(2), pp. 345–367.

Wightman, B., Ha, I. and Ruvkun, G. (1993) 'Posttranscriptional regulation of the heterochronic gene lin-14 by lin-4 mediates temporal pattern formation in C. elegans', *Cell*, 75(5), pp. 855–862.

Wingard, M. C. *et al.* (2020) 'Heart failure and diabetes: role of ATM', *Current Opinion in Pharmacology*, 54, pp. 27–35.

Winkler, G. *et al.* (2003) 'Expression of tumor necrosis factor (TNF)-α protein in the subcutaneous and visceral adipose tissue in correlation with adipocyte cell volume, serum TNF-α, soluble serum TNF-receptor-2 concentrations and C-peptide level', *European Journal of Endocrinology*, 149(2), pp. 129–135.

Wu, C. W. *et al.* (2013) 'MicroRNA-18a Attenuates DNA Damage Repair through Suppressing the Expression of Ataxia Telangiectasia Mutated in Colorectal Cancer', *PLoS ONE*, 8(2), p. e57036.

Wu, D. F. *et al.* (2005) 'Heterozygous mutation of ataxia-telangiectasia mutated gene aggravates hypercholesterolemia in apoE-deficient mice', *Journal of Lipid Research*, 46(7), pp. 1380–1387.

Xu, X. H. *et al.* (2017) 'Resveratrol transcriptionally regulates miRNA-18a-5p expression ameliorating diabetic nephropathy via increasing autophagy', *European Review for Medical and Pharmacological Sciences*, 21(21), pp. 4952–4965.

Xu, X. J. *et al.* (2012) 'Insulin sensitive and resistant obesity in humans: AMPK activity, oxidative stress, and depot-specific changes in gene expression in adipose tissue', *Journal of Lipid Research*, 53(4), pp. 792–801.

Yang, D. and Kastan, M. (2000) 'Participation of ATM in insulin signalling through phosphorylation of eIF-4E-binding protein 1', *Nature Cell Biology*, 2, pp. 893–898.

Ye, J. (2013) 'Mechanisms of insulin resistance in obesity', *Frontiers in Medicine*, 7(1), pp. 14–24.

Zhang, J. *et al.* (2015) 'ATM Functions at the Peroxisome to Induce Pexophagy in Response to ROS', *Nature Cell Biology*, 17(10), pp. 1259–1269.

Zhang, Y. *et al.* (1994) 'Positional cloning of the mouse obese gene and its human homologue', *Nature*, 372, pp. 425–432.

Zhang, Y. *et al.* (2018) 'Mitochondrial redox sensing by the kinase ATM maintains cellular antioxidant capacity', *Science Signaling*, 11(538).

Zhu, Y. *et al.* (2013) 'Regulation of fatty acid metabolism by mTOR in adult murine hearts occurs independently of changes in PGC-1α', *American Journal of Physiology: Heart and Circulatory Physiology*, 305, pp. H41–H51.

Appendix A

Procedures prior to the harvesting of the CM, as performed by Dr H. Sadie-van Gijsen

Animals

Dietary intervention

Animal work was performed from October 2018 to May 2019 by Dr H. Sadie-van Gijsen. The conditioned media used in the current MSc study was derived from animals that formed part of a larger study. Only the dietary information **(*Table A1*)** and biometrical data **(*Table A2*** and ***Figure A1*)** of the animals relevant to the current study will be included as described in the protocol by Dr H. Sadie-van Gijsen.

Briefly, ethical approval was obtained from the Stellenbosch University Research Ethics Committee: Animal Care and Use (ethics number ACU-2018-6786). Animals were housed at the Animal Research Facility, Tygerberg campus, Stellenbosch University. At 4 weeks after weaning (approximately 6 weeks of age, body weight 170-200g), male Wistar rats were started on either a standard laboratory control (CON) chow diet (n=4) or a high fat/fructose/cholesterol (OB2) diet (n=4). The OB2 diet (referred to in this study as the HFD) was prepared by combining CON pellets with large amounts of Holsum, fructose, cholesterol and casein. A breakdown of the macronutrient composition for each diet is listed in ***Table A1***. Animals had *ad libitum* access to food and water at all times and body weights were recorded weekly. Animals were sacrificed at 16 weeks by means of intraperitoneal injection with a lethal dose of sodium pentobarbital (160 mg/kg).

Table A1: Composition of the control (CON) and high-fat (OB2) diets.

	CON	OB2
Starch (g/100 g)	22.1	4.7
Glycaemic carbohydrate (g/100 g)	27.4	11.5
Total sugar (g/100 g)	5.2	6.7
Glucose (g/100 g)	0.1	0.2
Sucrose (g/100 g)	4.6	1.5
Fructose (g/100 g)	0.3	4.4
Other (maltose, lactose, galactose, trehalose) (g/100 g)	0.2	0.7
Total fat (g/100 g)	5.04	24.09
%kJ from fat	15.4	66.0

Saturated fat (g/100 g)	1.28	14.3
Mono-unsaturated fat (g/100 g)	1.28	7.42
Poly-unsaturated fat (g/100 g)	2.48	2.38
Cholesterol (mg/100 g)	44	440
Protein (g/100 g)	25.8	12.9
Fibre (g/100 g)	16.8	5.5
Energy (kJ/100 g)	**1225**	**1350**

Biometric data

The following biometric measurements relevant to the current MSc study were recorded per rat per diet group:

Table A2: Biometric measurements of control (n=4) and HFD (n=4) rats.

Animal	Total body weight (g)	Change in body weight (g)	OGTT (AUC)	PR fat weight one side (g)	% PR fat (of total body weight)
CON A	359	176	118.4	0.57	0.318
CON B	413	228	130.9	1.14	0.552
CON C	431	221	183.7	1.05	0.487
CON D	406	202	150.3	1	0.493
	402.25	**206.75**	**145.825**	**0.94**	**0.4625**
OB E	384	214	246.2	0.91	0.513
OB F	399	223	274.9	0.98	0.491
OB G	427	236	365	2.68	1.255
OB H	410	224	68.7	1.27	0.62
	405	**224.25**	**238.7**	**1.46**	**0.71975**

AUC: area under curve; OGTT: oral glucose tolerance test; PR: peri-renal

A two-tailed Student's t-test was performed to compare the biometric data of the two diet groups **(*Figure A1*)**.

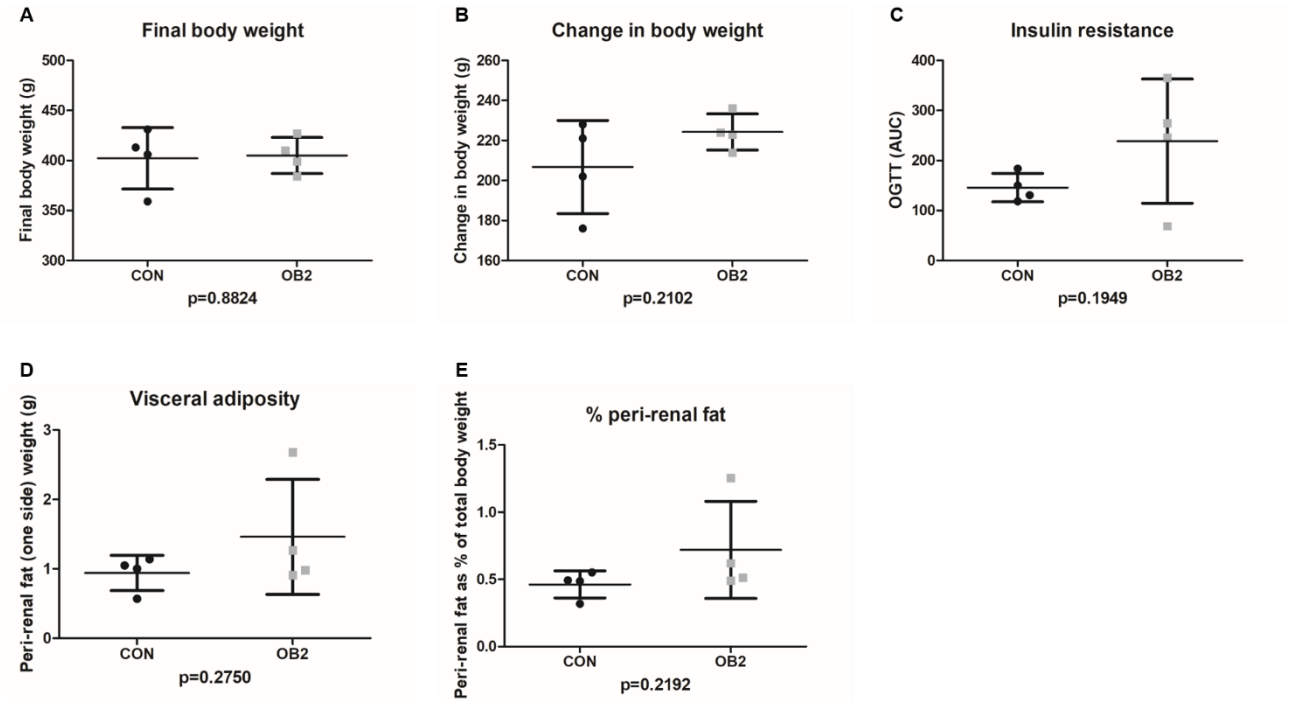

Figure A1: Biometric measurements of control diet animals (CON; n=4) and HFD animals (OB2; n=4). *No significant differences between the diet groups were observed (two-tailed Student's t-test; mean ± SD; $p<0.05$ considered statistically significant).*

ASC isolation and adipocytic differentiation

Briefly, the ASCs were harvested from the inguinal subcutaneous fat pad and the peri-renal (visceral) fat pad of control and HFD rats. The isolated ASCs were maintained in culture until post-confluency was reached, whereafter a subset of ASCs was induced to differentiate to mature adipocytes using adipogenic induction media. A detailed protocol for the harvesting, culturing and adipocytic differentiation of primary ASCs has been published (Sadie-Van Gijsen, Kotzé-Hörstmann and Huisamen, 2020). The lipid accumulation of differentiated adipocytes was determined by Dr H. Sadie-van Gijsen through Oil Red O staining and quantified using ImageJ software. A two-tailed Student's t-test was performed to compare the percentage staining of subcutaneous and visceral adipocytes in each diet group **(*Figure A2*)**.

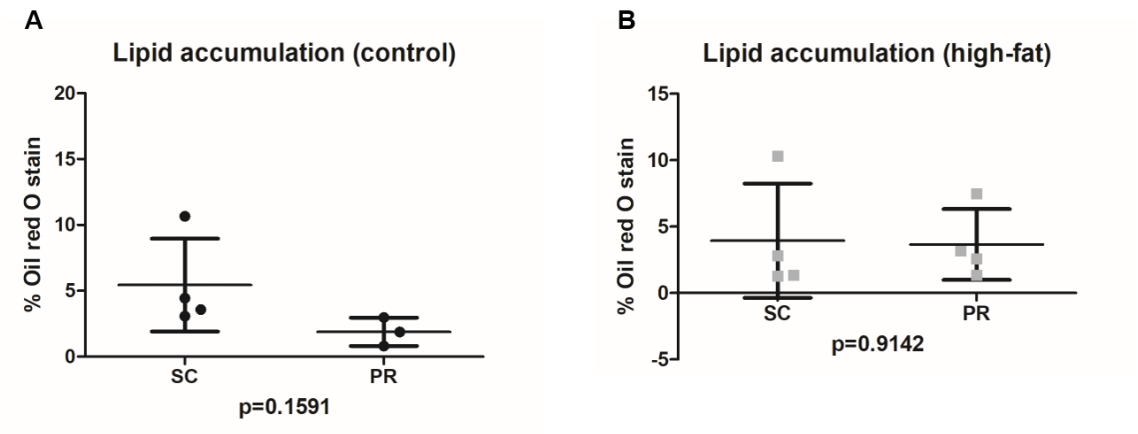

Figure A2: The lipid accumulation as determined by Oil Red O staining of subcutaneous (SC) and visceral (PR) adipocytes originating from control and HFD rats. *No significant differences in lipid accumulation between the fat depots were observed (two-tailed Student's t-test; percentage ± SD; $p<0.05$ considered statistically significant).*

Appendix B

Chapter 4: Additional information

MTT viability assay

The absorbance values (in triplicate) are displayed as OD (optical density) at 570 nm in ***Figure B1***.

	Raw Data (570)					
	1	**2**	**3**	**4**	**5**	**6**
A	0,069	0,077	0,073	0,068	0,072	0,068
B	0,082	0,077	0,066	0,081	0,083	0,064
C	0,077	0,076	0,078	0,073	0,074	0,075
D						

DMEM cnt | EtOH cnt | FFA | FFA + glu | Ins | Ins + FFA

Figure B1: The absorbance values (in triplicate) at 570 nm of H9c2 cells. *(1) DMEM control, (2) EtOH control, (3) FFAs (palmitic- and oleic acid), (4) FFA and glucose, (5) insulin, and (6) insulin and FFAs (technical n=3 per condition).*

Western blot analysis: membrane images used for total protein normalisation

The total protein of each sample lysate was transferred from hand-casted acrylamide gels onto stain-free membranes **(*Figure B2-B6)*** and imaged using the ChemiDoc™ system for normalisation analyses.

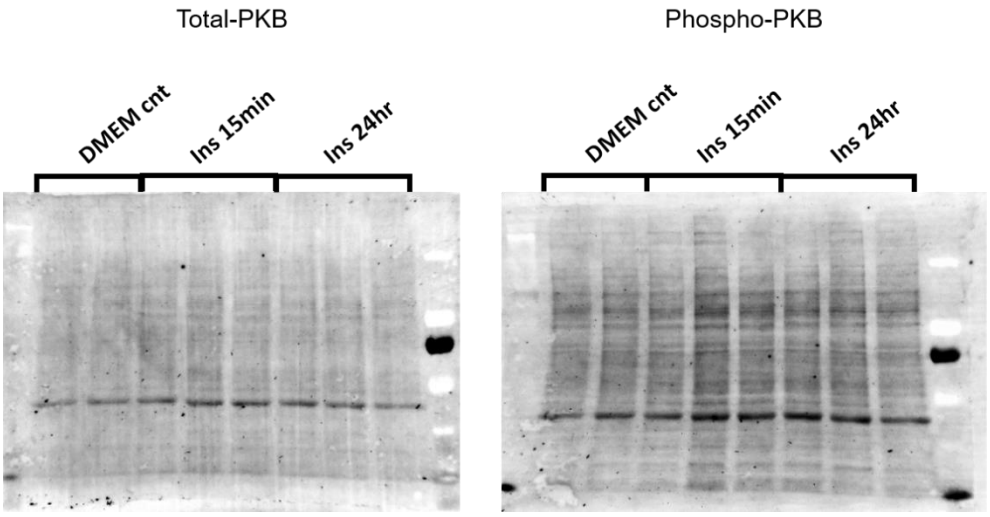

Figure B2: Membranes used for PKB normalisation.

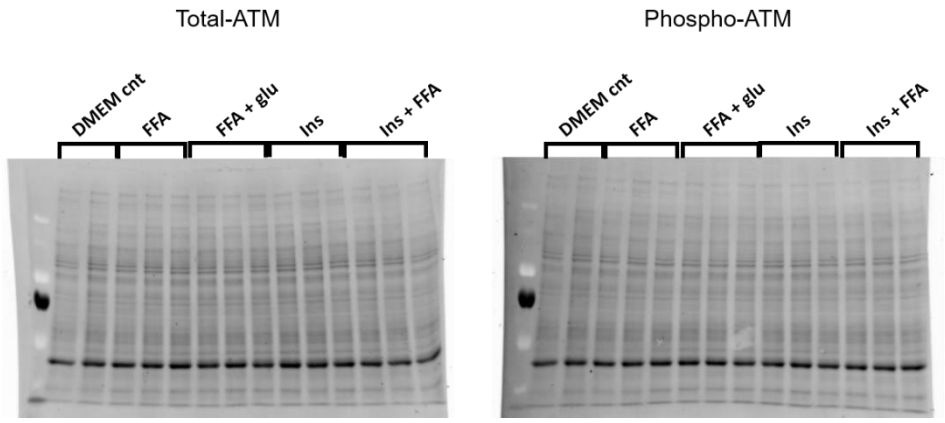

Figure B3: Representative membranes used for ATM normalisation.

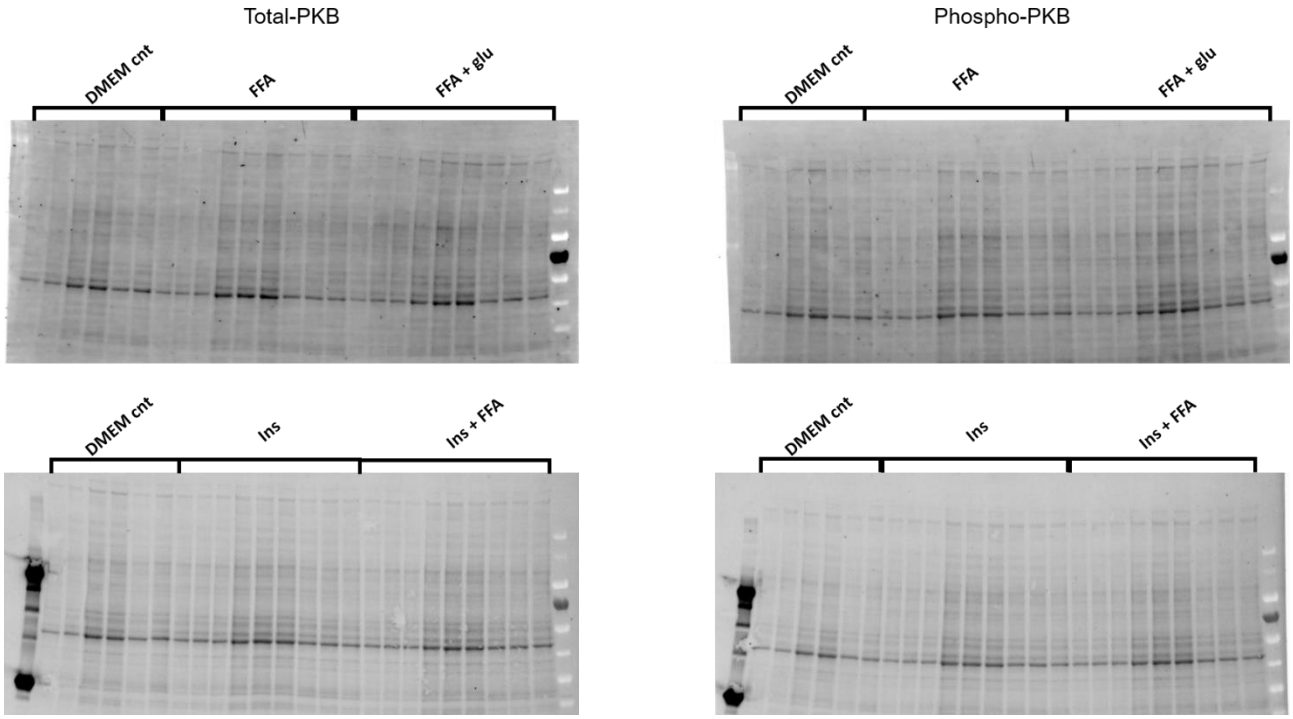

Figure B4: Membranes used for PKB normalisation.

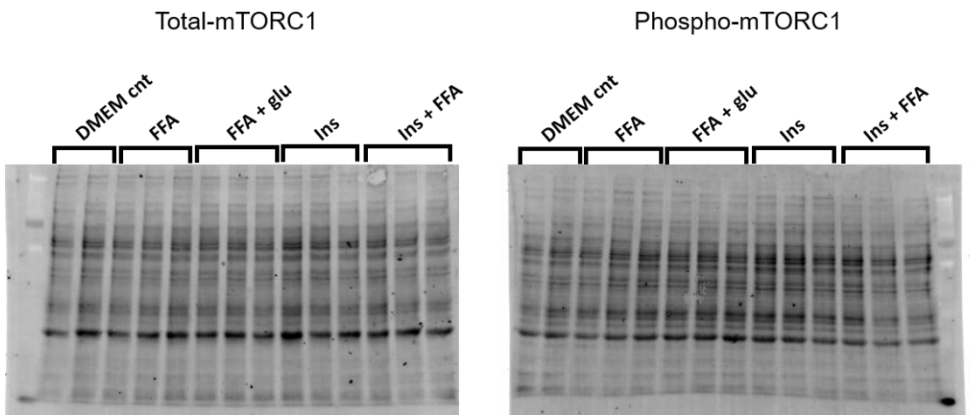

Figure B5: Representative membranes used for mTORC1 normalisation.

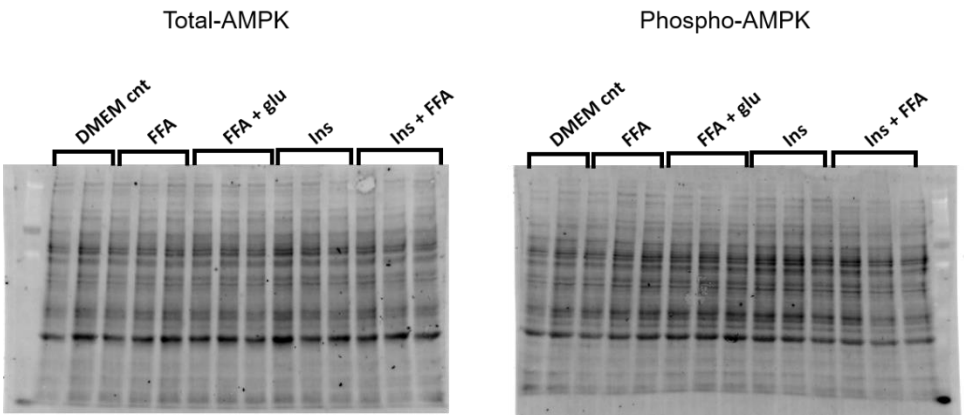

Figure B6: Representative membranes used for AMPK normalisation.

qRT-PCR analysis: RNA concentrations and purity, primer optimisation and U6 snRNA as an appropriate endogenous control miRNA

Total RNA concentration and purity (260/280 and 260/230 absorbance ratios) were determined using the NanoDrop™ 2000c spectrophotometer **(*Table B1*)**.

Table B1: Total RNA concentration and purity.

RNA sample	Concentration (ng/µl)	260/280 ratio	260/230 ratio
DMEM cnt 1	158.8	2.11	1.94
DMEM cnt 2	255.5	2.09	0.87
DMEM cnt 3	109.7	2.11	1.54
FFA 1	152.2	2.12	2.00
FFA 2	205.5	2.11	2.05
FFA 3	104.8	2.11	1.57
FFA + glu 1	154.6	2.12	1.89
FFA + glu 2	194.1	2.09	1.99
FFA + glu 3	88.1	2.12	1.84
Ins 1	147.9	2.11	1.65
Ins 2	193.0	2.12	0.87
Ins 3	107.6	2.12	1.75
Ins + FFA 1	147.4	2.13	1.88
Ins + FFA 2	208.8	2.11	1.60
Ins + FFA 3	120.7	2.12	1.41

A 10x dilution series, ranging from a 100% neat sample to a 0.001% dilution, using a pooled cDNA sample was used (see ***Figure B7*** for qRT-PCR plate layout) to construct amplification plots and linear

standard curves for all miRNA primers (miR-421, miR-18a and U6 snRNA) using the QuantStudio™ 7 Flex Real-Time PCR software. The amplification plots were used to assess whether the fluorescent signal from each miRNA primer could accumulate to threshold at a Ct-value below 35, whereas the standard curves were used to analyse the primer efficiencies, as well as identify the most optimal dilution factor for the cDNA samples.

	1	2	3	4	5	6	7	8	9	10	11	12
A	100	100	100	100	100	100						
B	10	10	10	10	10	10						
C	1	1	1	1	1	1						
D	0,1	0,1	0,1	0,1	0,1	0,1						
E	0,01	0,01	0,01	0,01	0,01	0,01						
F	0,001	0,001	0,001	0,001	0,001	0,001						
G	NTC	NTC	NTC	NTC	NTC	NTC						
H												
	miR-421		miR-18a		U6 snRNA							

Figure B7: The qRT-PCR plate layout for the standard curve using a 10x dilution series in duplicate from a pooled cDNA sample.

<u>miRNA-421</u>

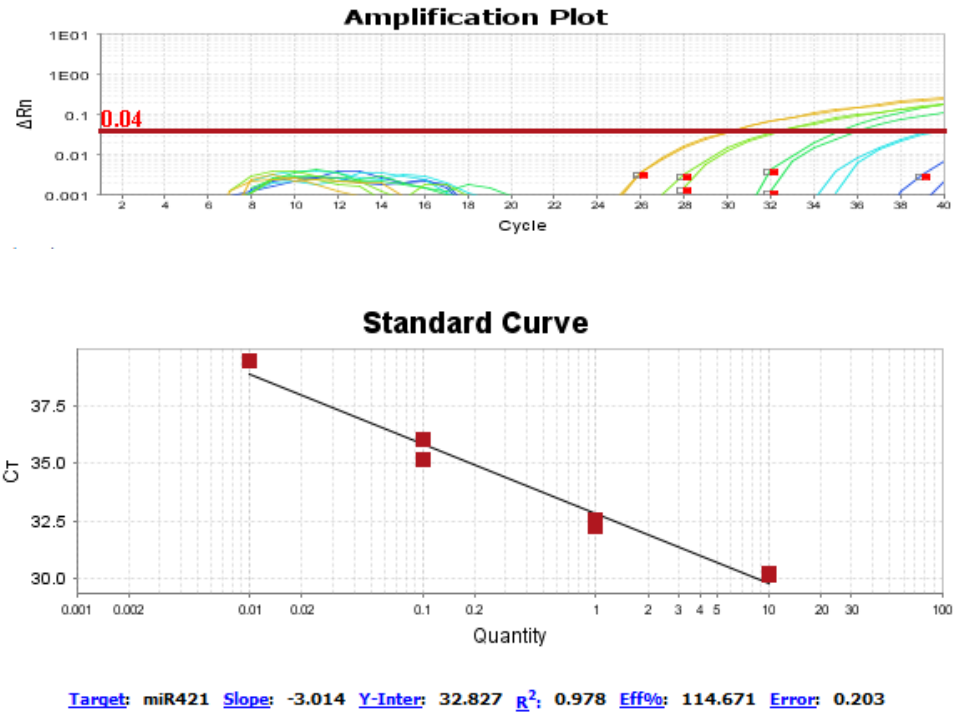

Figure B8: The amplification plot and standard curve of miR-421.

miR-18a

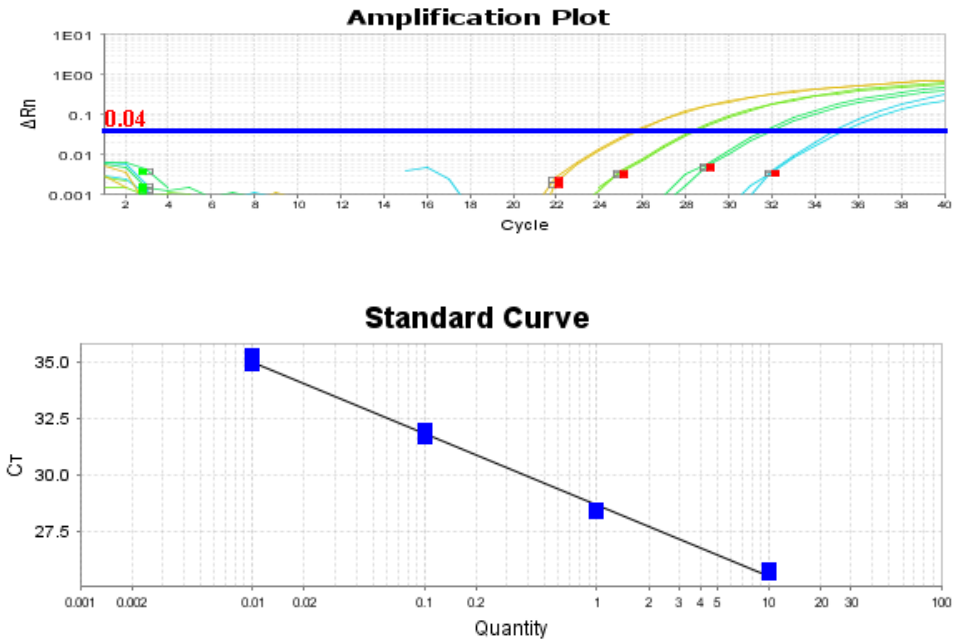

Figure B9: The amplification plot and standard curve of miR-18a.

U6 snRNA

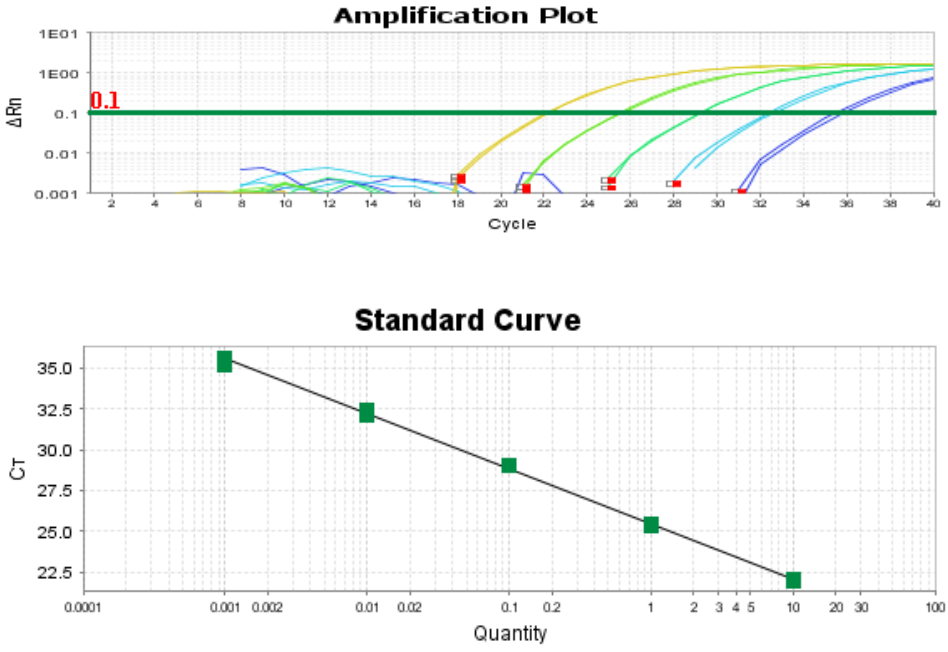

Figure B10: The amplification plot and standard curve of U6 snRNA.

The cDNA samples of a single animal were analysed in duplicate on the same qRT-PCR plate (see ***Figure B11*** for qRT-PCR plate layout).

	1	2	3	4	5	6	7	8	9	10	11	12	
A	cnt A	cnt B	cnt C	FFA A	FFA B	FFA C	FFA + glu A	FFA + glu B	FFA + glu C	Ins A	Ins B	Ins C	miR-421
B	cnt A	cnt B	cnt C	FFA A	FFA B	FFA C	FFA + glu A	FFA + glu B	FFA + glu C	Ins A	Ins B	Ins C	
C	Ins + FFA A	Ins + FFA B	Ins + FFA C	NTC	cnt A	cnt B	cnt C	FFA A	FFA B	FFA C	FFA + glu A	FFA + glu B	miR-18a
D	Ins + FFA A	Ins + FFA B	Ins + FFA C	Neg	cnt A	cnt B	cnt C	FFA A	FFA B	FFA C	FFA + glu A	FFA + glu B	
E	FFA + glu C	Ins A	Ins B	Ins C	Ins + FFA A	Ins + FFA B	Ins + FFA C	NTC	cnt A	cnt B	cnt C	FFA A	U6 snRNA
F	FFA + glu C	Ins A	Ins B	Ins C	Ins + FFA A	Ins + FFA B	Ins + FFA C	Neg	cnt A	cnt B	cnt C	FFA A	
G	FFA B	FFA C	FFA + glu A	FFA + glu B	FFA + glu C	Ins A	Ins B	Ins C	Ins + FFA A	Ins + FFA B	Ins + FFA C	NTC	
H	FFA B	FFA C	FFA + glu A	FFA + glu B	FFA + glu C	Ins A	Ins B	Ins C	Ins + FFA A	Ins + FFA B	Ins + FFA C	Neg	

Figure B11: The qRT-PCR plate layout for the cDNA samples in duplicate.

U6 snRNA is a common and widely-used endogenous control RNA used for normalising target miRNA expression. We have established that U6 snRNA is stably expressed in H9c2 cells treated with various combinations of FFAs, glucose and insulin **(*Figure B12*)**. Each sample (biological n=3) was analysed in duplicate and the mean Ct-values were compared by one-way ANOVA, followed by a Bonferroni post-hoc test. No statistically significant differences in mean Ct-values were observed among the different treatment groups, confirming its stable expression and deeming U6 snRNA an appropriate endogenous control for H9c2 cells in response to high concentrations of nutrients and/or insulin.

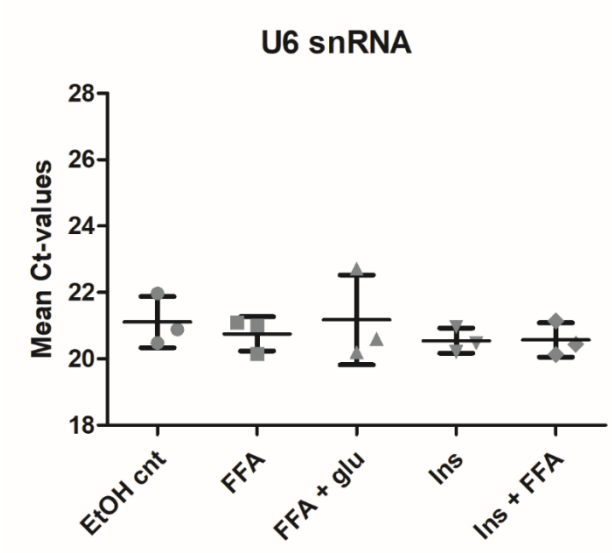

Figure B12: U6 snRNA displayed stable expression in H9c2 cells. *No significant differences in U6 snRNA expression were observed in H9c2 cells were treated with combinations of high FFAs, glucose and insulin (one-way ANOVA, Bonferroni post-test; mean Ct-value ± SD; $p<0.05$ considered statistically significant).*

Appendix C

Chapter 5: Additional information

Western blot analysis: membrane images used for total protein normalisation

The total protein of each sample lysate was transferred from hand-casted acrylamide gels onto stain-free membranes **(*Figures C1-C4*)** and imaged using the ChemiDoc™ system for normalisation analyses.

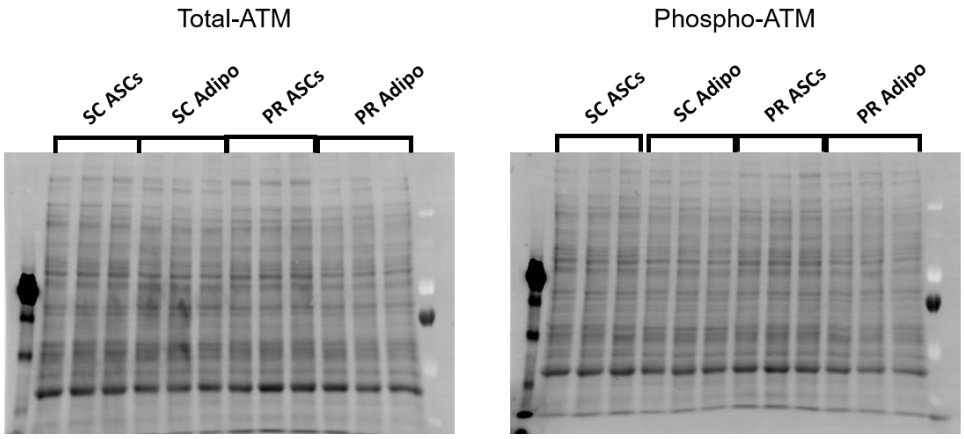

Figure C1: Representative membranes used for ATM normalisation.

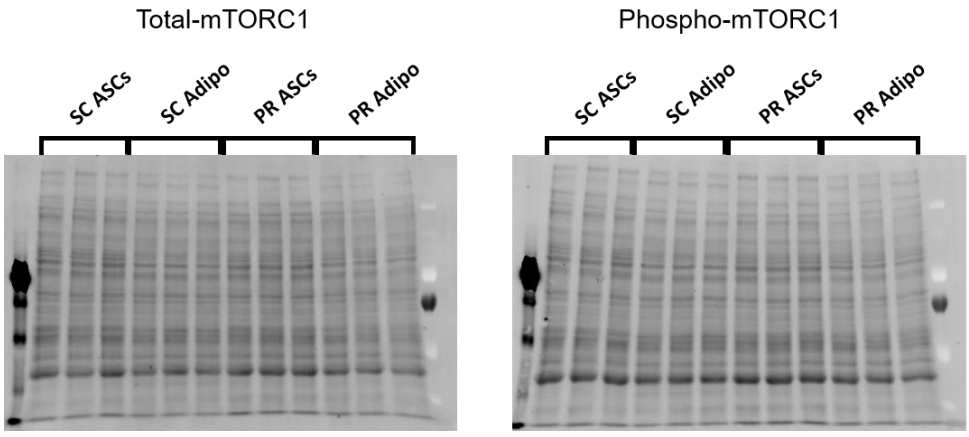

Figure C2: Representative membranes used for mTORC1 normalisation.

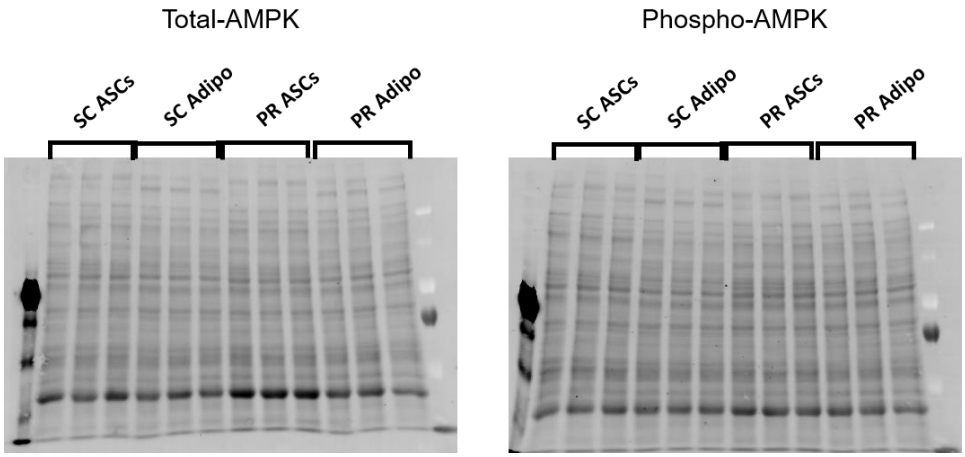

Figure C3: Representative membranes used for AMPK normalisation.

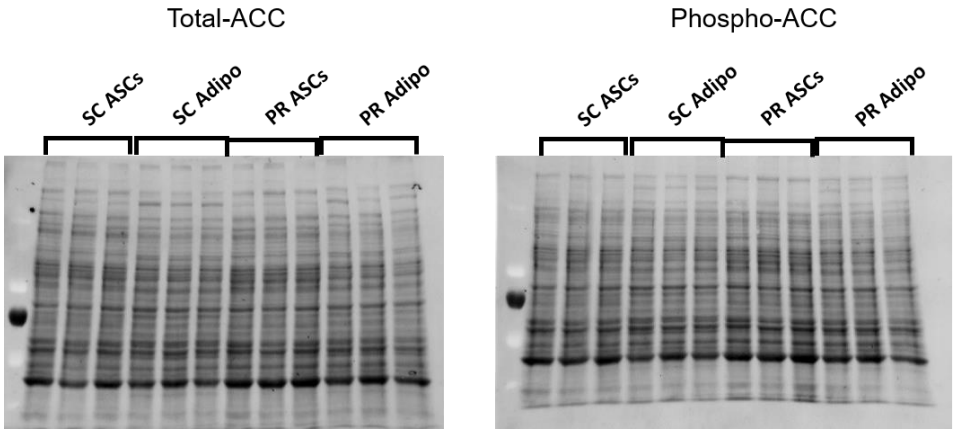

Figure C4: Representative membranes used for ACC (1,2) normalisation.

Appendix D

Chapter 6: Additional information

Western blot analysis: establishment of common DMEM control and membrane images used for total protein normalisation

To compare results between individual experiments (H9c2 cells treated with adipose-derived CM), a common control had to be established by comparing the DMEM control conditions for each individual experiment to ensure that no significant differences in metabolic protein activity were present to serve as a baseline. We compared the ATM total levels **(*Figure D1 A*)** and phosphorylated AMPK levels **(*Figure D1 B*)** between each DMEM control condition.

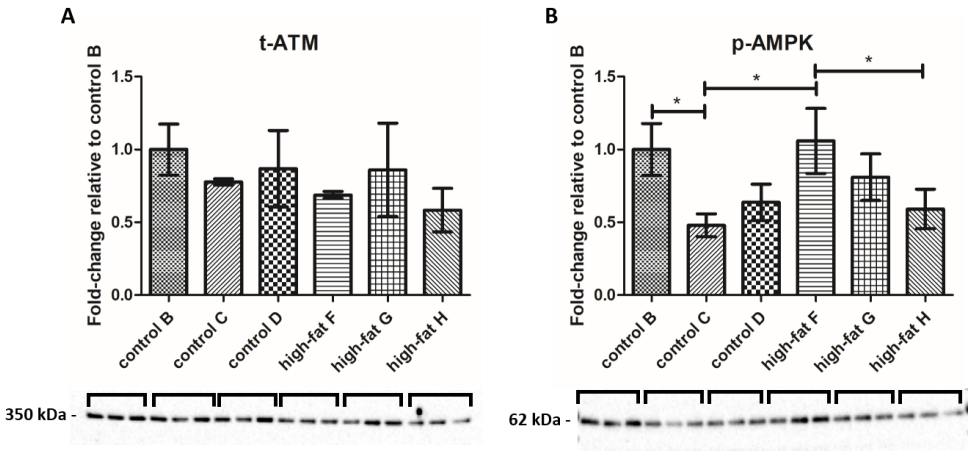

Figure D1: Total ATM levels (A) and phosphorylated AMPK levels (B) were determined between the DMEM control conditions of each experiment. *No significant differences were observed in total ATM levels, however significant differences were observed in phosphorylated AMPK levels (one-way ANOVA; Bonferroni post-test; *p<0.05).*

No significant changes were observed between the total ATM levels, however significant differences were observed in phosphorylated AMPK levels between experiments B and C ($p<0.05$), C and F ($p<0.05$), and F and H ($p<0.05$). The latter results are unexpected, as all the groups represent H9c2 cells treated with complete DMEM media only. H9c2 cells of similar passage (17 or 18) treated with complete DMEM media were incubated for the same duration (24 hours) in a similar sterile environment (at 37°C in 95% humidified air). Furthermore, the protein lysates were prepared to the same protein concentration per sample, and proteins were normalised to the total protein per lane following Western blot analysis to compensate for unequal loading. In an attempt to correct for the significant differences observed in phosphorylated AMPK levels in the control-treated cells, the protein lysates from experiments B (representing a control experiment) and G (representing an HFD

experiment) were pooled and served as a common DMEM control that was loaded onto each polyacrylamide gel.

The total protein of each sample lysate was transferred from Criterion™ TGX Stain-Free™ gels onto stain-free membranes **(*Figures D2* and *D3*)** and imaged using the ChemiDoc™ system for normalisation analyses. The control diet-derived CM-treated H9c2 cells are indicated in black, whereas the HFD-derived CM-treated H9c2 cells are indicated in grey.

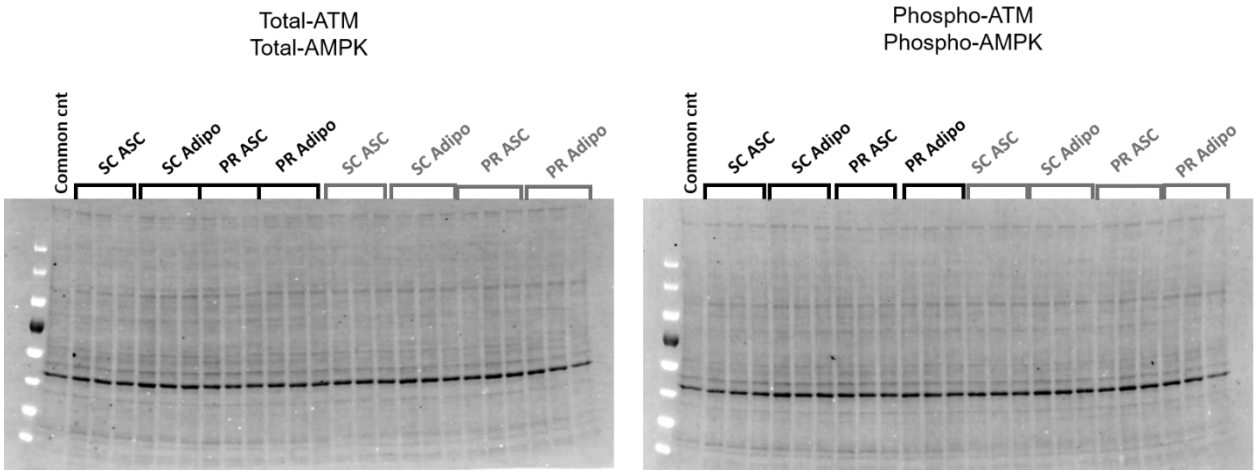

Figure D2: Representative membranes used for ATM and AMPK normalisation.

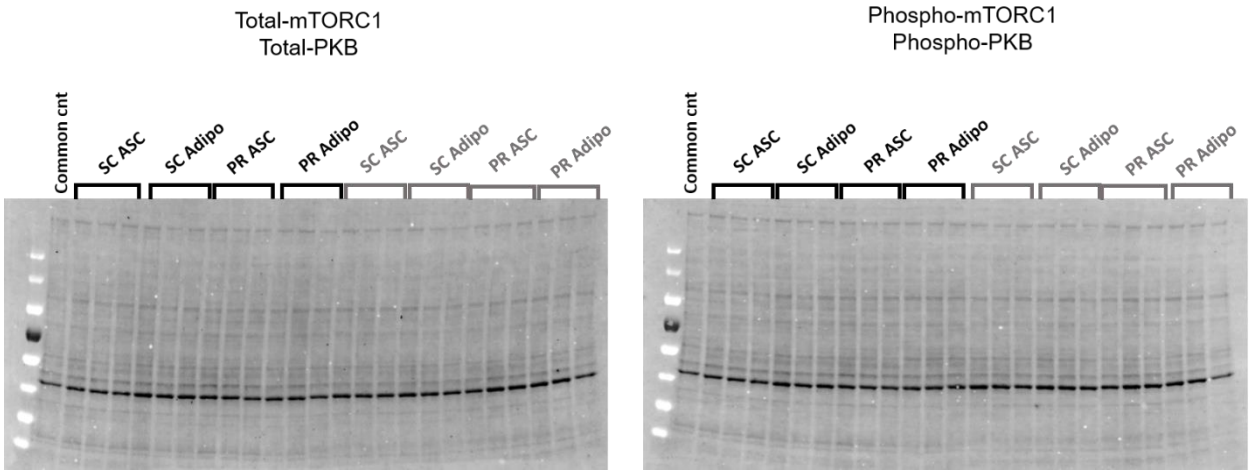

Figure D3: Representative membranes used for mTORC1 and PKB normalisation.

qRT-PCR analysis: RNA concentration and purity, RIN allocations, primer optimisation, U6 snRNA as an appropriate endogenous control miRNA, and establishment of common DMEM control

Total RNA concentration and purity (260/280 and 260/230 absorbance ratios) were determined using the NanoDrop™ 2000c spectrophotometer **(*Table D1*)**.

Table D1: Total RNA concentration and purity as determined by NanoDrop™ spectrophotometry.

RNA sample	Concentration (ng/µl)	260/280 ratio	260/230 ratio
DMEM cnt A	135.4	2.15	1.95
DMEM cnt B	189.2	2.09	1.69
DMEM cnt C	177.5	2.11	2.07
DMEM cnt D	224.5	2.13	2.07
DMEM cnt E	124.8	2.14	1.35
DMEM cnt F	191.6	2.13	2.21
DMEM cnt G	227.0	2.11	1.78
DMEM cnt H	128.6	2.14	1.71
SC ASC A	138.2	2.16	1.86
SC ASC B	165.9	2.11	1.85
SC ASC C	180.8	2.13	2.10
SC ASC D	178.5	2.14	1.92
SC ASC E	84.4	2.11	1.88
SC ASC F	136.6	2.12	2.13
SC ASC G	170.9	2.10	0.74
SC ASC H	105.1	2.14	1.45
SC Adipo A	146.7	2.16	1.87
SC Adipo B	173.1	2.11	2.15
SC Adipo C	153.9	2.12	2.18
SC Adipo D	166.8	2.14	2.04
SC Adipo E	102.5	2.13	1.98
SC Adipo F	120.6	2.14	2.24
SC Adipo G	177.1	2.11	2.16
SC Adipo H	95.0	2.13	1.32
PR ASC A	136.6	2.17	2.01
PR ASC B	173.1	2.11	1.75
PR ASC C	148.1	2.13	1.89
PR ASC D	189.6	2.13	1.62
PR ASC E	83.6	2.14	1.39
PR ASC F	124.8	2.14	2.24
PR ASC G	169.5	2.11	2.17
PR ASC H	98.3	2.11	1.34
PR Adipo A	134.6	2.16	1.36
PR Adipo B	162.8	2.12	2.17

PR Adipo C	163.8	2.11	1.46
PR Adipo D	164.0	2.13	1.54
PR Adipo E	80.7	2.13	0.80
PR Adipo F	111.6	2.13	2.24
PR Adipo G	149.5	2.10	2.14
PR Adipo H	92.2	2.14	1.43

12 total RNA samples were randomly selected across all 8 experiments and submitted to the Central Analytical Facility (CAF) for RNA integrity analysis (RIN allocation) with the Agilent 2100 Bioanalyzer. Briefly, the RNA samples were separated on an agarose gel by electrophoresis based on size and visualised through laser-induced fluorescence detection **(*Figure D4*)**. The gel image was used to compile RNA electropherograms **(*Figure D5*)** and the areas under the 18S and 28S ribosomal RNA (rRNA) peaks were calculated as a ratio of the total area under the curve (a high number indicates that little to no degradation has occurred). All 12 samples scored a RIN of 10, which confirms that the isolated RNA molecules were fully intact.

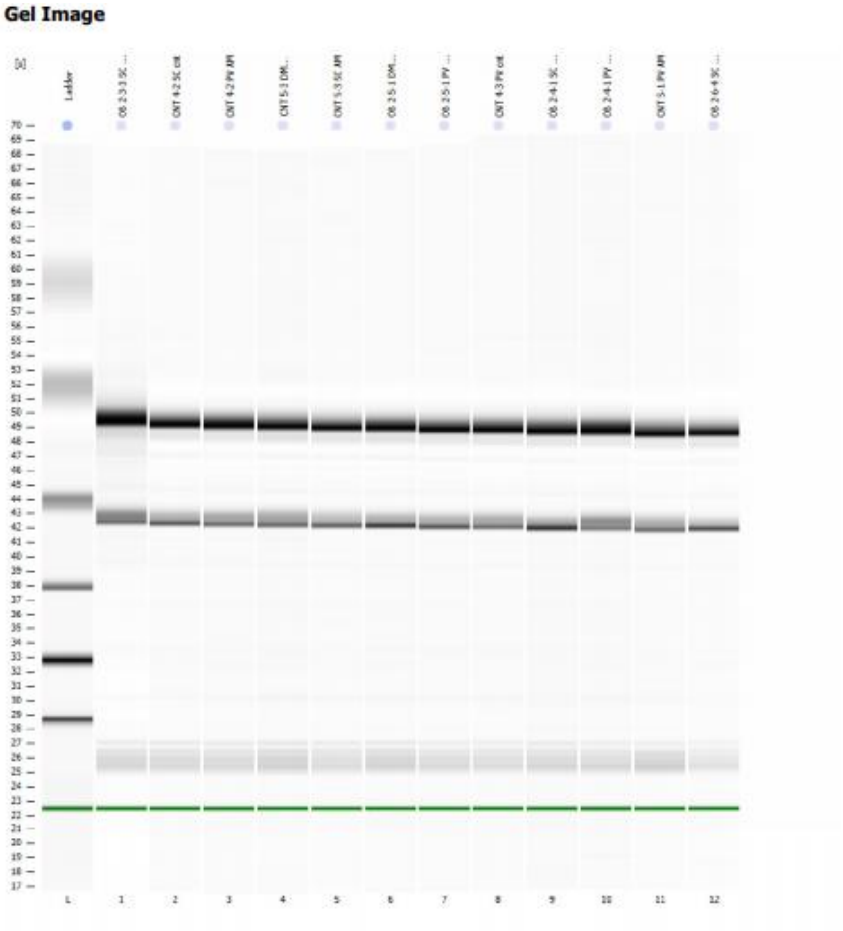

Figure D4: Image of the total RNA samples separated on an agarose gel.

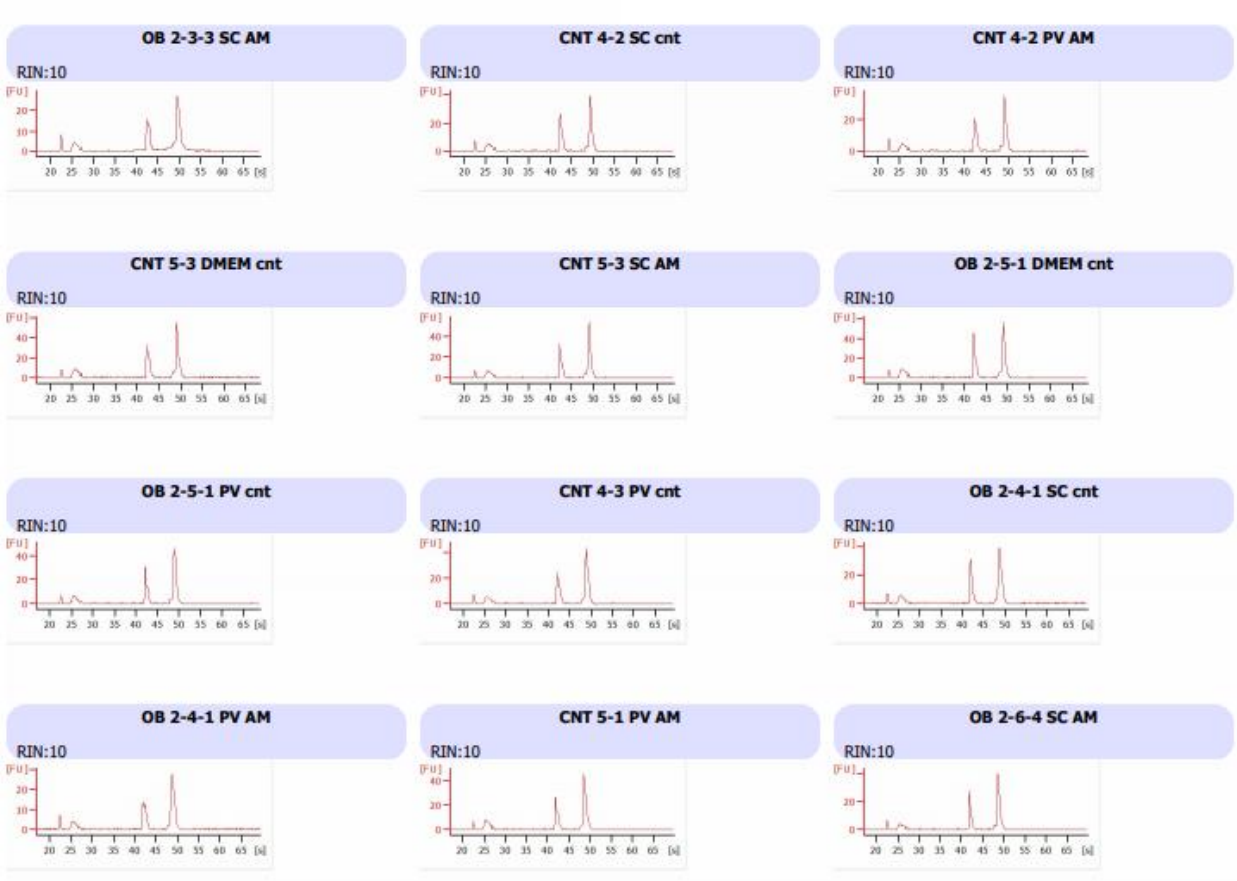

Figure D5: RNA electropherograms displaying the 18S and 28S ribosomal RNA peaks used to calculate the RIN. *Each RNA sample scored a RIN of 10, indicating high RNA integrity.*

A 10x dilution series, ranging from a 100% neat sample to a 0.001% dilution, using a pooled cDNA sample was used (see ***Figure D6*** for qRT-PCR plate layout) to construct amplification plots and linear standard curves for all miRNA primers (miR-421, miR-18a, miR-194, miR-210, miR-322, miR-181b and U6 snRNA) using the QuantStudio™ 7 Flex Real-Time PCR software. The amplification plots were used to assess whether the fluorescent signal from each miRNA primer could accumulate to threshold at a Ct-value below 35, whereas the standard curves were used to analyse the primer efficiencies, as well as identify the most optimal dilution factor for the cDNA samples.

Plate 1												
	1	2	3	4	5	6	7	8	9	10	11	12
A	100	100	100	100	100	100	100	100	100	100	100	100
B	10	10	10	10	10	10	10	10	10	10	10	10
C	1	1	1	1	1	1	1	1	1	1	1	1
D	0,1	0,1	0,1	0,1	0,1	0,1	0,1	0,1	0,1	0,1	0,1	0,1
E	0,01	0,01	0,01	0,01	0,01	0,01	0,01	0,01	0,01	0,01	0,01	0,01
F	0,001	0,001	0,001	0,001	0,001	0,001	0,001	0,001	0,001	0,001	0,001	0,001
G	NTC	NTC	NTC	NTC	NTC	NTC	NTC	NTC	NTC	NTC	NTC	NTC
H												
	miR-421		miR-18a		miR-194		miR-210		miR-322		miR-181b	

Plate 2												
	1	2	3	4	5	6	7	8	9	10	11	12
A	100	100										
B	10	10										
C	1	1										
D	0,1	0,1										
E	0,01	0,01										
F	0,001	0,001										
G	NTC	NTC										
H												
	U6 snRNA											

Figure D6: The qRT-PCR plate layout for the standard curve using a 10x dilution series in duplicate from a pooled cDNA sample.

miRNA-421

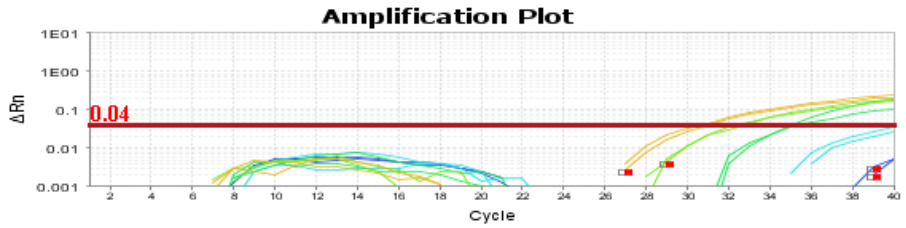

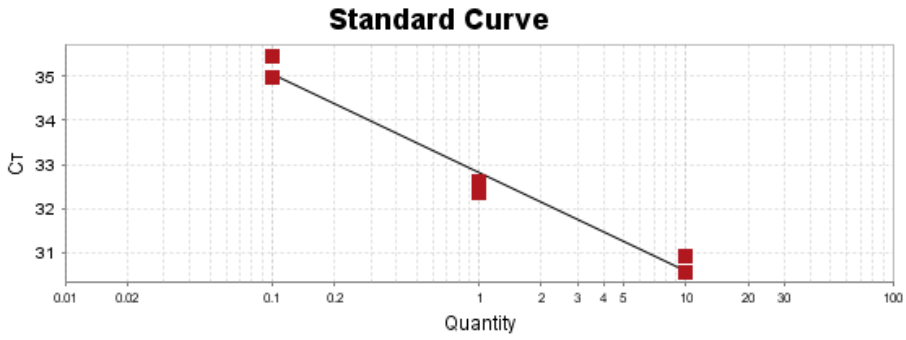

Target: 421 Slope: -2.239 Y-Inter: 32.816 R^2: 0.974 Eff%: 179.671 Error: 0.182

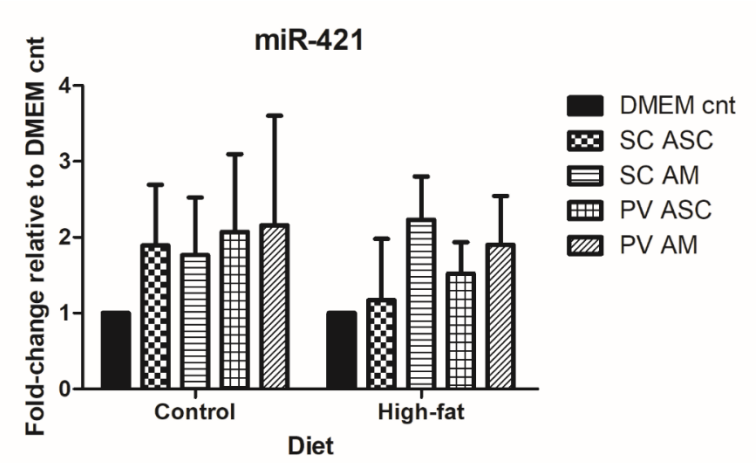

Figure D7: The amplification plot, standard curve and relative expression graph of miR-421. *The standard curve showed a primer efficiency outside of the normal range in H9c2 cells treated with adipose-derived CM. Therefore, no sound conclusions regarding the relative expression of miR-421 can be formulated.*

miRNA-18a

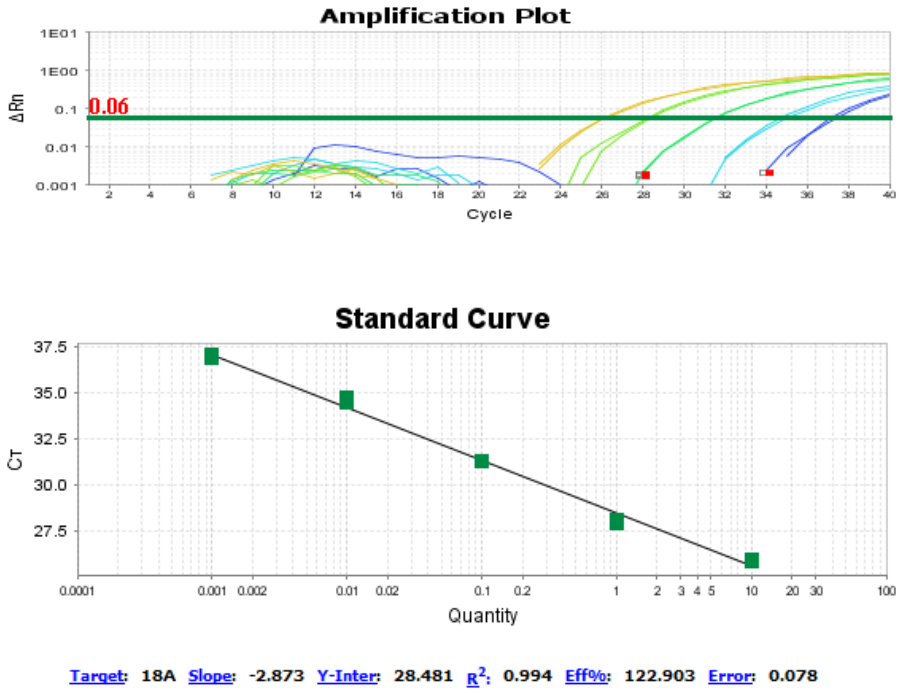

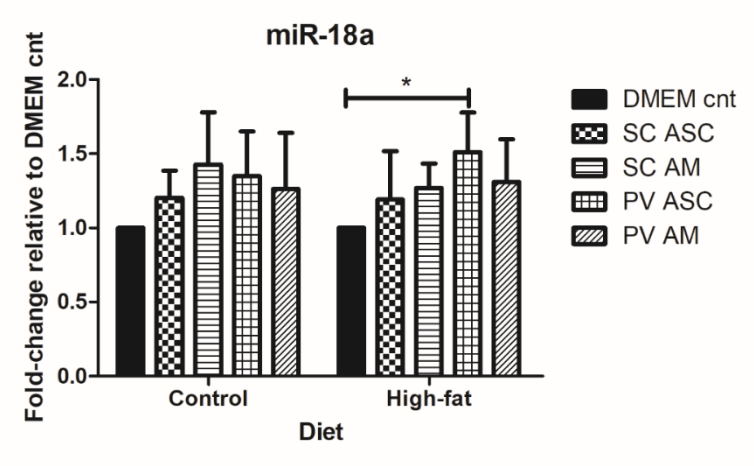

Figure D8: The amplification plot, standard curve and relative expression graph of miR-18a. *The standard curve showed a primer efficiency outside of the normal range in H9c2 cells treated with adipose-derived CM. Therefore, no sound conclusions regarding the relative expression of miR-18a can be formulated.*

miRNA-194

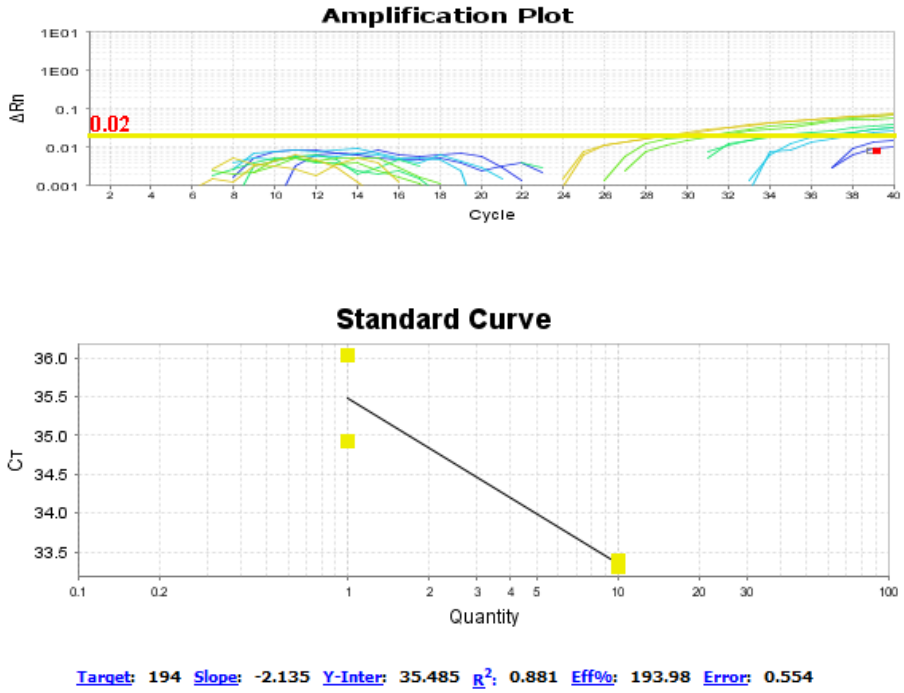

Figure D9: The amplification plot and standard curve of miR-194. *The standard curve showed a primer efficiency outside of the normal range in H9c2 cells treated with adipose-derived CM. Therefore, miR-194 was excluded from the qRT-PCR analysis.*

miRNA-210

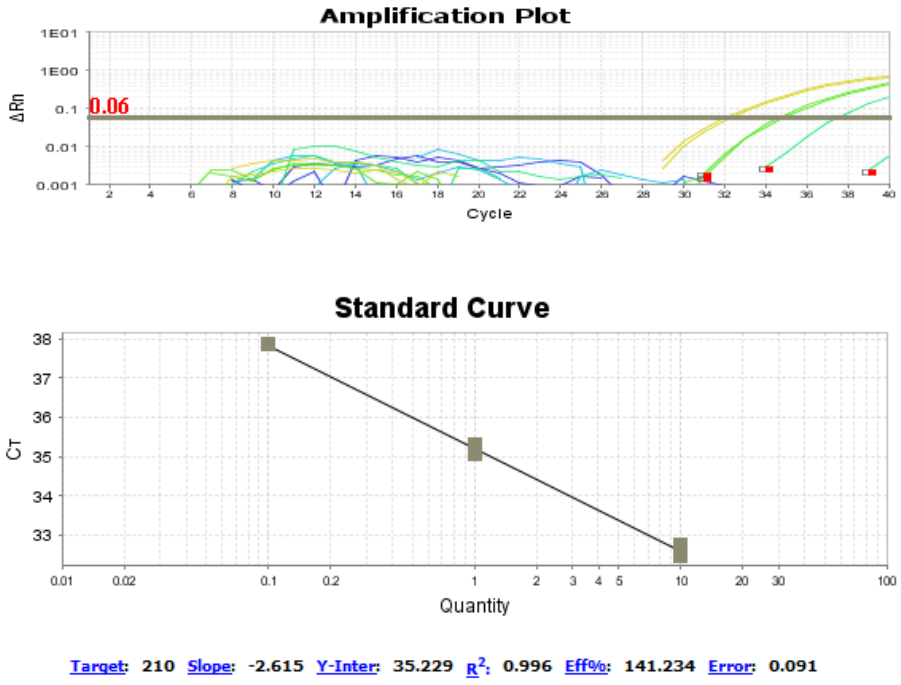

Figure D10: The amplification plot and standard curve of miR-210. *The amplification plot showed Ct-values of greater than 35 and the standard curve showed a primer efficiency outside of the normal range in H9c2 cells treated with adipose-derived CM. Therefore, miR-210 had to be excluded from the statistical analysis.*

miRNA-322

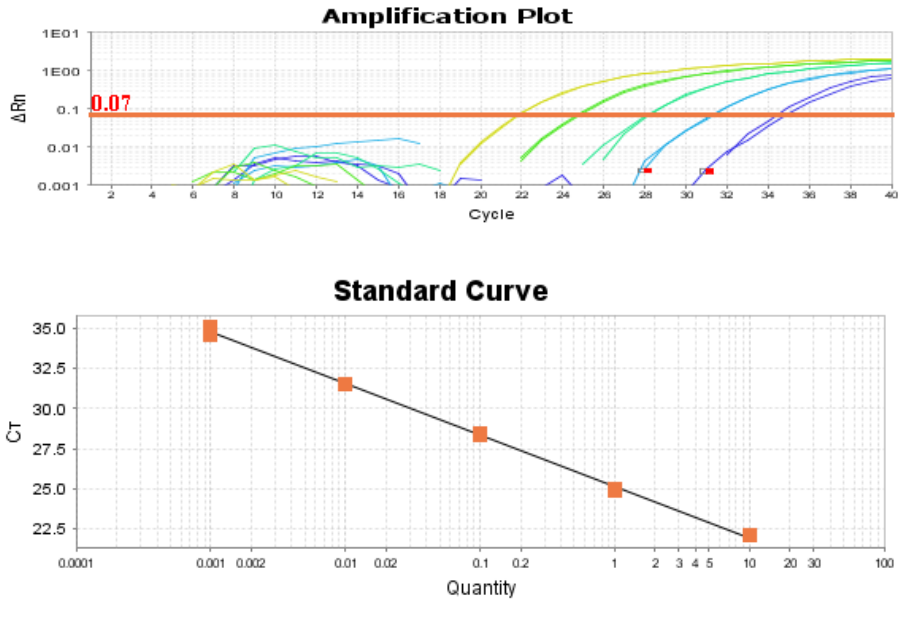

Figure D11: The amplification plot and standard curve of miR-322.

miRNA-181b

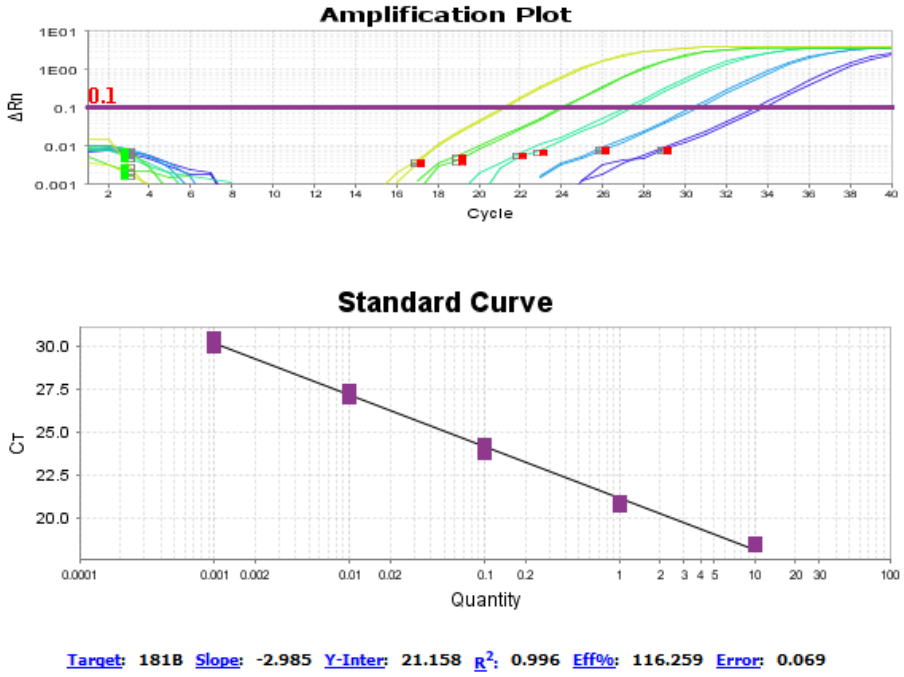

Figure D12: The amplification plot and standard curve of miR-181b.

U6 snRNA

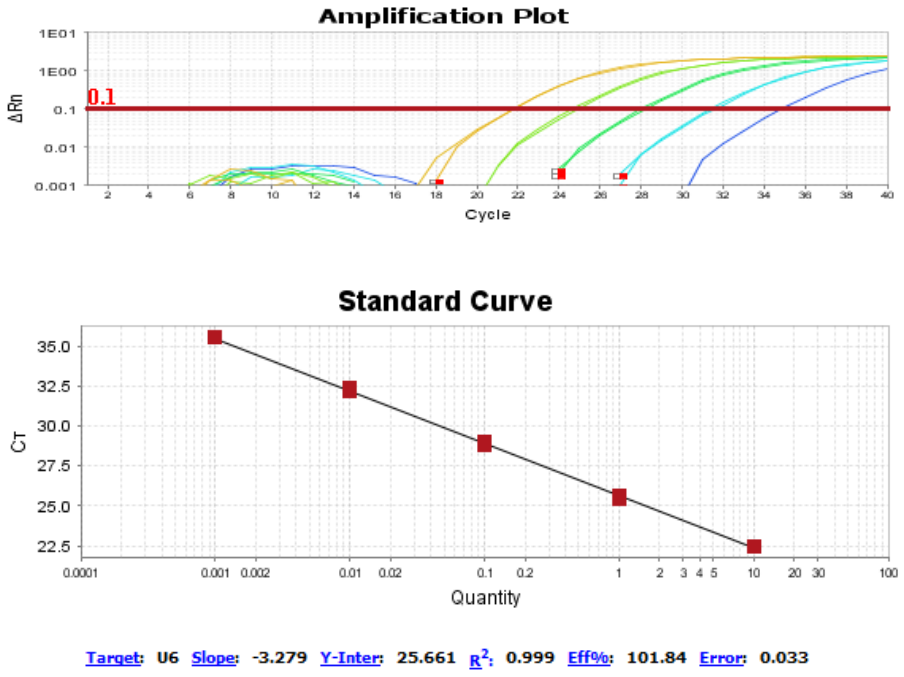

Figure D13: The amplification plot and standard curve of U6 snRNA.

The cDNA samples of a single animal were analysed in duplicate on the same qRT-PCR plate (see ***Figure D14*** for qRT-PCR plate layout).

Plate 1:	Animal A												
	1	2	3	4	5	6	7	8	9	10	11	12	
A	cnt	cnt	SC ASC	SC ASC	SC Adipo	SC Adipo	PR ASC	PR ASC	PR Adipo	PR Adipo	NTC	Neg	miR-421
B	cnt	cnt	SC ASC	SC ASC	SC Adipo	SC Adipo	PR ASC	PR ASC	PR Adipo	PR Adipo	NTC	Neg	miR-18a
C	cnt	cnt	SC ASC	SC ASC	SC Adipo	SC Adipo	PR ASC	PR ASC	PR Adipo	PR Adipo	NTC	Neg	miR-210
D	cnt	cnt	SC ASC	SC ASC	SC Adipo	SC Adipo	PR ASC	PR ASC	PR Adipo	PR Adipo	NTC	Neg	miR-322
E	cnt	cnt	SC ASC	SC ASC	SC Adipo	SC Adipo	PR ASC	PR ASC	PR Adipo	PR Adipo	NTC	Neg	miR-181b
F	cnt	cnt	SC ASC	SC ASC	SC Adipo	SC Adipo	PR ASC	PR ASC	PR Adipo	PR Adipo	NTC	Neg	U6 snRNA
G													
H													

Figure D14: The qRT-PCR plate layout for the cDNA samples in duplicate.

U6 snRNA is a common and widely-used endogenous control RNA used for normalising target miRNA expression. We have established that U6 snRNA is stably expressed in H9c2 cells treated with adipose-derived CM harvested from control and HFD rats **(*Figure D15*)**. Each sample (DMEM cnt, SC ASC, SC Adipo, PR ASC and PR Adipo) per experiment (biological n=4 per diet group) was analysed in duplicate and the mean Ct-values were compared by one-way ANOVA, followed by a Bonferroni post-hoc test. No statistically significant differences in mean Ct-values were observed among the different treatment groups, confirming its stable expression and deeming U6 snRNA an appropriate endogenous control for H9c2 cells treated with adipose-derived CM.

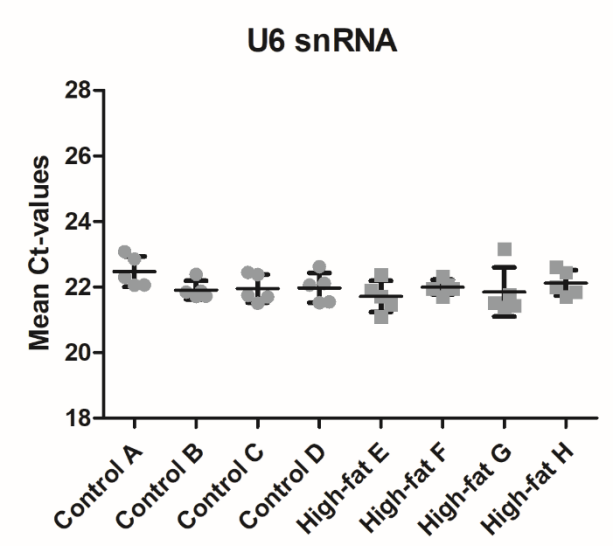

Figure D15: U6 snRNA displayed stable expression in H9c2 cells. *No significant differences in U6 snRNA expression were observed in H9c2 cells were treated with adipose-derived CM originating from control and HFD rats (one-way ANOVA, Bonferroni post-test; mean Ct-value ± SD; $p<0.05$ considered statistically significant).*

The Ct-values of the DMEM control groups for each experiment was compared to ensure that no significant differences in miRNA expression were present. No significant differences in Ct-values for miR-421, **(*Figure D16 A*)**, miR-18a **(*Figure D16 B*)**, miR-322 **(*Figure D16 C*)** and miR-181b **(*Figure D16 D*)** were observed between the DMEM control groups, therefore the Ct-values for each miRNA were averaged and used to calculate the fold-change for each treatment group.

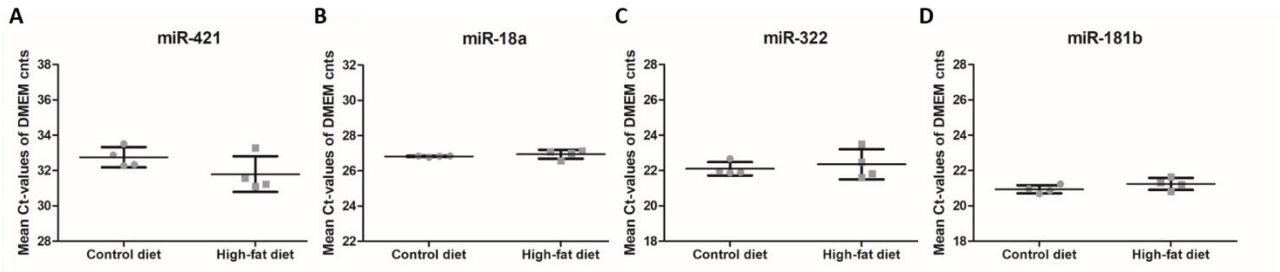

Figure D16: The stable expression of (A) miR-421, (B) miR-18a, (C) miR-322 and (D) miR-181b in H9c2 cells treated complete DMEM media to serve as control for H9c2 cells treated with CM originating from control and HFD rats. *No significant differences in miRNA expression were observed, therefore the Ct-values of H9c2 cells treated with complete DMEM media were pooled per primer and used as a common control for fold-change calculations (two-tailed Student's t-test; Bonferroni post-test; $p<0.05$ considered statistically significant).*